

THE GEOLOGY
of the
NGOYE GRANITE GNEISS FORMATION

by

Andrew John Scogings

Submitted in partial fulfilment of the requirements
for the degree of Master of Science
in the Department of Geology, University of Durban-Westville.

Durban, 1985

ABSTRACT

The Ngoye Granite Gneiss Formation is located in the Natal sector of the Proterozoic Namaqua-Natal Mobile Belt, about 10 km southwest of Empangeni. It forms a prominent east-west trending elongate whalebacked massif some 30 km in length, within amphibolitic gneisses and schists of the Tugela Group.

A suite of twelve different, gneissic granitoids has been recognised within the Ngoye Formation on the basis of field relationships, mineralogy and supportive geochemistry. They range in composition from peraluminous syenite to peralkaline granite. Peraluminous varieties are typically muscovite and garnet-bearing whereas metaluminous granites in the formation contain olive-green biotite and/or hornblende and sphene. Riebeckite, aegerine and yellow-brown biotite, with accessory fluorite and zircon are characteristic of the peralkaline granites. Geochemically, the samples analysed display a range in SiO₂ from 63,79 - 78,47%, are extremely depleted in CaO and MgO, while being enriched in Na₂O and K₂O. Depletion of CaO relative to alkalis is shown by an alkali-lime index of only 36, suggestive of an alkalic character. The agpaite index (A.I. = mole Na₂O + K₂O/AL₂O₃) of the peralkaline samples ranges between 1,02 and 1,16; which classifies them as granites of comenditic affinity. Various chemical classification schemes have been tested and evaluated, of which the R1 - R2 multicationic diagram provides results most similar to modally-derived terminology. Accordingly, the Ngoye granitoids are shown to range from minor syenites and alkali granites to predominant monzo - and syeno-granites.

Trace element data indicate that the peralkaline granites are enriched in Nb, Zr and Zn relative to the other, non-peralkaline, granites in the formation. In addition, radioactive, magnetite-bearing quartz-rich rocks associated with

the peralkaline granites, have extremely enhanced contents of Nb, Zr, Y, Zn, U, Th and to a lesser extent Sn and W. Peraluminous and near-peraluminous granites have the highest Rb/Sr and Rb/Ba ratios of all samples analysed, as well as enhanced Sn, U and Th contents while Zr is notably depleted. Small, muscovite-rich pods associated with muscovite-bearing granites are highly enriched in Sn.

The application of certain discriminants based on modal and geochemical parameters has shown the Ngoye Formation to comprise typical "A" - type granites. "A" - type granites are characteristically intruded as ring complexes into anorogenic or post-orogenic tectonic settings in attenuated or epiorogenically-domed continental crust. Comparison of the Ngoye Formation with the well-known "younger granite" complexes of Nigeria and Saudi Arabia reveals marked similarities. The inference is therefore that the Ngoye Formation represents a metamorphosed "postorogenic" granite complex with most of the hallmarks of "A" type or "within-plate" magmatism.

Four phases of deformation (D_1 to D_4) are recognised within the area mapped. Evidence of D_1 deformation is rare, but rootless folds within the transposed layering in the amphibolitic country rocks reflect the intensity of this prograde metamorphic event, M_1 , during which upper amphibolite grades were achieved. Field evidence shows that the Ngoye granites were intruded after the D_1 event and prior to D_2 . This latter event caused widespread folding about east-west F_2 axes, with the development of a pervasive S_2 planar fabric within the antiformally folded Ngoye Formation. S_2 is locally developed in the amphibolitic country rocks. The D_2 event culminated in the development of northward-directed overthrusting and retrogressive, M_2 , metamorphism of mylonitic thrust planes. Lateral shearing characterizes D_3 , with development of macroscopic mylonites and mesoscopic conjugate shear zones. This was in response to a sinistral sense of movement, as indicated by prominent sub-horizontal extension lineations (L_3) and microscopic asymmetric augen structures. D_4 is deduced from stereograms and is indicated as cross-folding of F_3 fold axes.

TABLE OF CONTENTS

	<u>page</u>
ABSTRACT	ii
LIST OF FIGURES	vii
LIST OF TABLES	xii
LIST OF PLATES	xiv
ACKNOWLEDGEMENTS	xv
CHAPTER 1: INTRODUCTION	1
1.1 General	1
1.2 Previous Investigations	4
1.3 Aims of Present Study	7
CHAPTER 2: FIELD AND PETROGRAPHIC DESCRIPTIONS	9
2.1 Petrographic classification	9
2.1.1 Modal analysis methods	14
2.2 Mesocrystic - biotite granite	18
2.2.1 Field characteristics	18
2.2.2 Petrography	20
2.3 Biotite-hornblende granite	21
2.3.1 Field characteristics	21
2.3.2 Petrography	23
2.3.3 Biotite-schist enclaves in the biotite-hornblende granite	27
2.4 Muscovite-biotite granite	29
2.4.1 Field characteristics	29
2.4.2 Petrography	29
2.5 Biotite-muscovite granite	31
2.5.1 Field characteristics	31
2.5.2 Petrography	32
2.6 Hornblende monzodiorite	35
2.6.1 Field characteristics	35
2.6.2 Petrography	35
2.6.3 Comments on the possible origin of the monzodiorite	39
2.7 Monzonite	40
2.7.1 Field characteristics	40
2.7.2 Petrography	40
2.8 Microsyenite	42
2.8.1 Borehole-core characteristics	42
2.8.2 Petrography	45
2.9 Riebeckite-biotite granite	46
2.9.1 Field characteristics	46
2.9.2 Petrography	48

	<u>page</u>
2.10 Riebeckite granite	49
2.10.1 Field characteristics	51
2.10.2 Petrography	51
2.11 Aegerine microgranite	52
2.11.1 Field characteristics	52
2.11.2 Petrography	54
2.12 Magnetite microgranite	55
2.12.1 Field characteristics	55
2.12.2 Petrography	57
2.13 Magnetite-quartz rock	58
2.13.1 Field characteristics	58
2.13.2 Petrography	61
CHAPTER 3: METAMORPHISM	64
3.1 Introduction	64
3.1.1 Review	64
3.2 Diagnostic assemblages in the Ngoye Formation	65
3.2.1 Calc-silicate minerals	67
3.2.2 Riebeckite	68
3.2.3 Colour of biotite and hornblende	69
CHAPTER 4: MAJOR AND TRACE ELEMENT GEOCHEMISTRY	70
4.1 Introduction	70
4.1.1 Physical and chemical alteration of geochemical samples	70
4.2 Major-element geochemical Characteristics	75
4.2.1 A review of the I-and S-type granitoid classification	76
4.2.2 Loiselle and Wones, A-type granitoids	78
4.2.3 Harker variation diagrams	78
4.2.4 DI Variation diagrams	80
4.2.5 Peacock alkali-lime index	82
4.2.6 Alumina saturation	82
4.2.7 Wright alkalinity ratio	84
4.2.8 Alkaline/Tholeiitic diagrams	84
4.3. Granitoid nomenclature based on major element chemistry	86
4.3.1 Harpum diagram	86
4.3.2 O'Connor's normative Ab-An-Or diagram	86
4.3.3 Streckeisen's Ab-An-Or diagram	88
4.3.4 Streckeisen and Le Maitre's orthogonal plot	90
4.3.5 De la Roche R1 - R2 diagram	90
4.3.6 Degree of Peralkalinity	93
4.3.7 Summary of the chemical classification of Ngoye granitoids	93
4.4 Trace-Element Geochemistry	94
4.4.1 Introduction	94
4.4.2 General characteristics of Ngoye trace elements	94
4.4.3 Large-ion lithophiles	94
4.4.4 Incompatible elements (Zr, Zn & Y)	100
4.4.5 Incompatibles U, Th, Pb W and Sn	101
4.4.6 Incompatibles and alkalis in the magnetite-quartz rocks	101

	<u>page</u>
CHAPTER 5: GEOCHEMICAL TECTONIC CLASSIFICATION OF THE NGOYE GRANITOIDS.	103
5.1 Introduction.	103
5.2 Tectonic Classification Schemes.	104
5.2.1 Differentiation Index.	104
5.2.2 AFM Diagrams.	104
5.2.3 Calc-Alkaline Index.	106
5.2.4 Alumina Saturation.	107
5.2.5 Parameters to distinguish granite environments.	107
5.2.6 QAP diagram.	111
5.2.7 Multicationic R1 - R2 diagram.	113
5.2.8 Trace-element tectonic discriminants for granitoids.	113
CHAPTER 6: STRUCTURAL GEOLOGY.	119
6.1 Introduction.	119
6.2 Terminology.	119
6.2.1 Previous investigations.	121
6.3 D ₁ event.	121
6.4 Intrusion of the Ngoye granites.	127
6.5 D ₂ event.	127
6.5.1 Amphibolitic country rocks.	128
6.5.2 D ₂ : Ngoye massif.	128
6.6 D ₃ event.	129
6.6.1 Shear zones: a review.	129
6.6.2 Mylonites: a review.	131
6.6.3 Conjugate shear zones in the Ngoye Formation.	132
6.6.4 East-west macro shear zones.	140
6.6.5 Composite planar fabrics.	140
6.6.6 Mylonites - mesoscopic observations.	143
6.6.7 Mylonites - microscopic observations.	143
6.6.8 Interpretation of folds in the mylonites.	143
6.6.9 Crenulations.	148
6.7 D ₄ event.	148
CHAPTER 7: DISCUSSION & CONCLUSIONS.	149
7.1 Modal and geochemical characteristics.	149
7.2 The significance of peralkaline granites in the Ngoye Formation.	151
7.3 The A-type classification.	154
7.4 Comparison of the Ngoye Formation with A - type granites.	157
REFERENCES.	159
APPENDIX A.	171
A.1 Introduction.	171
A.2 Geochemical exploration results.	172
A.3 Geophysical exploration results.	173
A.4 Targets.	175
APPENDIX B.	177
B.1 Major and trace element analyses.	177
APPENDIX C.	182
C Modal analyses of Ngoye granitoids.	182

LIST OF FIGURES

		<u>page</u>
Figure 1.1.	Map showing the northern portion of the Natal Sector of the Namaqua-Natal Mobile Belt.....	2
Figure 1.2.	Geology of the Ngoye Granite Gneiss Formation, after the 1975 Geological Survey map.....	5
Figure 1.3.	Geology of the Ngoye Granite Gneiss Formation, simplified after Charlesworth (1981).....	6
Figure 1.4.	Schematic down-plunge structural profile of the northern portion of the Natal Sector, Namaqua-Natal Mobile Belt.....	7
Figure 2.1	Simplified geological map of the Ngoye Granite Gneiss Formation.	10
Figure 2.2.	Triangular diagram after Streckeisen (1976 b) for the modal classification of igneous rocks.....	11
Figure 2.3.	Modal AQP plots of Ngoye granitoids.....	12
Figure 2.4.	Modal AQP plots of Ngoye granitoids.....	13
Figure 2.5.	Simplified geological map of the Ngoye Formation, showing the distribution of mesocrystic biotite granite.....	19
Figure 2.6.	Simplified geological map of the Ngoye Formation, showing the distribution of biotite-hornblende granite.....	22
Figure 2.7.	Simplified geological map of the Ngoye Formation, showing the distribution of muscovite-biotite granite.....	30
Figure 2.8.	Simplified geological map of the Ngoye Formation, showing the distribution of biotite-muscovite granite.....	33
Figure 2.9.	Simplified geological map of the Ngoye Formation, showing the location of monzodiorite outcrops.....	36
Figure 2.10.	Simplified geological map of the Ngoye Formation, showing the location of the monzonite outcrops.....	41
Figure 2.11.	Simplified geological map of the Ngoye Formation, showing the location of microsyenite intersections in borehole NG 2.	43
Figure 2.12.	Cross-section, looking East, of borehole NG2.....	44
Figure 2.13.	Simplified geological map of the Ngoye Formation, showing the distribution of riebeckite-biotite granite.....	47

	<u>page</u>
Figure 2.14.	Simplified geological map of the Ngoye Formation, showing the distribution of riebeckite granite. 50
Figure 2.15.	Simplified geological map of the Ngoye Formation, showing the location of the aegerine microgranite outcrop. 53
Figure 2.16.	Simplified geological map of the Ngoye Formation, showing the distribution of magnetite microgranite. 56
Figure 2.17.	Simplified geological map of the Ngoye Formation, showing the distribution of magnetite-quartz rock outcrops. 59
Figure 3.1.	Isobaric T - X CO ₂ diagram for reactions in the monzodiorite. 68
Figure 4.1.	Map of the Ngoye Formation showing geochemical-sample localities. 75
Figure 4.2.	Na ₂ O-K ₂ O plot for granitoids from the Ngoye Formation. 76
Figure 4.3	Harker variation diagrams of the Ngoye major element oxides. 79
Figure 4.4.	Variation diagrams of major oxides in weight percent against the differentiation index. 81
Figure 4.5.	Peacock's alkali-lime index diagram showing the alkalic affinities of the Ngoye granitoids. 83
Figure 4.6.	Wright variation diagram showing the essentially alkaline to peralkaline character of the Ngoye granitoids. 83
Figure 4.7a.	Plot of total alkalis versus SiO ₂ showing the sub-alkaline character of the Ngoye granitoids. 85
Figure 4.7b.	The subdivision of sub-alkaline rocks into calc-alkaline and tholeiitic varieties, using ratios of Al ₂ O ₃ to normative plagioclase. 85
Figure 4.8.	Plot of SiO ₂ against FeO : MgO ratios illustrating the predominantly tholeiitic character of the Ngoye granitoids. 85
Figure 4.9.	Classification of the Ngoye granitoids on the binary K ₂ O versus Na ₂ O diagram after Harpum (1963). 87
Figure 4.10.	Plot of normative Ab - An - Or for the classification of granitoid rocks, fields after O'Connor (1965). 87
Figure 4.11.	Classification of the Ngoye granitoids according to Ab - An - Or for silica-oversaturated igneous rocks on the basis of An / Or ratios, after Streckeisen (1976 a). 89

	<u>page</u>
Figure 4.12.	Normative classification of the Ngoye granitoids based on the quartz versus anorthite/orthoclase diagram of Streckeisen & le Maitre (1979). 91
Figure 4.13.	The R1 - R2 diagram showing igneous-rock fields relevant to the classification of the Ngoye granitoids, after de la Roche <u>et al.</u> (1980). 91
Figure 4.14a.	Classification schemes for peralkaline, quartz normative, extrusive rocks, after Macdonald & Bailey (1973). 92
Figure 4.14b.	Classification schemes for peralkaline, quartz normative, extrusive rocks.. . . . 92
Figure 4.15.	Plots showing the variation in Sr and Ba with Rb for the Ngoye granitoids.. . . . 97
Figure 4.16.	Triangular diagram illustrating the relative enrichment of Zn and Zr over Al in the peralkaline Ngoye granitoids.. . . . 97
Figure 4.17.	Plot of Zr concentrations (ppm) against the agpaitic index (AI) for peralkaline granitoids from the Ngoye Formation.. . . . 98
Figure 4.18.	Plots of Ngoye granitoid analyses showing the decrease in Zn and Zr concentrations with increasing aluminous character.. . . . 98
Figure 5.1a.	Histogram showing the distribution of chemical analyses in terms of the differentiation index - the Aleutian Islands orogenic-related suite.. . . . 105
Figure 5.1b.	Histogram showing the distribution of chemical analyses in terms of the differentiation index - the Iceland anorogenic suite. 105
Figure 5.1c.	Histogram showing the distribution of chemical analyses in terms of the differentiation index - the Ngoye analyses. 105
Figure 5.2.	AFM ternary diagram illustrating compressional and extensional-suite trends, after Petro <u>et al.</u> (1979).. . . . 105
Figure 5.3.	Variation diagram for $\text{CaO}/(\text{Na}_2\text{O}+\text{K}_2\text{O})$ vs SiO_2 106
Figure 5.4.	Plot of molecular SiO_2 , Al_2O_3 , and $(\text{Na}_2\text{O}+\text{K}_2\text{O})$ for comenditic and pantelleritic obsidians. 108
Figure 5.5.	Diagram showing variation of total iron (as FeO) against agpaitic index.. . . . 108

	<u>page</u>
Figure 5.6.	Diagram showing the discrimination of "type" extensional and compressional granites. 109
Figure 5.7.	QAP modal diagram showing fields of various granitoid series, after Lameyre & Bowden (1982)... 112
Figure 5.8.	Petrogenetic classification of granitoid series using the R1-R2 multicationic diagram, after Batchelor & Bowden (1985)... 112
Figure 5.9.	Ocean ridge granite (ORG) normalized trace element patterns for average analyses from Pearce <u>et al.</u> (1984)... 115
Figure 5.10.	Variation diagrams of Y, Nb and Rb against SiO ₂ for Ngoye granitoid analyses.. . . . 116
Figure 5.11a.	Nb - Y discriminant diagram for collision, volcanic-arc, within-plate, and ocean-ridge granites.. . . . 118
Figure 5.11b.	Nb+Y - Rb discriminant diagram for collision, volcanic-arc, within-plate, and ocean-ridge granites.. . . . 118
Figure 6.1.	Stereographic plots of structural data from the amphibolitic terrain. 123
Figure 6.2.	Stereographic plots of structural data from the granitic terrain.. . . . 124
Figure 6.3.	Map showing general structural features of the study area. 125
Figure 6.4.	Detail of layered plasticine model, showing conjugate shear zones developed during a bulk sinistral-shearing event (Harris & Cobbold, 1984)... 130
Figure 6.5.	Schematic representation of asymmetric directional criteria from shear zones, after Simpson & Schmid (1983)... 139
Figure 6.6.	Typical composite planar fabrics, shown as shear bands (c - surfaces) transecting mylonitic foliations (s - surfaces)... 142
Figure 6.7.	Block diagram illustrating the orientation of fabrics referred to in the text, with respect to the mylonitic foliation.. . . . 147
Figure 6.8.	Diagram showing how fold hinges may be rotated into parallelism with the direction of overthrusting.. . . . 147

Figure 7.1.	World map showing the distribution of peralkaline oversaturated igneous rocks.	152
Figure 7.2.	Examples of typical granitic ring complexes from Saudi Arabia & Sudan.....	155
Figure 7.3.	Example of a Nigerian "younger granite" complex, and the Ngoye Formation.	156
Figure A.1.	Location of exploration targets.....	174
Figure A.2.	Contours of Nb in panned samples.....	174
Figure A.3.	Contours of Sn in panned samples.	175
Figure C.1.	Location of additional modal analyses.	186

LIST OF TABLES

		<u>page</u>
Table 2.1.	Representative modal analyses of mesocrystic biotite granite.....	19
Table 2.2.	Representative modal analyses of biotite-hornblende granite.....	22
Table 2.3.	Representative modal analyses of muscovite-biotite granite.....	30
Table 2.4.	Representative modal analyses of biotite-muscovite granite.....	33
Table 2.5.	Representative modal analyses of hornblende monzodiorite.....	36
Table 2.6.	Representative modal analyses of monzonite.....	41
Table 2.7.	Representative modal analyses of microsyenite.....	43
Table 2.8.	Representative modal analyses of riebeckite-biotite granite.....	47
Table 2.9.	Representative modal analyses of riebeckite granite.....	50
Table 2.10.	Representative modal analysis of aegerine microgranite.....	53
Table 2.11.	Representative modal analyses of magnetite microgranite.....	56
Table 2.12.	Representative modal analyses of magnetite-quartz rock.....	59
Table 3.1.	Summary of metamorphic events in the Natal Nappe Complex...	65
Table 3.2.	Diagnostic mineral assemblages in the Natal Nappe Complex. ...	66
Table 4.1a.	Average chemical analyses, Ngoye non-peralkaline granitoids...	71
Table 4.1b.	Average chemical analyses, Ngoye peralkaline granitoids.....	72
Table 4.2a.	Average chemical analyses, Ngoye granitoids.....	73
Table 4.2b.	Average granitoids from published literature sources.....	74
Table 4.3.	Characteristics of I- and S-type granitoids.....	77
Table 4.4.	Mean trace-element contents in the Ngoye granites.....	95
Table 4.5.	Trace-element contents, Ngoye and Saudi-Arabian quartz rocks..	99

	<u>page</u>
Table 5.1.	Comparison of variables for granites in the SiO range 70 - 75%. 110
Table 6.1.	Summary of the structural terminology used in chapter 6..... 120
Table 6.2.	Summary of deformational events in the Ngoye area. 122
Table A.1.	Panned stream samples, statistical parameters..... 172
Table A.2.	Target 1, trench channel sample analyses..... 176
Table B.1.	Major-elements, selected trace elements, and C.I.P.W. norms.. 178
Table B.2.	Major elements, selected trace elements, and C.I.P.W. norms.. 179
Table B.3.	Major elements, selected trace elements, and C.I.P.W. norms.. 180
Table B.4.	Major elements, selected trace elements, and C.I.P.W. norms.. 181
Table C.1.	Additional modal analyses..... 182
Table C.2.	Additional modal analyses..... 183
Table C.3.	Additional modal analyses..... 184
Table C.4.	Additional modal analyses..... 185

LIST OF PLATES

	<u>page</u>
Plate 1. Ngoye landscapes.....	3
Plate 2. Polished slabs of Ngoye granitoids.....	16
Plate 3. Polished slabs of Ngoye granitoids.....	17
Plate 4. Enclaves in the Ngoye granites.....	24
Plate 5. Polished slabs and photomicrographs of zoned enclaves.....	25
Plate 6. Granite contacts and conjugate shear zones.....	26
Plate 7. Photomicrographs of hornblende monzodiorite.....	37
Plate 8. Photomicrographs of the magnetite-quartz lithology.....	60
Plate 9. Deformation styles within the study area.....	126
Plate 10. Conjugate shear zones in the Ngoye massif.....	134
Plate 11. Photomicrographs illustrating microstructural changes across ductile shear zones.....	135
Plate 12. Photomicrographs of microstructural shear-sense criteria.....	136
Plate 13. Photomicrographs of microstructural shear-sense criteria.....	137
Plate 14. S-C mylonites within the Ngoye massif.....	141
Plate 15. Typical D ₃ -related structures in the Ngoye massif.....	144
Plate 16. Photomicrographs of asymmetric structures in mylonites.....	145
Plate 17. Photomicrographs of asymmetric structures in mylonites.....	146

ACKNOWLEDGEMENTS

I wish to express my sincere thanks to Drs. I.F. Forster and G.A.D. Zelt for their continued support and enthusiasm throughout the duration of this project. Without the help and assistance of the Geology Department, University of Durban - Westville, this thesis would not have been completed.

The help given me by Dr. M. R. Cooper during the past year, in particular his constructive criticism concerning the text, artwork and diagrams, is gratefully acknowledged. Drs. C. A. Finlay and A. Kerr as well as Prof. P.E. Matthews are warmly thanked for their invaluable contributions and discussions with me. I am indebted to the technical staff, Mr. S. Pillay and Ashwin, who cheerfully and unflinchingly manufactured hundreds of high-quality thin sections, in addition to numerous polished rocks slabs.

I would like to thank Mining Corporation (now part of the S.A. Development Trust Corporation), in particular Dr. H. J. Hanekom and Mr. S. B. Gain for their enthusiasm and permission to use data from the Ngoye Project. Their generous assistance in having rock samples analysed for major and trace elements at Pretoria University is gratefully acknowledged. In addition, I would like to thank the Kwa-Zulu Government, and Mr. D. Freeman of the Kwa-Zulu Nature Conservation Department, for their permission to enter the Ngoye area. Sincere appreciation is extended to Rob Parker, John Adlam and other members of the Forestry Department, Port Durnford State Forest, for their hospitality while in the field.

I wish to thank Renee, my wife, for typing this difficult text, and also for her patience and encouragement during these last few hectic months. Without her help this thesis would not have been possible. Trevor Greening, thanks for the use of your word processor and home, and also for your unselfish help in printing and editing the final copy. Very special thanks to Mona Heine for printing the photographic plates.

Finally, thanks to all my festive friends, without whose help this thesis would have been completed six months earlier.

Chapter 1

INTRODUCTION

1.1 General

The 150 km² study area is situated in north-eastern Natal, South Africa (Fig. 1.1). Detailed investigations were carried out over the Ngoye Granite Gneiss Formation, which forms a prominent 32 km long east-west trending whale-back to the west of Felixton. A smaller 3 km long body crops out at Ninians, just to the north-west of Felixton. The main Ngoye range rises to 300m above the surrounding terrain and is dominated by (a) domical or bornhardt surfaces in the northern and eastern portions of the massif, and (b) all-slopes soil covered topography in the western areas (Plate 1). The undulating central and southern parts are covered by impenetrable indigenous forest (Plate 1). Forming a major watershed between the Mlalazi drainage system to the south and the Umhlatuzi system to the north, the Ngoye massif is characterized by strongly trellised drainage. Stream directions are controlled both by prominent north-south joints and by the regional east-west foliation in the gneissic granite. All streams in the area are perennial due to the high mean annual rainfall of 1400mm (measured at Port Durnford Forest Station). Maximum precipitation is during the hot subtropical summer months when temperatures of up to 43°C result in extremely humid field conditions.

Access via gravel roads and tracks to the area is good, although four-wheel drive is necessary during the wet summer months. Entrance to the Ngoye Forest Reserve is prohibited unless the required permit has been obtained from the Kwa-Zulu Nature Conservation Department.

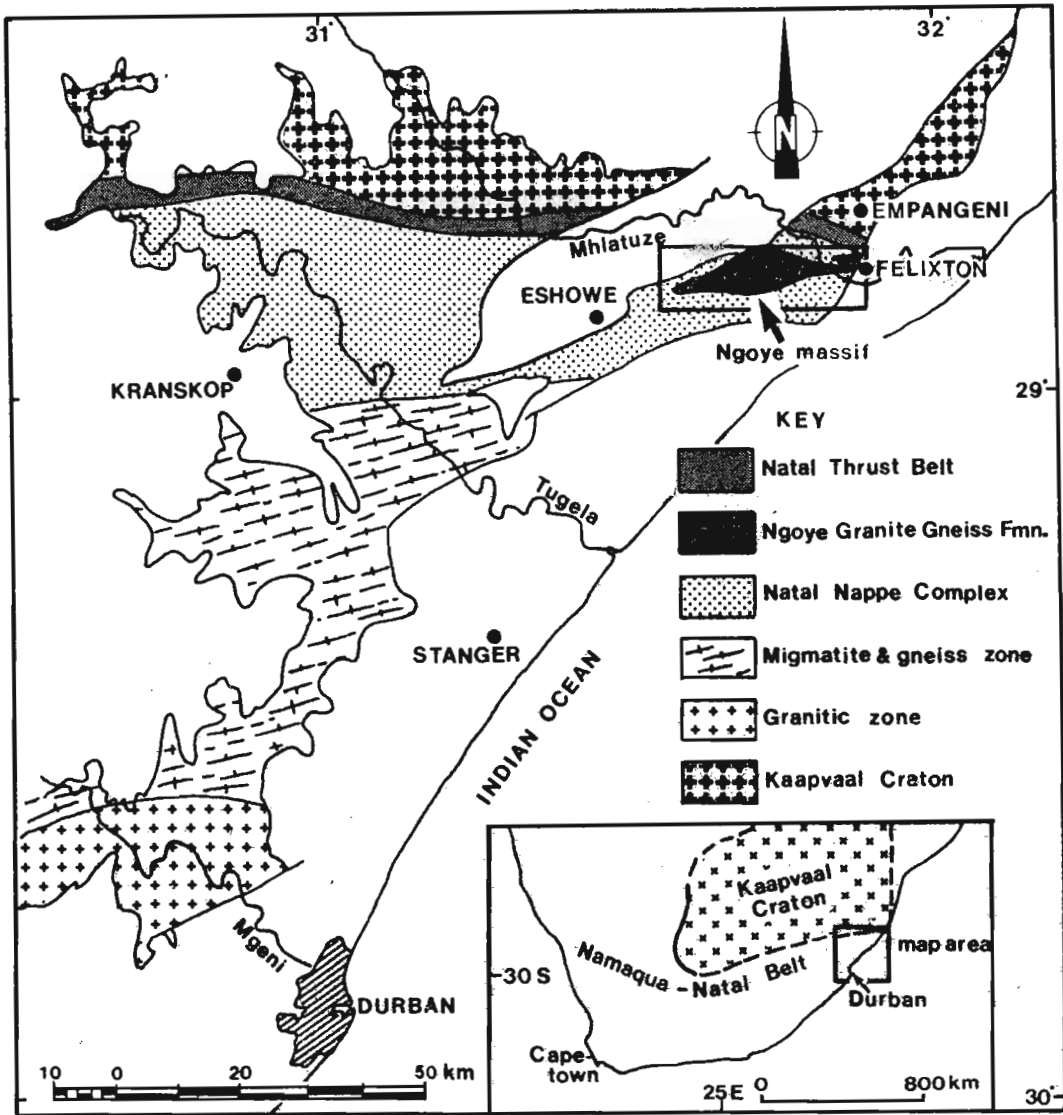


Fig. 1.1. Map showing the northern portion of the Natal Sector of the Namaqua-Natal Mobile Belt. Subdivision of the mobile belt is after Matthews (1981). The mapped area, i.e. the Ngoye Formation, is indicated as the Ngoye massif.

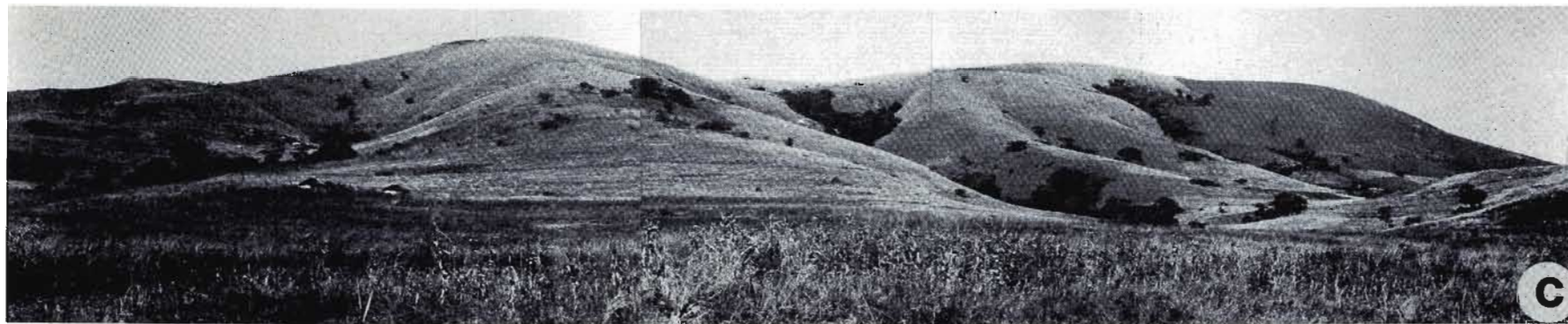
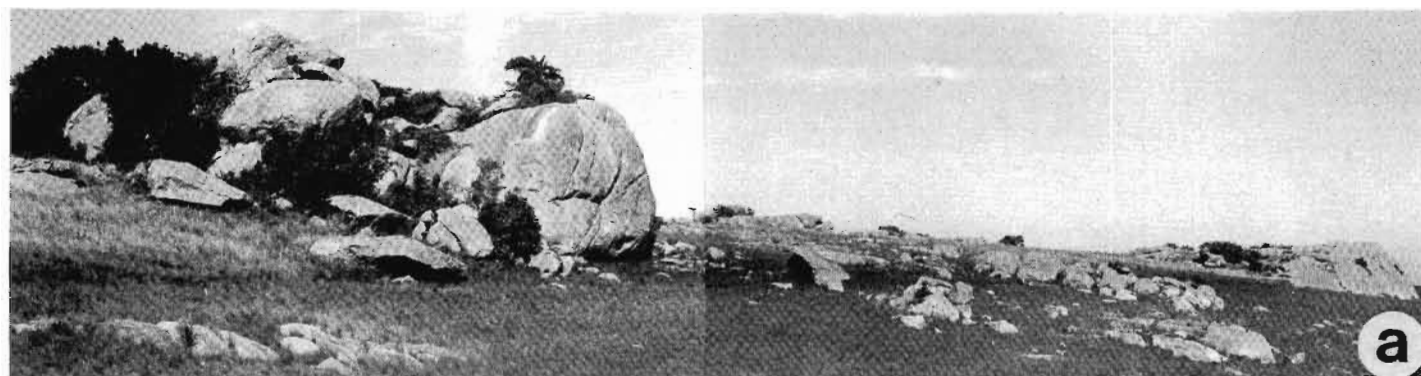


Plate 1. Ngoye landscapes. (a) Eastern Ngoye, looking South over mesocrystic biotite granite outcrops, field of view 300 m (map ref. 25 G). (b) Is a view northwards over the densely wooded summit of the Ngoye range, onto exfoliation domes of muscovite-biotite granite (map ref. 20 F). The western extremity of the range is shown in (c), a view southwards from the Umhlatuzana river (map ref. 5 I) showing the soil covered all-slopes topography typical of the area, field of view 1,5 km.

1.2 Previous Investigations

Prior to 1898 very little geological work had been done in Natal and Zululand. During 1899 William Anderson made a reconnaissance survey of eastern Zululand in which he outlined 300 square miles of granites, gneisses and schists to the east of Eshowe. He noted the granitic nature of the "Engoye Mountains" and stated: "The laminations of the gneisses and schists are usually inclined at a high angle.... away from the Engoye Mountains, which form the axis of this metamorphic belt" (Anderson, 1901: p. 60).

Mapping by McCarthy (1961) confirmed Anderson's original appraisal that the Ngoye range is at the core of a steep anticlinal structure. McCarthy distinguished the Ngoye lithology as biotite granite gneiss, composed of microcline, oligoclase, quartz and biotite with accessory sphene and zircon. A locally developed porphyroblastic (augen) gneiss fabric was also noted. Garnetiferous aplites on the north-eastern flanks of the massif were thought to have been derived from a sedimentary precursor. In concluding his discussion on the steep-dipping, westerly-striking Ngoye granite gneiss McCarthy drew attention to (a) the concordance of the granite gneiss with regional trends (b) the apparently gradational boundary between granite gneiss and surrounding schists and (c), the lack of increased metamorphic grade in the schists adjacent to the granite gneiss. A metasomatic origin for the Ngoye granite was proposed (McCarthy, 1961).

The Geological Survey (1975) produced a 1:50 000, 6 sheet compilation of the geology around Empangeni (Fig. 1.2). Du Preez (1982), in the unpublished explanation, suggested an origin by partial melting of a quartzo-feldspathic parent for the Ngoye granite body. He cited sharp, generally concordant contacts, as well as concordancy of granite-gneiss foliation with the regional country rock structure, as evidence for syntectonic intrusion.

Whereas McCarthy (1961) had assigned all granite gneisses in the area between Empangeni and Felixton to the Ngoye type, Charlesworth (1981) restricted the Ngoye Granite Gneiss Formation to those rocks constituting the "Umgoye" Massif, and to a smaller body at Ninians (Fig. 1.3). The remaining granitoid gneisses in the area were assigned to the Nseleni and Halambu Formations. He described the Ngoye granite gneiss as fine to medium

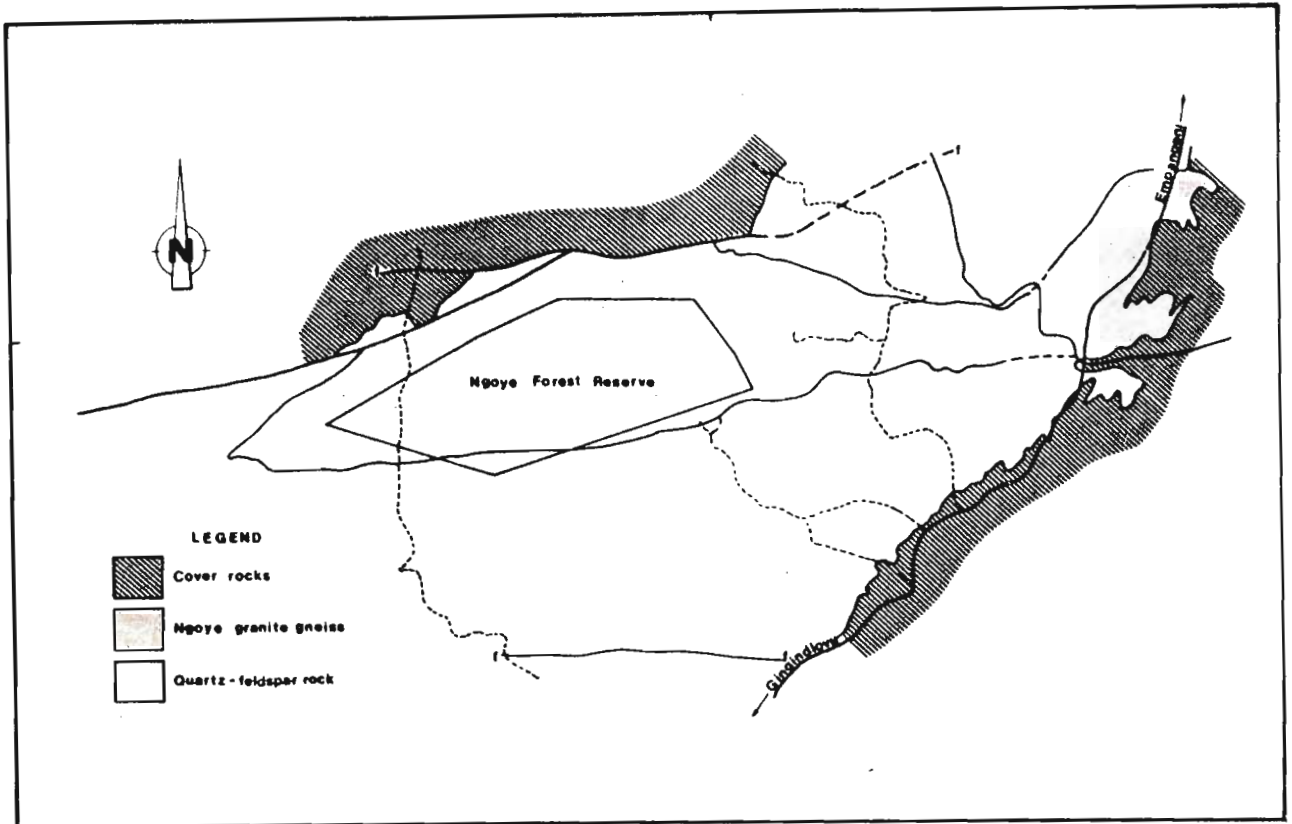


Fig.1.2. Geology of the Ngoye Granite Gneiss Formation (Geological Survey ,1975).

grained, noting the local development of megacrystic or sub-augen varieties and a strong penetrative gneissosity particularly towards the margins. Modal analyses showed approximately equal amounts of microcline and oligoclase, with biotite the characteristic mafic mineral. Accessory minerals included sphene, epidote, muscovite and garnet. Some hornblende-bearing varieties were observed although apparently not restricted to any particular area. Using Streckeisen's (1976) AQF diagram, Charlesworth classified the Ngoye as varying from quartz monzonite to granite. A prominent easterly-plunging lineation, defined by elongate biotite aggregates, was described from the southern margins of the main massif, as well as from the Ninians body. He furthermore proposed a transition from a central, remnant augen-gneiss core in the summit of the range, through well foliated gneissic varieties, to marginal mylonites. The mylonites were interpreted as thrust contacts, no evidence (enclaves or apophyses) being found for an intrusive relationship with the surrounding gneisses (Charlesworth, op cit.).

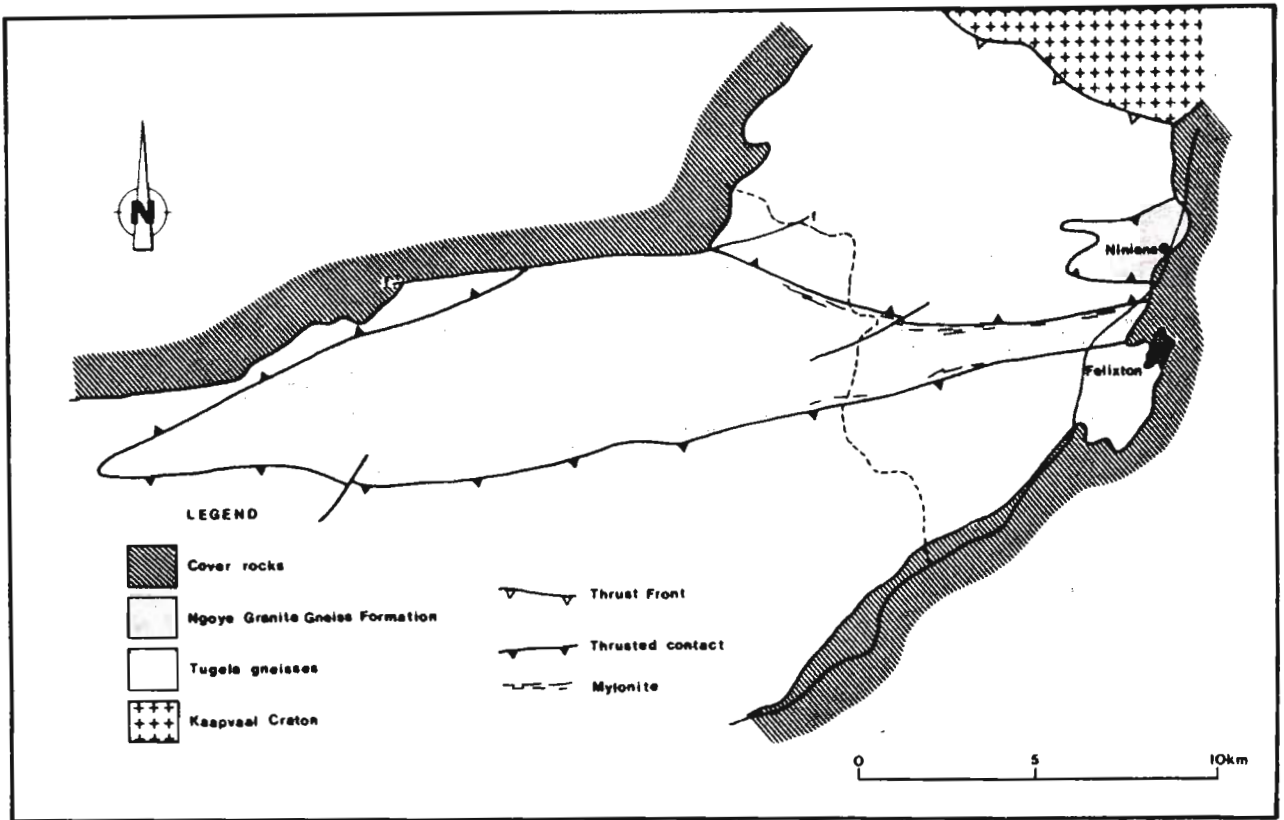


Fig. 1.3. Geology of the Ngoye Granite Gneiss Formation, after Charlesworth (1981).

Matthews (1981) subdivided the entire "Natal Metamorphic and Structural Province" into four major zones (Fig 1.1) on the basis of lithological, structural and metamorphic characteristics, as briefly described below:

- (i) a Northern Frontal Zone comprising the Natal Thrust Belt and the Nkomo, Madidima, Mandleni and Tugela Nappes (in ascending structural order) of the Natal Nappe Complex (Fig. 1.4);
- (ii) a 60 km-wide Migmatite and Granite Gneiss zone between Eshowe and Durban;
- (iii) a Granitic zone 120 km in width extending from just north of Durban to Port Shepstone in the south and
- (iv) the Southern Granulite Zone which extends to the Transkei border.

The Ngoye Granite Gneiss Formation was included as a concordant sheet at the top of the Nkomo Nappe by Matthews (1981) and Matthews & Charlesworth (1981), (Fig. 1.4).

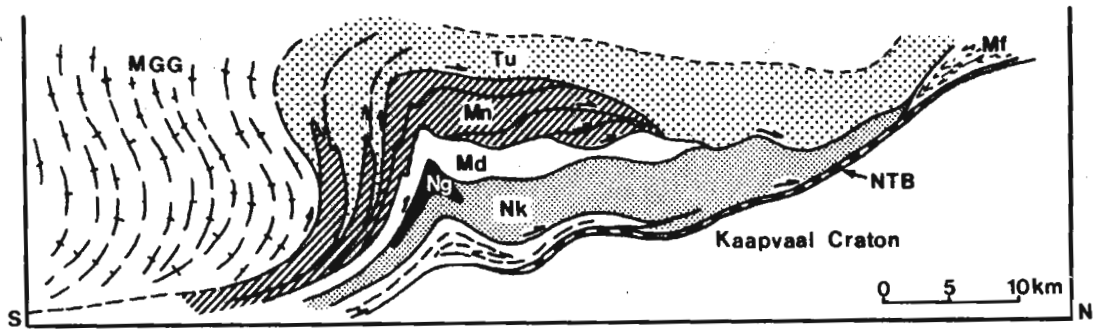


Fig. 1.4. Schematic down-plunge structural profile of the northern portion of the Natal Sector, Namaqua-Natal Mobile Belt. This section (adapted from Matthews, 1981) is across the western part of the map shown in Fig. 1.1. Ng=Ngoye Formation; Nk=Nkomo Nappe; Md=Madidima Nappe; Mn=Mandleni Nappe; Tu=Tugela Nappe; NTB=Natal Thrust Belt; Mf=Mfongozi schist; and MGG=migmatite and granite gneiss.

1.3 Aims of Present Study

Interest in the area was generated in 1981 with the discovery by Mining Corporation of radioactive, quartz-rich magnetite-bearing rocks along the southern margins of the Ngoye Granite Gneiss Formation. Subsequent stream sampling and geophysical work was conducted under the author's supervision from July 1982 to May 1983. This led to the delineation of several targets along this zone which were trenched and sampled, the most promising one of which was probed by two boreholes. Mineralization proved to be of low and irregular tenor over narrow widths and the project was discontinued in July 1983. Reconnaissance mapping by the author whilst employed by Mining Corporation indicated the presence of at least four distinctly different, mappable, granitic units within the formation.

The aims of my study, since having been employed as a research assistant in the University of Durban-Westville Geology Department, have therefore been to:

- (i) delineate and map (at a scale of 1:25 000) all lithologies present ;
- (ii) define and compare these lithologies utilizing microscopic and geochemical techniques;
- (iii) evaluate the structural and metamorphic history of the study area and to evaluate the formation of mylonites and shear zones; and to
- (iv) investigate and possibly reassess the tectonic environment in which the Ngoye granites were generated.

Chapter 2

FIELD AND PETROGRAPHIC DESCRIPTIONS

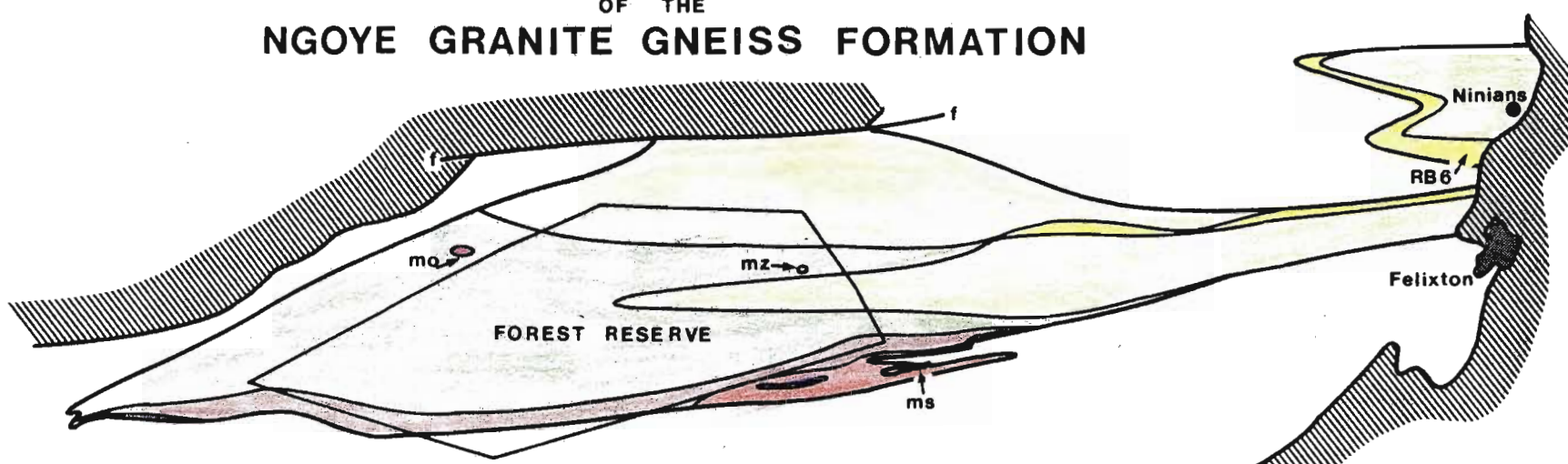
2.1 Petrographic classification

Twelve different granitoids have been recognized within the Ngoye Granite-Gneiss Formation on the basis of mineralogical composition and field characteristics (Fig. 2.1). Modal assemblages were calculated using thin sections stained for K-feldspar and plagioclase according to the methods described by Hutchison (1974). Following the I.U.C.S. subcommission proposal that the AQP-triangular diagram (Fig. 2.2) be used for igneous - looking rocks irrespective of their derivation (Streckeisen, 1976 b), this method of classification has been utilized for the Ngoye granitoids. To this end, and for rocks with a mafic component of less than 90%, the following mineral groups advocated by the I.U.C.S. subcommission have been adhered to:

- (i) A = alkali feldspar such as perthite or microcline and includes albite An_{00} to An_{05} ;
- (ii) P = plagioclase and scapolite; and
- (iii) Q = quartz

When plotted on the QAP triangular diagram a root name (eg, granite) is derived, which is preceded, in order of increasing amounts, by the characteristic mafic minerals. Thus a biotite-hornblende granite contains more hornblende than biotite (Streckeisen, 1976 b).

GEOLOGY OF THE NGOYE GRANITE GNEISS FORMATION



LEGEND

- Younger cover
- Peralkaline microgranites
- Riebeckite granite
- Riebeckite-biotite granite
- Microsyenite
- Monzonite
- Hornblende monzodiorite
- Biotite-muscovite granite
- Muscovite-biotite granite
- Biotite-hornblende granite
- Mesocrystic biotite granite
- Tugela & Matigulu gneisses

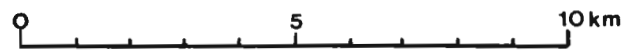


Fig. 2.1 SIMPLIFIED GEOLOGICAL MAP OF THE NGOYE FORMATION.

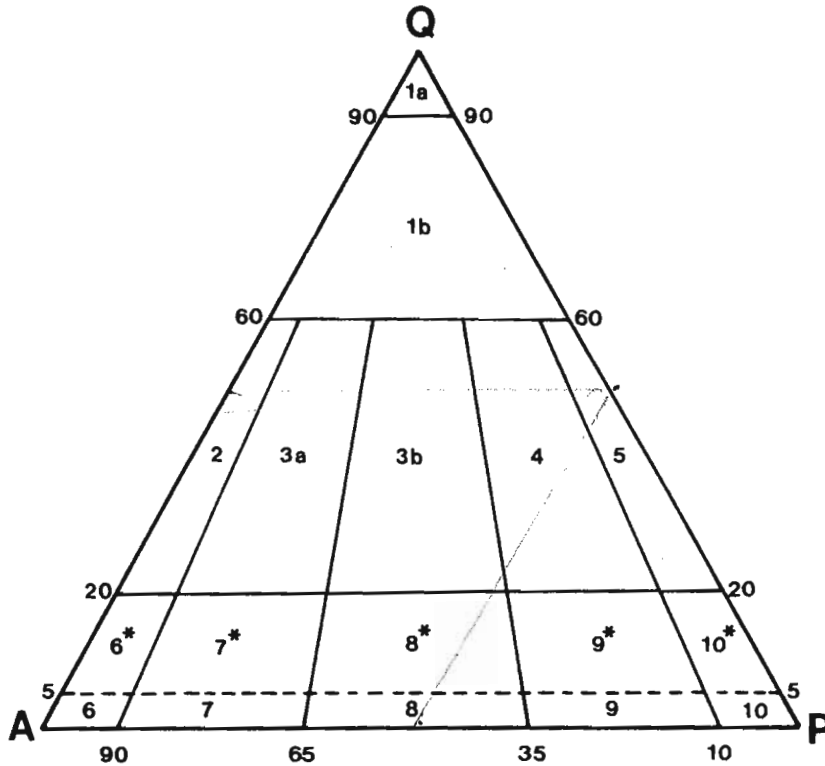


Fig. 2.2. Triangular diagram after Streckeisen (1976 b) for the classification of igneous rocks according to their modal mineral proportions, where $Q + A + P = 100\%$ (Q = quartz; A = alkali feldspar; P = plagioclase). The fields are numbered as follows: 1a, quartzolite; 1b, quartz-rich granitoids; 2, alkali-feldspar granite; 3a & 3b, granite (sensu stricto); 4, granodiorite; 5, tonalite; 6*, quartz alkali-feldspar syenite; 7*, quartz syenite; 8*, quartz monzonite; 9*, quartz monzodiorite; 10*, quartz diorite; 6, alkali-feldspar syenite; 7, syenite; 8, monzonite; 9, monzodiorite; 10, diorite.

Based on the Streckeisen classification, the following granitoids have been distinguished within the Ngoye Formation: (Figs. 2.3 & 2.4 and Plates 2 & 3)

- 1) Mesocrystic biotite granite
- 2) Biotite-hornblende granite and biotite-schist enclaves
- 3) Muscovite-biotite granite
- 4) Biotite-muscovite granite
- 5) Hornblende monzodiorite
- 6) Monzonite
- 7) Microsyenite
- 8) Biotite-riebeckite granite
- 9) Riebeckite granite
- 10) Aegerine microgranite
- 11) Magnetite microgranite
- 12) Magnetite-quartz rock (quartzolite).

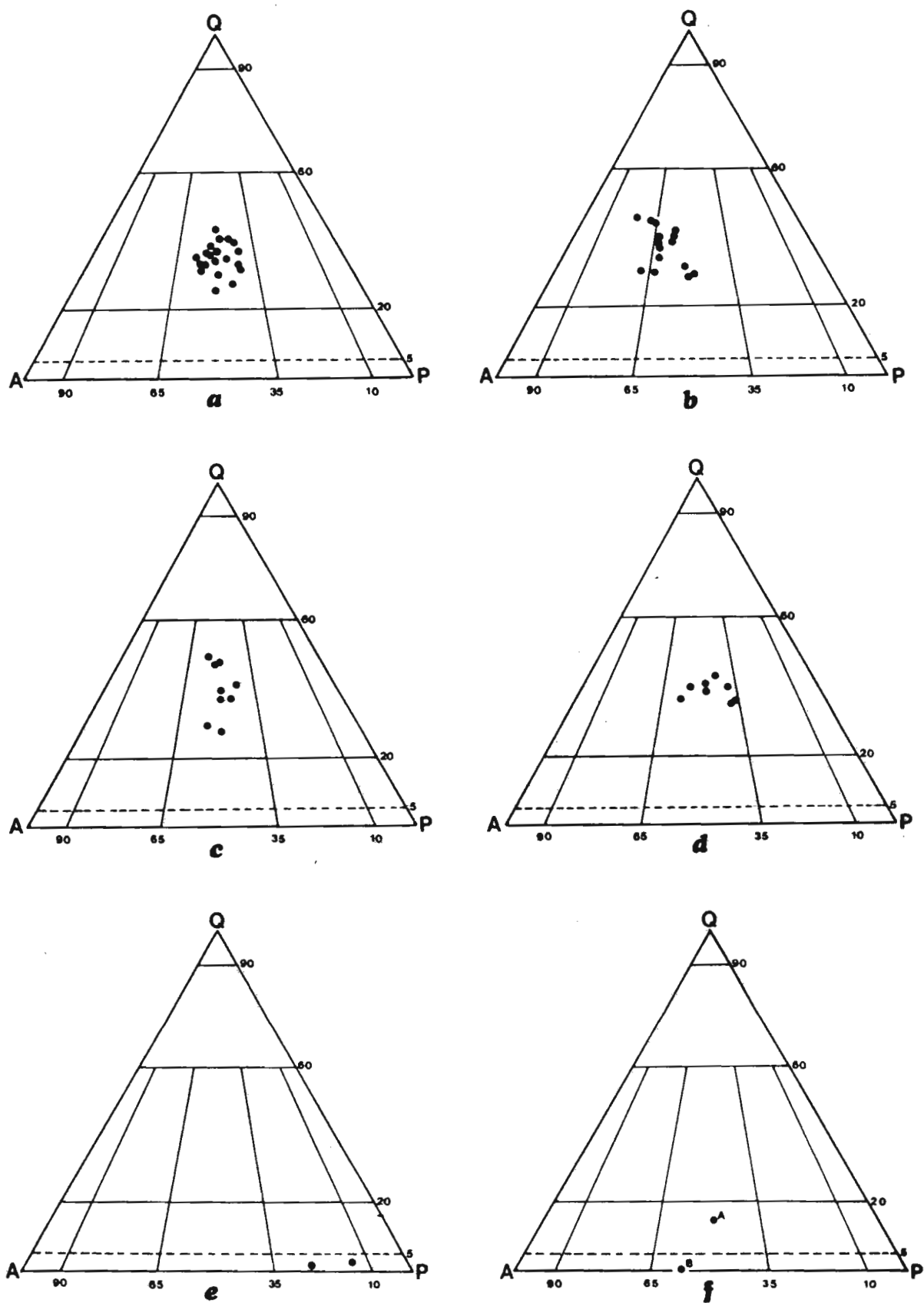


Fig. 2.3. Modal AQP plots of Ngoye granitoids: a, mesocrystic biotite granite; b, biotite-hornblende granite; c, muscovite-biotite granite; d, biotite-muscovite granite; e, hornblende monzodiorite; f, monzonite.

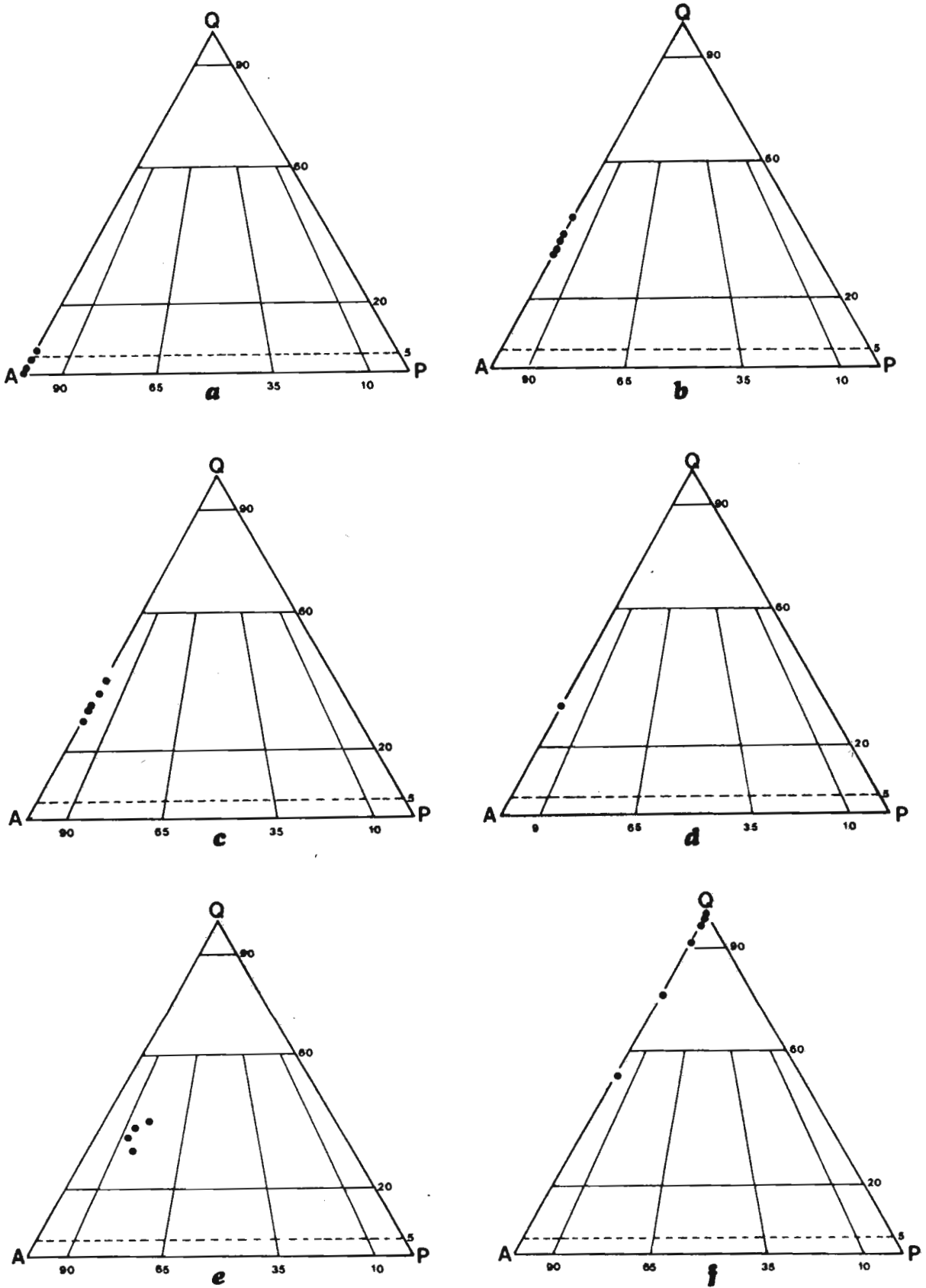


Fig. 2.4. Modal AQP plots of Ngoye granitoids: a, microsyenite; b, riebeckite-biotite granite; c, riebeckite granite; d, aegerine microgranite; e, magnetite microgranite; f, magnetite-quartz rock.

All of these rocks have a well developed regional, metamorphically induced foliation and in restricted areas have undergone later intense deformation as indicated by the presence of mylonites. As the Ngoye granitoids are probably of igneous origin (Charlesworth, 1981) they should strictly be termed "gneissic granitoids" or "orthogneisses." **However, for the purpose of the following discussion, which is essentially an attempt to describe, classify and characterize the various granitoids within the Ngoye Formation, the term gneissic will be omitted for simplicity. For example, the name "gneissic biotite-riebeckite granite" is referred to as biotite-riebeckite granite.**

2.1.1 Modal analysis methods

Modal analyses were carried out on specimens that had been stained for quartz, plagioclase and k-feldspar (Hutchison, 1974, p. 16). In the case of lineated samples, sections were cut both parallel and perpendicular to that lineation and the resulting mode is an average of an equal number of determinations from each direction. Approximately one thousand two hundred counts (plus-minus 200) were made on each section.

All modal analyses not given as representative samples in Tables 2.1 to 2.12 are tabulated in Appendix C. Sample sites, other than those shown in Figs. 2.5 to 2.17, are indicated in Fig. C.1. in Appendix C.

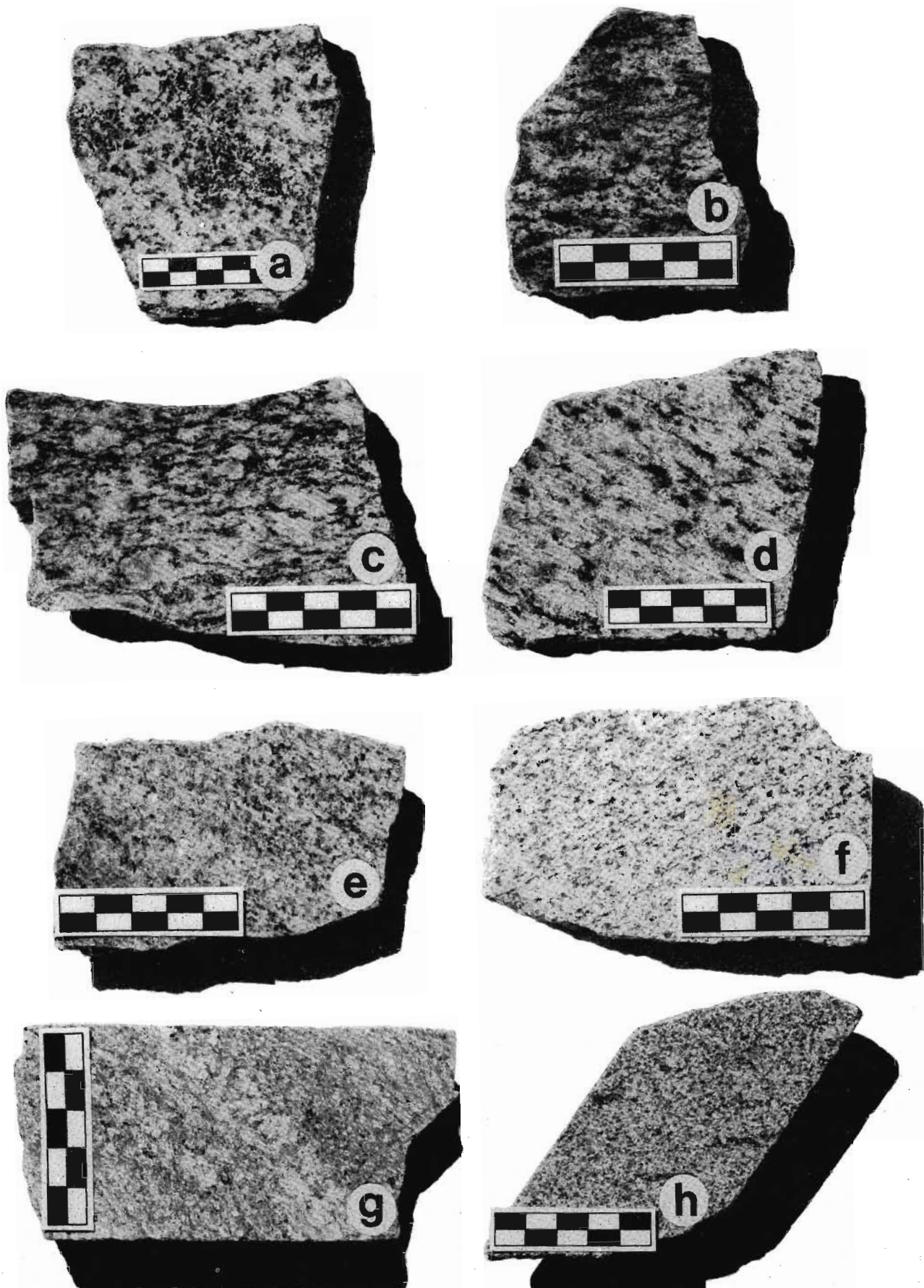


Plate 2. Polished rock slabs. (a), Hornblende monzodiorite; (b), monzonite; (c), mesocrystic biotite granite; (d), biotite-hornblende granite; (e), muscovite-biotite granite; (f), biotite-muscovite granite; (g), upper syenite; (h), lower syenite.

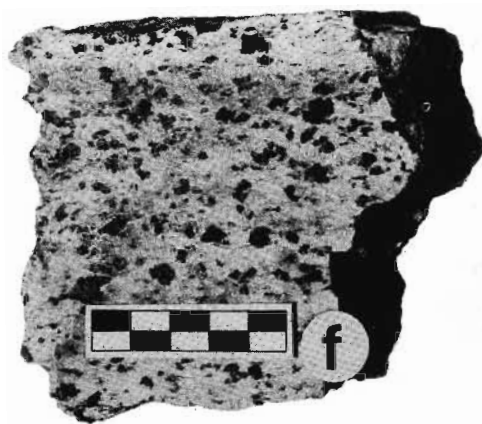
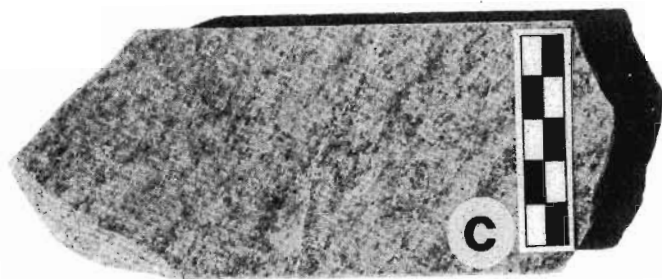


Plate 3. Polished rock slabs. (a), Riebeckite-biotite granite; (b), riebeckite granite; (c), magnetite microgranite; (d), aegerine microgranite; (e), mylonitized magnetite-quartz rock; (f), magnetite-quartz rock. Scale in cm.

2.2 Mesocrystic - biotite granite

This lithology was described by McCarthy (1961) and Charlesworth (1981) as the typical and predominant Ngoye Granite Gneiss, the type area being the "Kwa-Gugushe river, Ngoye area" (SACS, 1980). However, the present study has shown that this rock type constitutes only about 20% of the Ngoye formation and is restricted to the eastern and central portions of the main massif, as well as the smaller Ninians body (Fig. 2.5).

2.2.1 Field characteristics

The mesocrystic biotite granite is a resistant lithology and on weathering produces boulder-strewn outcrops and smooth bornhardt surfaces (Plate 1). Exposures, found predominantly in the main massif, become subdued and less frequent to the east of the Mhlatuze river and at Ninians. This rock type is characterized by ovoid pink microcline mesocrysts (up to 1,5 cm in length) in a foliated grey matrix of feldspar, quartz and biotite. Fresh samples, as found at a small quarry on the Ongoye-Ekupumuleni road (map ref. 29, F), show microcline mesocrysts rimmed by white plagioclase (Plate 2). Small crystals of yellow to off-white sphene are sometimes evident in hand specimens, especially in those from the Ninians body. Due to the smooth rounded morphology of outcrops, and the way in which the foliation wraps around the microcline mesocrysts, structural data are often difficult to obtain. However, several localities on the main massif indicate that microcline mesocrysts are ellipsoidal and define an east-west trending sub-horizontal linear fabric (Plate 2 c is of a section cut parallel to that fabric and perpendicular to foliation).

Occasional small (1cm x 10cm), biotite-rich enclaves were observed to be randomly distributed through this lithology, usually orientated parallel to the regional foliation. Contacts with adjacent granitoids along the southern limits of this lithotype are obscure, apart from along the south-eastern margins of the main massif where a sharp mylonitized contact with amphibolites is inferred. However, good exposures on the elevated northeast flanks of the range reveal a knife-sharp, strongly sheared contact with finer-grained muscovite-bearing granites (map ref. 30, F).

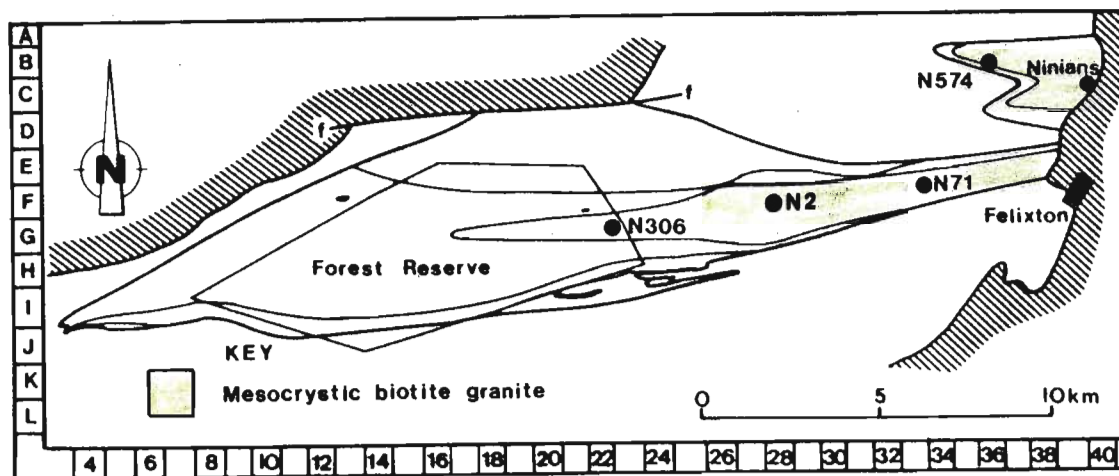


Fig. 2.5. Simplified geological map of the Ngoye Formation, showing the distribution of mesocrystic biotite granite.

TABLE 2.1

Representative modal analyses* of mesocrystic biotite granite

	N2	N71	N306	N574
microcline	36,1	25,3	35,0	23,0
plagioclase	28,4	21,9	34,6	32,2
quartz	28,7	38,2	23,2	36,2
biotite	4,6	3,9	5,6	5,1
muscovite	0,5	t	t	1,3
epidote	0,7	-	-	0,9
sphene	0,6	-	0,5	0,6
opaque	0,2	0,2	-	0,5

Notes:

Sample localities shown in Fig.2.5 above.

* : all values as volume percentages.

t : mineral species present but less than 0,2%.

- : mineral species not detected.

2.2.2 Petrography

Microscopically, the mesocrystic-biotite granite is heteroblastic, medium to coarse grained, and typically has mesocrysts or aggregates of microcline mantled by plagioclase. A poorly defined alignment of coloured minerals is generally apparent, especially in those sections cut parallel to the elongation direction of microcline mesocrysts. Samples from within or near mylonite zones show pronounced foliation and alignment of mafic minerals as well as decreased grain size. Representative modal analyses are presented in Table 2.1, and according to the AQP diagram (Streckeisen, 1976 b), this lithology is classified as monogranitic, with microcline and plagioclase present in almost equal amounts (Fig. 2.3). Xenoblastic to subidioblastic microcline occurs in two modes, either as crystalline or polycrystalline mesocrystic aggregates up to 15mm in size, or as small polygonal grains in the groundmass of thin sections. The mesocrysts, which display typical cross-hatch or gridiron twins, also contain occasional inclusions of quartz and plagioclase. Perthitic intergrowths are fairly common, with stringers, ribbons and occasional patch exsolutions present (Spry, 1969).

Plagioclase in the form of 1 to 3 mm diameter xenoblastic grains occurs predominantly in the groundmass, where it is associated with microcline, quartz and mafic minerals or as rims around the microcline mesocrysts. The contact zones of plagioclase grains against microcline are occasionally the sites of wormy myrmekitic intergrowths of quartz in the plagioclase. Polysynthetic twins are moderately well developed in the majority of plagioclase crystals, the extinction angles for which indicate compositions ranging from An_{20} - An_{26} (oligoclase). Most plagioclase crystals, like the microcline, are clear and free from secondary alteration.

Pale-yellow to olive-green biotite is the principle ferromagnesian mineral and occurs as broad ragged laths associated with clusters of epidote, sphene and rare hornblende. These minerals, which curve around and envelope microcline mesocrysts form fine layers which define the regional fabric.

2.3 Biotite-hornblende granite

Comprising about 45% of the outcrop, this lithology forms the bulk of the central to western parts of the Ngoye massif (Fig 2.6). Whereas outcrops in the central summit of the range are obscured by dense indigenous forest of the Ngoye Forest Reserve (Plate 1 b), the western exposures are relatively accessible from several jeep tracks maintained by the Kwa-Zulu Nature Conservation department.

2.3.1 Field characteristics

Biotite-hornblende granite exposures over the central Ngoye range are similar to those formed by mesocrystic biotite granite ie, bornhardt surfaces and boulder strewn outcrops. In contrast, the western part of the massif is characterized by deeply dissected all-slopes topography (Twidale, 1972) with abundant soil cover and rare, weathered outcrops of this granite type (Plate 1).

This essentially medium-grained lithology is discriminated, in the field, from the mesocrystic biotite granite by (a) a general lack of pink microcline mesocrysts and (b) the presence of clots and streaks of greenish-black hornblende (Plate 2d). The east-west regional foliation, with subvertical to moderate northerly dips, is readily apparent in the field and relatively easy to measure. Steep, northerly plunging linear structures in the foliation planes are sometimes developed and are due to the parallel elongation of minute biotite "needles". Single or conjugate pairs of ductile shear zones are occasionally developed and clearly postdate the formation of the regional east-west foliation (Plate 6). These structures are discussed in some detail in chapter 6.

Rare enclaves within the biotite-hornblende terrain comprise two varieties, namely (a) small biotite-rich streaks up to about 10 cm length and (b) elongate bodies of biotite-schist up to a metre or so in length (Plate 4). The latter, which are possibly xenoliths of country rock, display marked internal concentric zonation, from pale-grey biotite-schist cores to dark, hornblende rich margins (Plate 5). In addition, the structural fabric within the xenoliths is usually inclined obliquely to the contacts with surrounding granite.

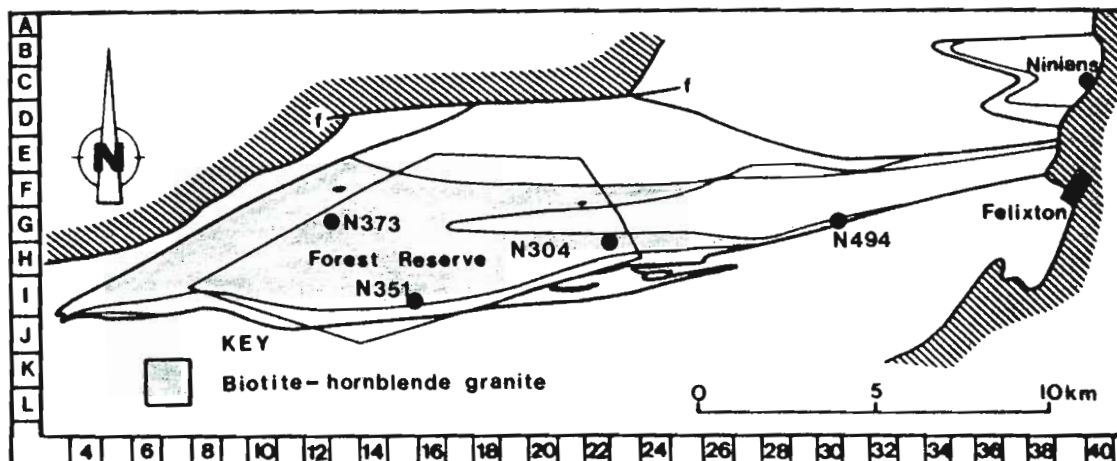


Fig. 2.6. Simplified geological map of the Ngoye Formation, showing the distribution of biotite-hornblende granite.

TABLE 2.2

Representative modal analyses* of biotite-hornblende granite

	N304	N351	N373	N494
microcline	35,2	30,9	30,9	43,2
plagioclase	20,1	22,5	27,0	23,1
quartz	37,4	39,4	29,5	28,1
biotite	2,3	2,0	3,5	1,1
hornblende	4,5	3,1	7,8	4,2
sphene	0,1	0,5	0,8	0,1
opaques	1,0	0,8	t	0,1

Notes:

Sample localities shown in Fig.2.6 above.

* : all values as volume percentages.

t : mineral species present but less than 0,2%.

- : mineral species not detected.

2.3.2 Petrography

Microscopically this lithology is distinguished from all others in the Ngoye massif by the presence of hornblende as the predominant ferromagnesian phase (Table 2.3). In addition to hornblende, variable amounts of biotite occur, with accessory minerals including sphene, zircon and epidote. Modal analyses fall within the alkali-feldspar enriched portion of field 3 (b) in Streckeisen's (1976 b) AQP diagram (Fig. 2.3). The regional east-west foliation is seen microscopically to be defined by thin stringers of very fine-grained (0,02-0,05 mm) polygonal quartz and feldspar grains, with aligned biotite laths and hornblende needles. These foliation planes which occur at 5 to 10 mm intervals are separated by broad zones of coarser minerals.

Microscopically, the dominant feldspar in most thin sections is microcline, which occurs predominantly as 2-4 mm grains and also as occasional "mesocrysts" up to 5 mm in diameter. Crystals are inclusion-free, unaltered, and display weakly developed spindle-shaped tartan twins. Ribbon and flame perthitic intergrowths (Spry, 1969) are occasionally present in microcline and for example in specimen N346A (map ref. 16, 1) sometimes display abundant exsolution phenomena. Plagioclase is generally xenoblastic and has polygonal to interlobate grain boundaries with adjacent microcline and quartz. Well defined polysynthetic albite twin lamellae indicate plagioclase compositions ranging from An_{20} - An_{26} , ie: oligoclase (determined using the Michel-Levy method described by Kerr (1959)). Quartz aggregates, alternating with feldspar-rich portions, define a crude gneissosity in most thin sections. Polygonal quartz grains vary from 2 to 4 mm diameter and are sometimes highly strained, displaying undulose extinction, serrated grain boundaries and peripheral sub-grain development (Bell & Etheridge, 1973).

Hornblende and biotite are the chief mafic constituents and occur in irregular elongate clots up to several millimetres in diameter.

The clots are generally aligned within the regional east-west foliation direction, and characteristically comprise randomly orientated intergrowths of biotite and hornblende. Hornblende is typically poikiloblastic, enclosing quartz blebs and displaying the distinctive pleochroic scheme: α = yellow green, β = deep green-blue and γ = deep green.

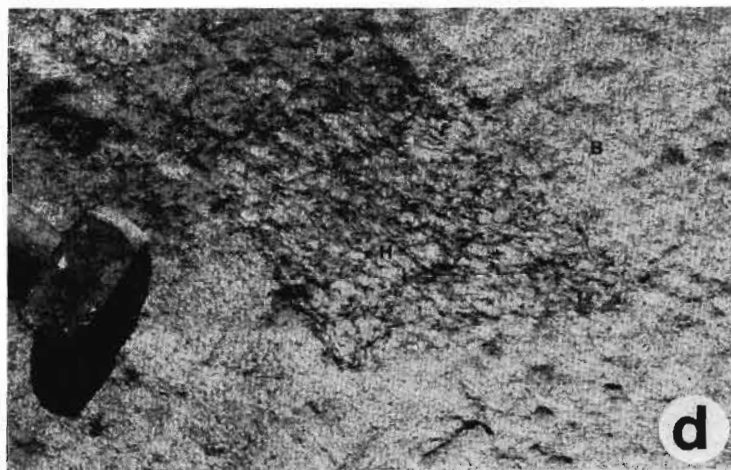
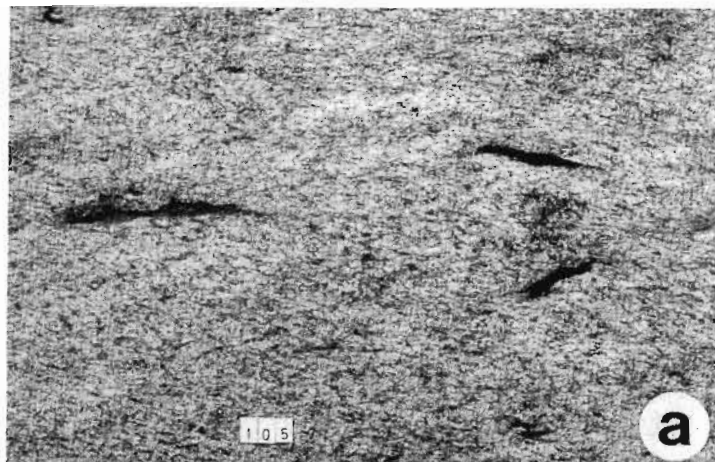


Plate 4. Enclaves in the Ngoye Granites. (a) Small, biotite-rich streaks in biotite-hornblende granite, map ref. 20 G. Plates 4 b & c illustrate biotite-schist bodies within biotite-hornblende granite (N447, map ref. 14 F). Note the concentric zonation within the enclave in (b) and the porphyroblasts developed within the enclaves in (c). The age relationship between the muscovite-biotite lithology and the biotite-hornblende granite is illustrated in (d), where a xenolith of biotite-hornblende granite (H, identified by thin section) is enclosed within the relatively younger muscovite-biotite granite (B). Scale in cm.

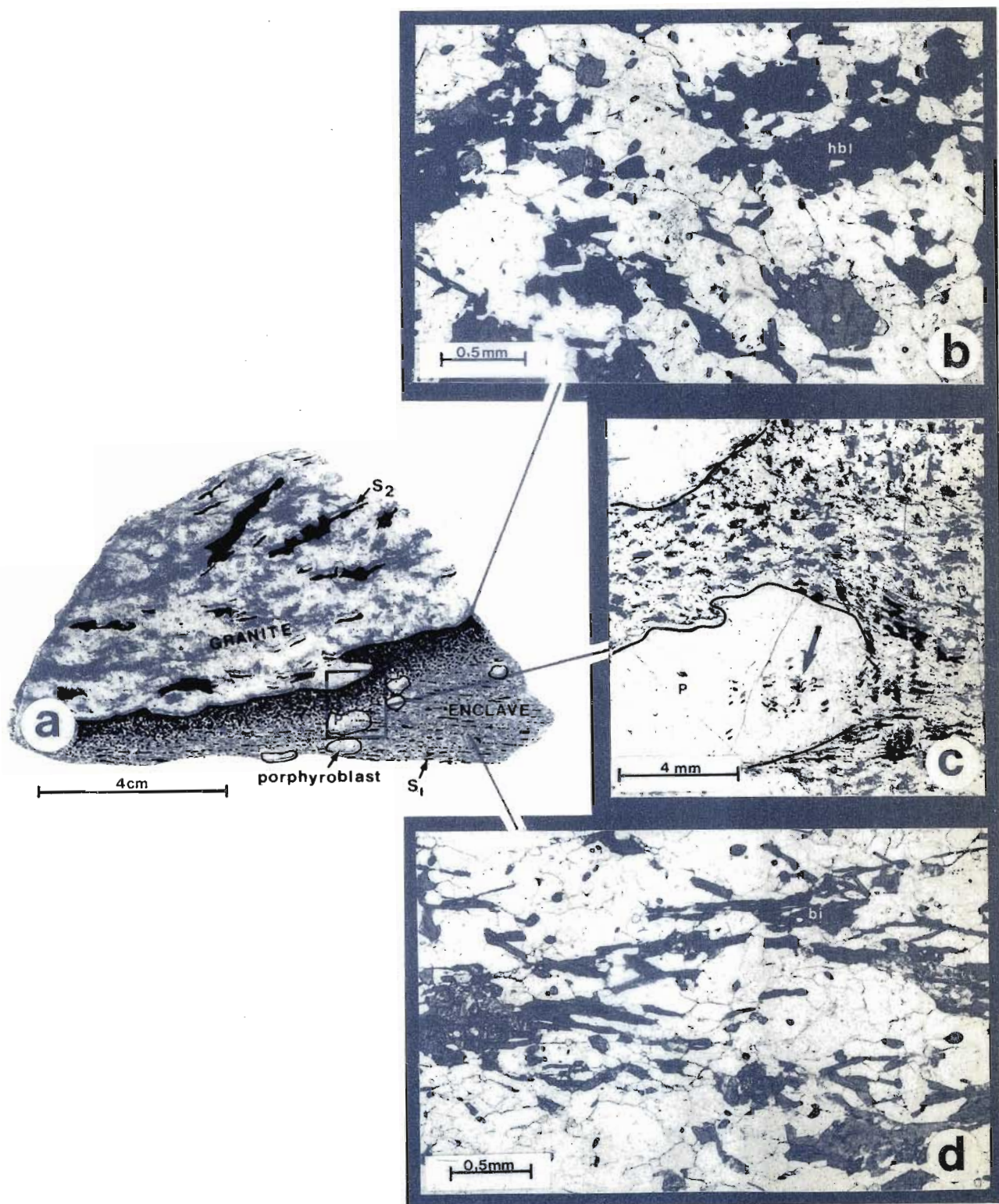


Plate 5. Polished slab and accompanying photomicrographs to illustrate mineralogical and textural variations across a biotite-schist enclave in biotite-hornblende granite (outcrop N447, map ref. 14 F). Note the hornblende-rich margin of the enclave (stippled in overlay), and the trail of biotite laths (arrowed) extending into the feldspar porphyroblast (P) in (c). The change in texture from schistose (d) to granoblastic-polkiloblastic (b) is readily apparent.

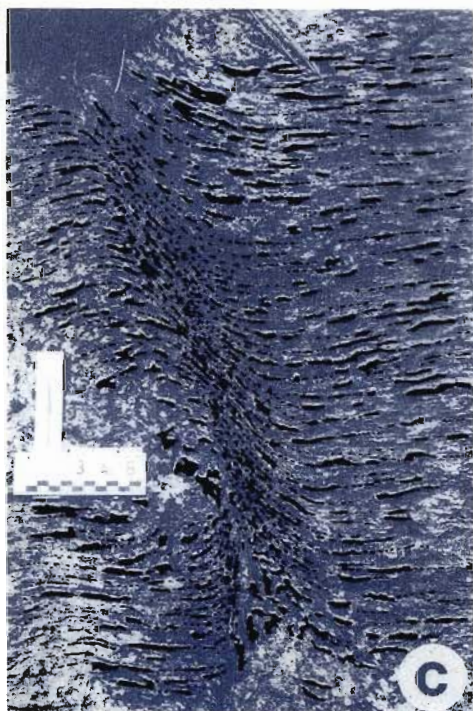
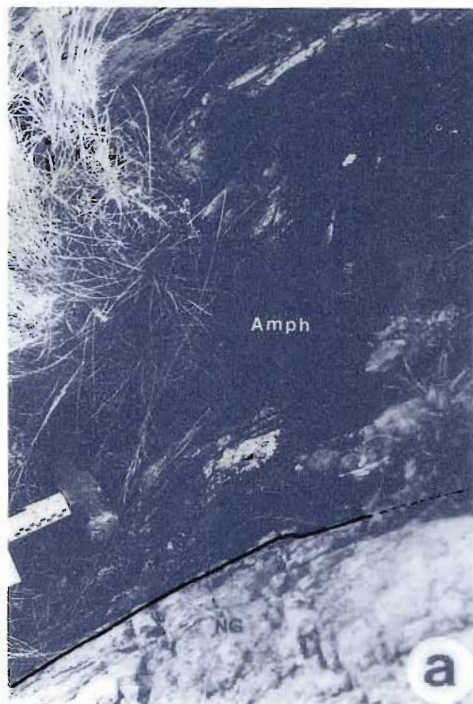


Plate 6. Granite contacts and mesoscopic shear zones. Plate 6 (a) shows the sharp southern contact of the Ngoye Formation (NG) against Endlovini amphibolite (map ref. 24 I). A sharp, highly sheared contact is evident in (b), between muscovite-biotite granite (B) and biotite-hornblende granite (H); photograph taken looking East at locality N107, map ref. 22 F. The lower photographs (c) and (d) illustrate the effect of conjugate (mesoscopic) ductile and ductile-brittle shearing on well foliated gneissic biotite-hornblende granite (map ref. 16 I) and Endlovini amphibolite (map ref. 24 I), respectively. Scales in cm, arrows point North.

These colours are characteristic of the iron-rich variety of hornblende, probably hastingsite, which, as pointed out by Deer et al. (1966) is the typical amphibole of alkali granites. Broad, ragged laths of yellow to olive green biotite are randomly orientated and, in general have cleavages enhanced by ore staining.

Sphene, zircon, opaque minerals, apatite and epidote are accessory minerals in this granite-type and are invariably associated with the biotite and hornblende clusters. Sphene occurs in two modes, namely (a) as subhedral lozenges and (b) as granular overgrowths on anhedral opaque grains. Euhedral zircon is a common accessory, and is distinguished from the associated sphene by its lower interference colours and diagnostic tetragonal crystal morphology.

2.3.3 Biotite-schist enclaves in the biotite-hornblende granite

As pointed out above (2.3.1), several biotite-schist enclaves occur within the biotite-hornblende granite at locality N447 (Map ref. 14, E). As illustrated in Plate 4, they are of variable size and range between about 20 cm and 1 m in length, being elongate and generally subparallel to the regional fabric in the surrounding granite. Field observations have shown (a), that the enclaves are distinctly zoned, from a dark-coloured outer margin into a light coloured core zone (b), that pinkish feldspar mesocrysts are occasionally present within the enclaves and (c) that the internal fabric within enclaves is often discordant with that in the surrounding granite. Using a polished slab and thin sections from the contact zone between an enclave and granite (Plate 5), the following observations are noted:

- (i) mesoscopically, a foliation (designated S_1) is well developed within the light-grey core of the enclave, this is shown microscopically to be due to the alignment of biotite and chlorite laths;
- (ii) foliation S_1 is at an oblique angle to the granite contact;
- (iii) there is a mesoscopically discernable foliation designated S_2 apparent in the granite which is oblique to the S_1 direction.

- (iv) microscopically, the pink feldspar "mesocryst" (P in Plate 5) is a polycrystalline aggregate consisting predominantly of microcline with minor amounts of plagioclase and quartz;
- (v) minute trails of biotite extend along the S_1 direction from the enclave into the feldspar aggregate (see arrow in Plate 5);
- (vi) there is a notable increase in grain size, moving outwards from the core to the margins of the enclave and;
- (vii) whereas the pale-grey core of the enclaves has a schistose fabric defined by elongate micaceous minerals, the outer shell has no discernible planar fabric;
- (viii) that the outer shell is depleted in microcline, biotite and calcite and enriched in hornblende relative to the core zone.

This overprinting of central schistose cores in the Ngoye enclaves is very similar to concentrically zoned enclaves in the Mt. Agamenticus granitic massif, described by Woodard (1957). He describes enclaves that have biotite-schist cores, surrounded by successive shells of hornblende and finally augite-rich rock adjacent to the granite and suggests that the zonation is due to a diffusion of elements between granite and enclave. The significance of the Ngoye enclaves is that they indicate thermal overprinting by the granite of a pre-existing metamorphic foliation within the enclaves, which probably represent fragments of older country rock. In addition, the polycrystalline nature of the "mesocrysts" within the enclaves, as well as the presence of biotite trails within the mesocrysts as shown in Plate 5, indicates that they post-date the schistose fabric and are thus possibly feldspar porphyroblasts.

2.4 Muscovite-biotite granite

Muscovite-biotite granite exposures are restricted to the northern summit and flanks of the main Ngoye range, comprising approximately 15% of the total outcrop area (Fig 2.7).

2.4.1 Field characteristics

The muscovite-biotite granite is essentially a rather homogenous rock which forms large, smooth, rounded exfoliation domes on prominent steep-sided spurs. Access to outcrops is restricted, due to a lack of roads as well as the heavily forested nature of much of the terrain (Plate 1 b). This lithology is distinguished in the field by its fairly consistent medium grain size and a low mafic content, i.e., as small flakes of biotite aligned parallel to the regional strike (Plate 2). Foliation is not always very obvious, due mainly to the leucocratic nature of the rock-type.

Contact relationships with the biotite-hornblende granite to the south are largely obscured due to soil cover. However, one pavement outcrop across the contact between these two granites shows it to be, in this instance, sharp and highly sheared (Plate 5). Relative ages across this contact were clarified by the discovery of several biotite-hornblende granite xenoliths within the muscovite-biotite granite (Plate 3). They are extremely variable in size, ranging from 0,5 m up to about 10 m diameter, and occur just north of the contact zone on the north-west flanks of the range (map ref. 16, F). These xenoliths strongly suggest that the muscovite-biotite granite is younger than and intrusive into the biotite-hornblende granite.

2.4.2 Petrography

The rock-type is essentially medium grained and microscopically is characterized by the occasional presence of microcline crystals up to 4mm in length. A poorly developed planar fabric is imparted on the rock by the alignment of sparse biotite laths which, on average, constitute only 3% of the rock. This notably low mafic-mineral content allows easy discrimination from

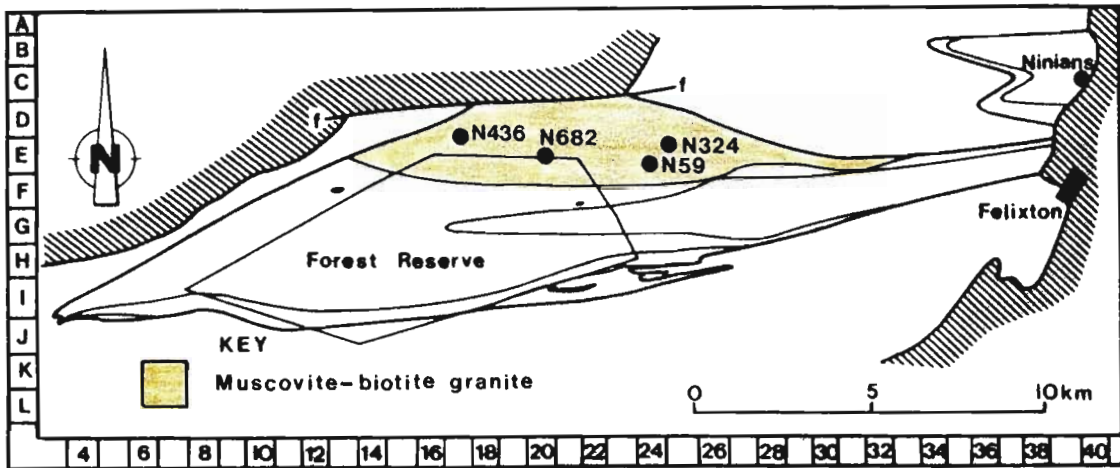


Fig. 2.7. Simplified geological map of the Ngoye Formation, showing the distribution of muscovite-biotite granite.

TABLE 2.3

Representative modal analyses* of muscovite-biotite granite.

	N59	N324	N436	N682
microcline	25,4	37,4	24,7	33,1
plagioclase	32,7	30,4	24,6	28,3
quartz	39,7	27,3	46,2	34,0
biotite	1,9	4,6	3,6	2,5
muscovite	0,2	t	t	0,3
opaques	-	t	-	t
fluorite	-	-	-	0,4

Notes:

Sample localities shown in Fig.2.7 above.

* : all values as volume percentages.

t : mineral species present but less than 0,2%.

- : mineral species not detected.

the mesocrystic and hornblende-bearing granites discussed previously (see 2.2 & 2.3). Concomitant with the leucocratic nature of this rock-type is an increase in quartz content, which ranges up to 48% and is distinctly higher than lithologies discussed earlier. Based on the Streckeisen QAP diagram (Fig. 2.3) the muscovite-biotite granite is classified as a monzogranite, indicative of almost equal alkali-feldspar and plagioclase contents (Table 2.3).

Xenoblastic to subidioblastic microcline occurs in two forms, either as (a) occasional mesocrysts up to 8 mm in length or (b) as approximately 3 mm sized grains in the groundmass of microcline, plagioclase and quartz. Very well-developed tartan twins characterize the microcline of this unit, while perthite is absent to rare in most thin sections. Xenoblastic to subidioblastic plagioclase grains (An_{24-27}) are distinguished by polysynthetic albite and occasional pericline twin lamellae. Notable, and in fact diagnostic of this lithology are ubiquitous beads and stringers, sometimes cauliflower-shaped, of myrmekitic intergrowths where plagioclase is in contact with microcline. Xenoblastic 2 - 3 mm quartz grains have polygonal to interlobate grain boundaries, with elongate aggregates helping to define a weak planar fabric.

Weakly aligned, broad, rather stumpy laths of biotite up to 2 mm in length are isotropically distributed throughout and are pleochroic from yellowish to olive-green. Muscovite occasionally accompanies biotite and occurs either as (a) crystals similar in size and shape to the biotite flakes or (b) as fine-grained, sometimes needle-like aggregates mantling the biotite.

Accessories include very rare zircon prisms, rounded xenoblastic opaque minerals, pale purple fluorite, and occasionally a yellow-brown mineral optically identified as allanite (see section 2.12 for the optical properties of allanite).

2.5 Biotite-muscovite granite

Outcrops of this lithology are confined to (a) a sheet-like zone between 200 and 500 m in width along the north-eastern margin of the main Ngoye body and (b), to a broad zone up to 800 m in width on the southern and south-western parts of the smaller Ninians body (Fig 2.8). This reversal of

succession, ie: from north of the mesocrystic granite in the main body, to south of the mesocrystic granite in the Ninians body is indicative of a possible fold closure between the two outcrops.

2.5.1 Field characteristics

Fresh exposures of this lithology which forms about 5% of the outcrop area, are entirely restricted to the RB. 6 quarry (map ref. 38, D) situated on the south-eastern margin of the Ninians body. Most other outcrops of biotite-muscovite granite comprise rounded residual boulders, often weathered to a friable sugary aggregate from which geochemically-fresh samples are only collected with great difficulty.

The lithology is subdivided, from field evidence, into two varieties on the basis of biotite content. Whereas the predominant type has approximately equal amounts of biotite and muscovite, a second subordinate variety is defined by the presence of small reddish garnets and the virtual absence of biotite (Plate 2). The latter forms a narrow sheet-like outcrop in the main Ngoye massif, as indicated in Fig. 2.8 and in addition, hosts microcline-quartz pegmatites and occasional muscovite rich pods.

The structural fabric is inconspicuous due to a paucity of ferromagnesian minerals. However, biotite-bearing varieties of this unit at the Ninians RB.6 quarry have a pronounced linear fabric due to the alignment of mafic aggregates which plunge moderately eastwards.

2.5.2 Petrography

As indicated, modal analysis of stained thin sections have shown that the biotite-muscovite lithotype can be subdivided into (a) varieties containing muscovite almost to the exclusion of biotite and (b) a more common type with sub-equal amounts of the two micas. In addition, the single-mica granite has a reduced microcline to plagioclase ratio as well as accessory garnet, compared with the two-mica variety which has no garnet, and a higher microcline content (Fig. 2.3 & Table 2.4). As the two varieties are similar in thin section they are discussed together.

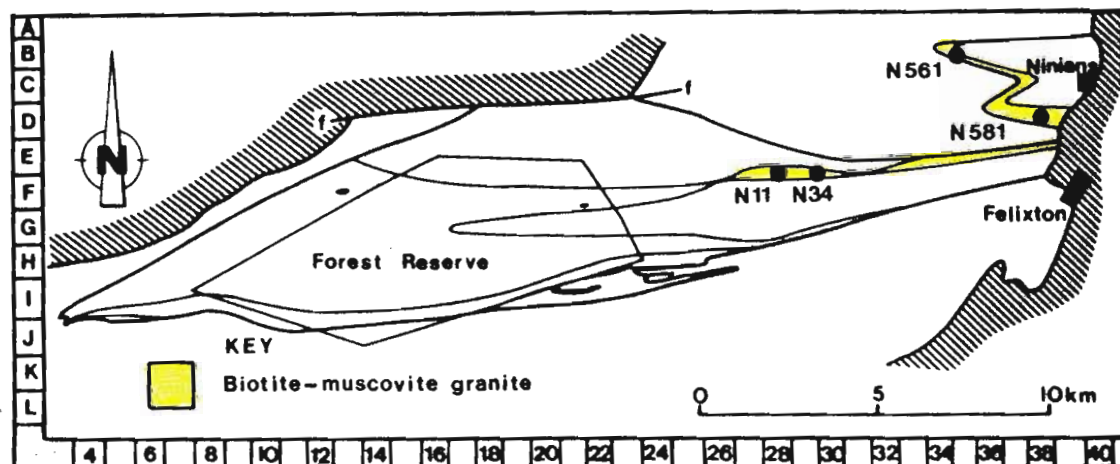


Fig. 2.8. Simplified geological map of the Ngoye Formation, showing the distribution of biotite-muscovite granite.

TABLE 2.4

Representative modal analyses* of biotite-muscovite granite

	N11	N34	N561	N581
microcline	26,0	30,4	35,7	31,8
plagioclase	29,8	36,1	25,5	26,3
quartz	39,4	28,8	36,4	39,7
muscovite	1,7	4,4	0,5	0,7
biotite	2,6	-	0,5	0,6
garnet	t	t	-	-
opaques	t	-	1,0	-
fluorite	-	-	0,2	-

Notes:

Sample localities shown in Fig.2.8 above.

* : all values as volume percentages.

t : mineral species present but less than 0,2%.

- : mineral species not detected.

Thin section examination reveals the biotite-muscovite granite to be essentially equigranular with polygonal to interlobate grains 2-3 mm in diameter. A weak planar fabric is produced by the alignment of sparse mica flakes. Clear, xenoblastic microcline is conspicuously twinned according to the albite and pericline twin laws, exhibiting well-defined cross-hatch structures. Exsolution phenomena are ubiquitous with excellent examples of broad ribbon and interpenetrant perthites, particularly in specimen N34 (map ref. 31, F). Xenoblastic to subidioblastic plagioclase (An_{10} - An_{15}) crystals are well twinned according to the Albite and sometimes Carlsbad twin laws. Although plagioclase is normally clear and free from alteration, tiny orientated muscovite needles are fairly common in the cores of some grains. Polygonal to interlobate quartz grains are equigranular and sometimes highly strained, but without evidence of recrystallization.

Poorly orientated mica flakes include both muscovite and biotite. The muscovite-rich (one-mica) granite type is characterised by orientated broad, stumpy muscovite laths and flakes which vary from 0,5 - 2,0 mm in length. In contrast, the two-mica variety has muscovite and biotite in about equal amounts, often as interpenetrant laths. Whereas the muscovite is typically colourless, the biotite exhibits pleochroism from α = very pale yellow-green to γ = pale olive-green to brownish. In addition, the biotites in one sample (N11, map ref. 29, F) are distinctly zoned, with pale greenish cores passing outwards into light brown-green pleochroic margins which in some cases, are surrounded by a thin rim of muscovite.

These rock-types are leucocratic and notably devoid of coloured accessory minerals. Minute, rounded, xenoblastic red-brown garnets and occasional opaque grains are typically present in trace amounts in the one-mica granite, whereas opaque ore and some fluorite characterize the two-mica variety.

2.6 Hornblende monzodiorite

Exposures of this lithology are restricted to a small knoll in the central part of the Ngoye range, about 3 km north of Amanzamnyama mission (map ref. 22, G). The outcrop pattern is semicircular over an area about 0,5 ha, just north of the mesocrystic biotite granite/biotite-hornblende granite contact zone (Fig 2.9).

2.6.1 Field characteristics

Monzodiorite outcrops are very similar to those underlain by the surrounding granitoids, forming large rounded boulders up to several metres in diameter. However, unlike the smooth granitic boulders, those formed by monzodiorite have distinctly pitted surfaces due to preferential leaching of carbonate minerals. The intervening areas between outcrops are soil covered, thus obscuring contact relationships with adjacent granite-types.

Fresh surfaces show this lithology to be equigranular and comprise mainly off-white feldspar with green- black hornblende the dominant mafic mineral (Plate 2). Irregular, rather diffuse patches and streaks of garnet-rich material constitute 10-20% of outcrops. These patches are distinctly different from the hornblende-bearing part of the outcrop and comprise red-brown garnet, off-white feldspar and green ferromagnesian minerals. Calcite is present in minor amounts, apparently distributed throughout the monzodiorite.

A weakly developed east-west, steep-dipping planar fabric is outlined by an indistinct alignment of hornblende crystals.

2.6.2 Petrography

The mesoscopic two-fold subdivision of outcrops into (a) hornblende-rich and (b) garnet-rich portions is confirmed microscopically by the following assemblages:

- (i) the bulk of the rock comprising: plagioclase + microcline + hornblende, with accessory calcite, sphene, allanite, epidote, zircon and quartz;

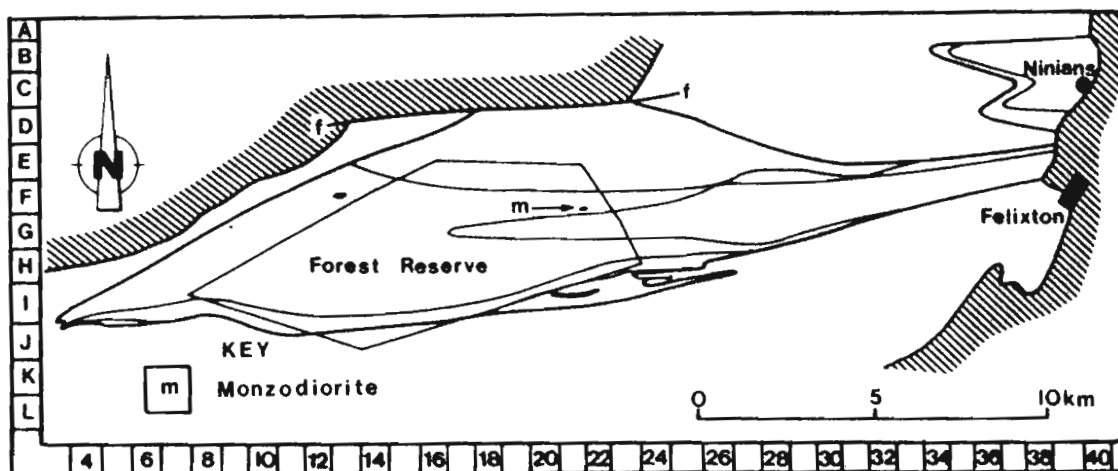


Fig. 2.9. Simplified geological map of the Ngoye Formation, showing the location of monzodiorite outcrops.

TABLE 2.5

Representative modal analyses* of hornblende monzodiorite

	N21b	N21x
microcline	9,1	19,0
plagioclase	69,5	60,7
quartz	2,2	1,6
hornblende	4,6	7,6
diopside	1,2	1,1
calcite	5,2	2,8
garnet	t	2,5
epidote	4,2	2,9
allanite	0,6	0,4
sphene	2,6	1,3
apatite	0,6	t

Notes:

Sample localities shown in Fig.2.9 above.

* : all values as volume percentages.

t : mineral species present but less than 0,2%.

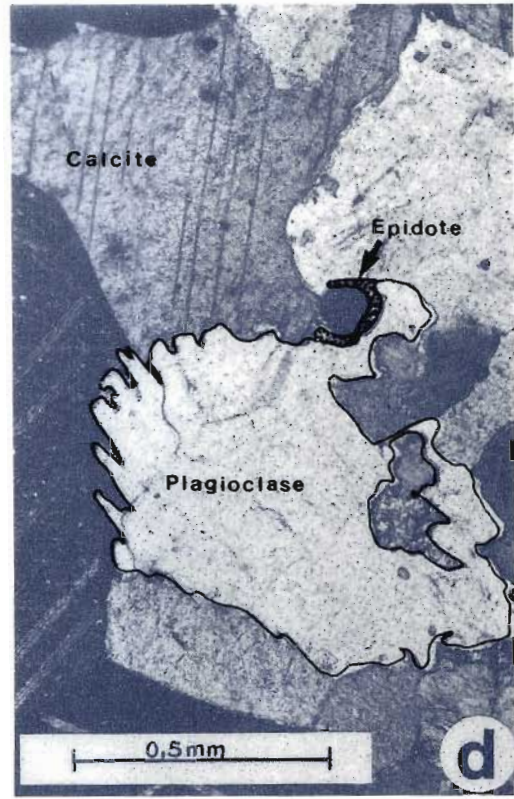
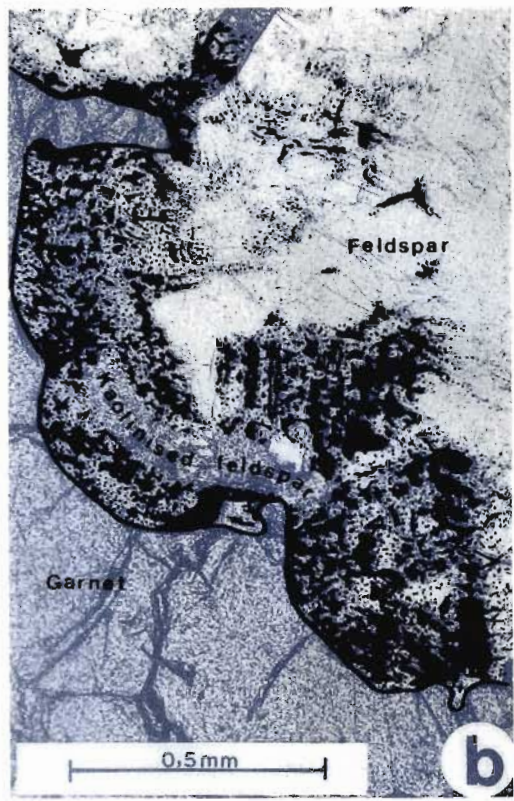
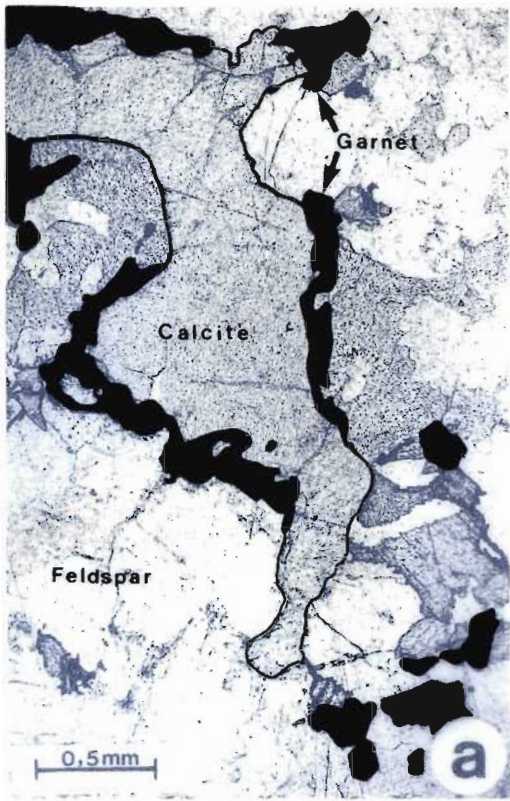


Plate 7. Photomicrographs of hornblende monzodiorite. (a) Plane-light image of calcite veinlet in stained thin section, showing garnet reaction rims (black) between calcite (grey) and feldspar (light grey). In (b), kaolinised feldspar is shown between feldspar (light grey, upper right) and garnet (dark grey, lower left). Photomicrographs (c) and (d) show examples of calcite replacing plagioclase along alternate twin lamellae. Also shown are garnet and epidote reaction rims (map ref. 22 G).

- (ii) the garnetiferous patches contain: garnet + calcite + diopside + hornblende with accessory epidote, allanite, sphene and quartz.

However a clear distinction between these two phases is not easy in thin section due to rather irregular, ill-defined boundaries. Therefore the modes plotted in Fig. 2.3 are averages of analyses over entire thin sections, which clearly show the monzodioritic nature of the bulk lithology (Table 2.5). Texturally, the rock is medium-grained (1,5-3mm) and essentially equigranular with polygonal to interlobate grain boundaries.

Plagioclase is the dominant mineral in all thin sections and is well twinned according to the albite and pericline twin laws. An anorthite content of An_{28-34} is indicated by twin-extinction angles as well as negative optic character. Although generally clear, plagioclase is sometimes altered to cloudy, kaolinitic material adjacent to garnet (Plate 7). In addition, plagioclase is in some instances selectively replaced by calcite along alternate, presumably Ca-rich, twin lamellae (Plate 7). Gridiron twinned microcline is a relatively minor constituent and occurs in two forms, namely (a) randomly distributed as discrete crystals or aggregates associated with the plagioclase or (b) as distinct rims around diopside-hornblende clusters. These latter occurrences comprise multigranular microcline aggregates characterised by (a) distinctly scalloped outer contacts against plagioclase in which microcline appears to replace plagioclase and (b) that the plagioclase adjacent to microcline is often myrmekitic.

Weakly aligned olive-green to deep-green hornblende is the predominant coloured mineral and forms between 5 and 10% of the modal analyses. It occurs as clusters of elongate xenoblastic to subidioblastic crystals and is usually associated with accessory sphene, epidote, zircon and allanite. Sphene forms grains and lozenges which are easily distinguished by birefringence, twinning and form from sharply euhedral zircons. Pleochroic, golden yellow to brown euhedral allanite crystals have typical six-sided basal sections and are invariably rimmed by colourless to yellow epidote. Quartz is an extremely rare mineral and occurs as discrete grains, usually interstitial between plagioclase crystals.

Calcite constitutes up to 5% of the bulk rock composition and is distinguished

by high relief, interference colours, twinning and negative optic character. This mineral is distributed throughout the lithology both as discrete grains, and also in irregular patches and veinlets where it is associated with garnet, diopside, hornblende and epidote. As illustrated (Plate 7), calcite appears to replace plagioclase along alternate twin lamellae. In addition, boundaries between calcite and plagioclase are often marked by a reaction rim of either garnet or epidote. Yellow-brown garnet is xenoblastic to subidioblastic and frequently surrounded by cloudy, kaolinised feldspar. Although impossible to ascertain optically, it is likely that the garnet is calcic (grossular or andradite) by virtue of its close association with calcite and diopside.

Pale green diopside occurs at the core of mafic aggregates which vary up to several mm in diameter. A distinct zonation is sometimes developed, from highly altered diopsidic cores outwards through hornblende to epidote. Associated minerals include sphene, quartz and calcite.

2.6.3 Comments on the possible origin of the monzodiorite

Three modes of origin for this unusual lithology have been considered. These are (a), that it is a meta-sedimentary raft or roof-pendant of calcareous country rock, (b) that it is a raft of older basic igneous rock, or (c) that it is a metamorphosed plug-like igneous intrusion younger than the surrounding mesocrystic biotite granite. Bearing in mind the apparent lack of similar calcareous country rocks around the Ngoye massif, it is considered unlikely that the monzodiorite represents a metasedimentary raft. Moreover, the occurrence of euhedral zircons (Poldervaart, 1956; see also page 62) within this lithology are diagnostic of an igneous derivation. The presence of calcite veinlets and patches indicate it may have undergone late-stage metasomatism by carbonate and / or CO₂ rich fluids. However, due to a lack of conclusive field evidence as well as geochemical data, no definite conclusions can be drawn at this stage regarding the origin of this interesting rock-type.

2.7 Monzonite

Outcrops are confined to a small hilltop just north of the forest reserve boundary, on the north western flanks of the main Ngoye massif (Fig 2.10; map ref. 13, F).

2.7.1 Field characteristics

The few outcrops observed are smooth and rounded, similar to those formed by the mesocrystic biotite lithology. Hand specimen examination shows this medium grained pink and grey rock to be mesocratic, and to have a fairly well defined foliation outlined by greenish to black mafic minerals (Plate 2 b). No quartz is visible, while yellowish sphene, greenish-yellow epidote and dark brown allanite are obvious in all exposures. Cross cutting epidote-quartz veinlets are common in the northern outcrops and may be related to the nearby Matshamhlope fault zone. Due to extensive soil cover around the outcrop area, no contact relationships could be established. No enclaves of any sort were apparent in the outcrops.

2.6.2 Petrography

Microscopic work reveals that some specimens are extremely brecciated, with unorientated angular fragments of feldspar set in a matrix of strain-free quartz grains which vary up to several mm in diameter. The quartz is crowded with substantial amounts of randomly orientated epidote and lesser quantities of blood-red to black hematite and chlorite. The unorientated nature of these inclusions and the feldspar fragments, as well as the unstrained nature of the silica cement, may indicate a late-stage introduction of quartz into a predominantly microcline and plagioclase lithology. This hypothesis may be explained in terms of brecciation associated with the nearby Matshamhlope fault, and subsequent introduction of silica-rich fluids.

Unbrecciated portions of the rock comprise almost equal amounts of microcline and plagioclase (An_{20-25}) with chlorite the dominant mafic mineral. Following the Streckeisen (1976 b) proposals, such an assemblage would be classified as a monzonite. However, if the modal analysis for the whole rock is taken into account, inclusive of the quartz veins,

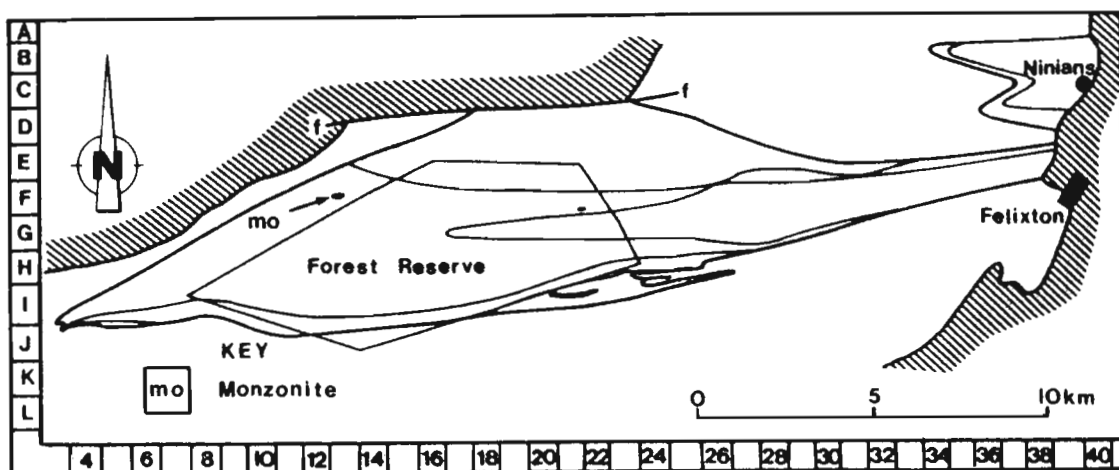


Fig. 2.10. Simplified geological map of the Ngoye Formation, showing the location of the monzonite outcrops.

TABLE 2.6

Representative modal analyses* of monzonite.

	N371A	N371B
microcline	34,7	45,2
plagioclase	36,8	49,1
quartz	12,1	t
chlorite	5,5	4,0
epidote	7,2	t
opaques	1,5	1,1
zircon	0,4	0,4
sphene	1,4	t

Notes:

Sample localities shown in Fig.2.10 above.

* : all values as volume percentages.

t : mineral species present but less than 0,2%.

N371A : modal analysis of whole rock.

N371B : modal analysis exclusive of quartz veins.

then the rock is classified as a quartz-monzonite (Fig. 2.3). The preferred name for the Ngoye occurrence, assuming late-stage introduction of quartz in a fault-related event, is therefore monzonite, the estimated mode for which is presented in Table 2.6. The component minerals are thus described below in terms of unbrecciated portions of the lithology.

The texture is inequigranular with 3-6 mm xenoblastic, interlobate microcline and plagioclase in a finer grained (1 mm) feldspathic matrix. Microcline displays typical cross-hatch twinning and is never perthitic. Plagioclase is twinned according to the albite law, with the extinction angles indicating an oligoclase composition. Both feldspar-types are clear and unaltered. Chlorite is the dominant ferromagnesian mineral and occurs as rounded to irregular polycrystalline masses, either interstitial between feldspar grains, or enclosed within plagioclase crystals. Accessories include euhedral zircon and brown allanite crystals.

2.8.0 **Microsyenite**

Two narrow horizons of this lithology were intersected in borehole NG 2, from 89,8 to 89,9 m and 93,9 to 94,5 m respectively, (Figs. 2.11 & 2.12). An intensive search of the projected outcrop area failed to outline similar lithologies, implying that this rock-type is of limited extent and/or extremely variable thickness.

2.8.1 Borehole-core characteristics

The two horizons differ markedly in hand specimen. The upper microsyenite between 89,8 and 89,9 m is a bright-pink leucocratic rock with small amounts of evenly disseminated chlorite throughout (Plate 2). In contrast the lower syenite is a fine-grained light-grey mesocratic rock, speckled with dark greenish-black chlorite aggregates which increase in concentration toward the lower contact at 94,5 m (Plate 2). Pyrite cubes up to 2 mm diameter are fairly common, especially between 94,3 and 94,5 m. No quartz is apparent in hand specimen. Contacts with the adjacent magnetite microgranite are

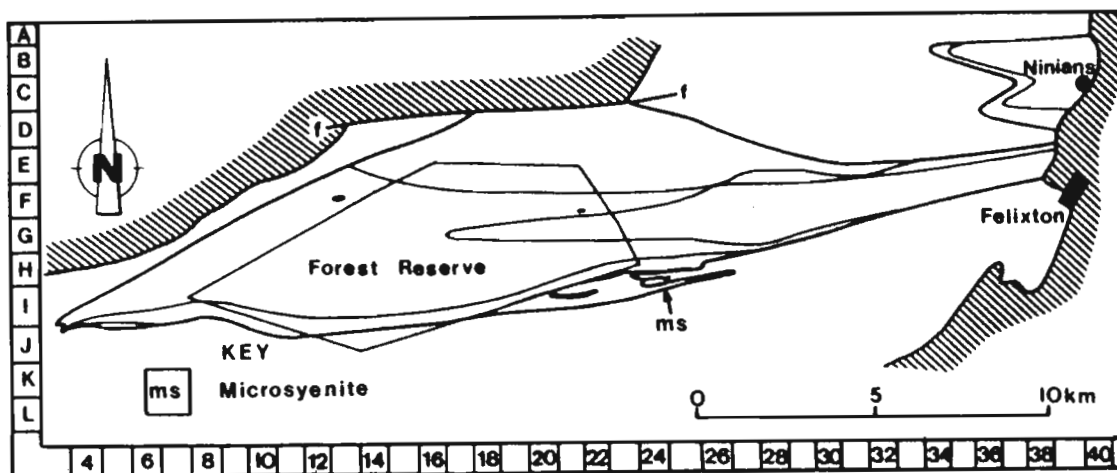


Fig. 2.11. Simplified geological map of the Ngoye Formation, showing the location of microsyenite intersections in borehole NG 2.

TABLE 2.7

Representative modal analyses* of microsyenite

	NG2 89,8m	NG2 93,9m	NG2 94,5m	NG2 94,8m
microcline	73,0	63,5	62,6	59,2
albite	21,8	18,1	24,4	26,9
quartz	1,3	6,7	3,6	0,2
chlorite	3,6	9,2	8,3	12,2
muscovite	0,3	t	t	t
opaque	0,2	0,9	0,8	0,4
zircon	t	t	t	t

Notes:

Sample localities shown in Figs.2.11 & 2.12.

* : all values as volume percentages.

t : mineral species present but less than 0,2%.

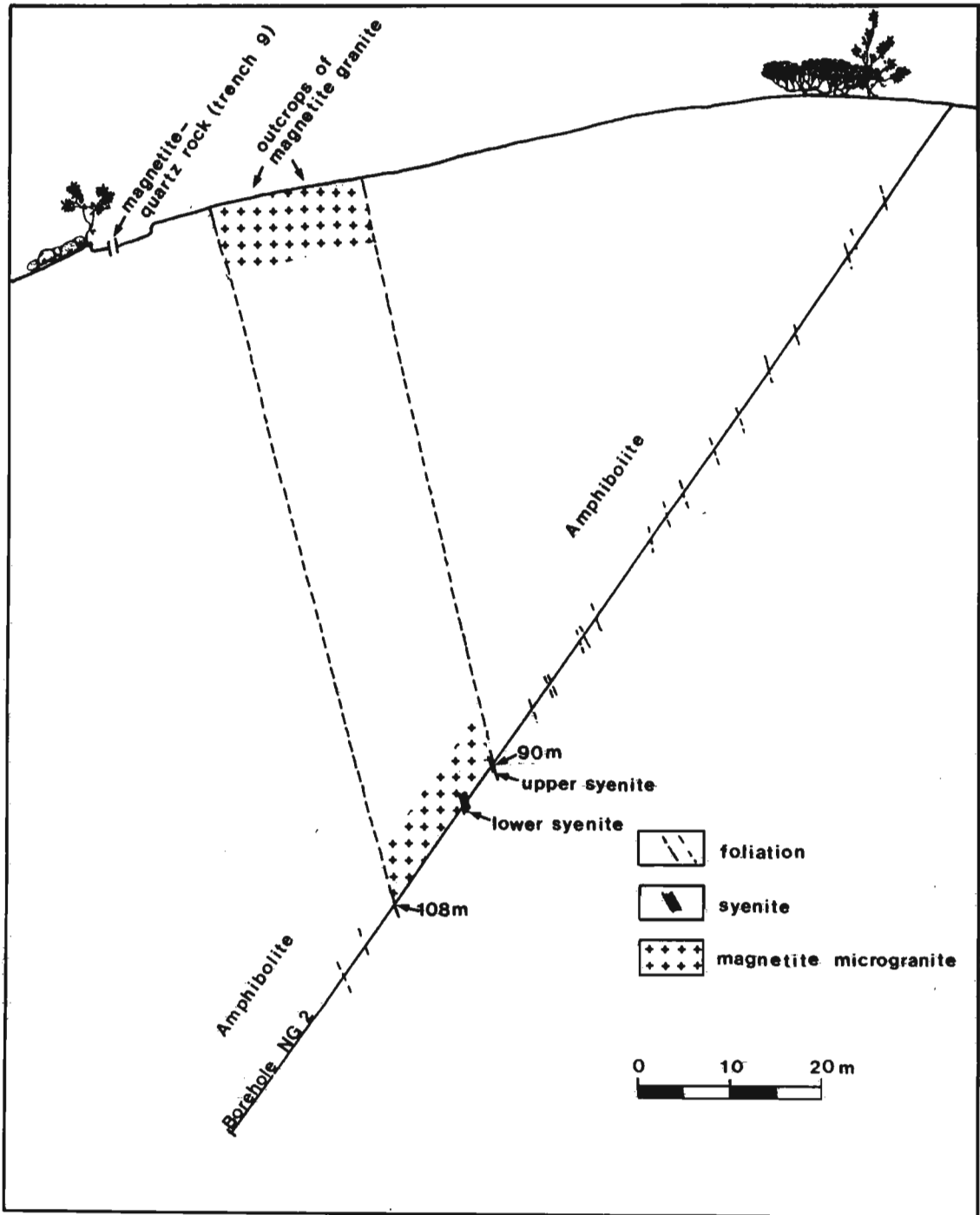


Fig. 2.12. Cross-section, looking East, of borehole NG2. Upper leucocratic syenite intersection from 89,8-89,9 m, lower mesocratic syenite between 93,9 and 94,8 m.

sharp and in one instance, at 94,5 m, possibly intrusive. The regional east-west foliation is well developed throughout both syenites and is penetrative across contacts. Both horizons are highly altered, with the upper syenite traversed by epidote veinlets parallel to a highly mylonitic contact at 89,9 m, while the lower syenite has a pitted surface and almost friable texture.

2.8.2 Petrography

The most diagnostic feature of these rocks is the high alkali feldspar content and virtual absence of quartz which is particularly obvious in stained sections. As shown in Fig. 2.4, all samples analysed plot along the AQ tie-line on Streckeisen's QAP triangle, and are thus classified as alkali-feldspar syenite. Microcline contents at 73% are notably higher in the upper intersection than the 61% of the lower, more mafic syenite. Quartz contents range from 0.2 - 4.1%. Chlorite is virtually the only mafic constituent and is present in amounts ranging from 4.1 to 10.3% in the upper and lower microsyenites respectively (Table 2.7).

Both microsyenites are essentially equigranular. Grains of about 1 mm diameter with occasional larger feldspars up to 2,5 mm noted. Xenoblastic microcline is the dominant mineral, displaying rather indistinct spindle-shaped tartan twins, while perthitic exsolutions are only rarely present. Plagioclase is well twinned according to the albite law and, based on extinction angles, is classified as albite An0 - An10. The characteristic coloured mineral, chlorite, occurs as intergrowths of 0,05 mm long vermicular chlorite. Pleochroism is strong from yellow-green to apple-green, while interference colours are typically low first order and generally masked by the chlorite's colour. Chlorite is present in two forms, either as rounded aggregates, up to 0,6 mm diameter wholly enclosed within plagioclase or as interstitial clots or stringers mantling euhedral feldspars. The small amount of quartz in these rocks is commonly associated with the chlorite in the interstices between feldspars. As chlorite is normally a secondary mineral and a sign of metamorphic downgrading, it is likely to have been derived by the breakdown of pre-existing mafic minerals such as pyroxene or amphibole, by the metasomatic action of hydrothermal fluids.

2.9 Riebeckite-biotite granite

This lithology is exposed intermittantly as a sheet-like body over a 20 km strike length, along the south to south-western flanks of the main Ngoye massif (Fig. 2.13). It is moreover, the predominant riebeckite-bearing granite in the Ngoye Formation and constitutes approximately 8% of the total outcrop.

2.9.1 Field characteristics

Riebeckite-biotite granite forms very similar outcrops to those underlain by the adjacent biotite-hornblende exposures to the north. Outcrops of this lithology are medium-grained and off-white in colour, being characterized by isotropically distributed fish-like aggregates of black mafic minerals (Plate 3). These range up to 1 cm in length and comprise mainly biotite, with lesser amounts of sodic amphibole and pyroxene. Although the sodic minerals are not readily indentifiable in hand specimen, the riebeckite-biotite lithology is distinguished from the superficially similar biotite-hornblende granite by: (a) the lack of green-black hornblende, (b) a lack of yellow sphene, (c) the larger size of the riebeckitic aggregates and (d) the essentially more "streaky" appearance of the latter granite. In addition to the above, riebeckite-biotite often has purple fluorite visible in hand specimen, this feature having not been seen in any of the other granitoids in the formation.

Structurally, riebeckite-biotite granite varies from almost unfoliated granite to occasional mylonitic types. Extreme extension of the initially ovoid ferromagnesian "clots" is indicated in some outcrops by the development of subhorizontal, linear, mafic aggregates that plunge either east-or westwards (Plate 15). Due to extensive soil cover, contact relationships with surrounding rock types are obscured, although inferred to be quite sharp. No enclaves were observed in this lithology.

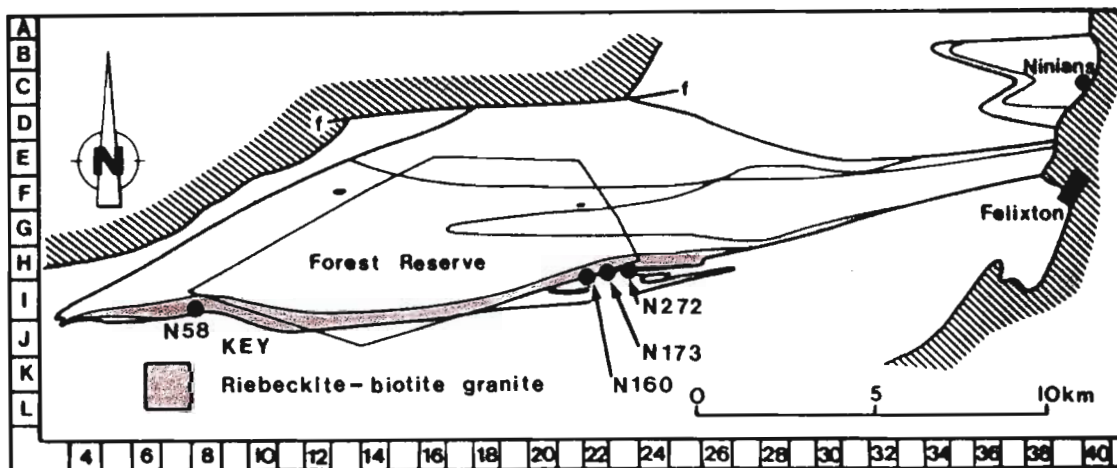


Fig. 2.13. Simplified geological map of the Ngoye Formation, showing the distribution of riebeckite-biotite granite.

TABLE 2.8

Representative modal analyses* of riebeckite-biotite granite

	N58	N160	N173	N272
microcline	29,7	34,0	30,9	32,5
albite	25,6	29,7	28,9	26,8
quartz	42,6	32,7	33,4	34,4
biotite	0,9	1,9	4,0	2,9
riebeckite	0,8	1,0	0,4	0,7
aegerine	-	-	1,4	-
opaque	t	t	0,3	2,0
fluorite	-	t	0,4	0,3
zircon	t	t	0,2	0,3

Notes:

Sample localities shown in Fig.2.13 above.

* : all values as volume percentages.

t : mineral species present but less than 0,2%.

- : mineral species not detected.

2.9.2 Petrography

The most distinctive feature of these rocks in thin section is the presence of clots of brightly coloured biotite, riebeckite and/or aegerine (Table 2.8). A relatively high alkali content is indicated by the occurrence of these minerals, and this observation is confirmed by the modal analyses which plot in Streckeisen's "alkali-feldspar granite" field (Fig. 2.4). The extreme plagioclase depletion inherent in such a classification indicates that the riebeckite-biotite granite has a low CaO content which, according to Bowden and Turner (1974), is typical of similar granites in the Nigerian younger granite province. Furthermore, the presence of sodic amphiboles and pyroxene in a granite is indicative of peralkaline chemistry, ie: depletion of Al relative to Na + K (Shand, 1947; Hyndman, 1972).

This lithotype is essentially equigranular (1,5 - 2,5 mm) although occasional larger microcline crystals up to 3,5 mm were noted in thin section. Xenoblastic microcline is generally quite well twinned according to the albite and pericline laws, which results in typical spindle-shaped twin lamellae and undulose extinction. Filmy micropertthitic intergrowths are ubiquitously developed in the microcline, with several crystals also displaying broad ribbons and wavy flame-exsolution phenomena. Plagioclase (Albite An 2 - 7) is xenoblastic and easily identified by well-defined polysynthetic albite lamellae as well as occasional broad Carlsbad-type twins. Albite and microcline are clear and unaltered and tend to form feldspar-rich aggregates that, by alternating with quartz rich aggregates impose a crude gneissosity on sections. Quartz grains vary from large (2 mm) highly strained, interlobate grains to smaller unstrained grains with polygonal boundaries.

Biotite and riebeckite are the chief mafic constituents and as mentioned above, occur in ovoid fish-shaped aggregates. These are developed within quartz-rich portions of the rock and characteristically comprise an open framework of randomly orientated biotite laths, with interstitial riebeckite, aegerine, opaque ore, sphene and fluorite. Quartz is frequently enclosed within these aggregates and also in some cases within spongy riebeckite crystals. Biotite is brightly coloured and pleochroic from golden-yellow to brown:- this colouration is distinctive and clearly different from the green biotite in other granites in the Ngoye formation. This trend is similar to

that noted by Bowden and Turner (1974) who found that brownish, iron-rich biotites were characteristic of peralkaline riebeckite granites and that green biotite characterizes non-peralkaline granites in the Nigerian "Younger Granite Province."

Biotite in the Ngoye samples is always the predominant ferromagnesian mineral, and in some cases is present to the virtual exclusion of riebeckite. Riebeckite (α =prussian-blue, β =grey-blue and γ =brownish-yellow), and aegerine (α =emerald-green, α =green and γ =yellow-green) are present in varying amounts. Aegerine occurs both intergrown with biotite and as overgrowths around biotite, whereas riebeckite clearly postdates both biotite and aegerine, occurring as rims around both the latter. The sequence of crystallization, from this evidence, is thus probably biotite \rightarrow aegerine \rightarrow riebeckite. This proposed late stage crystallization of riebeckite is corroborated by the spongy, poikilitic nature of some of the crystals, and is characteristic of the crystallization sequence in peralkaline granites (Bowden and Turner, 1974).

Xenoblastic sphene occurs either as discrete grains or more commonly as granular overgrowths on xenoblastic ore grains which are randomly distributed through the ferromagnesian aggregates. Zircon is always euhedral with square basal sections, and pale purple fluorite as irregular blebs and interstitial fillings is a common accessory, both minerals being associated with the mafic aggregates.

2.10 Riebeckite granite

This is one of the most distinctive and easily identifiable rock types in the Ngoye formation, and crops out along the southern marginal zone of the massif (Fig.2.14). The best exposures are in the vicinity of the Amanzamyama River (map ref. 22, 1) just south of the Forest-reserve fence, where riebeckite granite occurs as a sheet up to 50 m wide enclosed by magnetite microgranite.

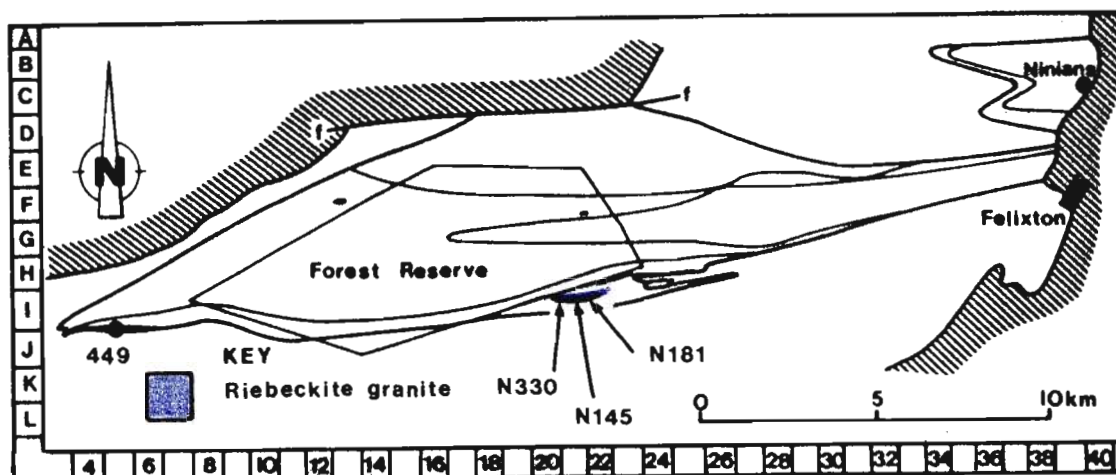


Fig. 2.14. Simplified geological map of the Ngoye Formation, showing the distribution of riebeckite granite.

TABLE 2.9

Representative modal analyses* of riebeckite granite

	N145	N181	N330	N449
microcline	28,5	32,3	31,0	28,2
albite	27,0	30,5	28,2	31,9
quartz	41,2	31,7	34,2	36,1
biotite	-	-	-	0,4
riebeckite	3,2	5,4	5,9	3,1
zircon	0,2	t	t	t
opaques	-	-	0,1	-

Notes:

Sample localities shown in Fig.2.14 above.

* : all values as volume percentages.

t : mineral species present but less than 0,2%.

- : mineral species not detected.

2.10.1 Field characteristics

Fresh outcrops are rare except in the Amanzamnyama area already described. This leucocratic medium grained rock-type is characterized by colourless to off-white feldspars and shiny blue-black riebeckite crystals (Plate 7 b). Riebeckite is the only ferromagnesian mineral present, aligned needles of which impart a prominent gneissosity on exposures. The only accessory minerals of any account are small, purple, well terminated zircons and occasional magnetite grains. Rare pegmatitic microcline and quartz streaks and irregular bodies contain riebeckite and euhedral zircons up to 1 cm in length. A foliation is consistently developed throughout the riebeckite granite which in places displays the effects of mylonitization to a spectacular degree (sample N142; map ref. 22, J).

Relationships with surrounding rock-types are unclear due to soil cover, rather poor outcrop quality and the highly sheared nature of most exposures. It can however be inferred from field data that contacts with adjacent magnetite microgranite (it's usual associate) are sharp. No enclaves of any sort were noted within riebeckite-granite outcrops.

2.10.2 Petrography

The modal analyses presented in Table 2.9 reveal that, on average, riebeckite-granite samples comprise predominantly alkali feldspar (microcline and sodic plagioclase) and quartz. Riebeckite (up to about 6%) is the only ferromagnesian mineral of significance in this lithology and is occasionally accompanied by minor amounts of biotite. Zircon is an ubiquitous accessory. According to the Streckeisen AQP ternary diagram (Fig. 2.4), the riebeckite granite is classified as an "alkali-feldspar granite". By the presence of the alkali-amphibole, riebeckite, it can also be termed a "soda granite" (Streckeisen, 1976 b).

Microscopic examination of thin sections reveals this rock-type to be fine to medium grained (1-2 mm) and essentially equigranular, although occasional larger microcline crystals up to 3 mm diameter were noted. Grain boundaries are interlobate to polygonal (feldspars) while quartz grains are generally polygonal. The mesoscopically visible gneissose texture of hand specimens is shown to be due to the alignment of elongate riebeckite crystals. A second

fabric, not visible in hand specimen, is caused by the presence of thin stringers of fine-grained material orientated approximately parallel to the gneissose fabric. Potash feldspar occurs as xenoblastic to sometimes elongate subidioblastic crystals that are twinned to varying degrees. Tartan twins are almost absent in some sections, and in these cases each potash-feldspar crystal has an untwinned core surrounded by a narrow mantle of well-twinned microcline. Although perthitic textures were noted, these intergrowths are notably poorly developed in the riebeckite granite. Xenoblastic plagioclase is sodic (An_{2-8}) and is poorly twinned although some broad lamellae and Carlsbad twins are present. Both plagioclase and microcline are clear and unaltered in all thin sections. Colourless xenoblastic quartz usually occurs as ribbons of 1 mm polygonal grains that define a planar fabric between elongate, composite feldspar aggregates.

Riebeckite, the characteristic mafic mineral of this rock-type, is normally xenoblastic to subidioblastic and occurs either as single crystals up to 2 mm in length or as multigranular aggregates. This mineral is distinguished by its pleochroic colours α = prussian blue, β = grey-blue and γ = brownish-yellow, typical amphibole cleavage, and an extinction angle of less than 20 (Deer et al., 1966). Whereas some crystals are inclusion-free, others are spongy and poikiloblastic, enclosing numerous quartz blebs. Ragged yellow-brown to brownish biotite is a rare accessory. Euhedral to subeuhedral zircons varying in length from 0,1 to 1,0 mm are a constant accessory in this lithology.

2.11 Aegerine microgranite

Outcrops of this minor lithology were found at only one locality, just to the south of the forest-reserve gate (map ref. 21, I), where it is closely associated with magnetite microgranite and riebeckite granite (Fig. 2.15).

2.11.1 Field characteristics

Weathered surfaces are superficially identical to those of adjacent magnetite-outcrops. However, close inspection of such surfaces reveals the presence of minute green crystals in the pale pink fine-grained quartzofeldspathic matrix, as opposed to the black magnetite grains in the surrounding rock types.

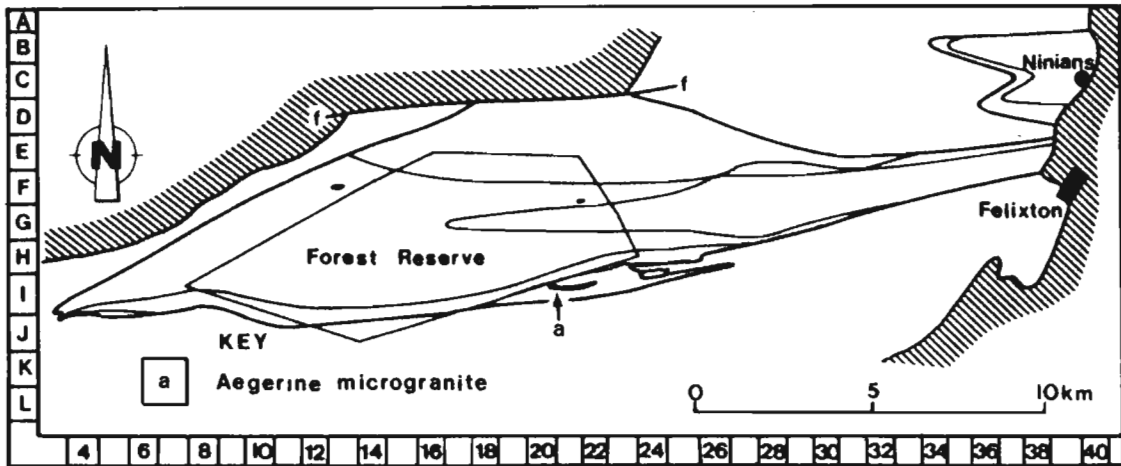


Fig. 2.15. Simplified geological map of the Ngoye Formation, showing the location of the aegerine microgranite outcrop.

TABLE 2.10

Representative modal analysis* of aegerine microgranite

N331	
microcline	40,2
albite	21,8
quartz	31,9
aegerine	5,1
riebeckite	t
opaque	t
zircon	t

Notes:

Sample locality shown in Fig.2.15 above.

* : all values as volume percentages.

t : mineral species present but less than 0,2%.

Fresh surfaces of this siliceous rock, which superficially resembles a sedimentary quartzite, are characterized by a dark grey colour and prominent conchoidal fracture (Plate 3). Due to the small size of the ferromagnesian minerals, metamorphic fabrics are not readily apparent in the field.

2.10.2 Petrography

Thin-section examination confirms the extremely fine, equigranular grain size which ranges from 0,3 - 0,5 mm. The predominant minerals are quartz and alkali feldspar, with the distinctive mineral, aegerine as virtually the sole mafic mineral (Table 2.10). As shown (Fig. 2.4), when plotted on a Streckeisen AQP diagram this lithotype is classified as aegerine alkali-feldspar granite, although in view of the fine grain size, it is here termed aegerine microgranite. The term "alkali" has been omitted, as the alkaline nature of the rock is implied by the presence of the alkali-mineral aegerine (Streckeisen, 1976 b). A fairly well-defined planar fabric is exhibited by alternating quartz-or feldspar-rich layers, as well as thin, extremely fine-grained (0,01 - 1,02 mm) quartzofeldspathic stringers parallel to the gross fabric.

The predominant mineral is xenoblastic, polygonal to interlobate microcline which constitutes about 40% of the rock. All microcline grains display gridiron twinning and are essentially non-perthitic, with only a few flame-like exsolutions noted. Most of the larger grains are surrounded by finely-recrystallized envelopes which impart on the rock a classic mortar texture. Xenoblastic plagioclase, similar in size (0,5 mm) to the microcline, comprises about 20% of the mode. Twinning is according to the albite and sometimes Carlsbad laws, extinction angles (Michel-Levy method; in Kerr, 1959) of which indicate that the plagioclase is highly sodic (An_{4-8}). Therefore, similarly to the riebeckite granite, all plagioclase in the aegerine microgranite has been included with microcline as alkali feldspar.

Polygonal quartz varies in grain size and is common in the fine-grained recrystallized stringers. The apparently low content of this mineral (32%) may be due to confusion with plagioclase, especially in the fine-grained portion of the rock. This possible source of error does not, however, materially affect the modal classification since the single analysis plots on the Q-A join, and is hence independant of plagioclase content.

The distinctive mineral of this lithotype, aegerine, forms xenoblastic, occasionally stumpy prismatic crystals isotropically distributed throughout the rock. They display the pleochroic scheme α = emerald green, β = green and γ = yellow green which, with characteristic low extinction angle and negative optic sign, serves to distinguish this mineral species from other pyroxenes. Furthermore, although not obvious, several crystals with characteristic pyroxene cleavage were noted.

Accessory minerals include small, elongate, riebeckite needles as rare overgrowths on aegerine, and occasional grains of opaque ore. The idioblastic habit and random orientation of the riebeckite needles is indicative of post-tectonic growth and the possible presence of sodic metasomatic fluids.

2.12 Magnetite microgranite

This granitoid forms a marginal phase along the south-central and south eastern boundaries of the Ngoye massif, with minor outcrops noted on the south-western margin near Endlovini mission (Fig. 2.16). In addition, the magnetite microgranite also extends (apophysis-like) from the massif into the amphibolitic terrain, where it forms a prominent concordant sheet of several kilometres strike length parallel to the southern contact of the Ngoye body (map ref. 24, H).

2.12.1 Field characteristics

Although relatively tough resistant rocks, fresh exposures of magnetite microgranite are uncommon. This fine grained, light pink lithology forms rounded, rather massive exposures characterized by minor amounts of granular magnetite, as the predominant and often sole, mafic constituent (Plate 3). A superficial resemblance to arkosic sandstone is a distinctive feature of outcrops. Field relationships with adjacent rocks are generally unclear, although contacts of magnetite microgranite against amphibolite in boreholes and trenches are knife-sharp. In addition, the apophysis-like form of the magnetite microgranite sheet into amphibolitic terrain (Fig. 2.16) is possible evidence of its younger, intrusive relationship.

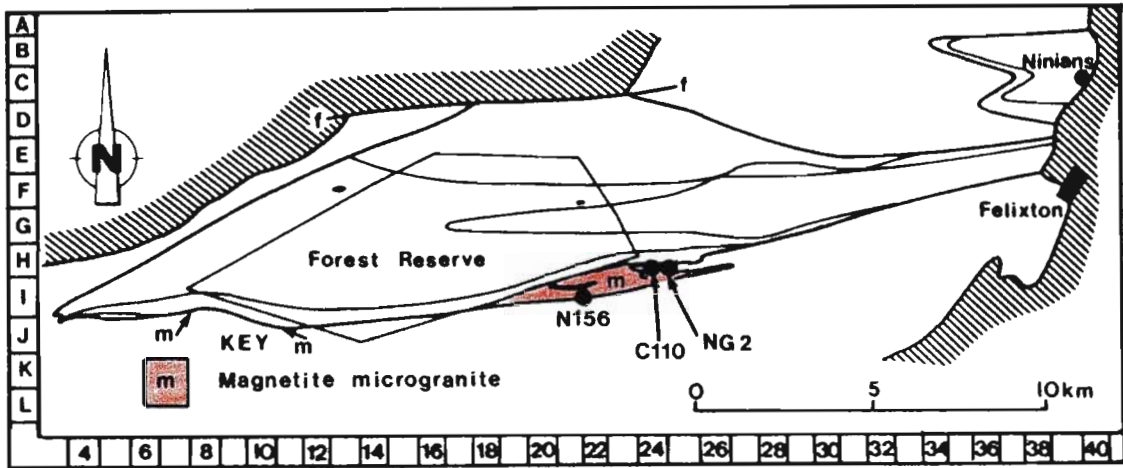


Fig. 2.16. Simplified geological map of the Ngoye Formation, showing the distribution of magnetite microgranite.

TABLE 2.11

Representative modal analyses* of magnetite microgranite

	NG2 90,4m	NG2 91,2m	C110	N156
microcline	54,3	51,3	47,2	53,5
plagioclase	8,4	9,0	11,0	8,5
quartz	35,7	37,6	38,9	36,0
opaques	1,3	2,1	2,6	1,9
zircon	t	t	t	t
fluorite	-	-	t	-

Notes:

Sample localities shown in Fig.2.16 above.

* : all values as volume percentages.

t : mineral species present but less than 0,2%.

- : mineral species not detected.

NG2 : borehole-core sample.

No enclaves were observed in any of the outcrops mapped, although the large body of amphibolitic rocks north of Amanzamyama mission (map ref 22, I may represent a xenolithic inclusion in the microgranite.

2.12.2 Petrography

The most conspicuous feature of this fine grained granitoid is the presence of magnetite as virtually the sole mafic mineral (Table 2.11). In addition, alkali-feldspar contents are extremely elevated, with microcline comprising more than 50% of most thin sections. Based on the Streckeisen (1976 b) modal classification, the magnetite microgranite is transitional between syenogranite and alkali granite (Fig. 2.3). Although apparently equigranular in hand specimen, thin sections exhibit bimodal grain-size distributions due to occasional 2-4 mm microcline crystals in a finer grained matrix (1 mm) of quartz and feldspar.

Microscopic work shows that microcline is the dominant mineral present. Microperthitic intergrowths, as well as coarse ribbon and flame exsolution phenomena, are variably developed though not conspicuous. Cross-hatch twins characterise all K-feldspars in the groundmass, in contrast to the "mesocrysts" which have untwinned cores. Plagioclase compositions are generally sodic and range between albite An_{5-10} according to extinction angles of broad polysynthetic albite twin lamellae.

Magnetite (up to about 3%) is virtually the sole mafic constituent in this leucocratic rock type, occurring as irregular, rounded to elongate, xenoblastic grains. They are normally evenly distributed throughout thin sections and define, albeit weakly, the regional foliation. Rare, elongate zones of increased grain size and enhanced magnetite concentration were encountered in samples from outcrops and drill core. Their margins are poorly defined and gradational which indicates that they are possibly pegmatitic segregations from the magnetite-microgranite host. Such magnetite-rich zones are characterized by unusual mineral phases such as fluorite, zircon and fergusonite (see discussion in 2.13.2 below). Erratically distributed accessories in the magnetite microgranite include yellow-green to olive-green biotite, subhedral to euhedral zircons up to 0,3 mm long, as well as light purplish fluorite as grains and interstitial fillings.

2.13 Magnetite-quartz rock

This unusual rock type is confined to the southern marginal zone of the main Ngoye massif and, spatially, is intimately associated with the peralkaline riebeckitic granites (Fig. 2.17). Outcrops are rare, with the best exposures to the north and northeast of Amanzamnyama mission (map ref. 25, I). These rocks occur as thin sheet-like bodies and elongate lenses, up to 50 m in length, in the amphibolitic country rocks immediately south of the granite contact. In addition, several small, irregular segregations up to a few metres in length were also found in the magnetite microgranite, both in outcrop and intersected by two boreholes.

2.13.1 Field characteristics

Fresh surface exposures of magnetite-quartz rock are rare and mainly confined to the boxed area shown in Fig. 2.17. In addition, further information about this lithology was obtained from several trenches which were dug to depths of between 2 and 3 metres over target 1 (Appendix A).

Magnetite is an essential constituent of this highly siliceous rock type and is always obvious in hand specimen. Creamy pink feldspar is often present in outcrop, but is generally absent or rare within highly siliceous, magnetite enriched varieties (Plate 3). Accessory minerals occasionally visible in hand specimens include euhedral zircons, off-white sphene and dark brown euhedral allanite prisms. Thin veinlets of dark purple fluorite were noted in one exposure (map ref. 23, I). Contact relationships with surrounding amphibolitic rocks are often obscured by soil cover, but evidence from trenches shows contacts to be sharp and approximately conformable with the host rock foliation. Exposures of magnetite-quartz rocks within the magnetite microgranite form irregular elongate pods bounded by apparently gradational contacts.

Structurally these rocks display variable fabric development, from isotropic pegmatite-like textures through to quite spectacular mylonitic varieties (Plate 3).

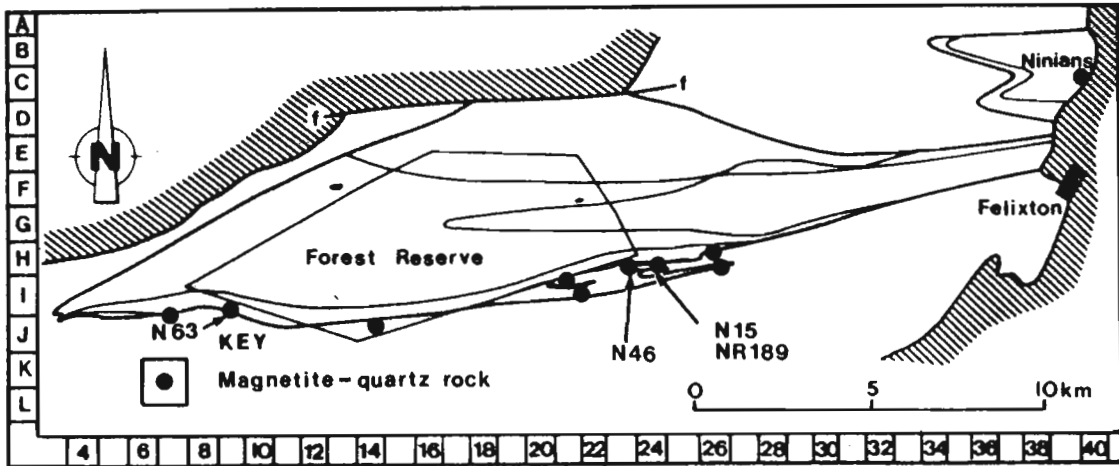


Fig. 2.17. Simplified geological map of the Ngoye Formation, showing the distribution of magnetite-quartz rock outcrops.

TABLE 2.12

Representative modal analyses* of magnetite-quartz rock

	N15	N46	N63	NR189
microcline	19,4	2,3	t	t
plagioclase	25,9	4,9	t	2,3
quartz	49,2	75,0	76,2	74,1
biotite	-	0,5	t	0,2
opaques	5,1	15,3	14,9	17,7
zircon	0,4	0,7	8,1	2,4
sphene	t	-	-	0,5
allanite	0,1	0,1	0,4	0,9
fergusonite	0,2	-	-	1,0

Notes:

Sample localities shown in Fig.2.17 above.

* : all values as volume percentages.

t : mineral species present but less than 0,2%.

- : mineral species not detected.

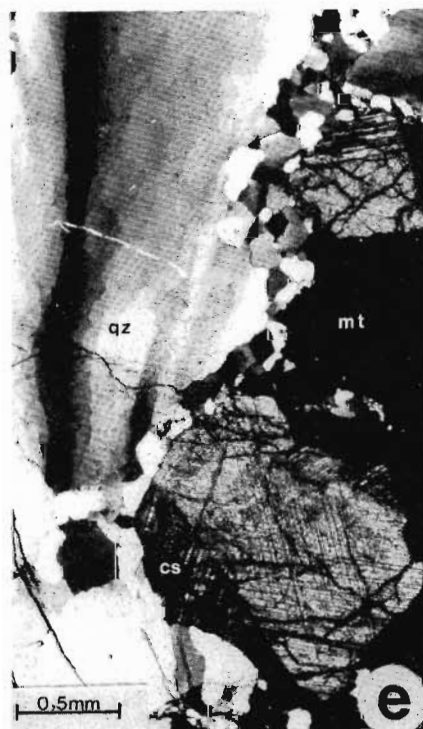
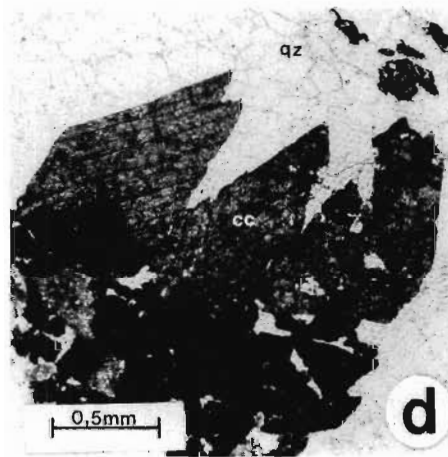
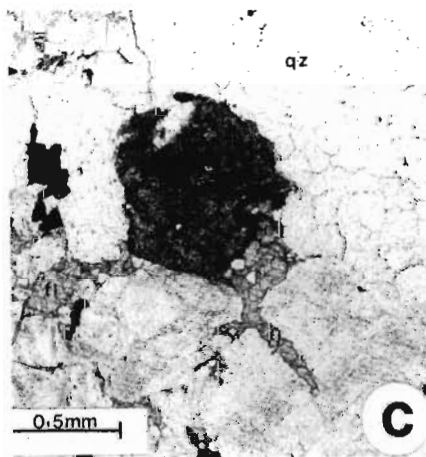
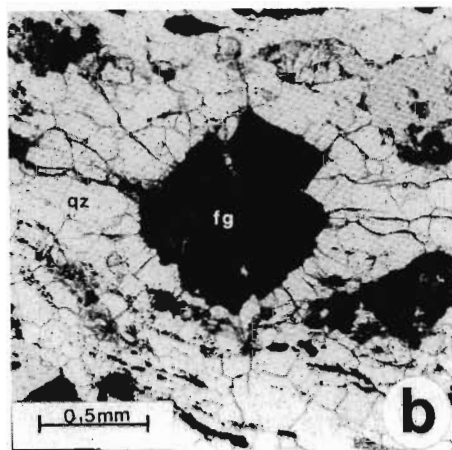
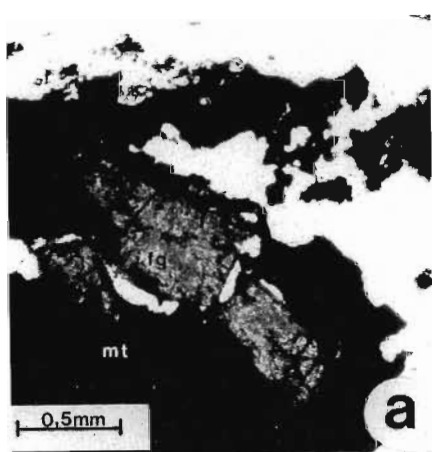


Plate 8. Photomicrographs of the magnetite-quartz lithology. (a) & (b) are typical fergusonite (fg) crystals (map ref. 25 I). Note the radial cracks in (b). In (c), anhedral allanite (dark grey) is shown with associated fluorite (fl) veinlets. Euhedral calcite (cc) crystals with magnetite and quartz (qz) comprise (d), from locality NR80, map ref. 25 I. (e) illustrates possible cassiterite (cs) with magnetite (mt) and highly strained quartz (qz) in thin-section NR189, map ref. 25 I. An euhedral, zoned zircon (zr) is

Mylonitized magnetite-quartz rocks have very well-developed planar and sometimes linear fabrics, with highly attenuated, streaked out magnetite grains defining a steep-dipping foliation and east-west orientated subhorizontal lineations.

2.13.2 Petrography

These rocks are highly variable in composition but essentially comprise quartz, magnetite and zircon with variable amounts of feldspar (Table 2.12). Plotting of the modes on the AQP diagram (Fig. 2.4) confirms their highly siliceous nature as they virtually all fall within Streckeisen's quartz-rich granitoid and quartzolite fields, ie: quartz more than 60%. Accessories include sphene, allanite, fergusonite, cassiterite, apatite and calcite.

As noted previously, quartz is the predominant constituent of all samples analysed and ranges from 49 to 84% by volume. Grain size is highly variable (0,2 to 5 mm), being finer in the more mylonitic, well foliated thin sections. Typically, the larger quartz grains have interlobate boundaries and, in some cases, display undulose extinction bands and peripheral subgrain development (Plate 8 e), whereas smaller quartz grains are polygonal and equigranular.

Xenoblastic microcline and well twinned plagioclase (An 0-5) are present in almost equal proportions, although total feldspar contents are highly variable and range from almost zero to as much as 50% by volume. Both microcline and plagioclase may form aggregates of interlobate, often kinked grains, or occur as single rounded crystals in the quartz matrix. Whereas quartz is normally fine grained (ie. totally recrystallized) in mylonitic examples, the feldspars are resistant, remaining as rounded clasts which do not display significant size reduction.

Opaque minerals, mostly magnetite, are essential constituent of all samples analysed. Concentrations range up to 20% by volume and have an inverse relationship with feldspar contents ie: magnetite rich specimens have virtually no feldspar. The magnetite grains are normally xenoblastic, but become increasingly lenticular; like feldspar they resist recrystallization and form porphyroclasts in mylonitic varieties of magnetite-quartz rock.

Subhedral to euhedral zircons ranging from 0,1 - 2 mm in length are

ubiquitous, with concentrations of up to 8%, although values of 0.1 - 2.0% are normal. Perfectly symmetrical zones of varying colour are frequently developed (Plate 8 f) and are visible both in prismatic sections and the square basal cuts so typical of this mineral. The highly radioactive nature of the zircons in the Ngoye samples is indicated by radial cracks in the material (usually quartz) around them (Plate 8 f). Zircons were extracted by heavy-media separation from several hand specimens after the method described by Poldervaart (1955). Inspection under the binocular microscope shows them to comprise euhedral, sharply terminated deep reddish-purple crystals. According to Poldervaart, euhedral zircons are diagnostic of a magmatic origin, the bipyramidal habit of many of those from magnetite-quartz rocks indicative of growth from an alkaline source magma (Poldervaart, 1956). Zircons in mylonitic varieties of the magnetite-quartz lithology exhibit brittle characteristics, with reduction in size by pull-apart mechanisms rather than as a result of recrystallization.

The two brown-coloured accessories seen in most sections have been tentatively identified as allanite and fergusonite. Allanite occurs either as tabular prismatic crystals with typical six-sided basal sections, or as anhedral masses up to 6 mm in diameter. Identification of this mineral has been by its crystal habit, biaxially negative optic sign, straight extinction and strong pleochroism. Colours in thin section are often zoned, ranging from yellow through yellow-brown to brown. Zones of metamict, isotropic, altered material are common and according to Deer *et al.* (1966) are a feature typical of allanite. Fergusonite is identified by its brown colour, tetragonal basal sections, and elongate prismatic habit (Plate 8 a & b). Its isotropic character, as observed in the Ngoye samples, is apparently due to a lack of crystalline atomic structure at temperatures below 400 c (Ford, 1932). Similarly to zircon, the highly radioactive nature of fergusonite is displayed by the occurrence of radiating cracks which form haloes in the matrix around crystals (Plate 8 b). Corroborative evidence for optical identification of fergusonite was supplied by a qualitative S.E.M. investigation of extracted fragments. This work, done by Mining Corporation at Pretoria University (Scogings, 1983) show it to comprise mainly Y, Ce, U, Nb and Ta which are essential constituents of fergusonite (Ford, 1932).

Sphene is a fairly common accessory varying from small subhedral crystals to

large masses several centimetres in length. It is distinguished by its characteristic birefringence, high relief, twinning and optical sign. Other accessories in the magnetite-quartz rock include biotite, fluorite calcite, and in one section, possible cassiterite (Plate 8 c, d & e).

Chapter 3

METAMORPHISM

3.1 Introduction

As shown in the previous chapters, the Ngoye Formation consists essentially of felsic, granitoid rock types of probable igneous origin (Charlesworth, 1981). In comparison with more diverse compositional groups such as calcareous, pelitic and mafic lithologies, the Ngoye specimens do not easily lend themselves to metamorphic investigations. This observation was noted by Charlesworth (1981) who on the basis of a regional investigation of the area between Eshowe and Empangeni, suggested that a lack of metamorphically-diagnostic mineral assemblages exists within the Ngoye Formation. However, current research has shown that meta-calc silicate rocks of limited extent (the monzodiorite lithology) do occur within the massif. Indicator minerals from this lithology may therefore be used to place some temperature and pressure constraints on metamorphic effects imposed on the study area. In addition, certain minerals (ie, riebeckite, biotite and hornblende) have supplied supporting evidence as to grade of metamorphism attained. In order to place these data in a regional context, an overall review of the literature is presented.

3.1.1 Review

Based on work by previous researchers (eg. Matthews, 1972) there is an apparent increase in grade southwards from the Kaapval Craton into the Natal Mobile Belt. However, as pointed out by Matthews (1981), the original

TABLE 3.1

Summary of metamorphic events* in the Natal Nappe Complex

Metamorphic event	deformation event	Metamorphic grade
M ₃	D ₃	very low grade, sparsely developed
M ₂	late D ₂	retrogressive, restricted mainly to mylonites between thrusts sheets
M ₁	D ₁ and into early D ₂ times	prograde to upper amphibolite facies

* = data from Charlesworth (1981)

zonation has been modified by northward overthrusting. In accordance with these aspects, Charlesworth (1981) recognized three metamorphic events (M₁, M₂, M₃) in the Natal Nappe Complex on the basis of field evidence and certain indicator minerals (Tables 3.1 & 3.2). The temperatures and pressures shown in Table 3.2 were derived by Charlesworth (1981) from the tabulated mineral assemblages.

3.2 Diagnostic assemblages in the Ngoye Formation

Current research has shown that the Ngoye Formation contains a far more varied mineral assemblage than previously believed. In this respect, calc-silicate assemblages in the monzodioritic lithology as well as the presence of riebeckite in the peralkaline granites are of particular interest.

TABLE 3.2

Diagnostic mineral assemblages*in the Natal Nappe Complex

Thrust unit	Lithology	Assemblage	T C	Pkb
Vuzane	Khomo amphibolite	oligoclase + green hornblende + garnet	550-600	4,5
Ngoye	Ngoye granite gneiss	not diagnostic		
Matigulu	Endlovini amphibolite	a)diopside + olive-green hbl. + andesine b)blue-green hbl. + andesine/labradorite	500	
	Intuze mica gneiss	a)sillimanite + muscovite + quartz b)fibrolite + biotite + garnet	610-650	4-5

Note

* = diagnostic minerals and lithologies from Charlesworth (1981).

3.2.1 Calc-silicate minerals

As noted in Chapter 2, the monzodioritic lithology contains a highly varied mineral assemblage comprising plagioclase, hornblende, calcite, diopside, epidote, calcic garnet and quartz. A detailed petrographic investigation of the specimens suggests, on the basis of reaction rims and mineral assemblages, that the following reactions have taken place:

(a) **2 calcite + 1 anorthite → 1 quartz + 1 grossularite + CO₂**(reaction 1) as shown in Plate 7(a), where a distinct reaction rim of garnet has been formed between calcite and plagioclase. The formation of grossularite as reported by Mukherjee and Rege (1972) is stable above a certain minimum temperature range defined by curves 1 and 4 in Fig. 3.1, where reaction 4 is given as **4 zoisite + 1 quartz → 1 grossularite and 5 anorthite + 2 H₂O** (Holdaway, 1972);

(b) the formation of epidote by the reaction of calcite and anorthite in the presence of water is illustrated in Plate 7 (c). This is fairly common in the thin sections examined and according to Storre & Nitsch (1973), the reaction: **2 zoisite + 1 CO₂ → 3 anorthite + calcite + 1H₂O** (reaction 2) takes place over a temperature range of greater than 150°C and is thus not very diagnostic;

(c) **1 grossularite + 1 quartz → 2 wollastonite + 1 anorthite**(reaction 3) defines the upper stability limit of grossular garnet in the presence of quartz (Boettcher, 1970). He does however point out that grossularite persists in the absence of quartz to temperatures of at least 875°C at Pt = 2 kb.

(d) the breakdown of diopside in the presence of CO₂ vapour is given by **1 tremolite + 3 calcite + 2 quartz → 5 diopside + 3 CO₂ + 1 H₂O** (reaction 5.). This reaction may explain the concentric zonation of amphibole, epidote and quartz seen around diopside cores in the thin sections examined. According to Metz & Trommsdorff (1968), the maximum temperature at which this reaction takes place is 650°C and is clearly dependant on CO₂ pressure (Fig. 3.1).

In conclusion, constraints derived from assemblages in the monzodiorite lithology are indicative of maximum metamorphic temperatures ranging between about 650°C and 725°C, at total pressures of 5 kb. These corroborate Charlesworth's (op cit.) research, from which he suggested a temperature range of 500-650°C at 4 to 5 kb pressure for the M₁ and early M₂ events. From the petrographic evidence, it is likely that reactions (1) and (2) above took place under prograde conditions, with the release of CO₂, which was then able to combine with diopside in a retrogressive reaction.

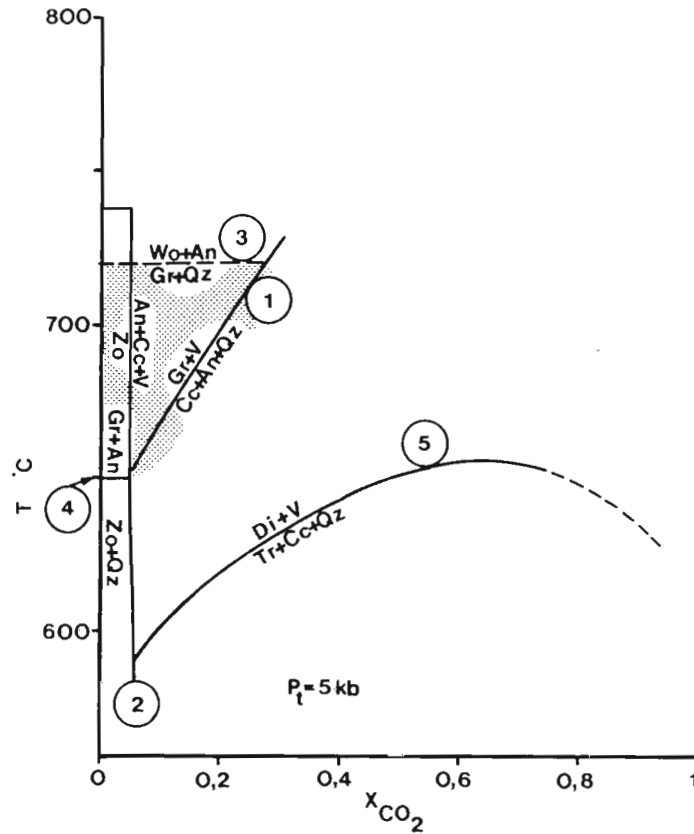


Fig. 3.1. Isobaric T - X CO₂ diagram at P_t = 5 kb for reactions in the monzodiorite (see text for sources). An_t anorthite, Cc calcite, Di diopside, Gr grossularite, Qtz quartz, Tr tremolite, V vapour, Wo wollastonite, Zo zoisite. Diagram adapted from Jackson, 1976. Stippled field is area of interest for Ngoye granitoids.

3.2.2 Riebeckite

The stability relations of magnesioriebeckite (part of the glaucophane-riebeckite series) according to oxygen partial pressure, temperature and vapour pressure have been investigated by Ernst (1960). He found that this mineral is stable over a wide range of P.T. conditions, from low temperature authigenic occurrences to magmatic-temperature conditions between the

stability limits of tremolite and pargasite. Ernst (op.cit.) concluded that the restricted occurrence of magnesioriebeckite is not due to attainment of specific metamorphic conditions, but results chiefly from the fulfilment of hypersodic (peralkaline) conditions. Moreover, the occurrence of riebeckite in metamorphosed rocks appears restricted to either peralkaline orthogneisses, or paragneisses derived from iron-rich sedimentary precursors (eg: crocidolite deposits, N. Cape). In view of these findings, it is unlikely that any useful P.T. estimates can be derived from the presence of riebeckite in the Ngoye Formation, other than to place an upper limit of about middle to upper amphibolite (650°C) facies metamorphism imposed on the granitoids.

3.2.3 Colour of biotite and hornblende

With an increase in metamorphic grade the colour of biotite and hornblende change according to compositional variations with increasing temperature (Engel & Engel, 1960; Binns, 1965). Biotite changes from green to brown to red, while hornblende varies from blue-green to green to brown, thought to be related to an increase in the Ti content (biotite) and Ti + Fe⁺ in hornblende. The greenish colour of biotite is often due to a high total content of iron. Although colour variations occur according to grade, the bulk composition of the host rock will have a significant bearing on the biotite colour. This latter observation is corroborated by the great variation in biotite colour throughout the Ngoye Formation, according to granite type. Thus the biotite within peralkaline granites is brown whereas greenish biotite characterises the metaluminous varieties and clearly reflect variations in host-rock chemistry.

Chapter 4

MAJOR AND TRACE ELEMENT GEOCHEMISTRY

4.1 Introduction

Ten specimens were collected for geochemical analysis during the mineral-exploration programme in 1982 and seventeen specimens during the present research period. (see Fig. 4.1 for locations; Tables 4.1a & 4.1b for average major element values, and Appendix B for individual analyses and C.I.P.W. norms). In accordance with grain size, 5 to 10 kg of each sample were crushed, milled and successively quartered to ensure an homogenous, representative final product.

4.1.1 Physical and chemical alteration of geochemical samples

It is important to note that the Ngoye granitoids have been metamorphosed, locally mylonitized, and exposed to aerial weathering effects. Chemical alteration is thus to be anticipated. Specimens were carefully inspected both megascopically and microscopically to ensure that they did not contain late introduced phases such as quartz veins, epidote or carbonate. Friable, bleached samples were easily recognized and rejected, and only hard, unweathered, unaltered material retained for the geochemical investigations. As none of the specimens analysed contained carbonate minerals, the volatile constituents of these rocks are presumed to be mainly H₂O. In all cases the volatile contents are low, less than 1%, which may be accounted by the presence of hydrous minerals such as biotite and hornblende.

TABLE 4.1a

Average chemical analyses*, Ngoye non-peralkaline granitoids.

	1 n=2	2 n=4	3 n=3	4 n=2	5 n=3
SiO ₂	64,45	73,09	74,45	76,38	76,27
TiO ₂	0,18	0,37	0,25	0,08	0,10
Al ₂ O ₃	18,01	12,26	12,95	12,16	13,19
FeO ^t	4,26	3,54	1,84	1,19	1,23
MnO	0,09	0,09	0,03	0,02	0,08
MgO	0,26	0,21	0,21	0,05	0,16
CaO	0,11	0,89	0,83	0,51	0,43
Na ₂ O	3,03	3,95	4,09	4,12	4,67
K ₂ O	9,50	4,73	4,87	4,62	4,52
P ₂ O ₅	0,02	0,06	0,07	0,01	0,03
L.O.I.	0,66	0,40	0,29	0,29	0,25
Total	100,57	99,59	99,88	99,43	100,93

Notes:

1 = microsyenite

2 = biotite-hornblende granite.

3 = mesocrystic biotite granite.

4 = muscovite-biotite granite.

5 = biotite-muscovite granite.

* = all values as percentages

FeO^t = total iron as FeO.

L.O.I. = loss on ignition including H₂O-.

TABLE 4.1b

Average chemical analyses*, Ngoye peralkaline granitoids.

	1 n=4	2 n=3	3 n=1	4 n=2	5 n=3
SiO ₂	76,86	77,32	76,77	77,20	69,24
TiO ₂	0,17	0,10	0,14	0,12	0,83
Al ₂ O ₃	11,44	10,94	11,26	11,22	2,60
FeO ^t	2,06	2,58	2,77	2,04	23,46
MnO	0,04	0,03	0,04	0,02	0,16
MgO	0,08	0,02	0,15	0,03	0,02
CaO	0,25	0,05	0,32	0,17	0,36
Na ₂ O	4,24	4,85	5,18	3,43	0,95
K ₂ O	4,58	4,16	4,15	5,48	1,02
P ₂ O ₅	0,04	0,01	0,01	0,02	0,08
L.O.I.	0,22	0,18	0,28	0,28	0,08
Total	99,98	100,24	101,07	99,99	98,80"

Notes:

1 = biotite-riebeckite granite.

2 = riebeckite granite.

3 = aegerine microgranite.

4 = magnetite microgranite.

5 = magnetite-quartz rock.

* = all values as percentages

" = total excludes 0,35% Nb; 1,2% Zr; 0,2% Y.

FeO^t = total iron as FeO.

L.O.I. = loss on ignition including H₂O-.

TABLE 4.2a

Average chemical analyses*, Ngoye granitoids.

	1	2	3
	n=22	n=12	n=10
SiO ₂	75,81	74,87	77,06
TiO ₂	0,18	0,22	0,14
Al ₂ O ₃	12,00	12,65	11,23
FeO ^t	2,19	2,11	2,28
MnO	0,05	0,06	0,03
MgO	0,12	0,17	0,06
CaO	0,46	0,70	0,18
Na ₂ O	4,27	4,19	4,35
K ₂ O	4,64	4,70	4,58
P ₂ O ₅	0,03	0,05	0,02
L.O.I.	0,27	0,32	0,21
Total	100,02	99,72	100,14

Notes:

1 = average Ngoye granite (excludes magnetite-quartz rock).

2 = average non-peralkaline Ngoye granite.

3 = average peralkaline Ngoye granite.

* = all values as percentages

FeO^t = total iron as FeO.

L.O.I. = loss on ignition including H₂O-.

TABLE 4.2b

Average granitoids* from published literature sources

	1	2	3	4	5
SiO ₂	58,58	62,03	71,30	75,22	75,47
TiO ₂	0,84	0,53	0,31	0,13	0,16
Al ₂ O ₃	16,64	16,39	14,32	9,93	10,72
FeO ^t	5,86	1,51	2,73	4,27	2,25
MnO	0,13	nd	0,05	0,17	nd
MgO	1,87	1,60	0,71	0,09	nd
CaO	3,53	3,60	1,84	1,08	0,25
Na ₂ O	5,24	1,08	3,68	4,78	4,20
K ₂ O	4,95	12,38	4,07	4,06	4,26
P ₂ O ₅	0,29	0,13	0,12	nd	0,07
L.O.I.	1,22	0,85	0,77	0,31	-
Total	99,98	100,24	101,07	99,99	98,80

Notes:

1 = average syenite, from Le Maitre (1976).

2 = orthoclase syenite, from Rosler & Lange (1972).

3 = average granite, from Le Maitre (1976).

4 = alkali granite, from Rosler & Lange (1972).

5 = riebeckite-aegerine granite, from Ekwere & Olade (1984).

* = all values as percentages

- = value not quoted in source literature.

nd = not determined.

FeO^t = total iron as FeO.

L.O.I. = loss on ignition including H₂O-.

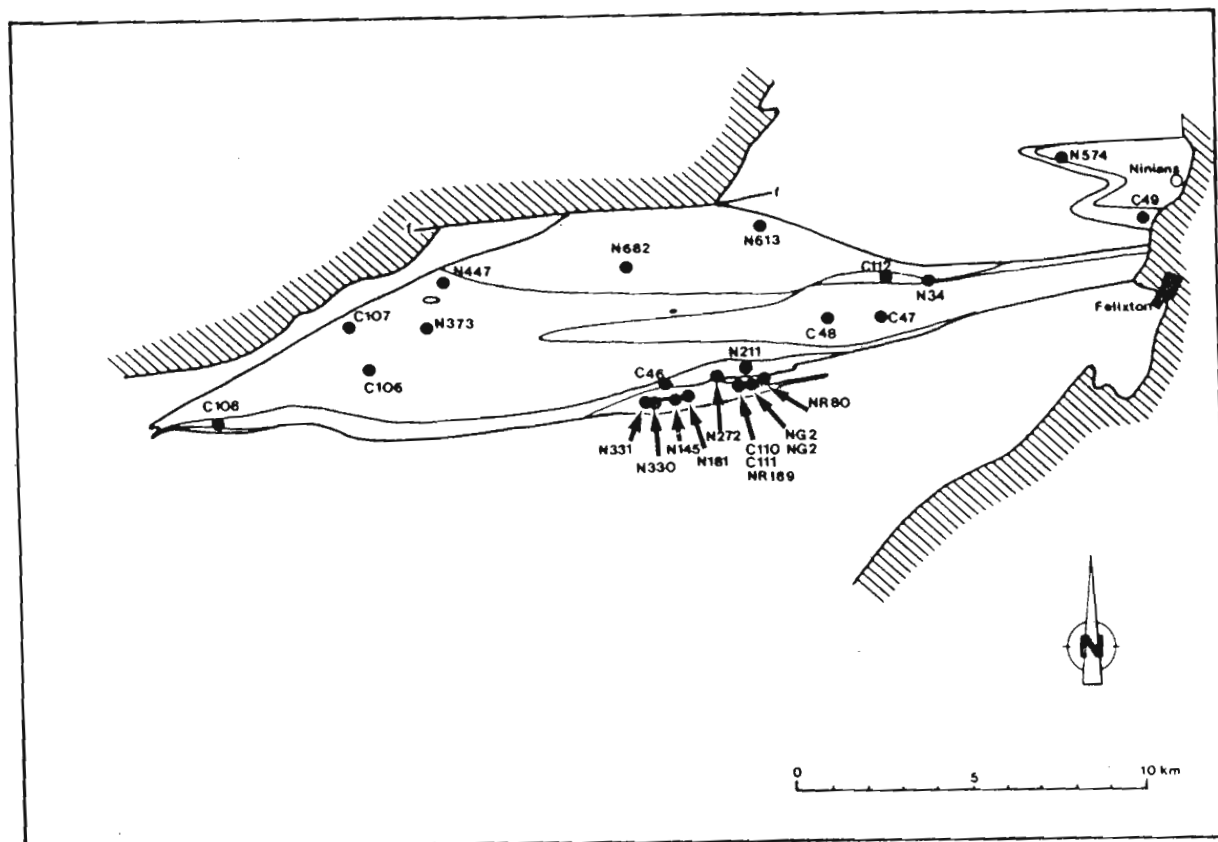


Fig. 4.1. Map of the Ngoye Formation showing geochemical-sample localities, see Appendix B for individual analytical results.

4.2 Major-element geochemical Characteristics

When compared with the chemistry of average granites as compiled by Le Maitre (1976), the Ngoye granites are depleted in Al_2O_3 , MgO and CaO (Table 4.2). Total alkalis ($Na_2O + K_2O$) and SiO_2 are, as indicated, notably enriched and are similar to the alkali granite of Rosler and Lange (1972). Comparison of the two Ngoye syenites with the orthoclase syenite of Rosler and Lange (1972) indicates strong similarities, although the Ngoye samples are relatively enriched in Na_2O and have highly depleted CaO and MgO contents.

4.2.1 A review of the I- and S-type granitoid classification

Chappell and White (1974) proposed that the source of granitic magmas within orogenic belts could be either: (a) by partial melting of igneous (I-type) or (b), by partial melting of sedimentary (S-type) precursors. Chemical and mineralogical differences were thus supposed to stem from variations in source-rock composition. Chappell and White defined I-type granitoids as hornblende-bearing, Al_2O_3 depleted (metaluminous) high Na_2O magmas, whereas sedimentary sources were suggested as giving rise to low Na_2O , high Al_2O_3 (peraluminous), muscovite-bearing, S-type granitoids of restricted SiO_2 range. The chemical parameters which Chappell and White (1974) found most useful in distinguishing granite types are summarized in Table 4.3. Comparison of the Ngoye granitoids with Chappell and White's (op.cit) parameters reveals them to have a pronounced I-type character although the Ngoye muscovite granite rock type has an S-type signature. Moreover, when plotted on a graph of Na_2O versus K_2O , (Hine et al., 1978) the Ngoye granitoids are provisionally classified as I-types (Fig. 4.2).

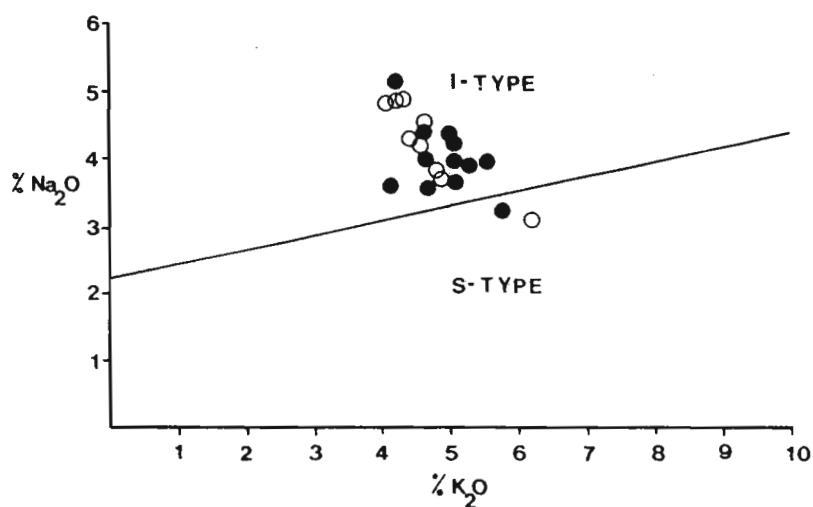


Fig. 4.2. Na_2O - K_2O plot for granitoids from the Ngoye Formation. The boundary between I- and S- types has been estimated from plots by Hine et al.(1978) for granitoids from Australia. Peralkaline granitoids are symbolized by open circles and non-peralkaline analyses by closed circles.

TABLE 4.3
 Characteristics of I- and S-type granitoids

S - type	I - type	Ngoye
low Na ₂ O, less than 3,2%	high Na ₂ O, more than 3,2%	granites average 4,3% Na ₂ O syenites range 2,2-3,9% Na ₂ O
Al ₂ O ₃ */(CaO+K ₂ O+Na ₂ O) 1,1	Al ₂ O ₃ */(CaO+K ₂ O+Na ₂ O) 1,1	granites range from 0,83-1,03 syenites range from 1,15-1,18
no normative diopside	C.I.P.W. normative diopside	most Ngoye samples have diopside
1% normative corundum	1% normative corundum	essentially less than 1% corundum
muscovite, garnet, monazite	sphene, hornblende, magnetite	predominantly biotite and hornblende
Sr ⁸⁷ /Sr ⁸⁶ 0,708	Sr ratios 0,704 - 0,706	Sr ratios 0,706**

Notes:

* = molecular proportions.

** = from Charlesworth (1981).

4.2.2 Loiselle and Wones, A-type granitoids

Loiselle and Wones (1979) extended the I & S concept to embrace what they proposed should be termed A-type granites. They derived the "A" prefix from several characteristics considered pertinent to such granites, including: Alkaline, Atlantic, Anorogenic, Anhydrous & After (in that they normally succeed I & S plutonism). According to Loiselle & Wones (1980), A-type granitoids usually contain hypersolvus feldspars and iron rich minerals such as aegerine, hastingsite and riebeckite, with zircon and fluorite as ubiquitous accessories. Chemically they are depleted in CaO, MgO and Al₂O₃ and enriched in Na₂O and K₂O relative to I- and S-types, and follow an iron enrichment trend on the AFM triangular diagram. Trace element contents are also distinctive, with A-type granitoids relatively enriched in Zr, Nb, Zn, REE and F whereas Sr and Ba are normally depleted. Loiselle & Wones (1979) also point out that A-type magmas are usually generated in stable, or tensional settings. Together with the frequent comagmatic development of rhyolitic lavas, the virtual absence of pegmatitic segregations is taken as evidence for shallow emplacement depths, and the anhydrous nature of such melts. Finally, both these authors and Collins et al. (1982) note the frequent association of A-type granites with syenitic rocks. In contrast, I- and S-types granitoids, which are tonalitic to granodioritic in composition, only very rarely have comagmatic syenites. The marked similarities between the Ngoye granitoids and the parameters presented by Loiselle & Wones strongly suggest that the Ngoye Formation has the hallmarks of A-type granite magmatism.

4.2.3 Harker variation diagrams

One of the earliest variation diagrams was devised by Harker (1909, in Cox et al., 1979) in which he plotted major oxides against SiO₂ contents for igneous rocks. Since SiO₂ is generally the most abundant oxide in rock analyses, it is obvious that as SiO₂ increases, the sum of all oxides must decrease. Negative correlations of most other oxides, irrespective of petrogenetic considerations, are thus to be expected in Harker diagrams (Cox et al., 1979). As pointed out by these authors, TiO₂, FeO, MgO and CaO generally fall together as SiO₂ rises while Na₂O and K₂O in contrast rise with SiO₂. Moreover, Al₂O₃ does not normally show as strong a variation as other oxides.

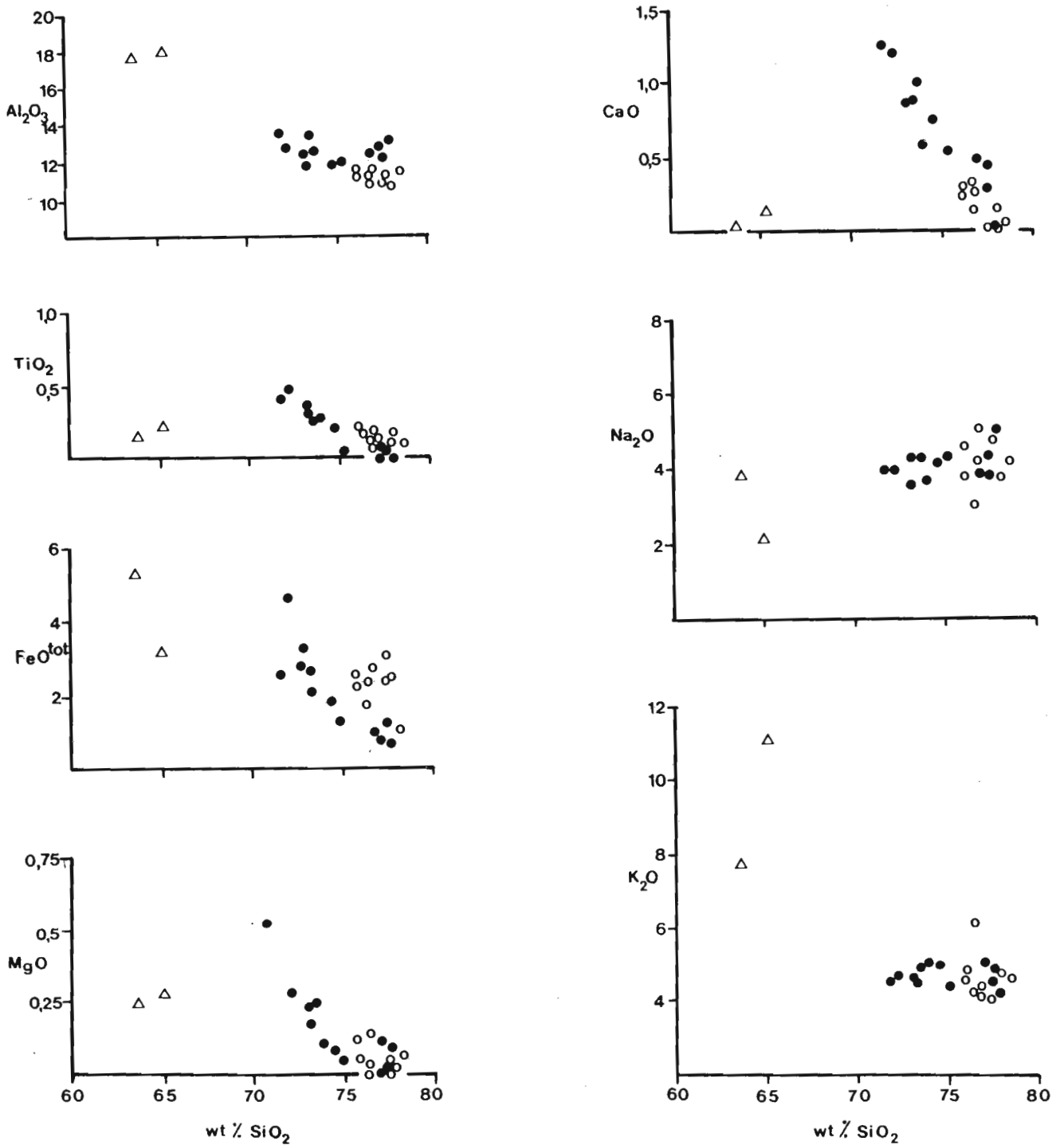


Fig. 4.3. Harker variation diagrams of the Ngoye major element oxides, in weight percent, plotted against silica. Open circles = peralkaline (riebeckitic) granites; closed circles = non-peralkaline (mica and/or hornblende) granites; triangles = syenites. $\text{FeO}^{(\text{tot})}$ = total iron, ie $\text{FeO} + 0,8998 \text{Fe}_2\text{O}_3$.

As shown in Figure 4.3, overall Ngoye major element variations for both peralkaline and non-peralkaline rocks are in accordance with these observations, in that:

- (i) TiO_2 , FeO , MgO and CaO in general vary inversely with SiO_2 contents;
- (ii) K_2O and Na_2O remain relatively constant and do not appear to covary with SiO_2 ;
- (iii) $\text{FeO}^{(\text{tot})}$ tends to be higher for a given SiO_2 content in the peralkaline granites than the other lithologies;
- (iv) Al_2O_3 is generally lower for a given SiO_2 content in peralkaline granites than the other samples.
- (v) The two chloritized syenites are highly enriched in alkalis, but depleted in TiO_2 , FeO , MgO and CaO and do not seem to follow the granite trends indicated in Fig. 4.3.

4.2.4 DI Variation diagrams

An alternative to plotting Harker diagrams is to plot major oxides directly against the differentiation index (DI) of Thornton & Tuttle (1960). The DI is computed as the sum of the weight % of normative quartz + orthoclase + albite, ie the total salic minerals less anorthite. This index is a natural quantity to use for variation diagrams as it is a measure of a rocks basicity. Thus the DI for an alkali granite would typically be about 93 whereas that for a basalt is only 35.

Compositional variations within the Ngoye granitoid suite are summarised in the major element - DI plots presented as Figure 4.4. The good positive correlation between SiO_2 and DI suggests that the elemental trends will parallel those on the customary Harker diagrams. This is indeed so, with TiO_2 , FeO , MgO and CaO all showing negative correlation with DI while Al_2O_3 and K_2O display no obvious covariance with differentiation. In addition, there is a marked tendency for the peralkaline granites to display restricted compositions, particularly with regard to Al_2O_3 , TiO_2 , MgO , CaO and to a lesser extent K_2O , which are all lower for a given DI than the non-

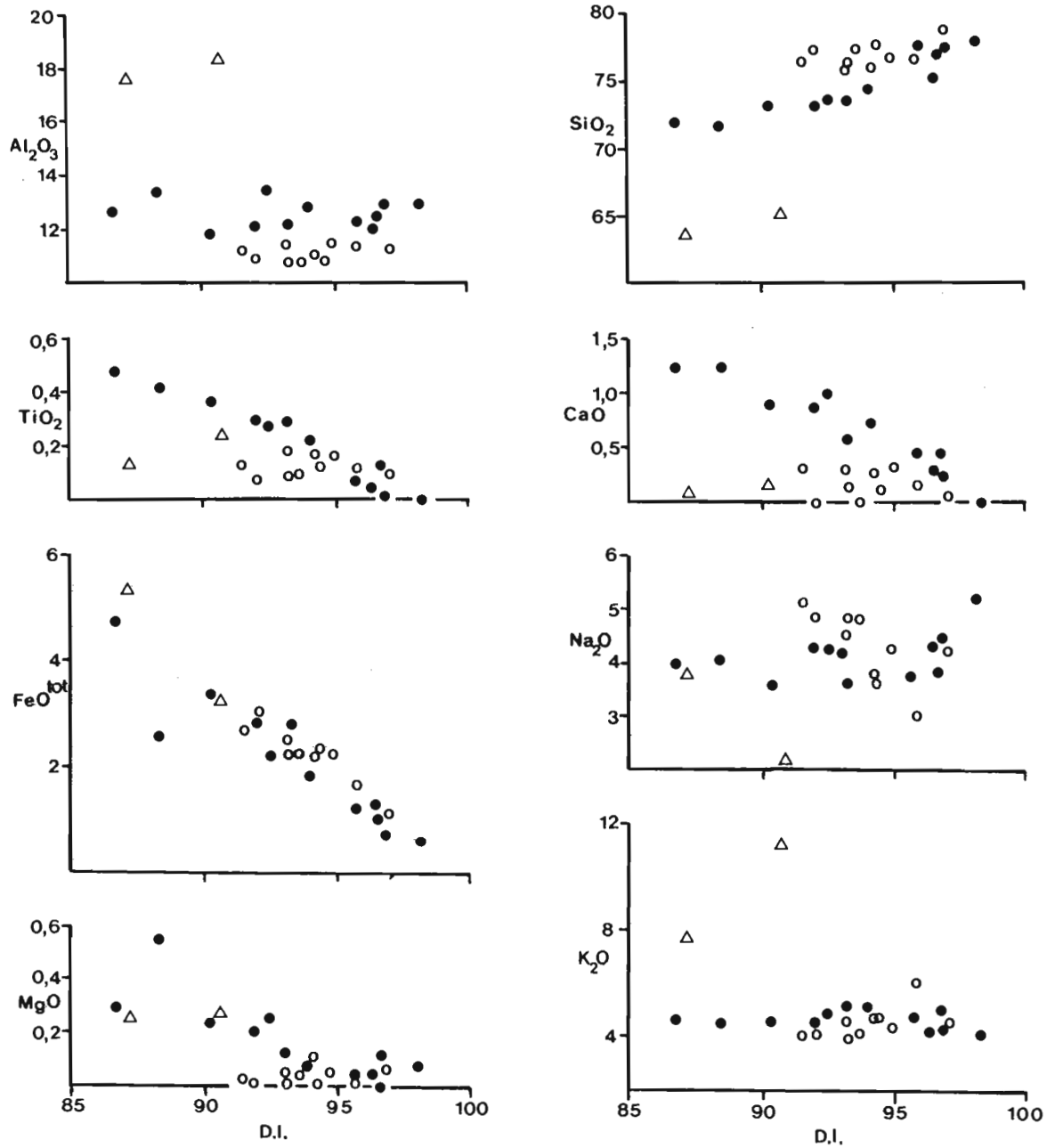


Fig.4.4. Variation diagrams of major oxides in weight percent against the differentiation index, where DI = normative quartz + albite + orthoclase. Ngye granitoid symbols as in Fig. 4.3.

peralkaline granites. As with the Harker diagrams, the DI plots isolate the microsyenite analyses which are significantly enriched in Al_2O_3 and K_2O , while extremely depleted in TiO_2 , SiO_2 and CaO . These aberrations may be due to metasomatic alteration of the syenites, for as mentioned in 2.7 above these rocks are characterised by epidotization and chloritization, typically secondary, low-grade minerals.

4.2.5 Peacock alkali-lime index

One commonly utilized method of classifying igneous rock suites is the alkali-lime index (ALI) of Peacock (1931) in which $(\text{Na}_2\text{O} + \text{K}_2\text{O})$ and CaO are plotted against SiO_2 , the ALI being the silica content where total alkalis are equal to lime (Fig 4.5). Peacock proposed four sequential rock series on the basis of this index: alkalic (less than 51), alkali-calcic (51-56), calc-alkaline (56-61) and calcic (index greater than 61). This method has been applied to the Ngoye granite (*sensu stricto*) analyses which, as a result of their limited silica range, do not form an intersection on the diagram (Fig. 4.5). However, the extension of calculated regression lines towards lower silica contents, suggests an alkaline (ALI=36) character for the samples. Similarly to the Harker and DI variation diagrams, the two syenitic analyses do not follow the apparent granitic trends on the Peacock diagram.

4.2.6 Alumina saturation

Shand (1947) subdivided igneous rocks into three groups according to Al_2O_3 concentrations relative to Na_2O , K_2O and CaO . A progressive depletion of Al_2O_3 relative to alkalis is apparent in the passage from peraluminous through metaluminous to peralkaline compositions. Concomitant with this Al_2O_3 variation is a change in characteristic modal and normative minerals. Thus, whereas peraluminous rocks are characterized by, for example, muscovite and garnet with normative corundum, peralkaline varieties typically contain sodic amphiboles and normative acmite. The absence of normative corundum and anorthite is, furthermore, diagnostic of peralkaline chemistry. Comparison of the Ngoye granitoid analyses with Shand's terminology shows a complete spectrum of compositions: from peraluminous syenite and muscovite granite, through metaluminous biotite and hornblende granites, to peralkaline riebeckite-bearing varieties (see Appendix B for norms).

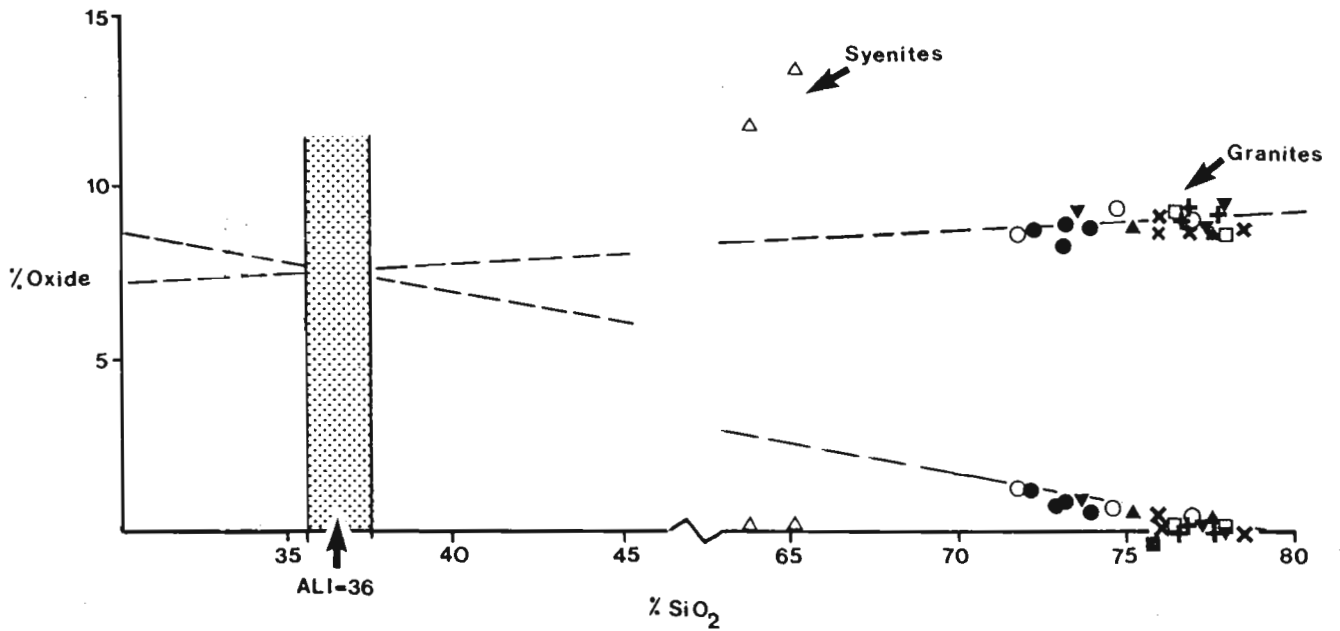


Fig. 4.5. Peacock's alkali-lime index diagram showing the alkalic affinities of the Ngoye granitoids. The calculated linear regressions $y = ax + b$ for (K_2O+Na_2O) and CaO versus SiO_2 are $y = 0,035x + 6,23$ and $y = 0,18x + 13,97$ respectively. Symbols \circ = mesocrystic biotite granite; \bullet = biotite-hornblende granite; \blacktriangle = muscovite-biotite granite; \blacktriangledown = biotite-muscovite granite; $+$ = riebeckite granite; \times = riebeckite-biotite granite; \square = magnetite microgranite; \triangle = syenite.

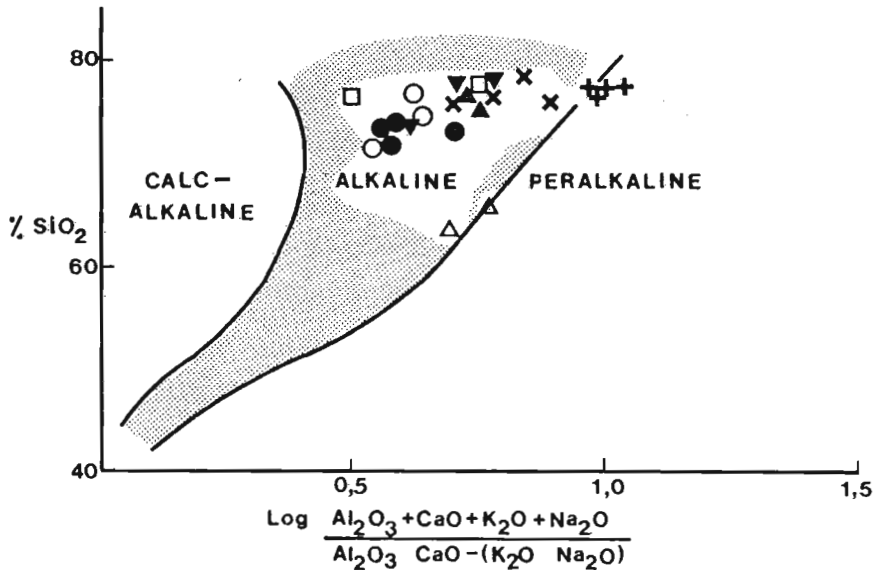


Fig. 4.6. Variation diagram showing the essentially alkaline to peralkaline character of the Ngoye granitoids, using the parameters suggested by Wright (1969). Symbols as in Fig. 4.5.

4.2.7 Wright alkalinity ratio

A classification system based on the Peacock index and the alumina saturation concepts of Shand was proposed by Wright (1969). Using the predominant major oxides present in granitic rocks, ie; Al_2O_3 , CaO , Na_2O , K_2O and SiO_2 , he devised a variation diagram which discriminates between calc-alkaline, alkaline and peralkaline chemical characteristics (Fig 4.6). In this respect, the Ngoye granitoids may be classified as alkaline to peralkaline, an evaluation that is in agreement with the conclusions derived using the parameters suggested by Peacock and Shand.

4.2.8 Alkaline/Tholeiitic diagrams

Further evidence for the non calc - alkaline nature of the Ngoye granitoids is provided by the variations between $(\text{Na}_2\text{O} + \text{K}_2\text{O})$ and SiO_2 (Fig. 4.7a). According to these parameters, igneous rocks may be classified as alkaline or subalkaline (Irvine & Baragar, 1971). These authors note that alkaline rocks are usually characterized by normative nepheline, whereas subalkaline varieties are typically quartz normative . A subdivision of the subalkaline field into tholeiitic and calc-alkaline members (Fig. 4.7b) was proposed, and based on normative anorthite versus Al_2O_3 contents (Irvine & Baragar., op.cit).

When plotted on these graphs the Ngoye granitoids are clearly subalkaline and tholeiitic. In contrast, the syenites which are significantly enriched in alkalis, are classed as alkaline. Furthermore, the tholeiitic nature of the Ngoye samples is corroborated (Fig.4.8) by their iron-rich character relative to MgO (Anderson et al., 1980).

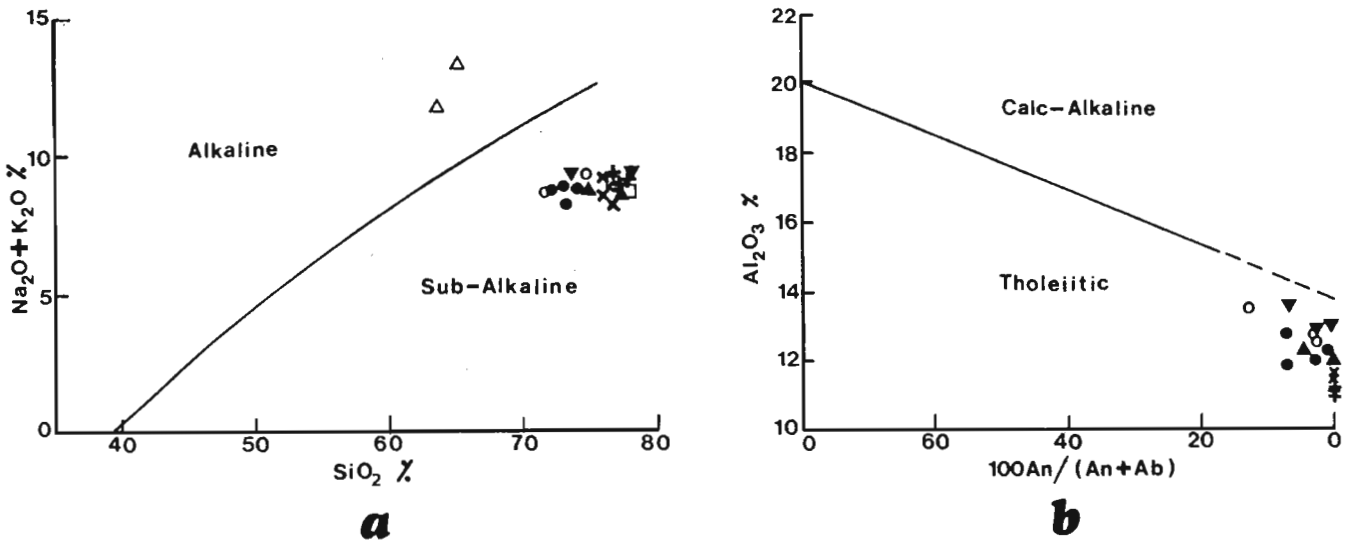


Fig. 4.7. Plot of total alkalis versus SiO₂ (Fig. 4.7a) showing the predominant sub-alkaline character of the Ngoye granitoids, according to the fields proposed by Irvine & Baragar (1971). Fig. 4.7b shows the subdivision of sub-alkaline rocks into calc-alkaline and tholeiitic varieties, using the ratios of Al₂O₃ to normative plagioclase suggested by Irvine & Baragar (op cit.). Symbols as in Fig. 4.5.

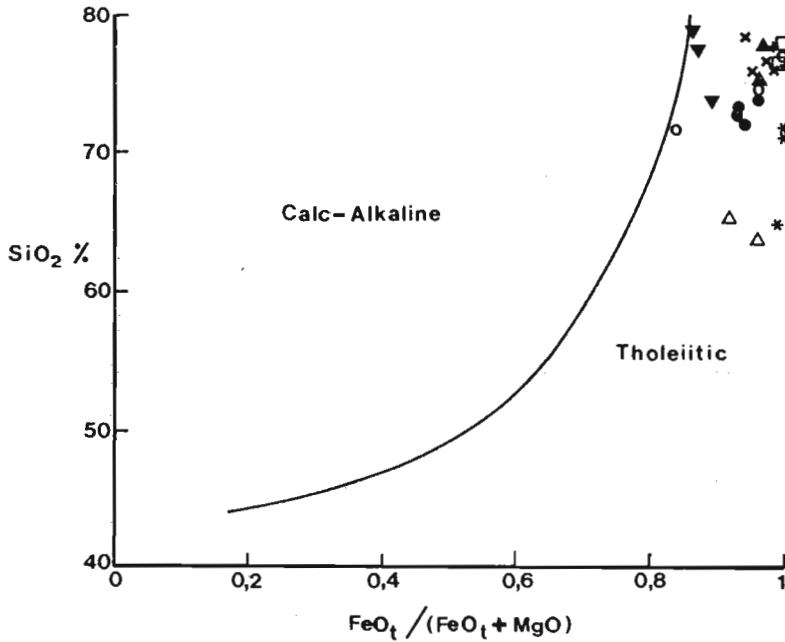


Fig. 4.8. Plot of SiO₂ against FeO : MgO ratios after Anderson et al. (1980). This illustrates the predominantly tholeiitic character of the Ngoye granitoids. Symbols as in Fig. 4.5.

4.3. Granitoid nomenclature based on major element chemistry

Modal analyses of the Ngoye specimens (chapter 2) have delineated 12 granitoid types. This section presents and compares chemically based classification schemes with the Steckensen (1976) modal approach.

4.3.1 Harpum diagram

A binary diagram of K_2O against Na_2O was proposed by Harpum (1963) as an aid to the classification of granitic rocks (Fig 4.9). A major deficiency inherent in the scheme is the exclusion of CaO and SiO_2 , which are major constituents of granitoid rocks. When plotted on this diagram, the Ngoye samples range from granodiorite to granite, with adamellite the dominant lithology. Adamellite, in this classification, embraces peraluminous and peralkaline varieties, while some of the peralkaline granites are classed as granodiorite. The two Ngoye syenites have been included in this plot to illustrate the effect the lack of a silica parameter has i.e. they both fall within the granite (*sensu stricto*) field.

In summary, the Harpum binary classification diagram does not provide compatible results with the modally derived terminology for Ngoye samples. In addition, this scheme does not allow discrimination between the various Ngoye lithologies.

4.3.2 O'Connor's normative Ab-An-Or diagram

The normative minerals albite, anorthite, orthoclase and quartz constitute the bulk of silica-oversaturated granitoid rocks. As O'Connor (1965) considered quartz to be a common factor such rock-types, he proposed a classification based on relative feldspar proportions only. This system represents a vast improvement on the simple, binary, Harpum diagram, but still suffers due to the omission of quartz on a discriminant. Thus, syenite and syenogranite samples with similar feldspar ratios cannot be distinguished on O'Connor's (*op.cit.*) diagram, and its use is therefore restricted to the

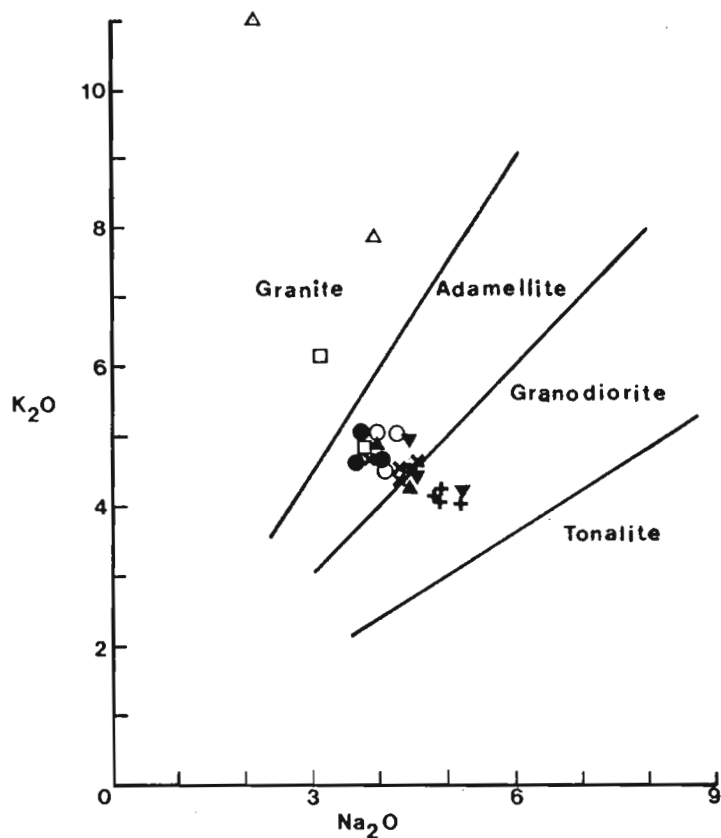


Fig. 4.9. Classification of the Ngoye granitoids on the binary K_2O versus Na_2O diagram after Harpum (1963). Symbols as in Fig. 4.5, with the two syenites included for comparison.

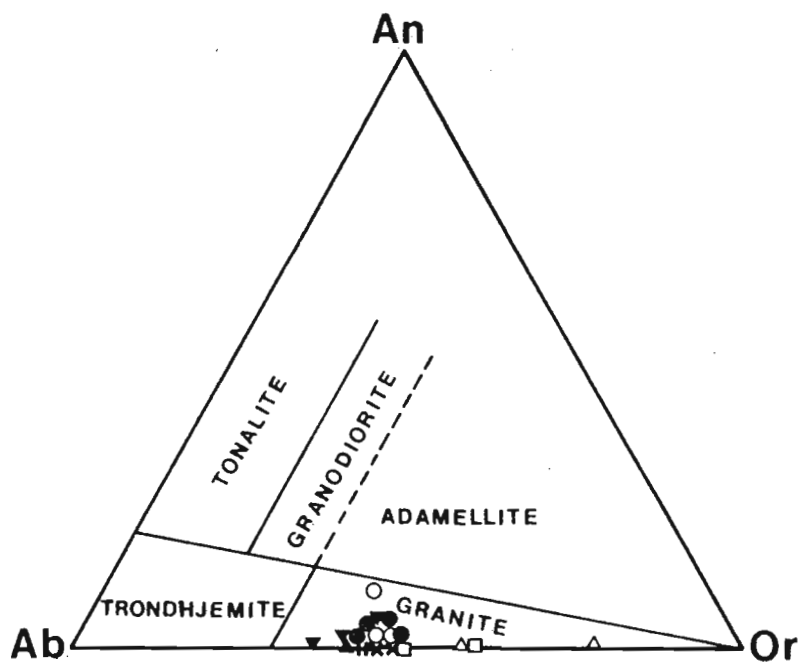


Fig. 4.10. Plot of normative Ab - An - Or for the classification of granitoid rocks, fields after O'Connor (1965). Symbols for Ngoye samples as in Fig. 4.5.

classification of silica oversaturated igneous rocks only. The resultant granitoid fields derived by O'Connor (1965) are shown in Figure 4.10. When the Ngoye normative feldspar contents are plotted on this diagram they all fall within the proposed granite (*sensu stricto*) field, close to the Ab-Or tie line. This confirms their depletion in CaO and approximately equal contents of Na₂O and K₂O, throughout the range of rock-types. For comparison, the two syenitic samples have been plotted and as it can be seen, the lack of silica saturation (normative quartz) parameter results in their falling within the granite field. In summary, this scheme does classify the Ngoye granitoids as granites but is unable to discriminate the syenitic samples, and furthermore, does not provide any real distinction between the various (*sensu stricto*) types as does the modal QAP diagram.

4.3.3 Streckeisen's Ab-An-Or diagram

Streckeisen (1976 a) suggested a different approach to the subdivision of the Ab-An-Or triangle from that proposed by O'Connor (1965). Whereas O'Connor plotted only silica oversaturated igneous rocks and did not realise the significance of feldspar ratios, Streckeisen found that:

- (i) there is a pronounced negative correlation between An and Or, whereas Ab remains fairly within igneous rock suites that vary from acid to basic. Thus, An increases and Or decreases from granite through granodiorite to tonalite, with a similar trend apparent from syenitic to gabbrocc compositions,
- (ii) the limits, 17% normative quartz and 7% normative feldspathoid correspond approximately to Quartz = 20 Feldspathoid = 10% of the modal QAPF classification.

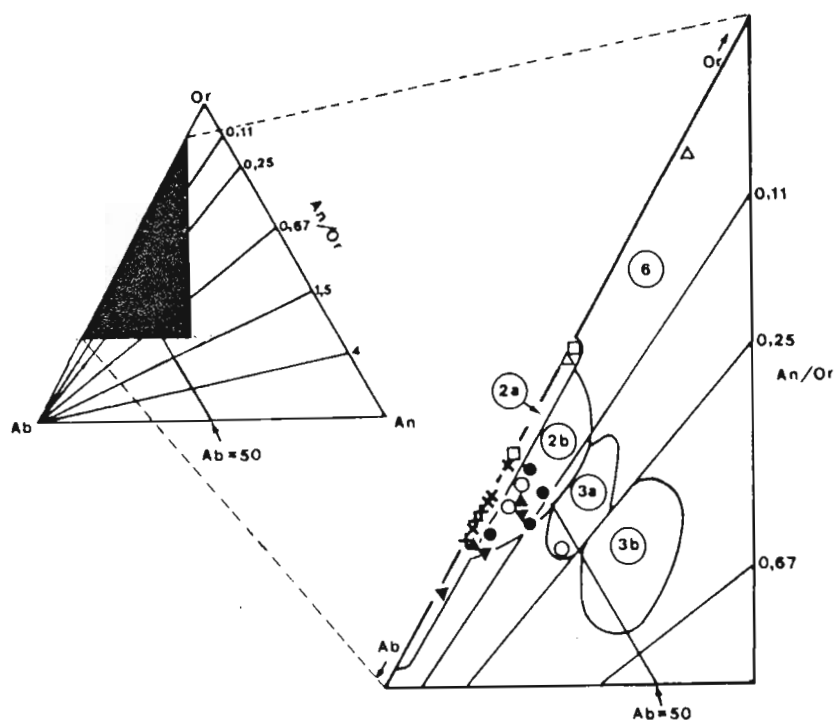


Fig. 4.11. Classification of the Ngoye granitoids according to Ab - An - Or for silica-oversaturated igneous rocks on the basis of An / Or ratios, after Streckeisen (1976 a). Numbered fields correspond with the rock groups of the modal QAP triangle, see Fig. 2.2. (Apart from group 2 which has been subdivided into fields 2a and 2b, or alkali granite and alkali-feldspar granite respectively). Symbols as in Fig. 4.5.

Streckeisen therefore proposed a classification within the normative Ab-An-Or triangle that was based on the An:Or ratio, for the three major rock groups listed below:

- (i) Quartz-feldspar rocks ($Q > 17\%$)
- (ii) Feldspar rocks ($Q < 17\%$, $F < 7\%$)
- (iii) Feldspar- feldspathoid rocks ($F > 7\%$)

When plotted on separate diagrams for each of the three groups, he found quite a good correspondence between modal and normative nomenclature (Fig. 4.11).

The majority of the Ngoye specimens with $Q > 17\%$ fall within the alkali granite and alkali-feldspar granites fields where $An:Or < 0,11$. One exception is a sample of mesocrystic-biotite granite which lies on the boundary between the syenogranite and monzogranite fields ($An:Or = 0,25$). The two syenites ($Q < 17\%$) when plotted on Fig. 4.11 do not correspond with any of the fields proposed by Streckeisen (op. cit.), indicative of their extreme calcium depletion relative to average syenites.

Streckeisen (op. cit.) also observed that alkali igneous rocks in the acid to intermediate silica range normally fall on the Ab-rich side of the Ab = 50 line (Fig 4.11), whereas calc-alkaline varieties always have Ab < 50. By analogy the Ngoye samples are alkaline, which is in agreement with the conclusions derived in 5 above.

4.3.4 Streckeisen and Le Maitre's orthogonal plot

This classification is based on the Streckeisen (1976 a) normative plot discussed above. Streckeisen and Le Maitre (1979) propose that, as the An:Or ratio appears critical in the classification of igneous rocks, the Ab factor may be discarded. This surmounts the difficult problem of how to distribute normative Ab between An and Or, which in the modal QAP diagram is achieved by combining albite of less than An₅ within the alkali-feldspar component. The omission of normative Ab from the abscissa of Streckeisen and Le Maitre's orthogonal plot (Fig. 4.12) enables Q to be included. This represents a significant advance over any of the previous classification systems in that silica saturation is now taken into account. These authors note however that even on this diagram the relationship between normative and modal classification is not always consistent. They point out, in particular, that granitic rocks of fields 3a and 3b in the modal QAPF diagram and with low An content in plagioclase, may plot in fields 2 and 3a of the normative diagram respectively.

Plots of the Ngoye samples on this diagram indicate compositions ranging from granite to alkali-feldspar granite, indicative of very low An content in the plagioclase feldspars. The two syenites are classified as alkali-feldspar quartz syenite.

4.3.5 De la Roche R1 - R2 diagram

The R1 - R2 diagram devised by de la Roche et al. (1980) is probably one of the most advanced chemical classification systems currently available. These authors note that all the chemical and normative classification schemes so far discussed essentially consider only the leucocratic components, such as alkalis and silica, or normative feldspars and quartz.

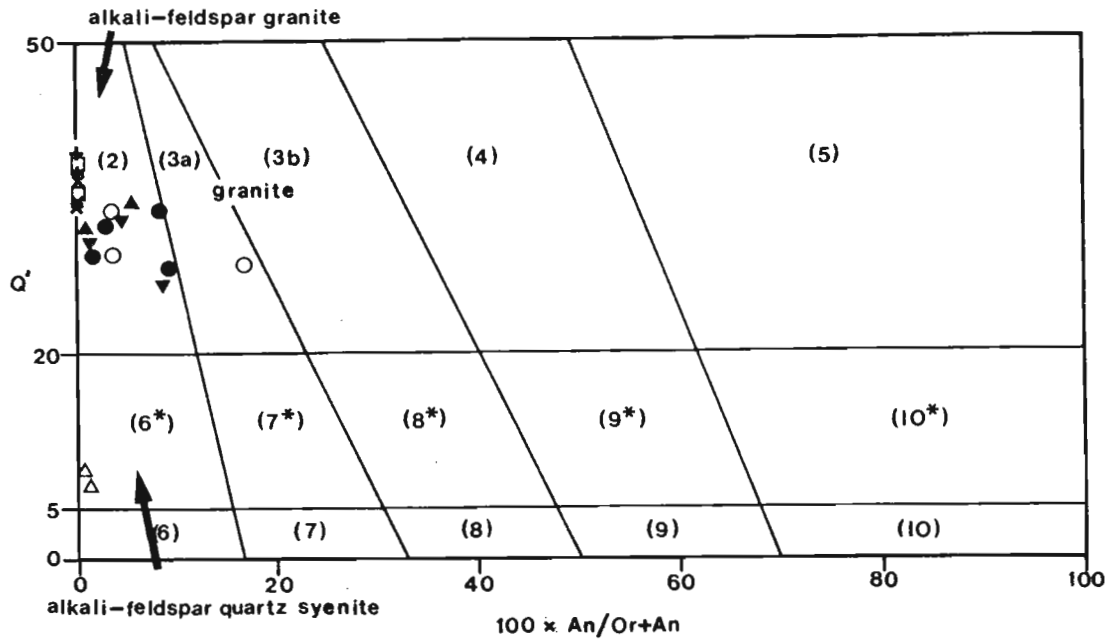


Fig. 4.12. Normative classification of the Ngoye granitoids based on the quartz versus anorthite/orthoclase diagram of Streckeisen & le Maitre (1979). The numbered fields (2), (3a), etc., correspond approximately to the fields 2, 3a, etc., of the Streckeisen (1976) QAP modal diagram. Symbols as in Fig. 4.5.

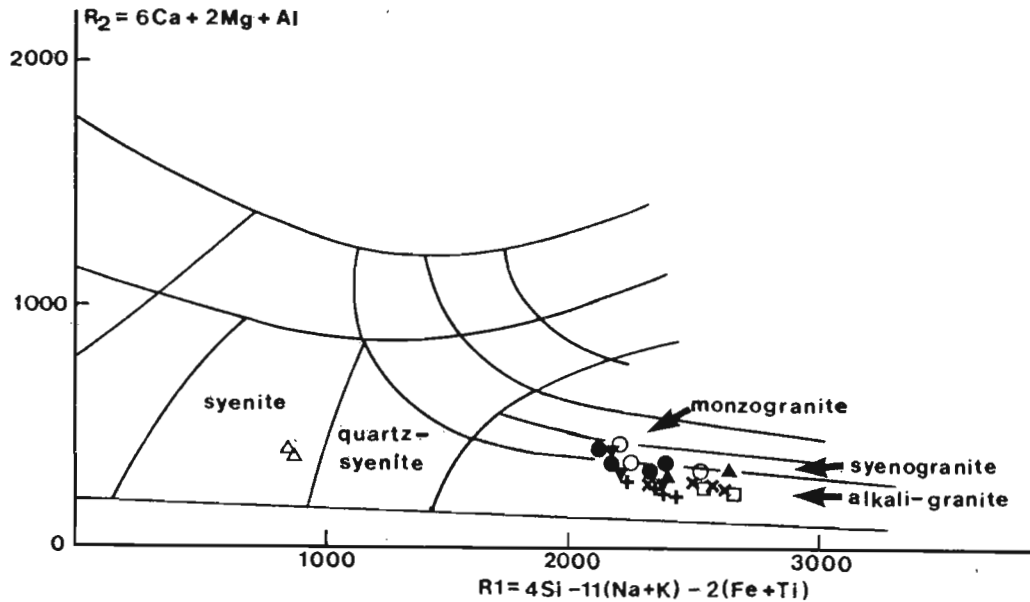
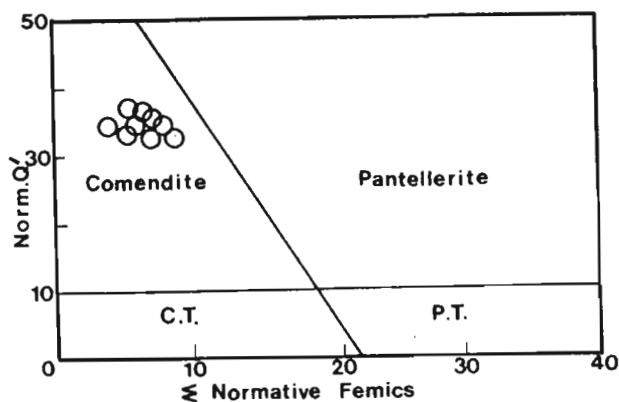
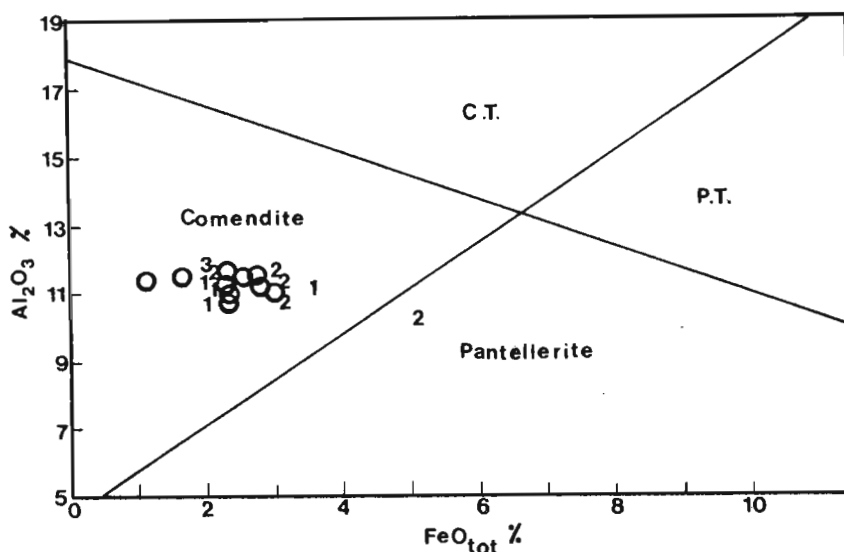


Fig. 4.13. The R1 - R2 diagram showing igneous-rock fields relevant to the classification of the Ngoye granitoids, after de la Roche *et al.* (1980). Symbols as in Fig. 4.5.



a



b

Fig. 4.14. Classification schemes for peralkaline, quartz normative, extrusive rocks. Fig.4.14a (after Macdonald & Bailey, 1973) is based on normative mineral proportions, whereas Macdonald's (1975) system utilizes Al : Fe ratios. The Ngoye are plotted as open circles, and in Fig. 4.14b are compared with typical peralkaline granites from Nigeria, Saudi Arabia and Sudan, numbered 1, 2 and 3 respectively. Analyses from Bowden, 1974; Neary et al., 1976; Radain & Kerrich, 1979; Harris & Marriner, 1980; Ekwere & Olade, 1984.)

They also point out that normative-based classifications rely, for mineral proportions, on the crystallization sequence inherent in norm calculations. De la Roche *et al.* (op. cit.) thus propose a bivariate chemical variation diagram that incorporates all major cations, and does not utilize normative proportions (Fig. 4.13), where $R1 = 4Si - 11(Na + K) - 2(Fe + Ti)$ and $R2 = 6Ca + 2Mg + Al$. Translation of the Ngoye data into these parameters shows that the samples range from syenite through monzogranite to alkali-granite, and accordingly bear a close resemblance to the nomenclature derived from the modal QAPF diagram.

4.3.6 Degree of Peralkalinity

Peralkaline granitoid rocks may be classified as either comenditic or pantelleritic (Macdonald & Bailey, 1973; Macdonald, 1975). These terms were introduced in the latter half of the last century to describe extrusive, peralkaline, silica-oversaturated rocks from the Mediterranean islands of Sardinia and Pantelleria, respectively. According to Macdonald (*op. cit.*), pantellerites are enriched in Fe_2O_3 , FeO , TiO_2 and MnO when compared with comendites, and have a higher agpaitic index due to a relative increase in the Na_2O to Al_2O_3 ratio. As pointed out by Macdonald (1975) comendites are purely transitional between rhyolite and pantellerite. Classification of the Ngoye peralkaline granites using the schemes suggested by the above authors (Fig. 4.14) indicates that they have comenditic affinities and are thus mildly peralkaline.

4.3.7 Summary of the chemical classification of Ngoye granitoids

All methods employed show the strongly granitic (*sensu stricto*) flavour of the Ngoye lithologies. However, significant discrimination of the samples is achieved only in the diagrams that incorporate normative quartz or silica in addition to feldspars and alkalis. The most powerful discriminatory diagram presently available for granite classification is that devised by de la Roche *et al.* (1980), which uses all major cations, and is able to separate the Ngoye granitoids into four groups that correspond closely to the modally derived terminology. According to the parameters of Macdonald (1975) the peralkaline granites within the Ngoye Formation are of comenditic affinity.

4.4 Trace-Element Geochemistry

4.4.1 Introduction

The Ngoye trace elements are discussed using the terminology of Shilling (1973) and Saunders *et al.* (1980). Cations with large radii and low charge are termed large-ion lithophiles (LIL), and include Rb, Ba and Sr. Lithophilic elements with low radius to charge ratios embrace the high-field strength (HFS) elements, and are generally referred to as incompatibles. This group incorporates the elements Nb, Sn, W, Th, Mo, Zr, and Y. Whereas the LIL elements substitute for major ions, eg: K and Ca in common silicate minerals such as feldspar, the incompatibles usually occur as discrete minerals, eg zircon, cassiterite and wolframite. The chalcophilic elements Pb and Zn, like the incompatibles, do not normally substitute for major silicate cations, but form discrete compounds in the residual liquids of fractionating magma systems (Mason, 1967).

4.4.2 General characteristics of Ngoye trace element abundances

Comparison of the Ngoye analyses (Table 4.4) with the average granite and syenite of Turekian & Wedepohl (1961) and Rosler & Lange (1972) reveals several substantial differences. The Ngoye specimens are generally enriched in Nb, Zr, Y, Zn and Th, while essentially depleted in Ba and Sr relative to the average granite and syenite. In addition, although Pb, Sn, W and Mo are generally of similar tenor to the average granite and syenite of Turekian & Wedepohl, several of the Ngoye lithologies have significantly enhanced contents of these elements.

4.4.3 Large-ion - lithophiles

As noted by Mason (1967) Ba and Sr have similar overall geochemical properties and are controlled by the major silicate phases, in particular alkali feldspar and plagioclase. McCarthy & Hasty (1976), and Hanson (1978) have examined fractionation trends within granitic bodies, and noted that plagioclase crystallization depletes Sr in the residual melt, while alkali

TABLE 4.4

Mean trace-element contents* in the Ngoye granites

	1 n=7	2 n=5	3 n=10	4 n=3	5	6 n=2	7
Nb	40	40	40	3580	200	89	35
Zr	484	102	547	12111	200	771	500
Y	72	44	78	1976	34	73	20
Zn	86	44	141	763	60	60	130
Pb	18	33	8	106	20	5	12
U	2	18	1	207	4	3	3
Th	16	40	8	434	18	22	13
W	1	5	1	172	2	-	1
Sn	2	18	6	84	3	6	1
Mo	2	2	-	35	1	3	1
Ba	812	23	112	42	830	438	1600
Sr	105	12	9	7	300	24	200
Rb	144	518	187	41	200	342	110
Rb/Ba	0,2	22,5	1,7	1,0	0,2	0,8	0,1
Rb/Sr	1,4	43,2	20,8	5,8	0,7	14,3	0,6

Notes:

- 1 = mean of early, metaluminous Ngoye granites.
- 2 = mean of younger, metaluminous and peraluminous Ngoye granites.
- 3 = mean of peralkaline Ngoye granites.
- 4 = mean of Ngoye magnetite-quartz rock samples.
- 5 = average granite (from Vinogradov, in: Rosler & Lange, 1972).
- 6 = mean of Ngoye microsyenites.
- 7 = average syenite (Turekian & Wedepohl, 1961).
- * = all values in parts per million.

feldspar fractionation shows a similar trend and also reduces Ba in the melt. The tendency of Ba and Sr to concentrate in early formed feldspars is a reflection of their high partition coefficient or K_D , ie "...the K_D is the...weight fraction of a given trace element in a mineral divided by the measured weight fraction of that element in a co-existing melt" (Hanson, 1978, p. 27).

In contrast, Rb, which is admitted in the place of potassium into alkali feldspar, has a low K_D and will thus tend to be concentrated in a co-existing melt. Therefore, due to their different partition coefficients as well as their affinity for major silicate phases, the trace elements Ba, Sr and Rb are particularly useful for modelling purposes in granitic systems. McCarthy & Hasty (1976) have shown that late stage granites within a differentiated complex should have high Rb:Sr and Rb:Ba ratios, indicative of extreme depletion in Sr and Ba in late melts. This observation was reiterated by Hanson (1978, p. 31) who stated that "if the element with a large K_D has a large variation within a suite, the main igneous process is differentiation". He noted that, within the early stages of the fractionation of a granitic magma, Ba and Sr vary greatly with very little change in Rb concentrations (Fig. 4.16). In contrast, Hanson (op. cit.) found, by geochemical modelling, that late stage partial-melt material shows the opposite trend and would be expected to have low Rb:Sr and Rb:Ba ratios.

Variation diagrams for the Ngoye samples are presented in Figures 4.15, and display very similar trends to the theoretical trends presented by Hanson (1978) and Robb (1983) for fractionated granite magma. These data corroborate the field evidence, which indicates that the muscovite-bearing granites (high Rb:Sr and Rb:Ba ratios) intrude and thus postdate the biotite and biotite-hornblende granites (low Rb:Sr and Rb:Ba ratios, see Table 4.4 on page 96). Moreover, if the Ngoye lithologies were the result of a partial melting sequence, the earliest intrusives should have had the highest Rb:Sr and Rb:Ba ratios, which is clearly not the case.

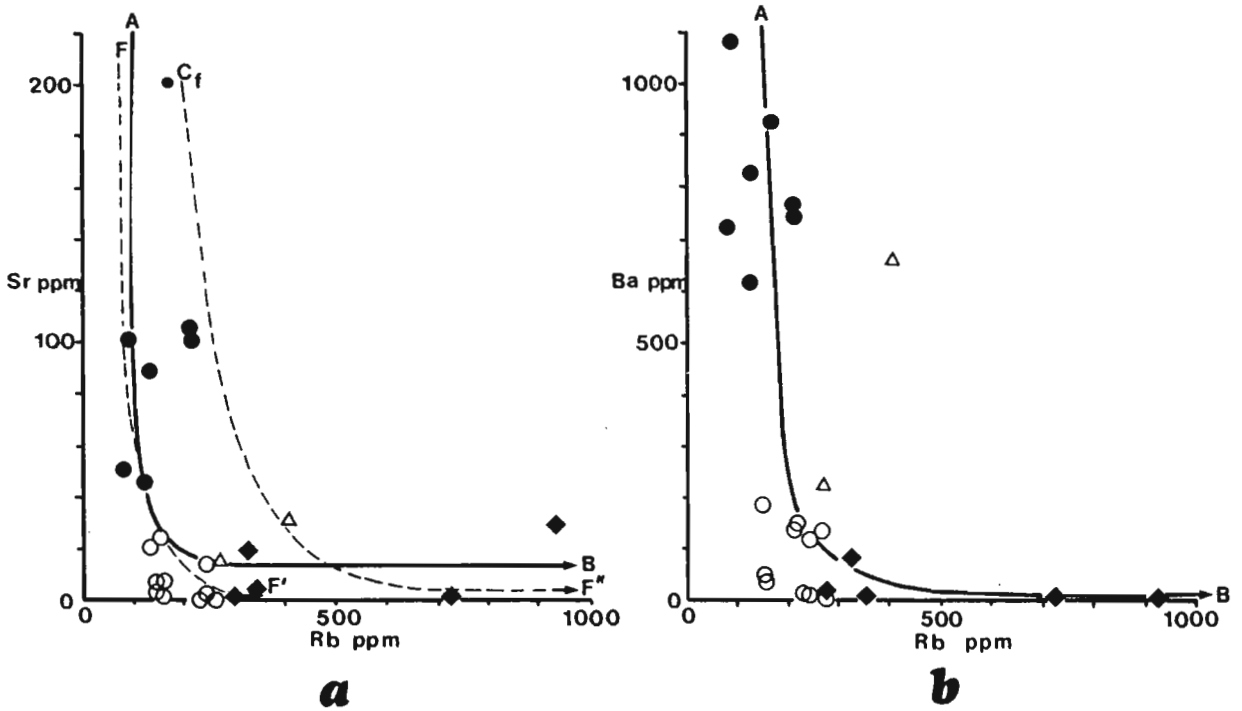


Fig. 4.15. Plots showing the variation in Sr and Ba with Rb for the Ngoye granitoids. Theoretical fractional crystallization curves for a melt of composition C_f have been modelled by Robb (1983) as follows: trace-element abundances of the fractionating solid phase vary along curve F - F' while those of the residual liquid vary along C_f - F'' (Fig. 4.15a). Note the extremely rapid depletion of Sr and Ba relative to Rb in the early phases of crystallization. Symbols as follows: solid circles = early non-peralkaline granites; solid diamonds = late non-peralkaline granites; open circles = peralkaline granites; triangles = syenite.

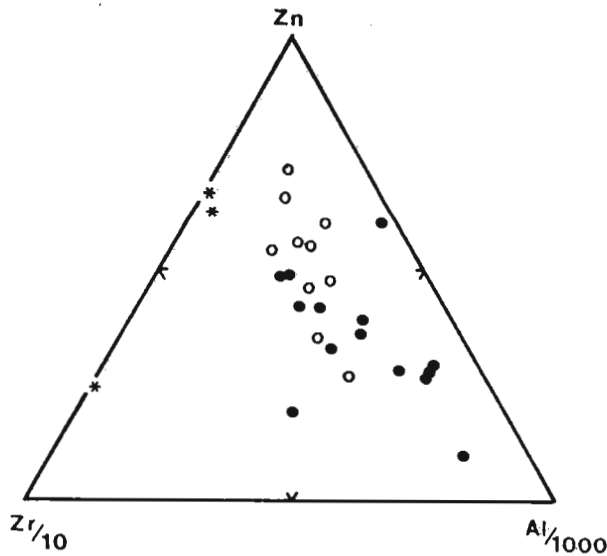


Fig. 4.16. Triangular diagram illustrating the relative enrichment of Zn and Zr over Al in the peralkaline Ngoye granitoids. Solid circles = non-peralkaline granitoids; open circles = peralkaline granitoids; asterisks = magnetite-quartz rocks. Concentrations in ppm.

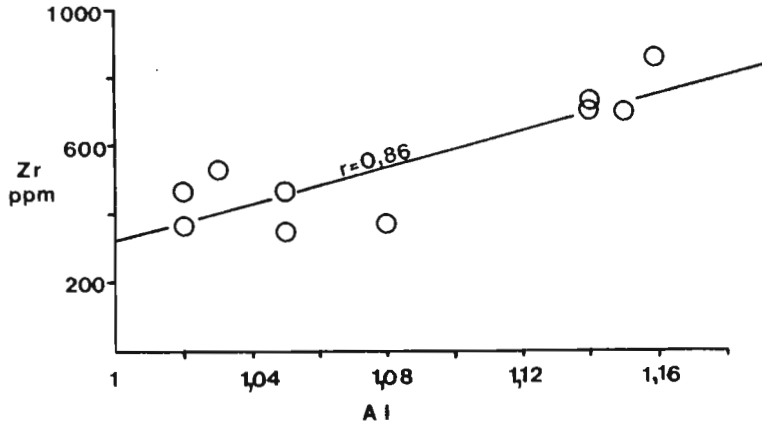


Fig.4.17. Plot of Zr concentrations (ppm) against the alpaaitic index (AI) for peralkaline granitoids from the Ngoye Formation. The calculated linear regression ($y = 2608x - 2280$) has a correlation coefficient (r) of +0,86.

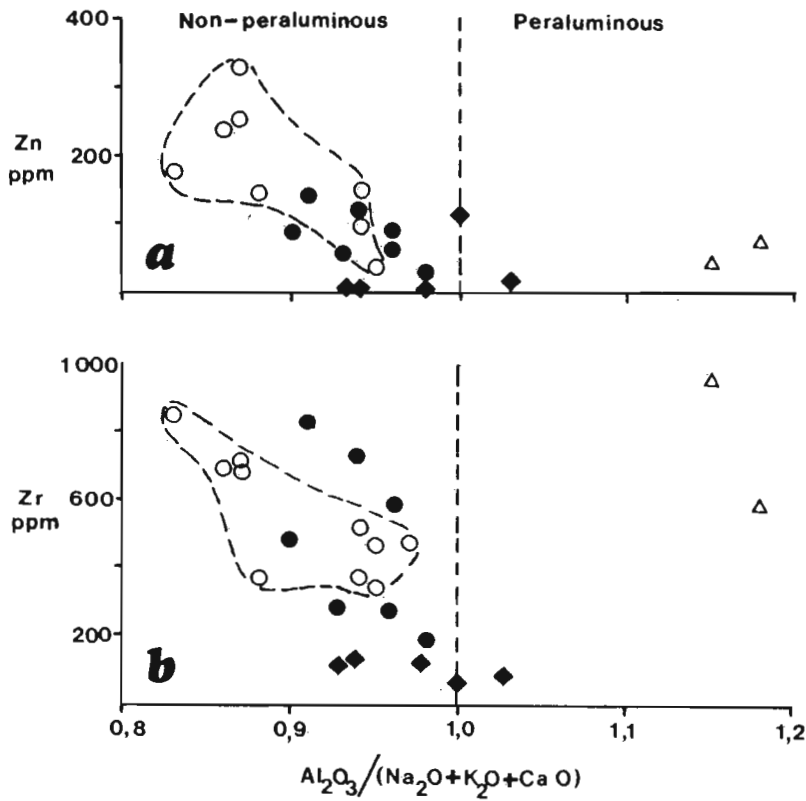


Fig.4.18. Plots of Ngoye granitoid analyses showing the decrease in Zn and Zr concentrations with increasing aluminous character. Symbols as in Fig. 4.16.

TABLE 4.5

Trace-element contents, Ngoye and Saudi-Arabian quartz rocks.

	C110	NR80	NR189	A	B
Na ₂ O	2,29	0,14	0,43	1,19	0,50
K ₂ O	2,58	0,04	0,45	1,99	4,65
Nb	1886	56	8797	5390	3337
Zr	3443	3285	29605	24089	11390
Y	1265	584	4080	2873	4783
Zn	622	681	985	-	-
U	141	85	394	363	-
Th	154	84	1065	590	827
W	14	40	462	-	-
Sn	113	26	115	-	-
Mo	nd	17	89	-	-
Ce	763	-	-	3157	-
Nd	669	-	-	1943	-
La	402	-	-	1505	2828
Ba	56	21	50	-	-
Sr	6	1	15	891	464
Rb	95	2	27	124	535

Notes:

C110, NR80, and NR189 are analyses of magnetite-quartz rock from Ngoye.

A & B are siliceous veins from the Midian Complex, Saudi Arabia (Harris & Marriner, 1980).

* = all values as parts per million, apart from Na₂O and K₂O which are percentages.

4.4.4 Incompatible elements (Zr, Zn & Y)

As noted above, the Ngoye granitoids (in particular the peralkaline granites) are enriched in incompatibles relative to the average granite and syenite of Turekian & Wedepohl (1961). Enhanced concentrations of HFS and other incompatibles are characteristic of peralkaline granites (Bowden & Turner, 1974; Gerasimovsky, 1974; Taylor et al., 1980; Brown et al., 1984). In addition, Taylor et al. (1980) have shown that peralkaline granites are typically enriched in Zr and Zn relative to Al contents. The phenomenon of Zr enrichment in peralkaline magmas has been attributed to an excess of alkalis over alumina (Watson, 1979) and thus directly related to the agpaite ratio ($A.I = \text{mole Na}_2 + \text{K}_2\text{O}/\text{Al}_2\text{O}_3$). Watson found that highly peralkaline liquids are capable of dissolving up to 3.9 wt % Zr, whereas peraluminous liquids reach saturation at only 100 ppm Zr. He concluded that Zr remained in solution until late in the crystallization sequence of peralkaline magmas due to the formation of alkali-zircono silicate complexes, ie: $(\text{Na,K})_4 \text{Zr}(\text{SiO}_4)_2$. He furthermore demonstrated a similar behaviour for Zn in peralkaline melts, where zinc-fluoride complexes increase the solubility of Zn. As suggested by Collins et al. (1982), the counter-ion effect noted by Watson (1979) may also be an important factor in the retention of the highly charged cations, such as Nb and Y, that are so characteristically enriched in peralkaline granites. Comparison of the Ngoye analyses with the above observations shows that; similarly:

- (i) Ngoye peralkaline granites & magnetite-quartz rocks are enriched in Zn & Zr relative to Al (Fig. 4.16);
- (ii) there is a trend of increasing Zr with increasing peralkalinity (Fig. 4.17).
- (iii) the most aluminous granites in the formation, i.e.: the biotite and muscovite-bearing varieties, have the lowest Zn and Zr concentrations (Fig. 4.18);
- (iv) the peraluminous syenites have similar Zr concentrations to the peralkaline granites, but are highly depleted in Zn;
- (v) the earliest non-peralkaline granites (biotite-hornblende

and biotite types) have higher Zr concentrations than the later muscovite-bearing varieties. This indicates precipitation of Zr early in the crystallization sequence of the non-peralkaline granites, leaving later magmas depleted in this element.

4.4.5 Incompatibles U, Th, Pb W and Sn

Although these elements are most abundant in the magnetite-quartz rocks, significant values also occur in the aluminous two-mica granites of the Ngoye Formation. As pointed out previously (4.5), field and geochemical evidence show that the muscovite bearing magma is probably related by fractional crystallization to the biotite and biotite-hornblende varieties. The enhanced contents of U, Th, Pb, W and Sn within the muscovite granite is therefore consistent with their tendency to concentrate in a residual magma (Mason, 1967).

4.4.6 Incompatibles and alkalis in the magnetite-quartz rocks

These fascinating and unusual rocks are highly enriched in incompatible elements (Table 4.5). Occurrences of similar rocks have been documented in Nigeria (Bowden *et al.*, 1979) and Saudi Arabia by Harris & Marriner (1980), and Harris (1981). The latter authors have mapped siliceous veins associated with the Midian peralkaline-granite complex which, like those at Ngoye, are comprised of at least 50% quartz, with lesser amounts of feldspar, zircon, allanite, sphene and calcite. Geochemical analyses of the Saudi Arabian occurrences reveal their peraluminous nature and extreme enrichment in Zr, Nb, Y, U and Th (Table 4.5). However, alkalis and fluorine are notably depleted relative to the associated granites. The suggested mode of origin is that such rocks form from a volatile-rich phase related to the peralkaline Midian granite, in which the compatibles are mobile, as fluoride, alkaline or carbonate complexes (Harris, 1981). The extreme depletion of F and alkalis (and hence the peraluminous chemistry) are ascribed to the complexing elements (F, Na, K, CO₂) having left the system after depositing the highly charged lithophiles (Harris *op. cit.*).

Comparison of the Ngoye magnetite-quartz rocks with the data presented by Harris & Marriner (op. cit.) and Harris (op.cit.) reveals the following striking similarities:

- (i) the Ngoye samples always contain modal zircon while sphene is also commonly present;
- (ii) they are highly enriched in incompatibles and are highly radioactive;
- (iii) alumina saturation is variable, although generally of peraluminous nature;
- (iv) the Ngoye rocks are highly depleted in alkalis;
- (v) a low F content is inferred from the virtual total lack of fluorite in thin sections, compared with the peralkaline granites which frequently have modal fluorite up to 1%;
- (vi) calcite is sometimes present, indicative of a CO₂ volatile phase and
- (v) outcrops of the magnetite-quartz rocks are always intimately associated with peralkaline granites on the southern flanks of the Ngoye massif.

Thus, in conclusion, it is apparent that the magnetite quartz rocks are very similar to the Saudi-Arabian siliceous veins, and likewise probably represent late stage liquids and volatiles derived from the crystallization of peralkaline magma. The extremely high incompatible element concentrations are consistent with this mode of derivation, while the low alkali contents may be ascribed to removal of the Na and K as volatile phases.

Chapter 5

GEOCHEMICAL TECTONIC CLASSIFICATION OF THE NGOYE GRANITOIDS

5.1 Introduction

Iddings (1892) classified igneous rocks into two major groups, alkali and subalkali. Following this, Harker (1897) and Becke (1903) noted that the folded mountains of the circum-Pacific orogenic belt were characterized by sub-alkali igneous rocks, while the islands of the non-orogenic Atlantic basin were dominated by alkali rocks. These two divisions were accordingly referred to as "Pacific" and "Atlantic" (Harker, 1897). A refinement of this classification introduced by Benson (1926) recognised two broadly different igneous suites related to tectonic settings. The first he termed "Cordilleran, always formed during a period of great lateral pressure," and the second he termed "Lacomorphic" magmatism, which is "not accompanied by marked lateral pressure." (Benson, 1926, pp. 5-6). Although he did not relate these suites to petrographic provinces, he suggested that the tectonic settings "controlled in some degree, the processes of magmatic differentiation" (Benson, *op.cit.*, p. 77). Subsequent workers, eg. Barth (1962) have reviewed Harker's two-fold subdivision and emphasized the correlation between "Pacific" type and orogenic activity, as well as between "Atlantic" type and non-orogenic activity.

It must be stressed that the simple two-fold subdivisions discussed above are arbitrary, and that transitional rock types and tectonic settings must occur between the two extreme end members. The purposes of this chapter is to evaluate the chemical and mineralogical features of the Ngoye granitoids

and compare these data with "tectonic setting" parameters derived by other workers.

5.2 Tectonic Classification Schemes

One of the first quantitative evaluations of the relationship between plate-tectonic setting and chemical compositions of associated igneous rocks was by Martin and Piwinskii (1972). They postulated a two-fold classification, i.e.; a calcalkaline suite related to convergent, compressional plate boundaries, and an alkaline suite associated with divergent, extensional plate boundaries. Subsequent work by Petro et al. (1979) substantiated the chemical signatures described by Martin & Piwinskii. The most important contributions of these authors are outlined below and compared with the Ngoye granitoids.

5.2.1 Differentiation Index

Martin and Piwinskii (1972) distinguished between orogenic and anorogenic-related igneous suites on the basis of the differentiation index, where $DI = \text{normative } Q + Or + Ab$. They found on the basis of the frequency distribution of DI that unimodal (intermediate) distributions are typical of orogenic suites whereas bimodal (acid-basic) distributions characterize anorogenic suites (Fig. 5.1). However, unimodal acid (high DI) distributions in areas dominated by granites (*sensu stricto*) may be ambiguous (Petro et al., 1979). By comparison, (Fig. 5.1) the Ngoye data do not provide conclusive evidence as to their tectonic origin, although they bear some resemblance to the acidic portion of the proposed anorogenic distribution.

5.2.2 AFM Diagrams

Martin and Piwinskii (*op. cit.*) and Petro et al. (*op. cit.*) state that igneous rock suites related to extensional tectonic environments have more scatter along the AF tie-line of AFM diagrams than do compressional suites and show very little Mg enrichment. Inspection of their proposed fields (Fig 5.2) reveals a considerable amount of overlap towards the A apex of the triangle. The Ngoye granitoids occupy an extended linear area along the A-F tie line,

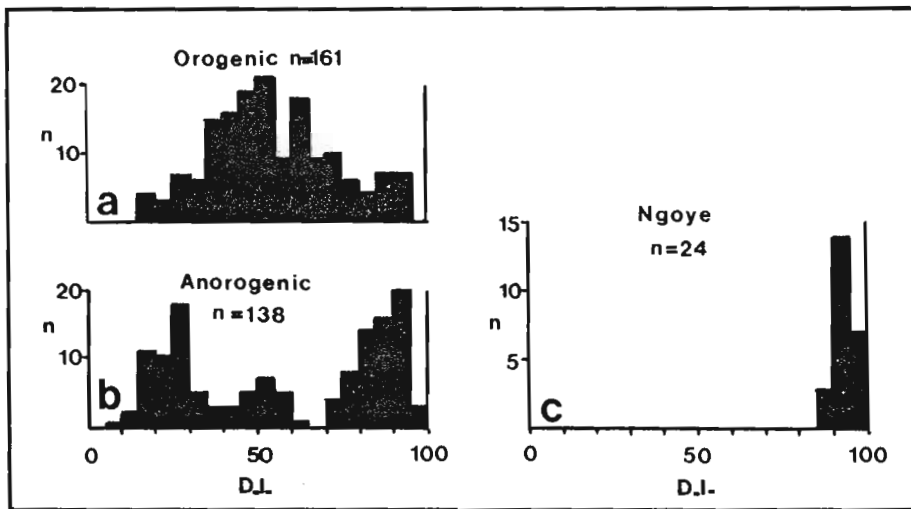


Fig.5.1. Histogram showing the distribution of chemical analyses in terms of the differentiation index (DI of Thornton & Tuttle, 1960). Fig. 5.1a is from the Aleutian Islands orogenic-related suite; Fig. 5.1b is the Iceland anorogenic suite; and Fig. 5.1c is the distribution of Ngoye analyses.

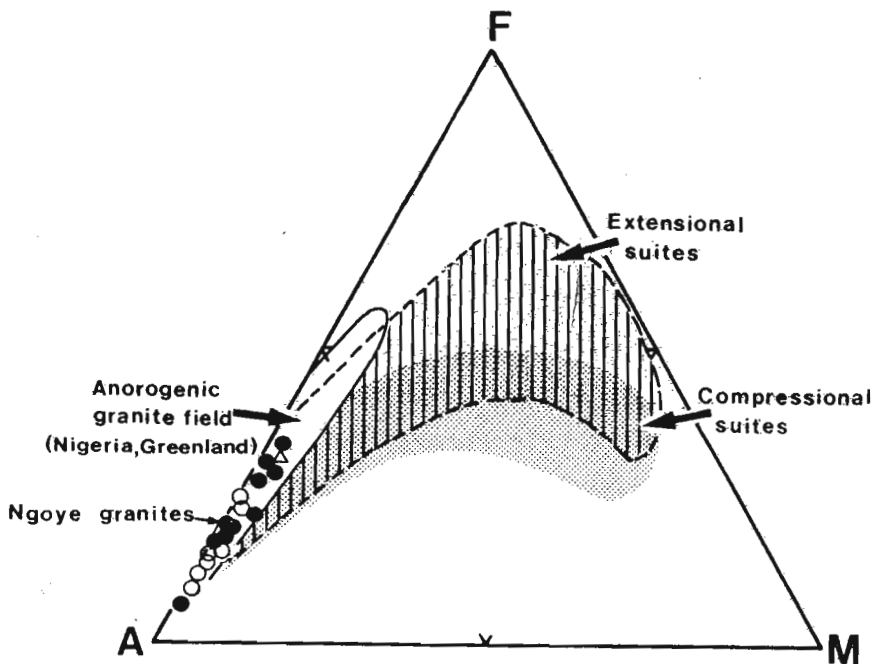


Fig.5.2. AFM ternary diagram illustrating compressional and extensional-suite trends, after Petro et al. (1979). The anorogenic-granite field is from Collerson (1982). Symbols for the Ngoye granitoids as in Fig.4.3. A= $K_2O + Na_2O$; F= total iron as FeO; M= MgO.

within the field defined by Collerson (1975) for granitoids from Nigeria and other anorogenic provinces. Although the Ngoye data are ambiguous and occupy the overlap between extensional and compressional fields, the extremely low Mg content of these samples is consistent with emplacement within an extensional environment (Fig. 5.2).

5.2.3 Calc-Alkaline Index

Petro et al. (1979) using analyses from known tectonic settings, found that the Peacock calc-alkali index could be applied as an index for compressional suites (ALI = 60 to 64) and extensional suites where ALI < 56. This is analogous to saying that compressional suites are calc - alkaline, whereas extensional suites are alkaline and characterized by depressed CaO relative to alkalis. By comparison, the highly alkaline (ALI = 36) Ngoye granites were probably emplaced within an anorogenic environment. Petro et al. (op. cit.) have portrayed the above graphically, (Fig. 5.3), on a $\text{CaO}/(\text{Na}_2\text{O} + \text{K}_2\text{O}) - \text{SiO}_2$ diagram. This displays the relatively low CaO content relative to alkalis which is considered diagnostic of extension-related igneous suites. When plotted on this graph the Ngoye granitoids may be considered to yield a trend similar to that of the type extensional suites, although they plot predominantly in the overlap zone defined by the two trends.

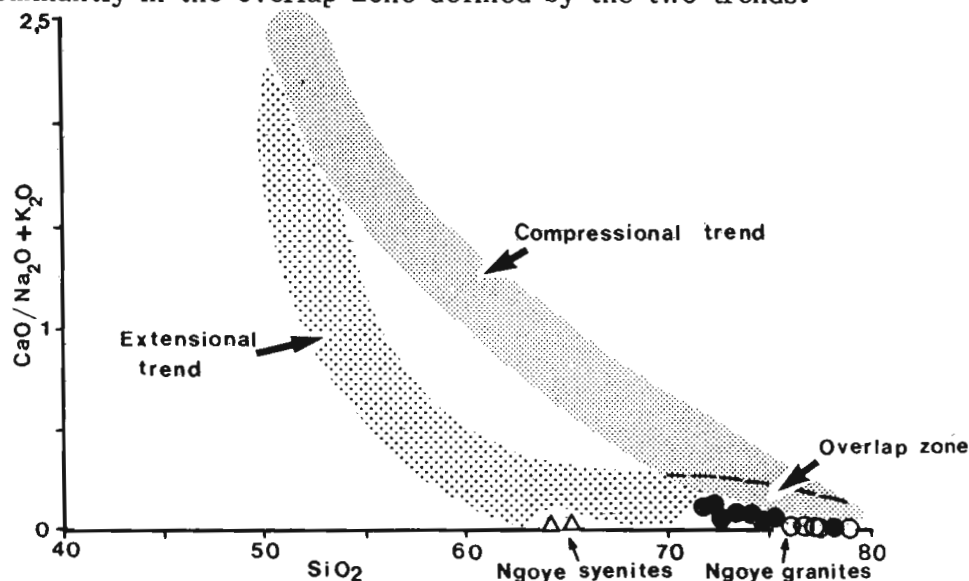


Fig. 5.3. Variation diagram for $\text{CaO}/(\text{Na}_2\text{O}+\text{K}_2\text{O})$ vs SiO_2 . Approximate compressional and tensional trends after Petro et al. (1979), from the Sierra Nevada and Iceland-Greenland suites respectively. Note that the Ngoye analyses plot in the overlap zone between the two trends, symbols as in Fig. 4.3.

5.2.4 Alumina Saturation

Petro et al. (op. cit.) plotted frequency distributions of peraluminous, metaluminous and peralkaline granitoids and were able to show that only extensional suites have associated peralkaline magmatism. Moreover, whereas peraluminous and metaluminous rocks are common to both settings, compressional suites tend to have higher frequencies of peraluminous lithologies. In addition, Bailey and Macdonald (1970) have shown that peralkaline rhyolites, generally considered to be equivalent to peralkaline granites, may be subdivided into two groups, namely continental and oceanic comendites (Fig. 5.4). They found that;

- (i) Continental comendites have a strong correlation with experimentally determined quartz-feldspar minima; and that
- (ii) Oceanic specimens have a wide compositional spread from trachytic towards the quartz feldspar cotectic zone.

The Ngoye peralkaline granites, when plotted on Figure 5.4 cluster within Bailey and Macdonald's (op. cit.) continental comendite field. The authors also point out that when total iron as FeO is plotted against agpaite index, the continental comendites have a good positive correlation with peralkalinity, whereas the oceanic varieties have highly variable, scattered iron contents (Fig. 5.5). The Ngoye data when plotted in Figure 5.5 have a fairly good positive correlation ($r = 0,63$), with a very similar trend to that proposed for continental comendites by these authors. A pronounced continental signature is thus apparent for Ngoye peralkaline granites.

5.2.5 Parameters to distinguish granite (sensu stricto) environments

However, Petro et al. (1979) noted that whereas their "type" suites contained a wide range of rock compositions, in many areas granites are the predominant and often only type present. Therefore they attempted to differentiate between variables from granites (sensu stricto) derived from known tectonic settings. They randomly extracted data from granites in the

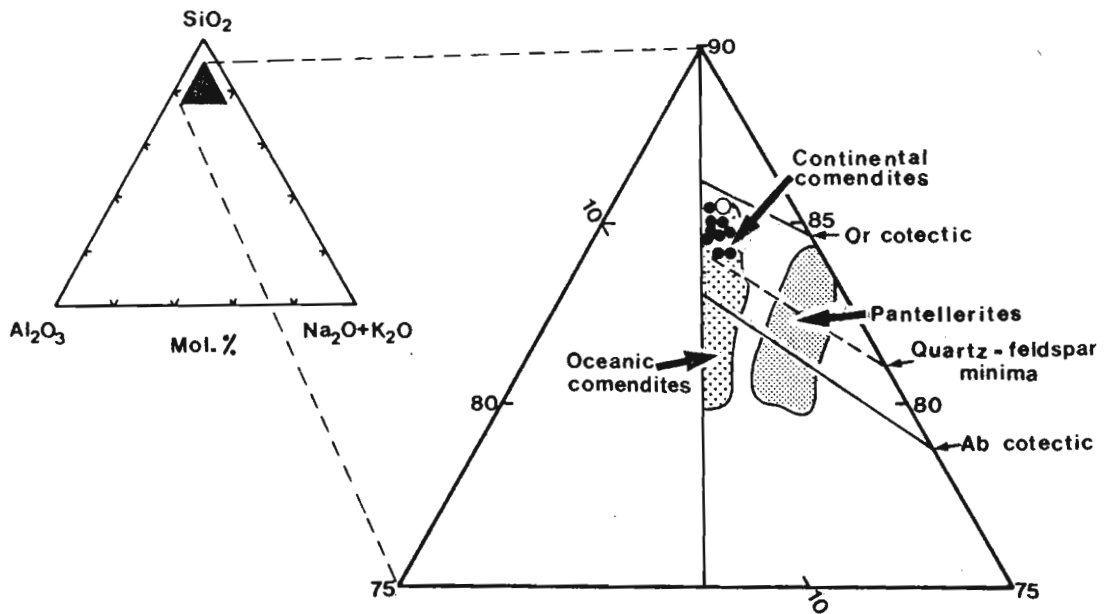


Fig.5.4. Plot of molecular SiO₂, Al₂O₃, and (Na₂O+K₂O) for comenditic and pantelleritic obsidians. The comendite and pantellerite fields are represented by widely and closely spaced dots respectively, after Bowden (1974). The typical Sardinian comendite is represented by an open circle (Bowden, 1974), Ngoye peralkaline granitoids by closed circles. The basic diagram is modified from Bowden (op. cit.).

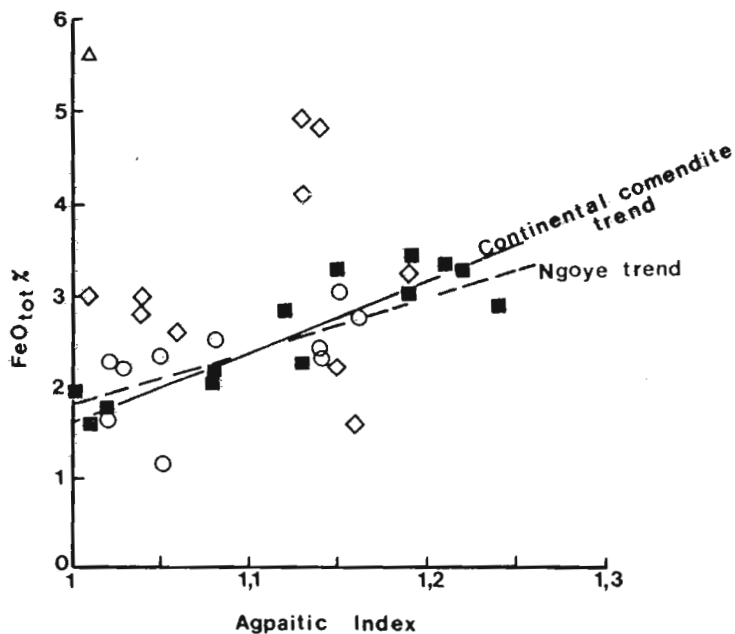


Fig.5.5. Diagram showing variation of total iron (as FeO) against agpaitic index. The solid line represents the axis of distribution of continental comendites (solid squares) after Bailey & Macdonald (1970). The dashed line is the calculated trend ($r=0,63$) for the Ngoye peralkaline samples (open circles). Oceanic comendites are given as open diamonds. The diagram is from Bailey & Macdonald (1970).

70 to 75% SiO₂ range and computed the average chemical variables shown in Table 5.1. Petro et al. (1979) considered the parameters most significantly different to be D.I., CaO, total alkalis, Ca/(Na₂O + K₂O) and FeO^(tot) / (Fe^(tot) + MgO) (Petro et al., 1979). In order to test the effectiveness of these discriminants, a graph of CaO/Na₂O + K₂O versus FeO^(tot)/FeO^(tot) + MgO was plotted (Fig. 5.6). In addition to the average Ngoye granite, several Cape Granite analyses were plotted (data from Schoch et al., 1977). The following points are noted:

- (i) based on the Ca/alkali ratios alone, the majority of the Cape granites are tension-related,
- (ii) when the FeO/FeO + MgO ratio is applied then most of the Cape samples are compressional granites and
- (iii) the average Ngoye sample plots close to the proposed tensional granites.

The Cape granites are therefore clearly ambiguous, and indicate that the parameters suggested by Petro et al., (op. cit.) should be treated with caution when evaluating tectonic settings of granite bodies. Nevertheless, the close correspondence of the Ngoye analyses with data from classical type-localities is strongly indicative of their "extensional" character (Table 5.1).

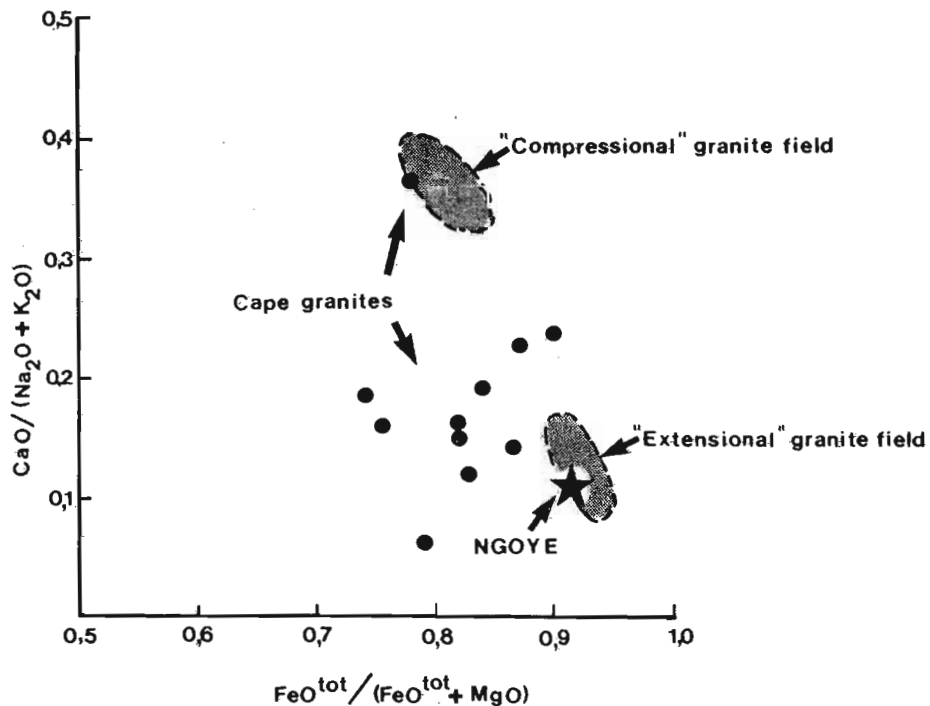


Fig. 5.6. Diagram showing the discrimination of "type" extensional and compressional granites (within the 70-75% SiO₂ range) on the basis of parameters suggested by Petro et al. (1979). The average Ngoye analysis (n=5) is represented by a closed star, while Cape granites from Schoch et al. (1977) are closed circles.

TABLE 5.1

Comparison of variables for granites in the SiO₂ range 70 - 75%

	average anorogenic n = 40	average Ngoye n = 5	average compressional n = 40
DI*	90,42	90,65	83,22
Al ₂ O ₃	13,29	12,82	14,43
FeO	2,79	3,00	2,19
MgO	0,27	0,27	0,53
CaO	1,05	1,00	2,31
Na ₂ O	4,07	4,12	3,81
K ₂ O	4,43	4,73	3,02
TiO ₂	0,28	0,35	0,26
Na ₂ O + K ₂ O*	8,50	8,85	6,83
CaO			
Na ₂ O + K ₂ O	0,13	0,11	0,36
FeO			
FeO + MgO	0,92	0,92	0,81

Notes:

* indicates parameters considered most significant by Petro *et al.* (1979) for discriminating between granites from contrasting tectonic environments.

DI = differentiation index.

FeO = total iron as FeO.

The average anorogenic and average compressional related granites are from Petro *et al.* (op. cit.), p. 229.

5.2.6 QAP diagram

Although never intended for use other than systematic igneous rock classification, Lameyre and Bowden (1982) recognized on Streckeisen's QAP modal diagram four distinct trends for rock suites from geochemically and tectonically distinct regions (Fig. 5.7). These suites are characterized as follows:

- (a) Calc-alkaline trends which range from early-orogenic low-K, to late-orogenic high-K magmatism, the granitoid rocks varying from granodioritic to monzonitic respectively;
- (b) Alkaline series granitoids which lie on or above the A-P silica-saturation line and show quartz enrichment only along the A-Q join. Such suites are usually located in areas of continental rifting (eg: Nigeria), and are late orogenic or anorogenic;
- (c) Tholeiitic series which follow the P-Q boundary in the Streckeisen diagram and include plagiogranites from the Skaergaard intrusion; and
- (d) Mobilizates - these are leucogranites and quartzofeldspathic leucosomes developed in migmatitic terrains. Characterized by peraluminous chemistry, their modes occupy a restricted field aligned parallel to the A-P base of the QAP triangle. They are not comagmatic with basic and intermediate rocks.

When plotted on the QAP diagram, the Ngoye granitoids coincide with the calcalkaline monzonitic, alkaline-silica oversaturated, and mobilizate fields (fields 4, 5 & 6 respectively, Fig. 5.7). The wide range of silica contents, the presence of basic (monzodioritic) rocks within the Ngoye formation, and the lack of migmatites precludes the derivation of these rocks solely by crustal anatexis (Lameyre & Bowden, op. cit.) The conclusion, therefore, is that the Ngoye granitoids are in fact coincident with the calc-alkaline monzonitic and alkali-silica oversaturated fields proposed by Lameyre and Bowden (op. cit.). This is indicative of a late-orogenic to post-orogenic (or anorogenic) time of emplacement for the rocks examined.

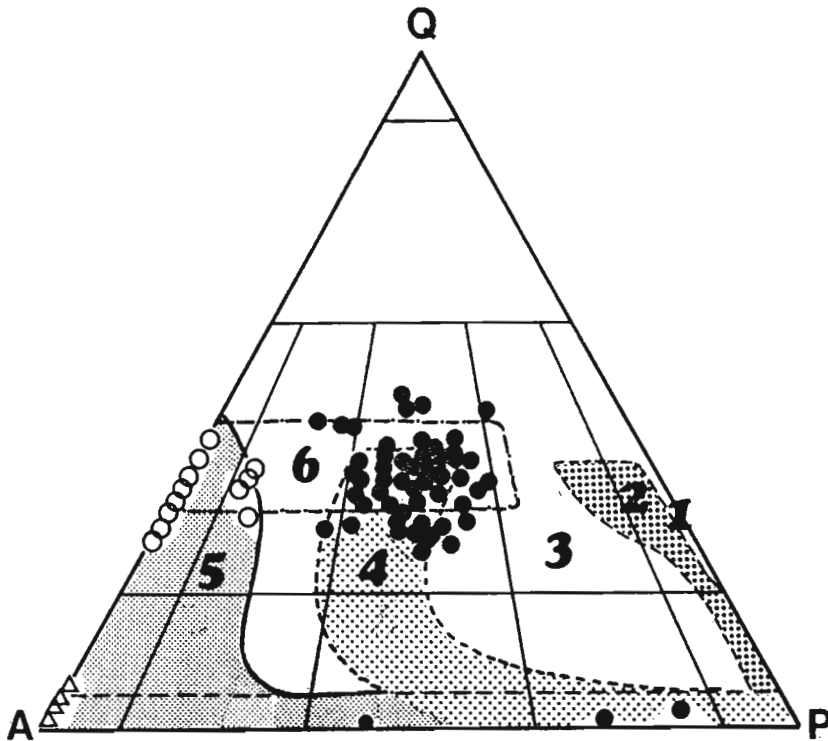


Fig. 5.7. QAP modal diagram showing fields of various granitoid series, after Lameyre & Bowden (1982). They are numbered as follows: 1, tholeiitic; 2, calc-alkaline (low K); 3, calc-alkaline granodioritic (medium K); 4, calc-alkaline monzonitic (high K); 5, aluminous, alkaline and peralkaline of the alkaline provinces; 6, overlapping field of granitoids formed by crustal fusion. Ngoye modal analyses; closed circles=non-peralkaline granitoids; open circles=peralkaline granitoids; triangles=syenite.

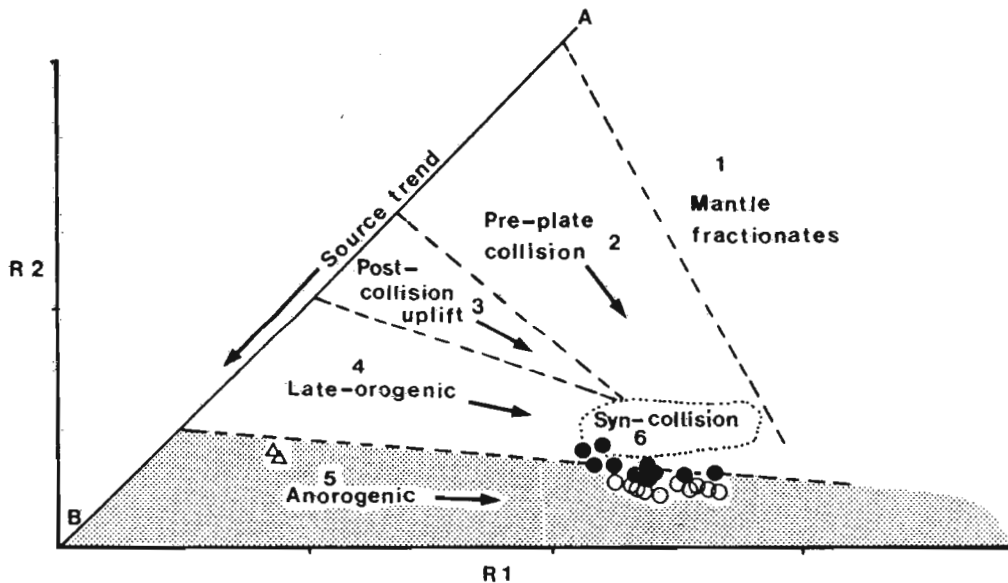


Fig. 5.8. Petrogenetic classification of granitoid series using the R1-R2 multicationic diagram, after Batchelor & Bowden (1985). The major granitoid associations (eg, Pre-plate collision) are from Pitcher (1983). The petrological equivalents are: group 1 = tholeiitic; group 2 = calc-alkaline low-and medium-K; group 3 = calc-alkaline high-K; group 4 = monzonitic; group 5 = alkaline and peralkaline; group 6 = anatectic granites (Lameyre & Bowden, 1982). Symbols as in Fig. 5.7.

5.2.7 Multicationic R1 - R2 diagram

Batchelor & Bowden (1985) have amended the De La Roche et al. (1980) R1 - R2 diagram so that 6 tectonically distinct igneous rock groups are defined (Fig. 5.8). They propose that the line A-B in Figure 5.8 is indicative of a change in source composition through an orogenic cycle. Any trends perpendicular to this are referred to as series trends. Concomitant with the change in source composition along line A-B, Batchelor and Bowden noted a change in tectonic setting of magma generation, from group 2 (subduction, pre-plate collision) to the late orogenic plutons of group 4. Group 5 is representative of anorogenic/post-orogenic "A" type magmas, whereas syn-collision "S" type granitoids are allocated to group 6 which is also the minimum melting or granitic composition of Tuttle & Bowen (1958).

The Ngoye analyses suggest two series trends on the R1 - R2 diagram (Fig.5.8). The non-peralkaline Ngoye granites straddle the late-orogenic/anorogenic boundary, while the peralkaline granites and peraluminous syenites fall within the anorogenic field proposed by Batchelor and Bowden (op. cit.).

The data may be interpreted according to the R1 - R2 diagram as follows :

- (a) that the Ngoye non-peralkaline granites are possibly late orogenic and
- (b) that the syenites, peralkaline granites and magnetite-quartz rocks are possibly post-orogenic in nature.

5.2.8 Trace-element tectonic discriminants for granitoids

Trace element diagrams have been used for some time as a means of distinguishing the tectonic settings of the basic extrusives. Their application to granitic rocks, however, has been hampered by (a) the difficulty of sampling granites of known tectonic setting due to the long time interval between emplacement and final exposure at the surface and (b) the highly complicated petro-genetic history of granites which is often modified by

crustal assimilation (Pearce et al., 1984). This led Pearce and coworkers to adopt the approach of grouping Phanerozoic granites of well-known tectonic setting, and statistically investigating their trace element characteristics and mineralogy. Some 600 analyses were grouped into four major types:

- (i) Ocean-ridge granites (ORG) - these are the so called plagiogranites, falling into Streckeisen's quartz diorite and tonalite fields. They may be metaluminous or peraluminous with hornblende the dominant mafic mineral and are calcic or calc-alkaline according to the Peacock alkali-lime index;
- (ii) Volcanic-arc granites (VAG) - these are similar to ORG but vary from quartz diorite to tonalite and granodiorite, while hornblende is still the principle mafic constituent. These rocks are generally metaluminous and calcic according to Peacock's lime index;
- (iii) Collision granites (COLG) - these have been subdivided by Pearce et al. into (a) syntectonic types that plot in Streckeisen's granite (*sensu stricto*) field and comprise S-type, peraluminous, muscovite-bearing granites, and (b) a post-tectonic group falling in the quartz diorite, tonalite and granodiorite fields which, according to Shand's alumina saturation index, are predominantly metaluminous. In addition, they are characteristically hornblende and biotite bearing, and thus similar to the I-type granites of Chappell & White (1974);
- (iv) Within-plate granites (WPG) - these have been divided on the basis of their mineralogy into (a) those intruded into continental crust of normal thickness, as well as into oceanic lithosphere, which have sodic amphiboles and pyroxenes as typical coloured-mineral phases. They constitute alkalic suites characterized by highly variable alumina saturations and vary from peraluminous to peralkaline. The second subgroup (b) comprises those intruded into highly attenuated continental crust and are characterised by calcic amphiboles and pyroxenes.

To illustrate the salient features of the chemical analyses associated with those four major groups, Pearce *et al.* (op.cit.) plotted ORG/normalized trace element diagrams (Fig. 5.9).

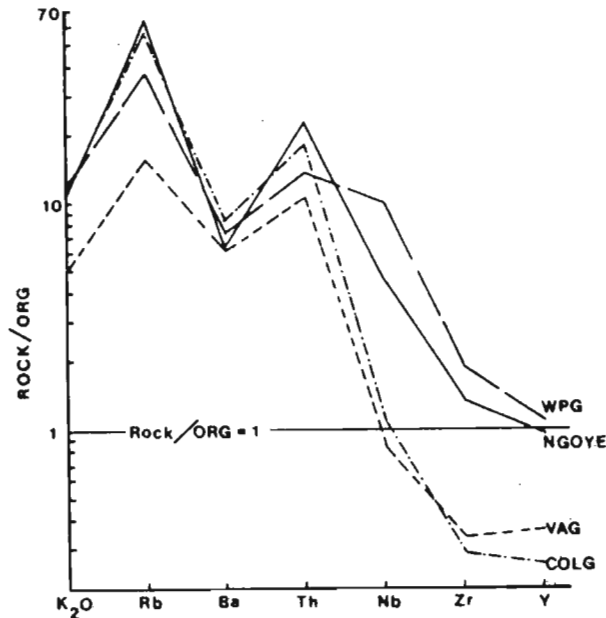


Fig. 5.9. Ocean ridge granite (ORG) normalized trace element patterns for average analyses from Pearce *et al.* (1984). The average Ngoye analyses are included for comparison.

- (i) VAG have enhanced K_2O , Rb and Th whereas Nb, Zr and Y are depleted;
- (ii) COLG are similar to VA granites but are characterized by exceptionally high Rb; and
- (iii) that WPG are highly enriched in K_2O , Rb, Th and Nb while Zr and Y are similar to ORG concentrations.

When the average ORG - normalized Ngoye data are plotted on Figure 5.9 a pronounced WPG signature is evident, though Nb, Zr and Y are marginally lower than the average WP granite of Pearce *et al.* (1984).

The latter workers further demonstrate, by plotting Y, Nb and Rb against SiO_2 , that, (a) Y and Nb are generally higher in ORG and WPG than in VA granites and, (b) that Rb is an excellent discriminant between ORG and WPG,

and also between COLG and VAG. Inspection of Figures 5.10 (a) and 5.10 (b) shows that Ngoye granitoids have within-plate characteristics, although the elevated Rb concentrations in Figure 5.10 (c) are similar to those of COL granites (Pearce et al., 1984).

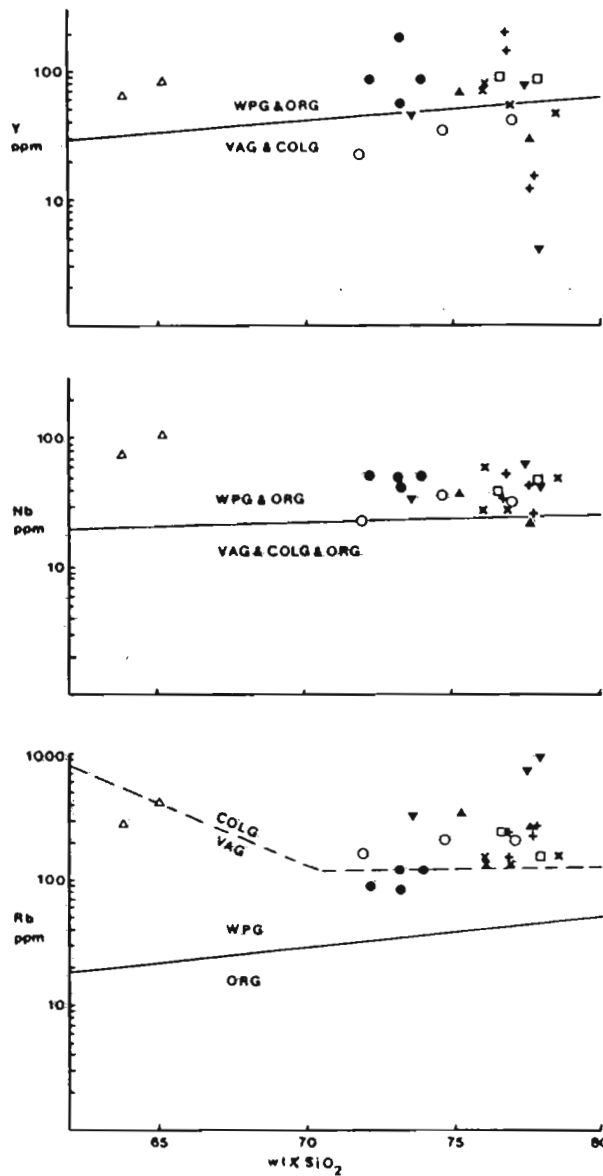


Fig. 5.10. Variation diagrams of Y, Nb and Rb against SiO_2 for Ngoye granitoid analyses. Boundaries between proposed tectonic settings from Pearce et al. (1984), for discussion see text. Ngoye symbols as in Fig. 4.5.

Further to the above findings, these workers concluded that, of the elements studied, Rb, Y and Nb contents were the most effective discriminatory parameters in granite analysis. Thus, in general, plots of Nb against Y (Fig. 5.11 a) provide a clear separation of VAG and WPG whereas there is blurred overlap between WP and OR granites (Pearce et al., 1984). However, as these workers point out, this zone of overlap is of no significance since WP and OR granites have highly contrasting petrographical characteristics. The plotting of Ngoye analyses on this bivariate diagram (Fig. 5.11a) shows that most samples have a strong affinity for the WPG/ORG overlap zone, with only a few falling marginally into the VAG + COLG field. However, based on their mineralogy, all Ngoye samples in the overlap zone can be classified as having WPG characteristics on the presence of sodic amphiboles, as well as granite (*sensu stricto*), syenite and alkali granite modal compositions (Pearce et al., *op. cit.*).

Pearce et al. (1984) considered the most successful discriminatory diagram to be a plot of Rb against Nb + Y (Fig 5.11b). They found that these parameters gave virtually complete separation of their type magmas. It is significant that the Ngoye samples, when plotted on this graph exhibit an extremely strong affinity for the WPG field. Moreover, while they cluster around the Nigerian and Skye suites (continental crust environment), none of the Ngoye analyses plot in the Ascension Island field (oceanic crust environment), see Fig. 5.11b. This is a reflection of the enhanced Rb content in Ngoye granitoids, which has been ascribed to contamination of mantle-derived magmas by continental crust (Pearce et al., 1984). Therefore, the use of trace-element discrimination diagrams reveals a pronounced within-plate (WPG) signature for most of the Ngoye samples, although the muscovite-bearing granites exhibit collision-granite (COLG) tendencies.

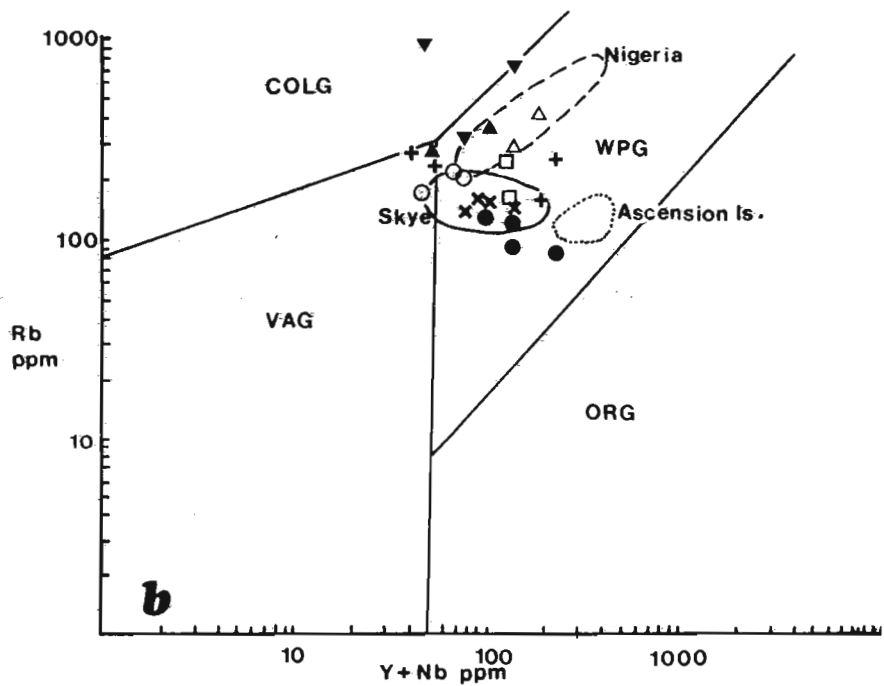
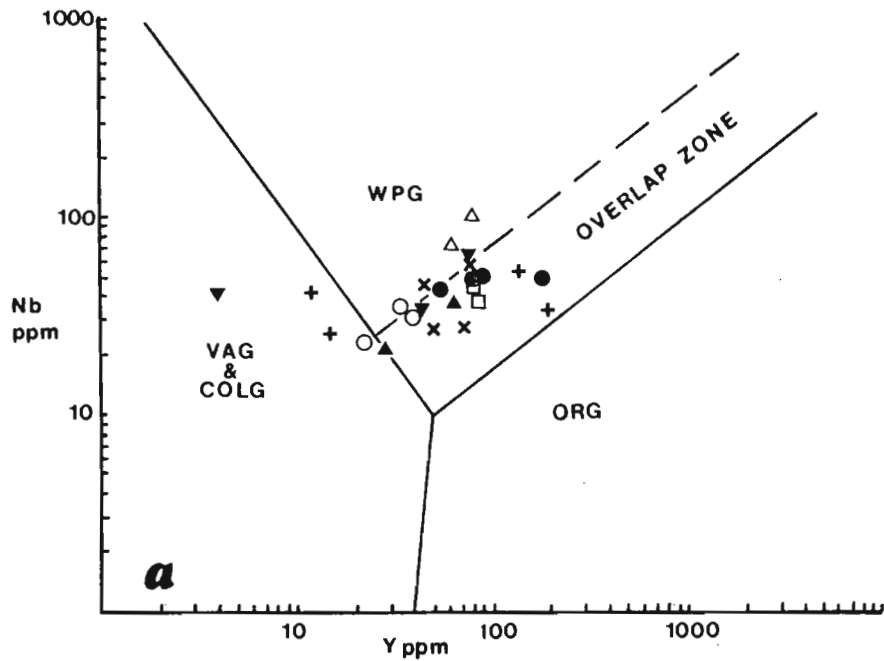


Fig. 5.11. Nb - Y, Fig.5.11a; and Rb - Y+Nb, Fig.5.11b discriminant diagrams for collision granites (COLG); volcanic-arc granites (VAG); within-plate granites (WPG); and ocean-ridge granites (ORG). For comparison the Ngoye granites are plotted, and display similarities with the Nigerian and Skye granitoid fields of Pearce *et al.* (1984).

Chapter 6

STRUCTURAL GEOLOGY

6.1 Introduction

The object of this section is to relate the structural evolution of the study area to the formation and metamorphism of the Ngoye granitoids and its surrounding country rocks. In this respect the intrusion of the Ngoye granitoids as well as later overthrusting and associated mylonitization provide the basic structural framework. Within this framework, the major fold and fabric elements and how they may be separated from one another on a time basis are discussed with respect to descriptive structural geology.

6.2 Terminology

The term foliation is used here in the sense of Turner and Weiss (1963) to describe all types of mesoscopically recognisable s-surfaces of metamorphic origin. The term therefore covers schistosity, crenulation cleavage, axial plane cleavage and gneissose foliation. The s-surfaces are referred to as $S_0, S_1 \dots S_n$. S_0 refers to a bedding or original surface, while S_1 is the earliest recognisable s-surface related to a tectonic origin. Successive subscripts denote the relative order of development. In some cases however, it was not possible to distinguish between various s-surfaces due, for example, to the effect of transposition layering.

Following Turner and Weiss (1963) and Hobbs et al. (1976), the term "lineation" is used in this study to embrace linear features which are

penetrative in hand specimen and in small outcrops. This term includes several varieties, eg: intersection of s-surfaces, linear preferred orientation of prismatic minerals and elongate mineral aggregates. On a mesoscopic to macroscopic scale (see below), fold axes, mullions and rods are referred to as linear structures (Hobbs et al., 1976) as opposed to lineations. As in the case of s-surfaces, successive generations of lineations, ie: $L_1, L_2 \dots L_n$ denote order of development, while $B_1, B_2 \dots B_n$ are applied to fold axes.

The term "fold" implies a geometric deviation from an original planar, surface, ie: a curve. In this section it is felt that the earliest identified folds (F_1) conform to this definition (in that it has affected a pre-existing planar surface, S_0) while subsequent episodes of folding ($F_1, F_2 \dots F_n$) are viewed as having refolded existing folded surfaces. The term "deformation" implies a metamorphic, that is a thermal and structural event. These individual and consecutive events are designated D_1, D_2 etc., (Table 6.1).

The use of an appropriate system is of paramount importance in structural geology. In this chapter the nomenclature of Hobbs et al. (1976) has been adopted. "Microscopic" scale refers to structural features which can only be observed using an optical or electron microscope, eg. the deformational features of individual grains. A "mesoscopic" structure is visible without the aid of microscope, for example a hand specimen or a single outcrop or continuous geological body. "Macroscopic" refers to bodies of rock that are incompletely exposed and from which any interpretation is based on observing a number of outcrops.

TABLE 6.1

Summary of the structural terminology used

Deformation events	D_1	D_2	D_3	D_4
Folds	F_1	F_2	F_3	F_4
Fold-axes	B_1	B_2	B_3	B_4
Lineations	L_1	L_2	L_3	L_4
Axial planes	S_1	S_2	S_3	S_4

6.2.1 Previous investigations

Anderson (1901, p.69) first noted the antiformal nature of the Ngoye hills and stated that "the laminations of the gneisses and schists are usually inclined at a high angle away from the Engoye (sic) Mountains, which form the axis of this metamorphic belt." McCarthy (1961) confirmed Anderson's appraisal of the antiformal Ngoye structure. He also pointed out that the "form of the granite gneiss is concordant with the foliation and structure of the schists" surrounding it (McCarthy, 1961, p.26). Following a comprehensive investigation of the northern margin of the Namaqua- Natal Mobile Belt, Charlesworth (1981) recognised the following structural sequence:

- (i) an early prograde tectono-thermal event (D_1), characterized by isoclinal folding and widespread transposition of lithological layering (within the Ngoye granite and surrounding rocks) into S_1 ;
- (ii) a second event, D_2 , caused by large-scale northward overthrusting when S_1 is deformed into east-west trending folds;
- (iii) thrust planes late in the D_2 event truncate earlier D_2 structures and mylonites were developed along thrusts, sometimes associated with retrogressive metamorphism and,
- (iv) late stage D_3 warping about north-south axes.

My research has indicated four structural events in the Ngoye area, and furthermore that the Ngoye granite was intruded after the D_1 event. These divisions are summarized in Table 6.2.

6.3 D_1 event

The oldest observed penetrative planar fabric (S_1) occurs in the amphibolitic country rocks which surround the Ngoye massif. This deformational phase has been recognised in the field by the local survival of small rootless (intrafolial) folds, designated F_1 . These, as shown in Plate 9a,

TABLE 6.2

Summary of deformational events in the Ngoye area

Rock type	Macroscopic effect	Mesoscopic effect	Structural fabric	Event	Grade
Granite and country rocks			all previous fabrics deformed about a N-S axis.	D4	
Ngoye Granite	kilometric, E-W trending lateral shears	1) conjugate ductile shears 2) late crenulations	intense mylonitic fabrics S3 parallel to S2, also along conjugate shear directions. Development of composite fabrics in mylonites. Extensional L3 lineations	D3	retrogressive to lower amphibolite
Country rocks		1)conjugate brittle shears			
Ngoye granite	folded into a tight, E - W trending anti-form structure		pervasive S2 axial-planar fabric; alignment of elongated mafic aggregates	D2	
Country rocks	S1 foliation is folded into a W-plunging closure around western end of massif	moderate to tight folds about E-W axes and deform S1	local S2 axial-planar fabric, L2 & B2 lineations and fold axes		Amphibolitic T=500-600 C P = 4 - 5 kb
Intrusion of Ngoye granites					
Country rocks, biotite schist & amphibolite	widespread transposition of lithological layering	intrafolial F1 folds	S1 axial-planar surfaces, L1 lineations and B1 fold axes	D1	prograde to amphibolitic

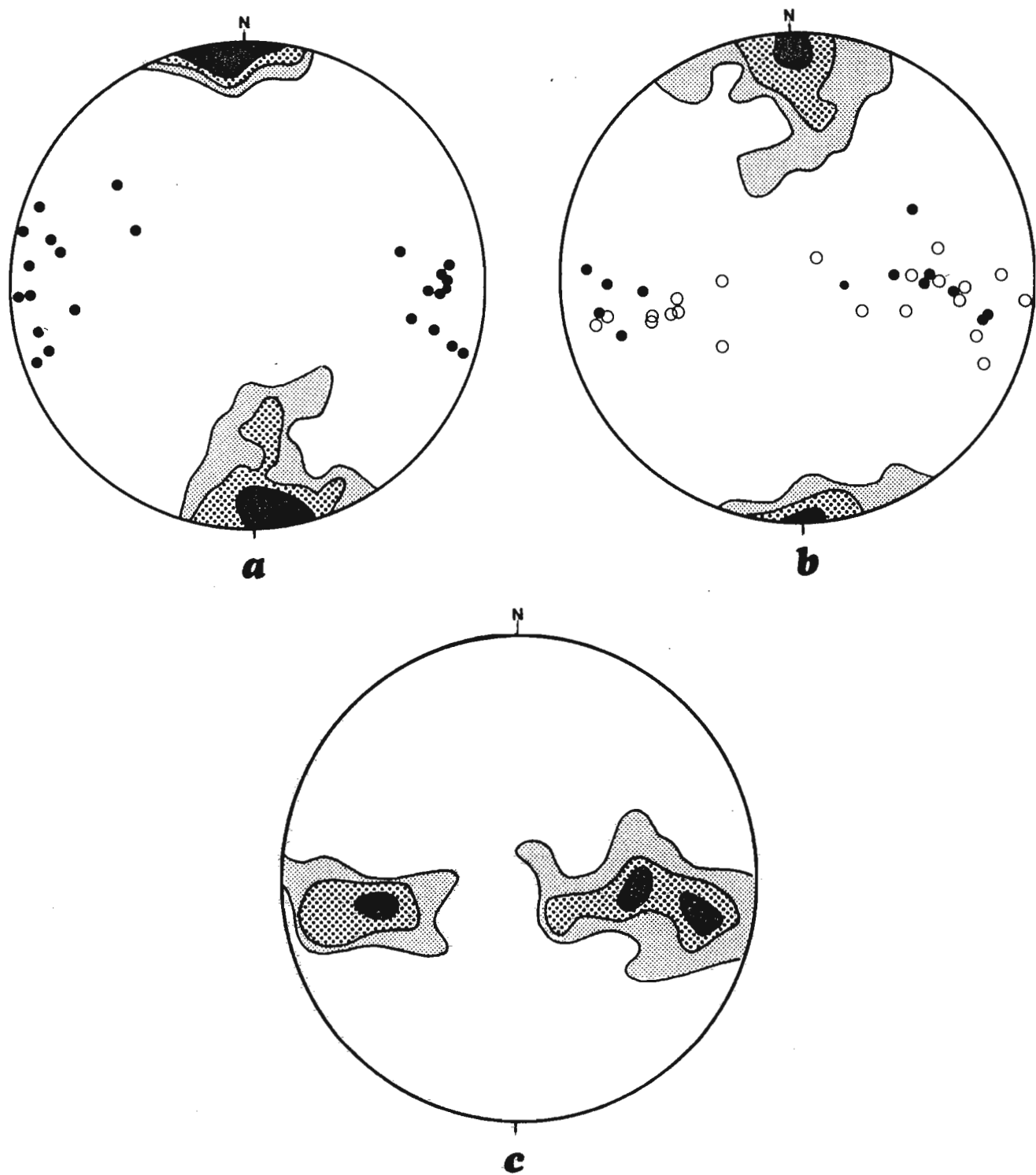


Fig. 6.1. Stereographic plots of structural data from the amphibolitic terrain surrounding the Ngoye Granite Gneiss Formation. Figs. 6.1 (a) and 6.1(b) show the distribution of poles to 70 S_1 and 96 S_1 foliation planes from the western and eastern domains respectively. Fig. 6.1(c) shows the the distribution of 34 B_2 fold axes and L_2 mineral lineations from the eastern domain country-rocks. All contours at 2,5 ; 5 & 10% per 1% area. See Fig. 6.3 for location of the eastern and western domains. Closed circles are L_2 lineations from the western ($n = 24$) and eastern ($n = 13$) domains respectively. Open circles are B_2 fold axes ($n = 21$) from the eastern domain.

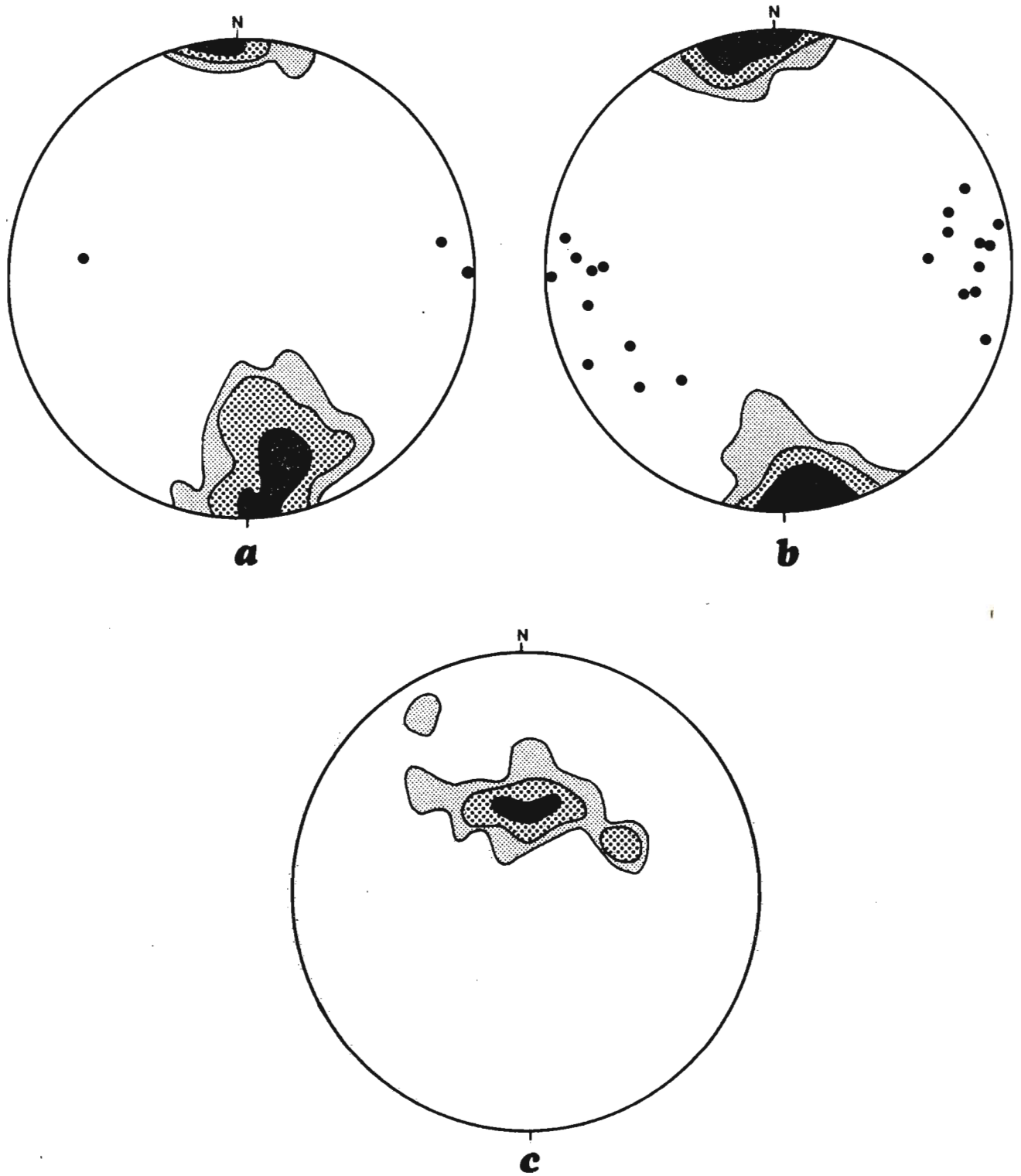


Fig. 6.2. Stereographic plots of structural data from the Ngoye Granite Gneiss Formation. Figs. 6.2(a) and (b) show the distribution of poles to 86 S_2 foliation planes and 176 S_2 foliation planes respectively. Fig. 6.2 (c) gives the distribution of 14 biotite lineations within S_2 planes from the western domain. All contours at 2,5 ; 5 & 10% per 1% area. Closed circles are L_3 mylonitic lineations, elongate mafic aggregates and elongate microcline crystals from the western ($n = 3$) and eastern ($n = 21$) domains, respectively.

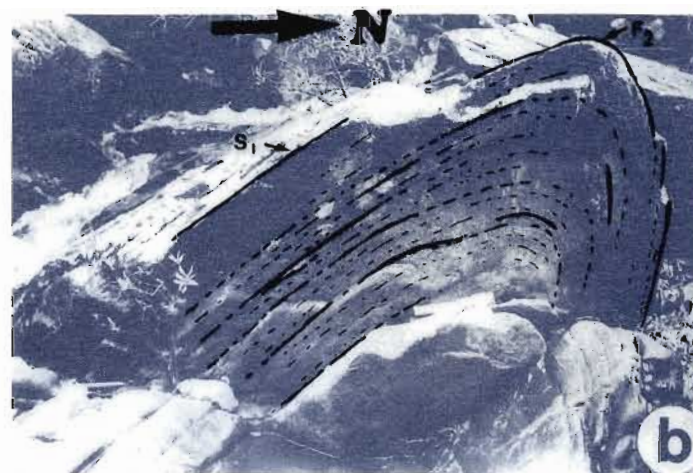


Plate 9. Deformation styles within the study area. The first apparent phase of deformation within the area is recognized by the local survival of small intrafolial folds in the amphibolitic terrain (a), map ref. 12 K. The effects of the second deformation D_2 is illustrated in (b), where the S_1 foliation has been folded into a northward verging F_2 fold (map ref. 27 J, looking West). Post D_2 northward overthrusting was observed in the amphibolitic terrain (map ref. 27 J, looking East) and is shown in (c). Late-stage crenulation of the pervasive foliation within the Ngoye Formation (map ref. 33 F) is illustrated in (d) and may be related to D_3 lateral shearing according to the extensional-crenulation model of Platt (1984). Scale in cm.

126

are considered evidence for the widespread transposition of an original S_0 lithological layering into parallelism with a metamorphic (S_1) axial planar foliation. As pointed out by Charlesworth (1981), the widespread transposition of S_0 into S_1 and subsequent sub-parallel orientation of fold limbs, makes D_1 related fold structures difficult to recognize in the study area. In addition, he proposed that D_1 event was accompanied by prograde M_1 metamorphism, probably attaining amphibolite grade.

6.4 Intrusion of the Ngoye granites

Field evidence, as listed below, strongly indicate that the intrusion of the Ngoye granites postdated the D_1 event:

- (i) biotite-schist (country rock) xenoliths within the granite show evidence of thermal and structural over-printing (see Plate 5 and accompanying description, chapter 2; section 2.3.2)
- (ii) D_1 -related fabrics were not observed in the Ngoye Formation, though this may be a reflection of the lack of colour-contrasted lithologies within the granitic terrain;
- (iii) the deformation of S_1 planar fabrics in the amphibolitic country rocks into an antiformal closure around the western extremity of the massif. In addition, the foliation in the Ngoye range at its western closure is sharply discordant with that in the country rocks (Fig. 6.3).

6.5 D_2 event

Effects of the D_2 event predominate throughout the Ngoye granite gneiss in that it produced a fairly homogenous east-west penetrative planar fabric. The results of this event are recorded somewhat differently in the amphibolitic terrain, which had previously been subjected to the D_1 deformation. Each terrain is discussed independently below.

6.5.1 Amphibolitic country rocks

F_2 fold structures result from the D_2 deformation which has overprinted the D_1 -associated fabrics. The resulting close to tight folds are characterized by interlimb angles between 45° and about 10° . As noted by Charlesworth (1981) an axial planar fabric (S_2) is frequently developed although often not obvious in outcrop. D_2 fold axes, designated B_2 are variable in orientation and, on the stereonet (Fig. 6.1), define two distinct maxima that plunge to both the east and west. L_2 lineations, as defined by elongate hornblende prisms within S_1 and parallel to B_2 are prominently displayed throughout the amphibolitic terrain. In addition, L_2 linear structures in the form of rods, within quartzo-feldspathic horizons characterize these lithologies.

F_2 folds sometimes display pronounced vergence to the North (Plate 9) while S_2 axial planes are steeply inclined to both north and south (Charlesworth, 1981). Continuation of northward translation after the formation of D_2 related structures is illustrated by planar thrusts of possible D_3 age that truncate F_2 folds (Plate 9).

6.5.2 D_2 : Ngoye massif

A pervasive planar fabric within the Ngoye granitoids is marked by elongate lenses and clots of mafic minerals. These define a regional east-west striking, steep dipping foliation that is essentially parallel, or nearly so, to that of the surrounding amphibolitic envelope. As shown in Fig. 6.2, dips in the eastern half of the massif are steeply to north and south, whereas foliations in the western portion are inclined steeply to moderately northwards. A major exception to the general concordance of structures in the massif and envelope occurs at the western extremity of the main body, near Mbangayiya store (Fig. 6.3). Here, as noted in 7.3 above, the east-west foliation in the Ngoye formation is sharply discordant with S_1 foliations in the country rocks, which define an overturned, westerly plunging antiformal F_2 closure around the granitic rocks. This structure indicates that the foliation in the Ngoye granitoids is probably axial planar to the D_2 event.

6.6 D₃ event

The D₃ event is characterized by the development of (a), conjugate north-west and north-east trending mesoscale ductile shear zones and (b) east-west striking, steep dipping, macroscale shear zones in the Ngoye massif. Similar macroscale shear zones along proposed thrust-planes have been described from the amphibolitic terrain around the Ngoye formation (Charlesworth, 1981). In addition, extensional lineations and minor crenulations have been ascribed to the D₃ event.

A summary of the general features regarding shear zones and mylonites is given below, after which an assessment of the Ngoye occurrences is made. Special reference is given to the use of mylonitic microstructures in determining the overall sense of displacement across shear zone, and a comparison made with published data on the subject.

6.6.1 Shear zones: a review

Ramsay & Graham (1970) and Hobbs et al. (1976) have defined a shear zone as a zone in which deformation has taken place by simple shear. Simple shear refers to a type of strain in which particles in a rock are thought to have been displaced along a sequence of parallel planes. Ramsay (1980) divided shear zones into 2 major groups, (a) "zones" of brittle shear (faults) where a clear discontinuity exists between the displaced sides of the "zone" and (b), ductile structures where deformation by ductile (plastic) flow results in no visible discontinuity at outcrop scale. In addition he showed that a ductile shear zone (which is the entire zone of reorientation of fabric) displays maximum displacement in its core where mylonitic rock types may develop subparallel to the shear direction. The core represents the final stage in the growth of a shear zone. Deformed planar surfaces have a characteristic sigmoidal form across the shear zone boundaries (SZB), with surfaces in the core zone approximately parallel to the SZB (Fig. 6.6).

Shear zones may occur as conjugate pairs or in parallel sets. The problem of how shear zones (or bands) develop in gneissose rocks has been addressed for example, by Harris & Cobbold (1984).

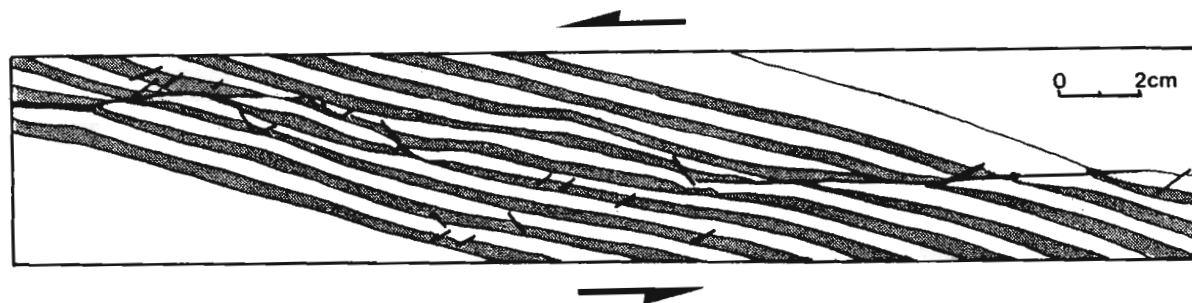


Fig. 6.4. Detail of layered plasticine model, showing conjugate shear zones developed during a bulk sinistral-shearing event. Plasticine layers were originally inclined at 15° to the shearing planes (illustration after Harris & Cobbold, 1984).

They state that conjugate shear bands (in rocks possessing a strong planar fabric) displaying "normal-fault" geometry are often cited as evidence for coaxial shortening (eg, Ramsay, 1980). Harris & Cobbold (op cit.) point out, however, that conjugate shear sets have also been observed in areas having a non-coaxial deformation history. Using layered plasticine models, these authors were able to reproduce the formation of conjugate shears by non-coaxial simple shear (Fig. 6.4). Moreover, and of great significance, the model shear bands always developed at approximately 40° to the plasticine layers, irrespective of initial layer-orientation to the simple-shear direction. They were able to reach the conclusion that conjugate shears are not necessarily diagnostic of a regional bulk coaxial deformation, but may be formed during bulk simple shearing when sliding along a foliation takes place (Harris & Cobbold, op cit.). This agrees with earlier work by White et al. (1980) who noted that shear zones are examples of inhomogeneous deformation initiated by material heterogeneities such as foliations or localized stress concentrations.

6.6.2 Mylonites: a review

Mylonites have been defined as : "narrow planar regions in which deformation is intense relative to the country rocks" (Hobbs et al., 1976, p. 418). This term (from the Greek mylon = mill) was first used by Lapworth in 1885 to describe rocks from the Moine Thrust in Scotland (Bell & Etheridge, 1973). He considered such rocks to have been derived by mechanical crushing, grinding and dragging-out of the country rocks, with only minor recrystallization of the mineral constituents. This emphasis on the mechanical cataclastic derivation of mylonites persisted, and was propagated by authors such as Waters & Campbell (1935) and Higgins (1971). The latter in his lengthy definitive paper on the subject quoted that "...mylonites generally show re-crystallization to a limited degree, but the dominant texture is cataclastic" (Higgins, *op cit.*, p. 7).

This cataclastic, brittle origin of mylonites remained the universal view until relatively recently, when research by Bell & Etheridge, and others in the 1970's indicated syntectonic re-crystallization and ductile deformation as dominant processes in mylonite formation. Bell & Etheridge (1973) described microstructural changes during the progressive mylonitization of an "acid gneiss", noting that the observed structures were comparable with those formed by the ductile deformation of crystalline materials such as metals. They suggested that mylonites (including Lapworth's original example) form by (a), ductile deformation and recrystallization of minerals, (b) brittle fracture and crushing of grains and (c) growth of new, smaller, grains. With regard to the fabric and appearance of mylonites, Hobbs et al. (1976) note that mylonitic rocks are generally finer grained than the rocks from which they are derived. Furthermore, these rocks are often strongly layered, with prominent extensional lineations commonly parallel to the axes of intrafolial folds within the mylonite zone. Occurring in a diversity of rock-types and metamorphic terrains, mylonites are characteristically developed on thrust-planes and within shear zones, often being associated with retrogressive metamorphism (Hobbs et al., *op. cit.*).

6.6.3 Conjugate shear zones in the Ngoye Formation

Mesoscale shear bands were recognized in the field, particularly in the central and eastern parts of the main massif. They are 1 to 2 metres in length, subvertical and characterized by ductile deformation of the regional D_2 -related foliation. As illustrated in Plates 6 & 10, they may occur as individuals or as conjugate sets symmetrically disposed at angles of up to 50° with the S_2 foliation. The sense of shear in the bands has been deduced from the deflection of planar fabrics across the shear-zone boundaries. Thus north-west striking shear zones have a dextral displacement sense, whereas sinistral movement characterizes north-east striking exposures.

The conjugate shear zones shown in Plate 10 have been investigated from both mesoscopic and microscopic points of view, with the object of assessing the microstructural effects of ductile shearing. The observations are summarized below:

(i) Mesoscopic observations

- (a) shear bands of opposite shear sense anastomose around relatively poorly foliated gneissic granite (see overlay, Plate 10)
- (b) planar fabrics (as shown by Ramsay, 1980) become notably intensified within the shear zones,
- (c) subhorizontal lineations indicate the movement to have been approximately horizontal i.e. in the plane of the pavement exposure and,
- (d) a planar fabric within the shear zones, sub parallel to the shear zone boundaries, is apparent.

(ii) Microscopic observations

Horizontal thin sections were cut from orientated hand specimens collected at the sites shown in Plate 10. Such sections are perpendicular to foliation and parallel to the lineation, or shear direction.

N302 A is an equigranular rock with essentially polygonal grain boundaries. A weak planar fabric is imparted on the specimen by the east-west alignment of broad, yellow-brown biotite laths (Plate 11). This microscopic observation is in accordance with the weakly foliated nature of the rock apparent in hand specimens.

N302 B was taken from just within the boundaries of a dextral shear zone. It is inequigranular and is transected by two planar fabrics, labelled C and S (these terms described in section 6.6.5 below). Whereas the fine-grained c-surfaces are orientated parallel to the SZB, those designated S are oblique to the SZB, curving asymptotically into the c-foliations (see overlay, Plate 12).

N302 C was collected from the core of a shear zone and displays a marked increase in the proportion of fine-grained material (Plate 11). Concomitant with this is an increased intensity of c-foliations, between which remnant feldspar porphyroclasts commonly exhibit brittle shear along the S direction.

N302 E has been included to show evidence for the post-tectonic growth of riebeckite (Plate 11). In addition, this slide is representative of a transitional structural stage between the poorly foliated N302 A sample and the highly foliated examples from within the shear zones.

N302 G shows that the central portion of this intensely sheared rock is characterized by a narrow 0,5 to 1 mm wide mylonitic zone. Classic mortar textures are displayed on either side of the core, with finely recrystallized minerals surrounding larger quartz and feldspar clasts (Plate 12). Towards the core, the degree of anisotropy increases and quartz grains become progressively more ribbon-like, appearing to stream out from polygonal grains at the core margins (Plate 12). A comparison of Plate 12 (b) (cut parallel to the mesoscopic lineation) with Plate 12 (d) (cut approximately normal to lineation) reveals that quartz ribbons are relatively elongate in the lineation direction. Moreover, as most of the quartz ribbons are in optically similar orientations, use of the gypsum lambda plate has enabled an approximate determination of the c-optic axis direction to be made (overlay).



124

Plate 10 Conjugate shear zones in pavement exposure of fine-grained riebeckite-biotite granite, southern flanks of Ngoye massif. Orientated specimen sites shown thus: N 302 A, B, C, E & G. Outcrop N 302, scale in cm.

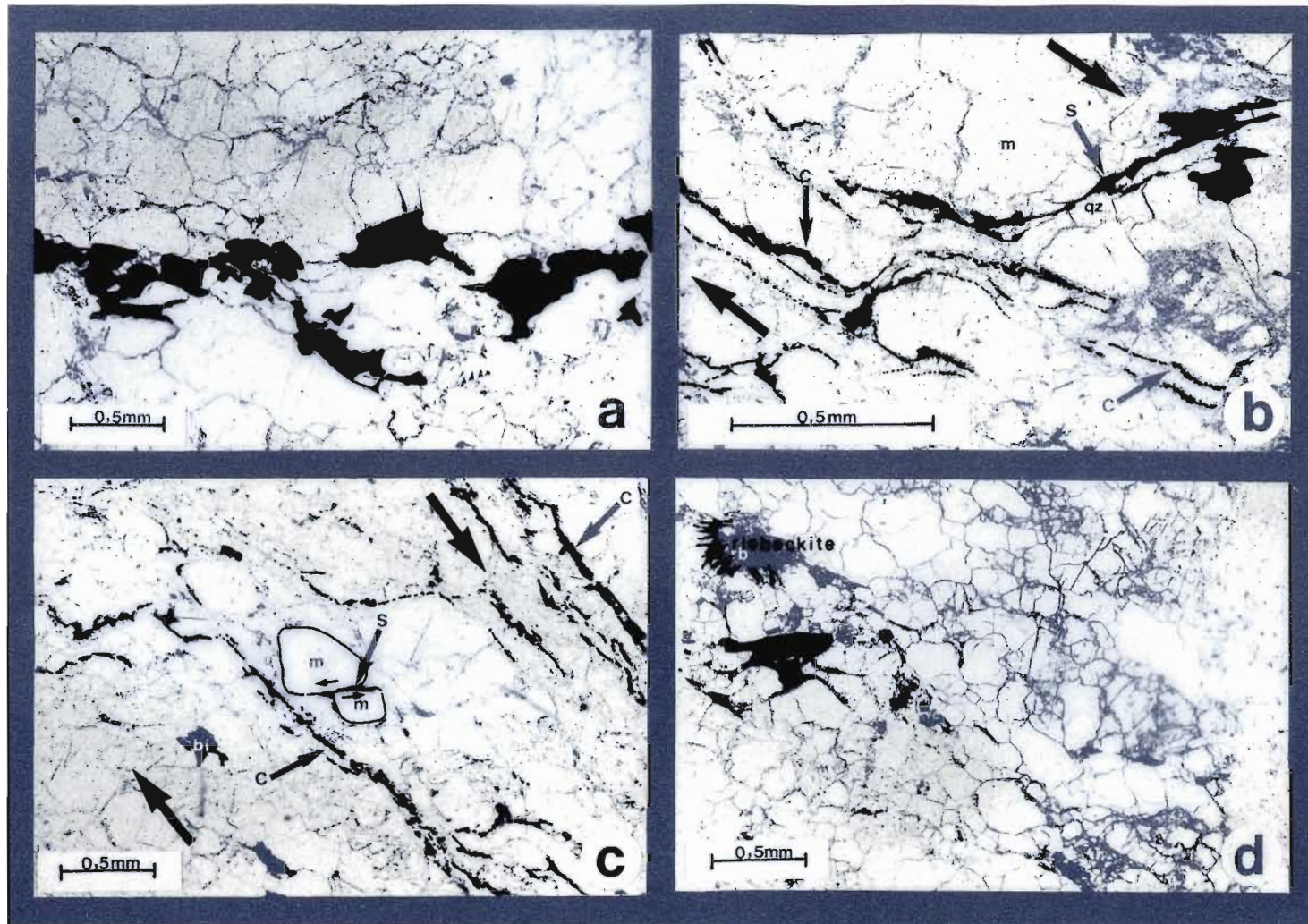


Plate 11. Photomicrographs illustrating microstructural variations across Ngoye conjugate ductile shear zones, locality N302 (map ref. 23 I, see Plate 10). (a) is of thin section N302A from a relatively undeformed portion of the outcrop and exhibits a weak foliation due to the alignment of broad biotite laths. Composite planar fabrics (labelled c & s) and illustrated in (b) and (c) are from sites 302B & 302C (see Plate 10). Note the apparently opposite sense of shear indicated by the displacement of feldspar clast (m) in (c). The bulk shear sense along foliation c is dextral (see arrows on overlay). (d) is from a relatively undeformed part of outcrop N302 (thin section 302E) and has been included to illustrate the post-tectonic growth of riebeckite (rb) needles.

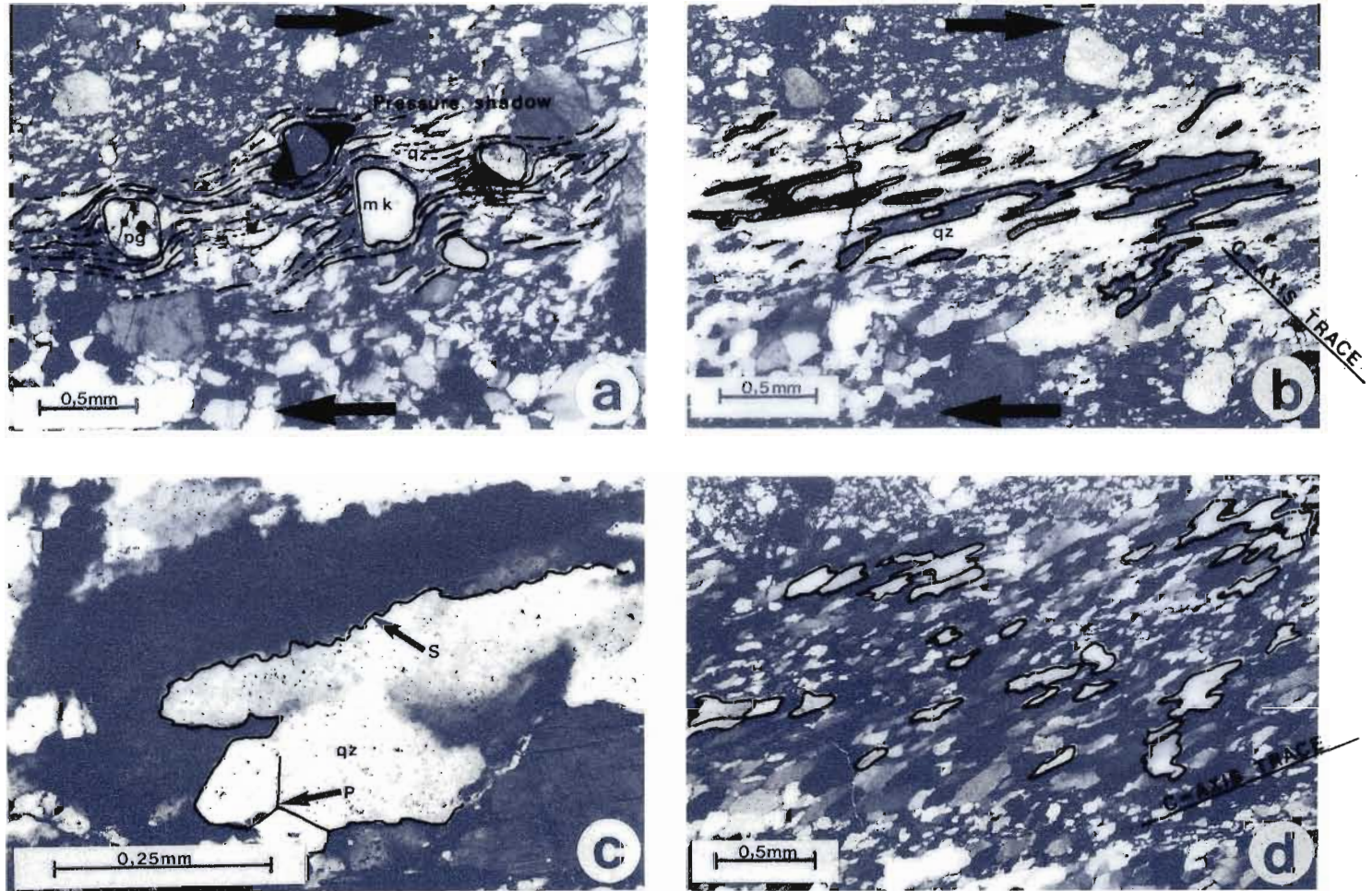


Plate 12. Photomicrographs illustrating microstructural criteria used to deduce shear sense from the mylonitic core of a dextral shear zone at locality N302 (map ref. 23 1). (a), Typical asymmetric quartz-filled (qz) pressure shadows around feldspar clasts (pg=plagioclase, mk=microcline) indicative of dextral shear sense in the x-z plane. (b) is from the same thin section as (a), showing elongate quartz (qz) ribbons with flattening planes oblique to the shear direction (see arrows on overlay). Quartz c-axis traces are oblique to the mylonite-zone boundaries. (c), Monocrystalline quartz ribbons "streaming out" from polygonally-bounded (p) quartz (qz) grains at the boundary of the mylonite zone. Note the serrated margins (arrowed s) of the quartz ribbon, indicating new-grain development (Bell & Etheridge, 1973). (d) Thin section cut normal to that illustrated in (b), showing c-axis orientation (see overlay).

137

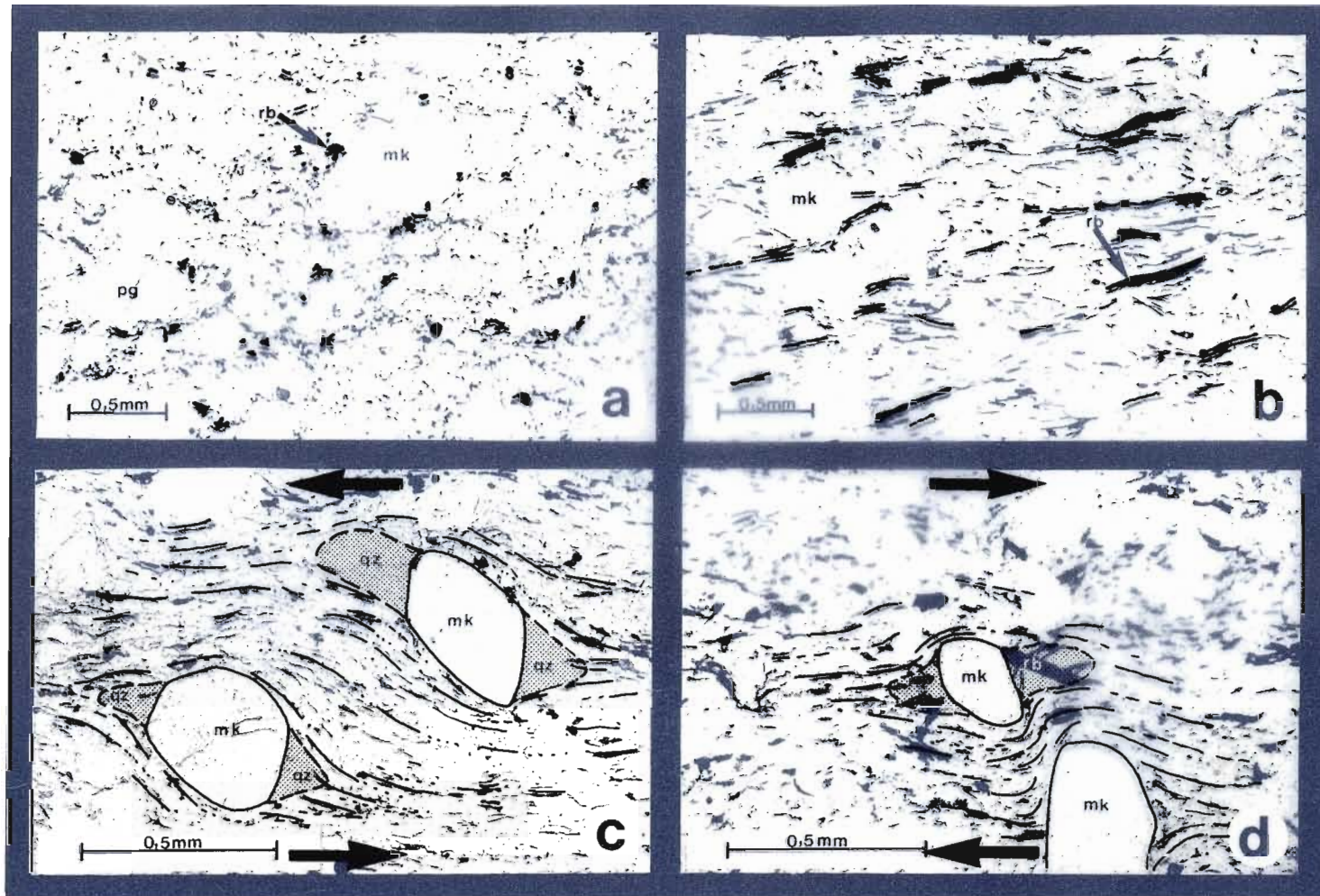


Plate 13. Photomicrographs of microstructural shear-sense criteria. Plates 13 (a) and (b) are from thin sections (map ref. 22 J) cut normal and parallel to the extension lineation direction, respectively. Note the basal sections of recrystallized riebeckite (rb) in (a), compared with elongate needles in (b), cut in the X - Z plane. Photomicrographs (c) and (d) in the X - Z plane illustrate asymmetric pressure shadows around feldspar porphyroclasts (pg=plagioclase, mk=microcline) containing quartz (qz) and riebeckite needles (rb), respectively showing sinistral and dextral shear (see overlay). Plate 13 (c) is from location N218 (map ref. 22 G), a macroscopic shear zone; and (d) is from a conjugate mesoscopic shear zone outcrop (N302, map ref. 23 I).

Moreover, most ribbons in horizontal sections wrap around feldspar clasts (Plate 12) to define asymmetric "tails" or "wings". Some of these tails are occupied by quartz and recrystallized riebeckite needles (Plate 13) and therefore are probably pressure-shadow areas. In this particular section (N302 G) which is cut perpendicular to foliation and parallel to lineation, there is a consistent sense of asymmetry about feldspar clasts (Plate 12). In each case the "uppermost" tail is on the righthand side of the clast, and the closest spaced foliation on the "upper" left. Those features are indicative of an overall dextral shear sense according to Simpson & Schmid (1983). They note that there is a tendency for a pre-existing foliation to be "closer spaced on the upper left hand and lower right hand side of clockwise (dextral) rotating grains" (Simpson & Schmid, *op.cit.*, p. 1283). By analogy with this observation the asymmetry of the foliation around feldspar clasts in the N302 G example is consistent with the dextral shear sense derived from field evidence.

Further microscopic evidence concerning overall shear direction can be obtained from the orientation of recrystallized quartz ribbons and grains. This follows research by Schmid *et al.*, (1981) and Simpson & Schmid (1983) who found that the flattening planes or long axes of recrystallised grains are oblique to the macroscopic foliation, and point in the direction of shear sense. Comparison of the obliquity of the quartz ribbons in Plate 12 with the data presented by Simpson (1983) confirms the dextral shear sense within this ductile shear zone.

Displaced broken grains, such as that shown in Plate 11, occur frequently in sheared rocks (Simpson & Schmid, *op. cit.*). Quoting the "sheared card pack" modal of Etchecopar (1974), Simpson and her coworker showed that displaced grains may be used to determine the overall displacement sense in shear zones, although the displacement along microfractures is usually opposite the overall direction (Simpson & Schmid, 1983). By analogy, the displaced grain outlined in Plate 11 is indicative of an overall dextral shear sense.

In conclusion, the microstructural data from outcrop N302 confirm the original (mesoscopic) impression of dextral shear within north-west striking shear zones over the outcrop. The criteria recognized in this example are in agreement with published information and include;

- (i) asymmetric augen structures;
- (ii) rotated grains with asymmetric pressure shadows; and
- (iii) displaced, broken grains with opposite displacement sense to the overall shear direction. Examples are shown in schematically in Fig. 6.5.

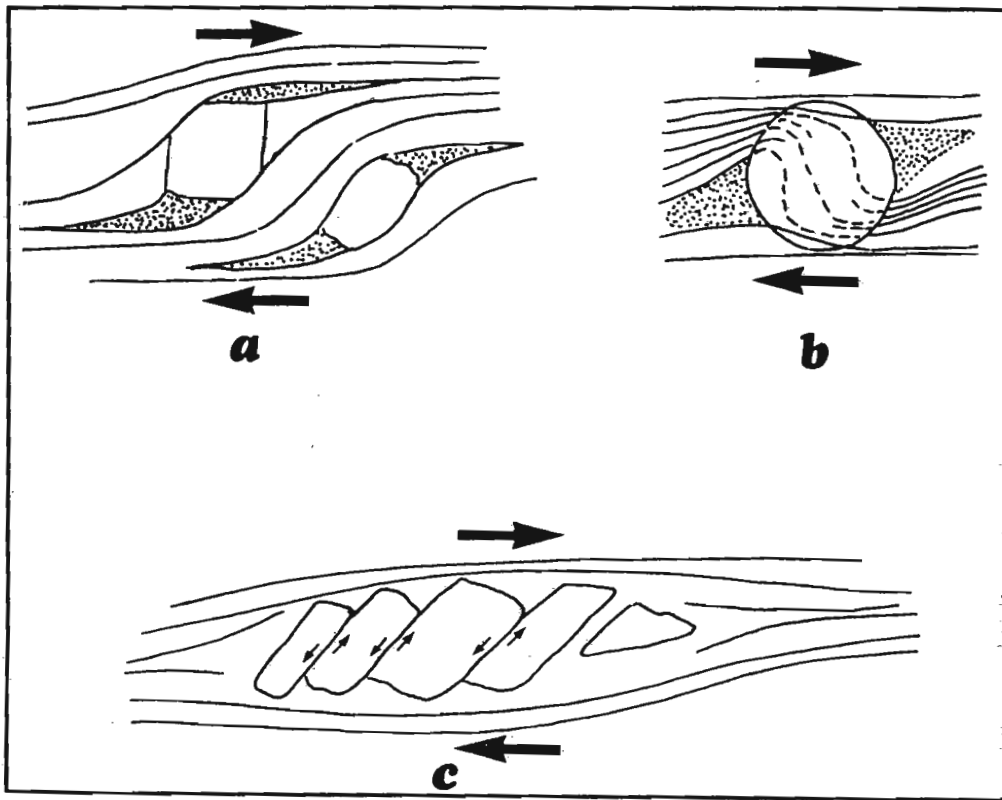


Fig.6.5. Schematic representation of asymmetric directional criteria from shear zones, after Simpson & Schmid (1983). (a) Asymmetric augen structures, (b) rotated grains with asymmetric pressure shadows, and (c) broken and displaced hard grains in a ductile matrix.

6.6.4 East-west macro shear zones

Several sub-vertical planar zones characterized by intense reworked and development of composite planar fabrics were mapped in the Ngoye range. Occurring predominantly in the eastern half of the outcrop they vary up to a few hundred metres width and several kilometres in length. These shear zones overprint, in a discontinuous fashion, the gneissic granites and are separated from each other by broad domains of less intensely deformed gneissic granites (Fig. 6.3). An increase in heterogeneous simple shear strain towards the shear zone centre is probable, where mylonites are commonly developed. The mylonites are typically fine-grained and have ubiquitously developed sub-horizontal extension lineations which imply "stretching" in a east-west direction. Rootless, similar style folds with axes aligned parallel to the extension lineations, occur in some of the mylonites. The development of composite planar fabrics and core zone mylonites are discussed separately below, and an attempt is made to deduce shear sense.

6.6.5 Composite planar fabrics

The onset of mylonitic deformation in the Ngoye Formation is characterized by the appearance of two foliations in the gneissic granite (Plate 14). Initially orientated at about 35° to each other, this angle decreases until approximate parallelism is achieved within the mylonitic shear zone centre. Salient features concerning the composite planar fabrics are (a), that the planar east-west striking foliation (labelled **c**) is parallel to the shear zone boundary and (b) that the second (labelled **s**) is oblique to the SZB and is sigmoidal, anastomosing asymptotically with the **c**-fabric.

This fabric development is very similar to those observed by Berthe et al. (1979) who described the gneissification of granite within the South Armorican Shear Zone (France). In this example the simultaneous appearance of two sub-vertical planar fabrics was noted, these being described as **c**- (cisaillement or shear) and **s** - (schistosite or foliation) surfaces respectively (Fig. 6.6). They defined the **c**-surfaces as always aligned parallel to the main shear zone boundary with progressive deformation, and considered to be spaced slip surfaces with a shear sense the same as that of the main shear zone.

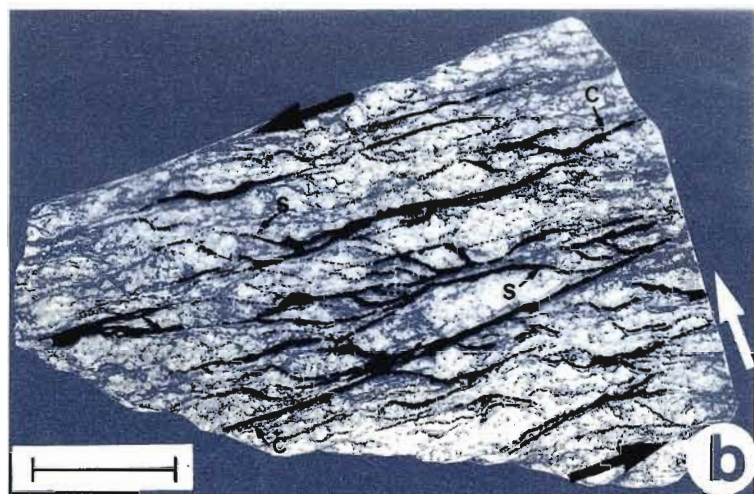


Plate 14. S-C mylonites from the Ngoye massif. Plates 14 (a), (b), & (c) (map ref. 26 H) show s-foliations anastomosing in and out of planar c-surfaces (see overlay). Note the decrease in angle between the two surfaces as c-surface concentration increases from (a) to (c). Approximate parallelism is achieved in the mylonite (phylionite) shown in (d) (map ref. 25 G). The asymptotic curvature of the s-surfaces is indicative of a bulk sinistral shear-sense, as shown by the arrows on the overlay. All illustrations are in the horizontal plane (X - Z of the strain ellipsoid), with arrows on the right hand side of the photographs indicating north. Scale bar in (b) is 5 cm long, all other scales in cm.

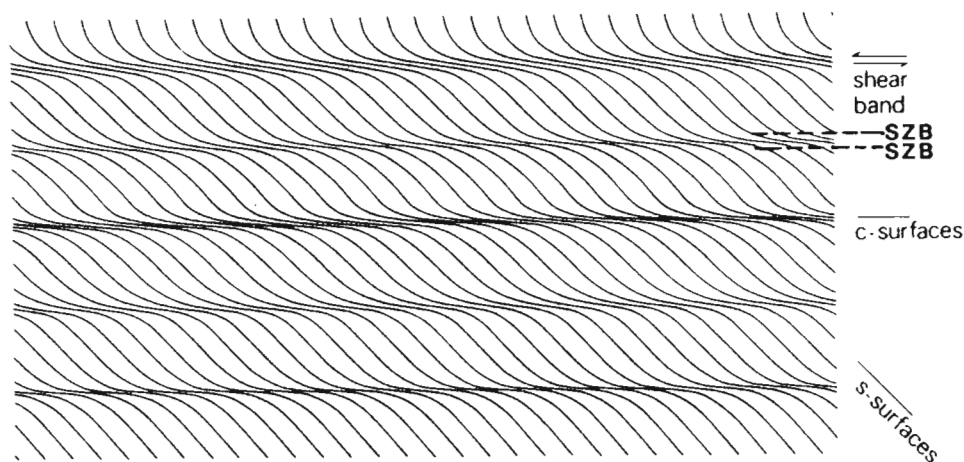


Fig.6.6. Typical composite planar fabrics, shown as shear bands (**c** - surfaces) transecting mylonitic foliations (**s** - surfaces), from Lister & Snoke (1984). Compare with Plate 14.

Furthermore, Berthe et al. (op cit.) found that **c**-surface spacing decreases towards the shear zone centre, and that **c**-surface concentration increases with increasing deformation. On the other hand, these authors noted that **s**-surfaces are sigmoidal and initially orientated at 45° to **c**-surfaces with this angle decreasing to near parallelism in the core-zone. Berthe et al. (1979) were also able to show that the asymptotic "tails" of **s**-surfaces defined the over-all dextral sense of shear within their example; that is, the tails curve into **c**-surfaces in the direction of the shear. By comparison then, the Ngoye examples shown in Plate 14 indicate sinistral lateral shear within zone 3.

Recent work by Lister & Snoke (1984) has suggested that not all composite planar fabrics, in what they term S-C mylonites, need develop simultaneously as proposed by Berthe et al. (1979). Three alternative derivations indicated are: (a) synchronous development of **s**- and **c**- surfaces, (b) late stage development of narrow shear bands (**c**-surfaces) during the same deformation that produced the **s**-surfaces and (c) a pre existing foliation cut by later narrow shear bands or **c**-surfaces (Lister & Snoke, 1984).

6.6.6 Mylonites - mesoscopic observations

As noted in 7.5.4 above, mylonites within the Ngoye macro-shear zones are characterized by the following:

- (i) a prominent, subvertical foliation (S_3);
- (ii) ubiquitous subhorizontal lineations (L_3) within the foliation planes plunge at shallow angles to both east and west (see stereoplot, Fig. 6.2);
- (iii) tight, appressed fold the compositional banding within the mylonites and vary from isoclinal to rootless, intrafolial fold-closure remnants (Plate 15); and that
- (iv) all folds have axes plunging parallel to the L_3 lineation.

6.6.7 Mylonites - microscopic observations

Petrographic studies have been based on orientated thin sections of mylonites from localities N142, N218 and N248 (Fig. 6.3, page 125). Sections were cut in two directions, either parallel to lineation and perpendicular to foliation, or normal to both foliation and lineation (Fig. 6.7). Microscopically, the sections cut parallel to L_3 are marked by (i) cataclasis where brittle minerals such as feldspars and opaque-ore grains have been pulled apart, and (ii) recrystallization where pressure shadows or prismatic amphiboles are orientated along L_3 (Plate 13). In contrast, thin sections normal to L_3 reveal virtually none of these structures, indicative of maximum extension parallel to the lineation direction. Following Mattauer et al. (1981) and Evans & White (1984) it is assumed that the lineation corresponds to the maximum extension direction X (where $X > Y > Z$) and that the S_3 foliation is parallel to the X-Y, or flattening plane of the strain ellipsoid (Fig. 6.7). This proposed orientation of X, Y and Z axes is corroborated by the orientation of recrystallized riebeckite needles within sample N142, where the obtuse cleavage angles (156°) in basal sections are generally orientated perpendicular to the S_3 foliation (Fig. 6.7; Plate 13).

According to Simpson & Schmid (1983), sections cut in the XY plane are most useful in deducing displacement sense across large-scale shear zones where no deflected marker horizons are apparent.

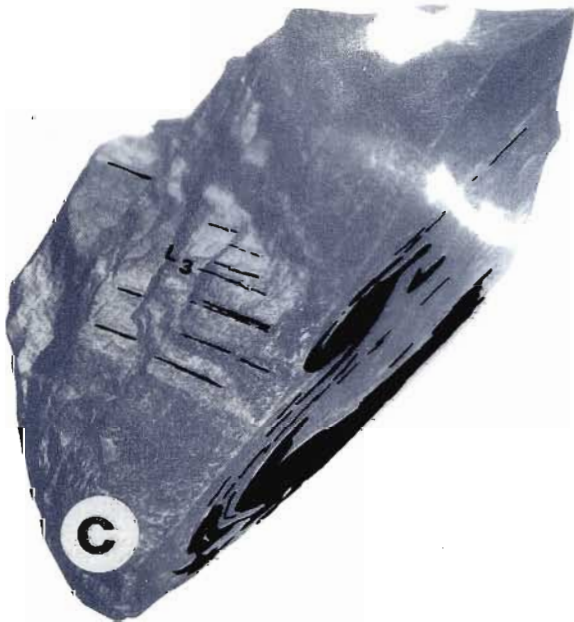


Plate 15. Typical D_3 -related structures in the Ngoye Formation. (a) shows eastward-plunging L_3 lineations defined by elongate mafic aggregates in riebeckite-biotite L_3 granite (map ref. 23 I). (b), Small isoclinal folds in mylonite, looking East (map ref. 25 G). Two aspects of a hand specimen from the same locality as (b) are shown in (c) & (d). These illustrate the parallelism of intrafolial fold axes with the extensional lineation L_3 , typical of the Ngoye mylonites. An orientated view eastwards of the sample in (d), showing that a previous mylonitic fabric has been folded during progressive mylonitization (see overlay).

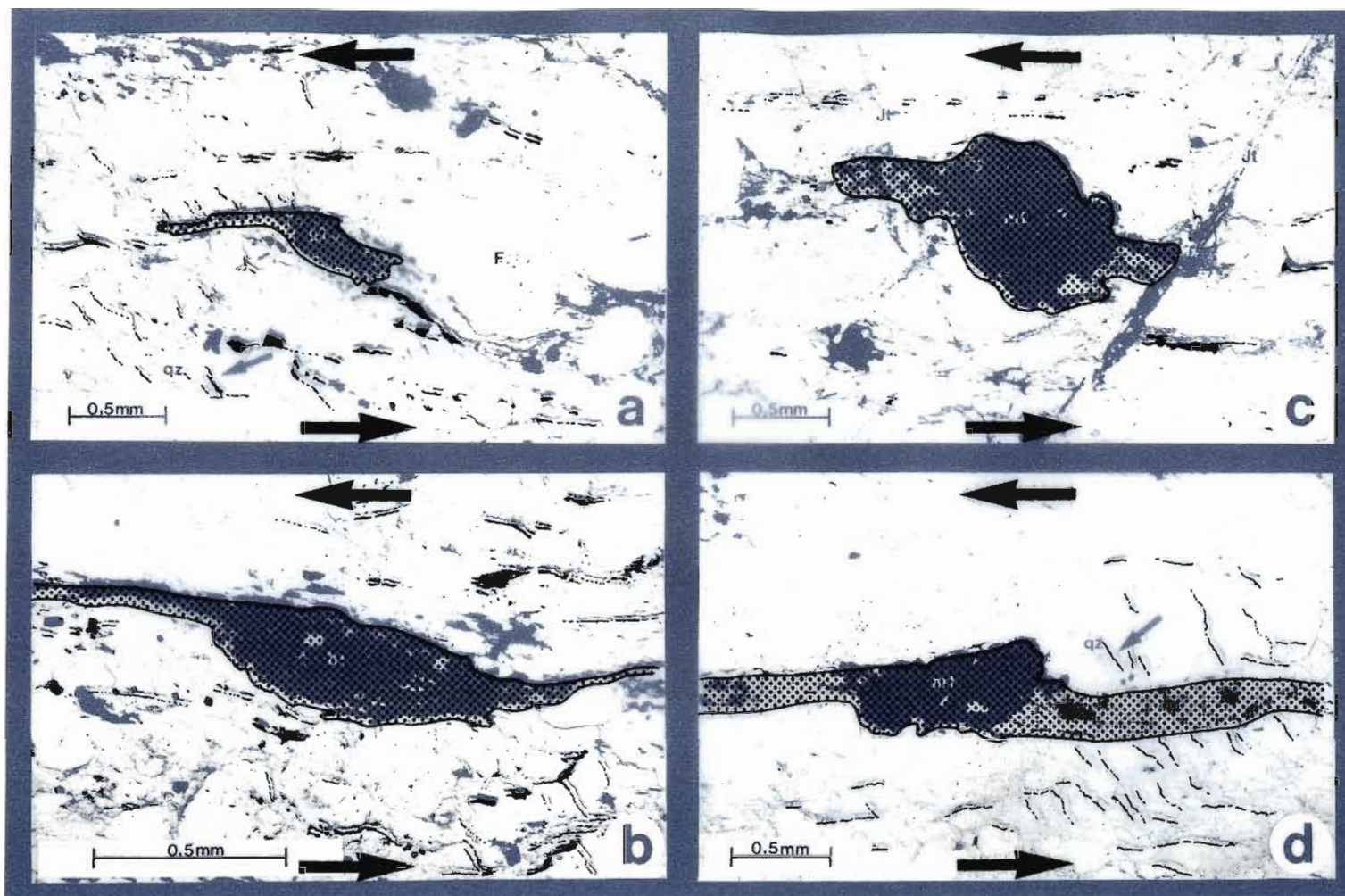


Plate 16. Photomicrographs of asymmetric structures in mylonitized magnetite microgranite (N248, map ref. 25 I). Examples (a) & (b) are fish-shaped biotite (bi) porphyroclasts whereas (c) & (d) are magnetite (mt) clasts. The asymmetry of the tails, which extend along the east-west foliation, indicate a sinistral shear sense. Similarly, elongate quartz (qz) grains with long axes oblique to the regional foliation (arrowed on a & d) are indicative of sinistral displacement. All thin sections cut in the X - Z plane with North at the top of illustrations.

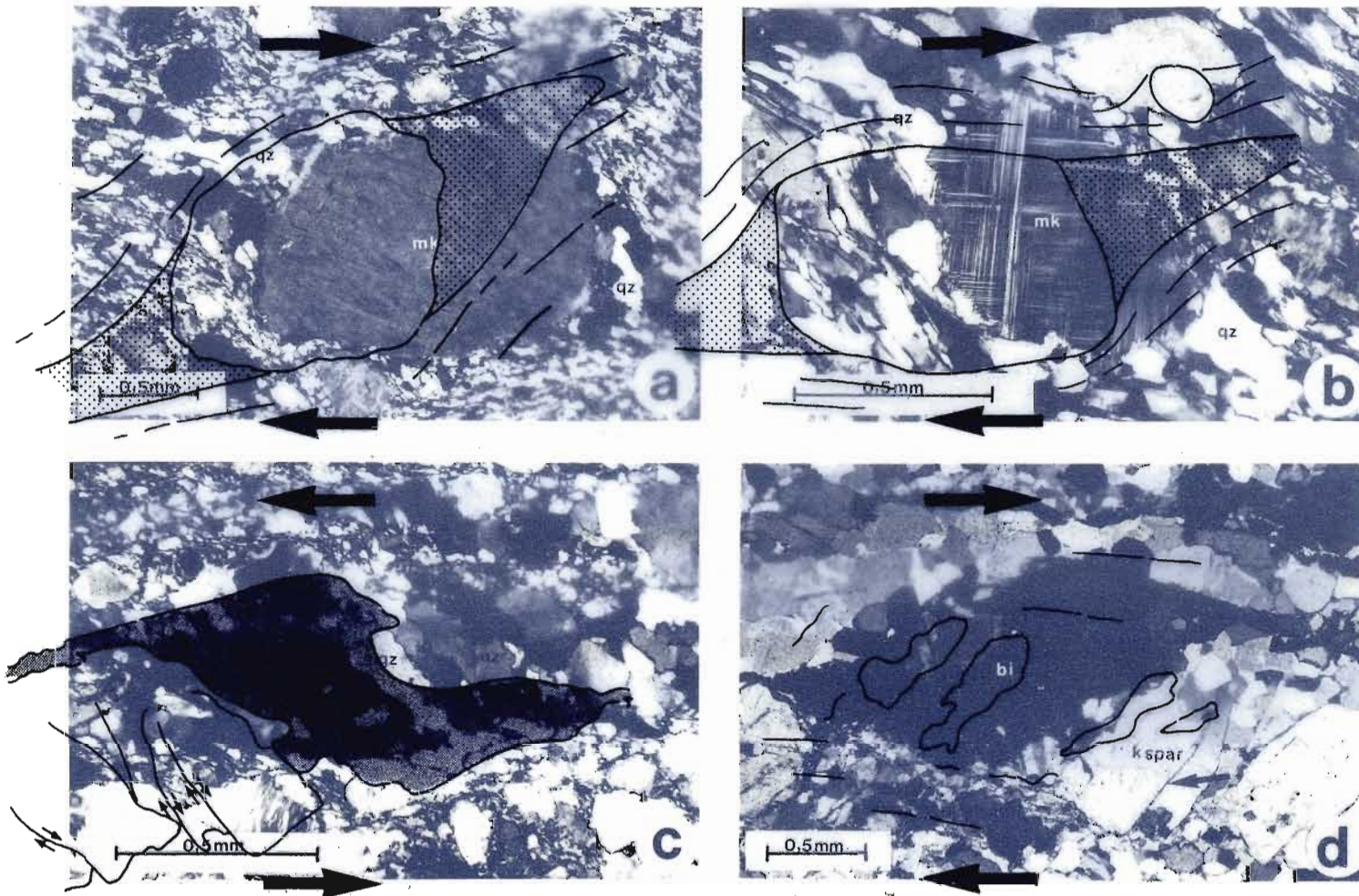


Plate 17. Photomicrographs of asymmetric structures in mylonites. Plates 17 (a) and (b) show asymmetric quartz (qz) pressure-shadow "tails" around microcline (mk) porphyroclasts, in a macro-shear zone mylonite from sample N218 (map ref. 25 H), indicative of sinistral shear. The elongate, obliquely orientated, quartz (qz) grains from sample N248 (magnetite microgranite) similarly indicate sinistral shear in (c). For comparison, photomicrograph (d) with asymmetric biotite "fish" (bi) and a fractured K-feldspar (k spar) grain is indicative of dextral movement, in a mesoscopic shear zone. All sections cut in the X - Z plane and are approximately horizontal, with North at the top of the plate.

146

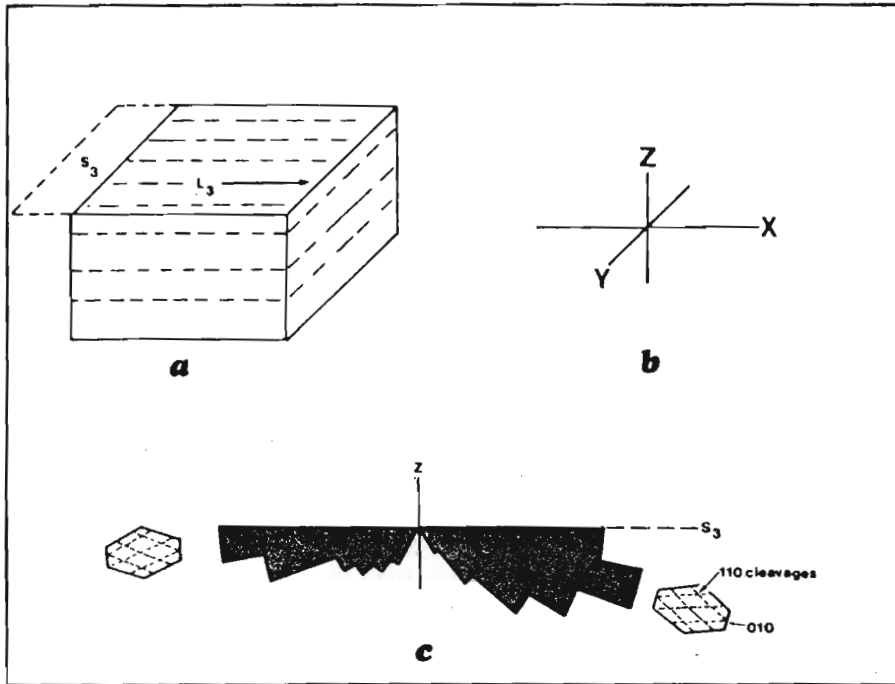


Fig.6.7. Block diagram illustrating the orientation of fabrics referred to in the text, with respect to the mylonitic foliation (S_3), mylonite lineation (L_3) and X, Y & Z axes of the finite strain ellipsoid, Fig. 6.7a & b. The orientation of riebeckite crystals with respect to S_3 , from thin sections normal to X, are shown in Fig. 6.7b.

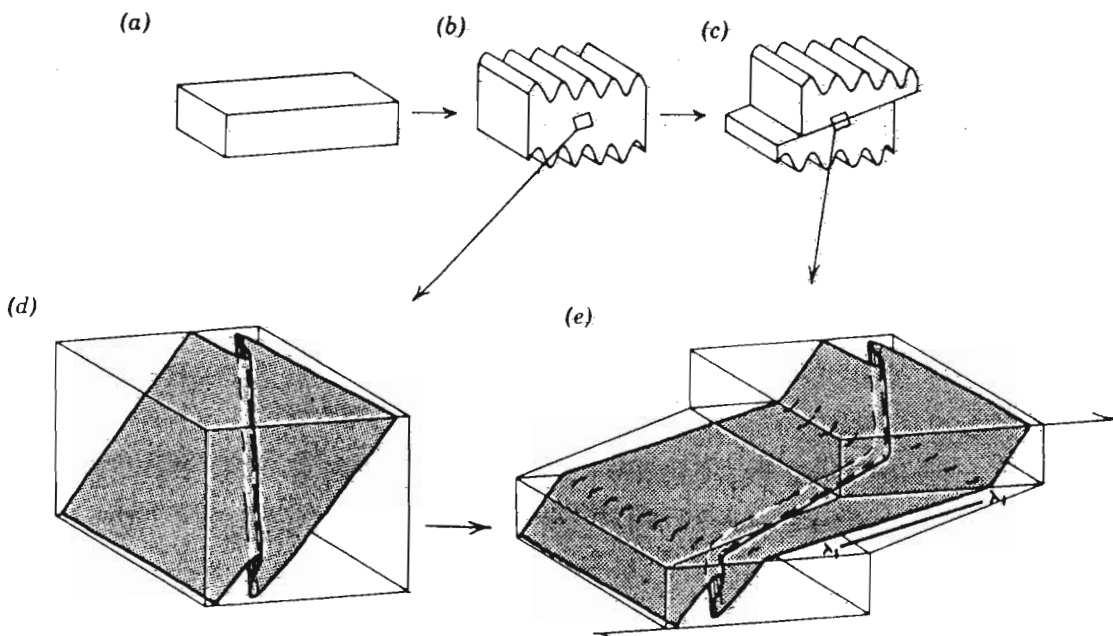


Fig.6.8. Diagram showing how fold hinges may be rotated, within a zone of intense deformation along a thrust plane, into parallelism with the direction of overthrusting. (taken from Hobbs, et al., 1976).

By comparison with the microstructural criteria deduced from the Ngoye conjugate shear zones, as well as data presented by Simpson & Schmid (op. cit.) in section 6.6.3 above, the asymmetric structures shown in Plates indicate a lateral, sinistral shear sense in the macro-shear zones. This displacement is compatible with the sinistral shear sense derived from the orientation of composite planar fabrics observed in mesoscopic exposures (see 6.6.5).

6.6.8 Interpretation of folds in the mylonites

From the above observations, it is now apparent that the isoclinal folds mentioned in 6.6.6 above have their axes orientated parallel to the maximum extension direction X. This represents a very special case, for as pointed out by Hobbs et al. (1976), although some extension may occur parallel to fold axes, the maximum extension is generally perpendicular to the fold axis (thus fold axes are generally parallel to Y of the strain ellipsoid). A possible solution to this problem is that folds in mylonites develop and refold continuously during shearing with the result that linear and planar fabrics rotate with increasing strain in shear zones, and that folds originally formed at an angle to the extension direction eventually rotate into approximate parallelism (Fig. 6.8) with the extension direction (Kvale, 1953; Bryant & Reed, 1969; Carreras et al., 1977; Evans & White, 1984).

6.6.9 Crenulations

Small crenulations in the S_2 foliation were observed on the north-eastern flanks of the massif (Plate 9). The deformation of S_2 indicates that they are post - D_2 in age, and by analogy with data published by Platt (1984) are probably extensional crenulation cleavages (ecc) related to sinistral lateral D_3 shearing.

6.7 D_4 event

Although not observed in the field, this event has been deduced from the stereograms which indicate gentle warping about north-south axes, of all pre-existing fold axes (Fig. 6.1).

Chapter 7

DISCUSSION & CONCLUSIONS

7.1 Modal and geochemical characteristics

Petrographic, geochemical and field evidence has defined 12 different gneissic granitoids within the Ngoye Formation. These have been classified using the QAP-modal system and range from monzodiorite through syenite, to alkali-feldspar granites and monzogranites. Geochemically they range from peraluminous to peralkaline on the basis of Shand's (1947) alumina-saturation classification. According to this approach the muscovite and garnet-bearing granitoids on the north-eastern flanks of the Ngoye massif have an excess of alumina over alkalis and calcium and are **peraluminous**. The predominant lithologies within the formation, constituting the summit and northern flanks of the range, are hornblende and/or biotite-bearing and **metaluminous**. **Peralkaline** riebeckite and aegerine-bearing gneissic granites are restricted in occurrence to the southern margin of the main massif, and according to Shand's definition, have an excess of alkalis over alumina. The two narrow gneissic syenite horizons intersected in borehole NG2, and closely associated with peralkaline magnetite microgranite are peraluminous.

The samples analysed display a range in SiO_2 content from 63.79 to 78.47%, are depleted in CaO and MgO, while enriched in Na_2O and K_2O relative to published average values for syenites and granites. When the major oxides are plotted (a) against SiO_2 as Harker variation diagrams and (b) against the differentiation index, fairly distinct trends are shown by TiO_2 , FeO, MgO and CaO, which in general vary inversely with SiO_2 contents and D.I., while Na_2O and K_2O do not covary with either SiO_2 or D.I. That the two syenitic

analyses do not follow these observed trends may be related to metasomatic alteration, as shown by their chloritized appearance.

No intersection was obtained on the Peacock (1931) alkali-lime diagram, although extension of the calculated trends to lower silica values indicates that the Ngoye gneissic granitoids are alkalic, and are highly depleted in CaO relative to $(Na_2O + K_2O)$. Application of the parameters suggested by Wright (1969) supports the alkaline nature of the samples. According to the schemes devised by Irvine & Baragar (1971) the Ngoye granitoids are tholeiitic, i.e. enriched in FeO relative to MgO and furthermore are subalkaline to peralkaline in nature.

Bearing in mind the nomenclature derived for the Ngoye granitoids from the QAP modal diagram, several chemically-based classificatory schemes were evaluated. It was found that those devised by Harpum (1963), O'Connor (1965) and Streckeisen (1976) have serious deficiencies due to the omission of a silica-saturation component. The most useful of these three schemes is that proposed by Streckeisen (op. cit.) in which he took cognisance of anorthite/orthoclase ratios, and which yields results similar to those derived from the modal QAP triangle. The orthogonal plot of normative constituents suggested by Streckeisen & Le Maitre (1979) provided reasonable discrimination between samples, and due to the inclusion of normative quartz is able to discriminate syenitic rocks. Probably the most advanced diagram available for granitoid classification by chemical means, is that devised by de la Roche et al. (1980). This scheme, which uses all the major cations present in granite analyses, was able to separate the Ngoye samples into four groups that correspond closely to the modally-derived terminology. Finally, the degree of peralkalinity was assessed using the methods of Macdonald (1975), which shows that the gneissic riebeckite and aegerine-bearing granitoids are mildly peralkaline and of comenditic affinity.

The Ngoye gneissic-granites and syenite are enriched in Rb and incompatible elements, while depleted Ba and Sr relative to published data for the average granite and syenite. Whereas the peralkaline types have restricted Ba and Sr contents, the metaluminous and peraluminous varieties display Ba and Sr depletion trends to Rb, indicative of derivation of the various lithologies by fractional crystallization processes, (Robb, 1983). Accordingly, the youngest, peraluminous granites have higher Rb/Ba and Rb/Sr ratios than the older

(from field evidence) metaluminous granites. A notable exception to this trend is shown by the incompatibles, Zr and Zn, which are depleted in the younger peraluminous granites relative to the older metaluminous types. In contrast, the peralkaline granitoids are highly enriched in Zr and Zn. This has been explained in terms of experimental data (Watson, 1979) who demonstrated that these elements are capable of remaining in solution to high levels within peralkaline magmas, whereas saturation levels are extremely low in metaluminous and peraluminous melts. It would thus be expected that late-stage residual fluids derived by the fractional crystallization of a peralkaline magma would be enriched in Zr and Zn as well as other incompatibles. This observation is consistent with the occurrence of radioactive, siliceous rocks associated with the gneissic peralkaline-granites along the southern flanks of the massif, which contain high concentrations of Zr, Zn, U, Th, Nb and REE. These rock-types are similar to siliceous veins associated with peralkaline granites in Saudi-Arabia and Nigeria (Harris, 1981).

7.2 The significance of peralkaline granitoids in the Ngoye Formation

The distribution of peralkaline silicic intrusive and extrusive rocks has been discussed at length by Murthy & Venkataraman (1964), Bowden (1974), and Macdonald (1975). In addition the occurrence of metamorphic peralkaline gneisses has been reviewed by Floor (1974), although in view of their often uncertain origins these are omitted from the following summary.

Peralkaline silicic rocks are located in both continental and oceanic environments although by far the overwhelming majority (about 90%) are found in the continental rift environment (Macdonald, 1975), see Fig. 7.1. Attempts by Bowden (1974) and Macdonald (1975) to relate peralkaline magmatism to plate tectonic settings have resulted in the three major subdivisions given on page 153.

(i) **continental doming and rifting in non-orogenic regions** (eg the African Plate) is often accompanied by peralkaline magmatism. This may occur from the pre-rift (epiorogenic-doming) stage through to the continued rifting (crustal-attenuation)stage. According to Bowden (op. cit.) each stage is characterized by various suites and varying proportions of silicic and associated rocks. Comendites form in the doming stage, while their relative proportions diminish as rifting evolves and they are replaced by pantellerites. In well-developed rift systems comenditic lavas are virtually absent (Mohr, 1970; in Macdonald, 1975). Where crustal extension is extreme the principle rock types are basaltic with only small quantities of peralkaline rhyolites. The intrusive equivalents of comendite and pantellerite, the peralkaline granites, are commonly found as subvolcanic ring structures in continental areas of pre-rift doming. Bowden (1974) considers that peralkaline plutonism is an essential part of pre-rift tectonics, with such granites generally restricted to this environment. He does note however, that xenoliths of peralkaline granite and syenite have been recorded from peralkaline lavas erupted on oceanic islands above actively spreading ridges, which suggests that peralkaline plutonism may be a minor but important early stage in most areas of tensional tectonics. The proportion of comagmatic basic rocks in ring complexes is generally very small and of the order of a few percent.

(ii) **Oceanic Islands** situated on or near actively spreading ridge crests (Fig. 7.1) have peralkaline rocks as their characteristic acidic phase. Comendites are the dominant silicic rock type, but they are of minor proportions compared with the volumes of alkali basalt, trachytes and phonolites at each centre.

(iii) **Back-arc magmatism** occurs either behind oceanic-island arcs (eg Dawson Strait in Papua New Guinea, Fig. 7.1), or inland from active subduction zones along continental margins (eg: Great Basin, Nevada, Fig. 7.1). These regions have been demonstrated (Saunders & Tarney, 1979) to be centres of spreading or extensional tectonics behind active andesitic volcanic arcs. There is thus one factor that links these various tectonic environments: they are characterized by tensional crustal conditions. According to research done by Macdonald (1975) there is no clear example of peralkaline silicic rocks having been emplaced under compressional stresses, and concludes that the presence of these rock-types is evidence of tensional crustal conditions at the time of emplacement. The question that now arises

with respect to the Ngoye peralkaline granites is : into which environment (continental, back-arc or oceanic) they were emplaced? As noted in Chapter 5, the Ngoye peralkaline rocks exhibit a very similar iron enrichment trend to that proposed by Bailey & Macdonald (1970) for continentally emplaced comendites. In addition, the overwhelming preponderance of silicic (> 99%) to basic rocks within the Ngoye Formation is akin to the proportions (basic rocks generally less than a few percent) observed in intracratonic granite complexes (Bowden, 1974). The hypothesis therefore is that the Ngoye granitoids were emplaced in a continental-crust environment undergoing tensional tectonics, either intracratonic doming and rifting, or attenuation in a marginal back-arc situation.

7.3 The A-type classification

The above observations are corroborated by the application of various discriminants based on geochemical parameters, which strongly suggest that the Ngoye Formation comprises typical anorogenic/post orogenic, or within-plate granitoids (Martin & Piwinski, 1972; Petro *et al.*, 1979; Lameyre & Bowden, 1982; Batchelor & Bowden, 1985; and Pearce *et al.*, 1984). The characteristics of such granites have been summarized by Loiselle & Wones (1980), who extended the I and S-type granite classification of Chappell & White (1974) to embrace what they termed "A" type granites. These authors note that A-type granite suites:

- (i) are often peralkaline and contain iron-rich minerals such fayalite, riebeckite, aegerine and hastingsite;
- (ii) are highly depleted in CaO, MgO and Al₂O₃ relative to I & S -types;
- (iii) display an iron enrichment trend when plotted on an AFM diagram and are hence tholeiitic;
- (iv) contain enhanced concentrations of the trace elements Zr, Nb, Zn, REE and F, whereas Ba and Sr are depleted;
- (5) are anhydrous or contain little H₂O, and intrude to shallow or sub-volcanic levels in the crust;
- (vi) often form ring complexes which are invariably intruded into continental crust, eg. the Nigerian, Sudanese and Saudi-Arabian "younger granite" provinces.

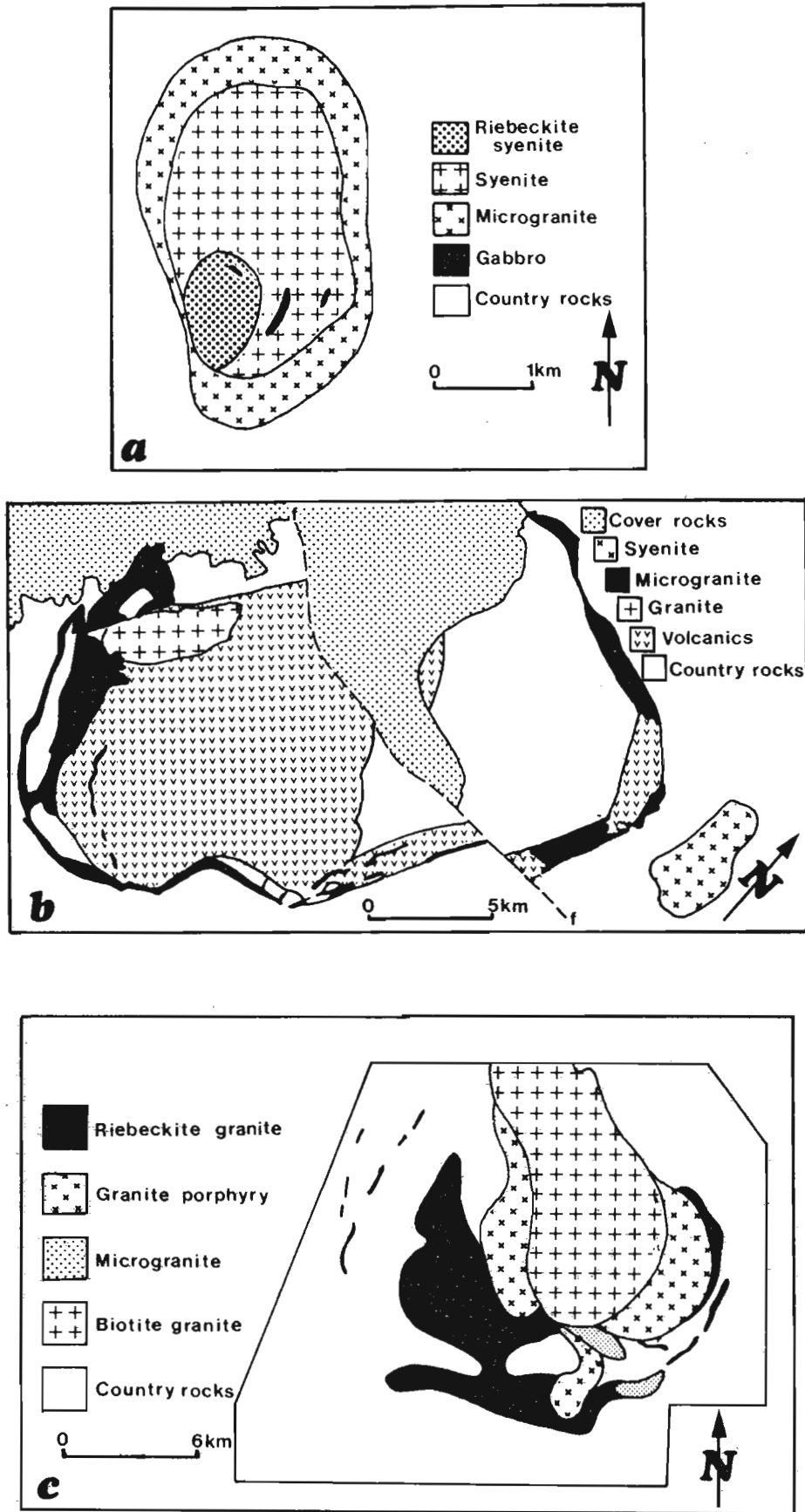


Fig. 7.2. Examples of typical granitic ring complexes. (a), Qeili and (b), Sabaloka in Sudan (after Almond, 1979); (c), Hadb-Aldyaheen, Saudi Arabia (after Radain & Kerrich, 1979).

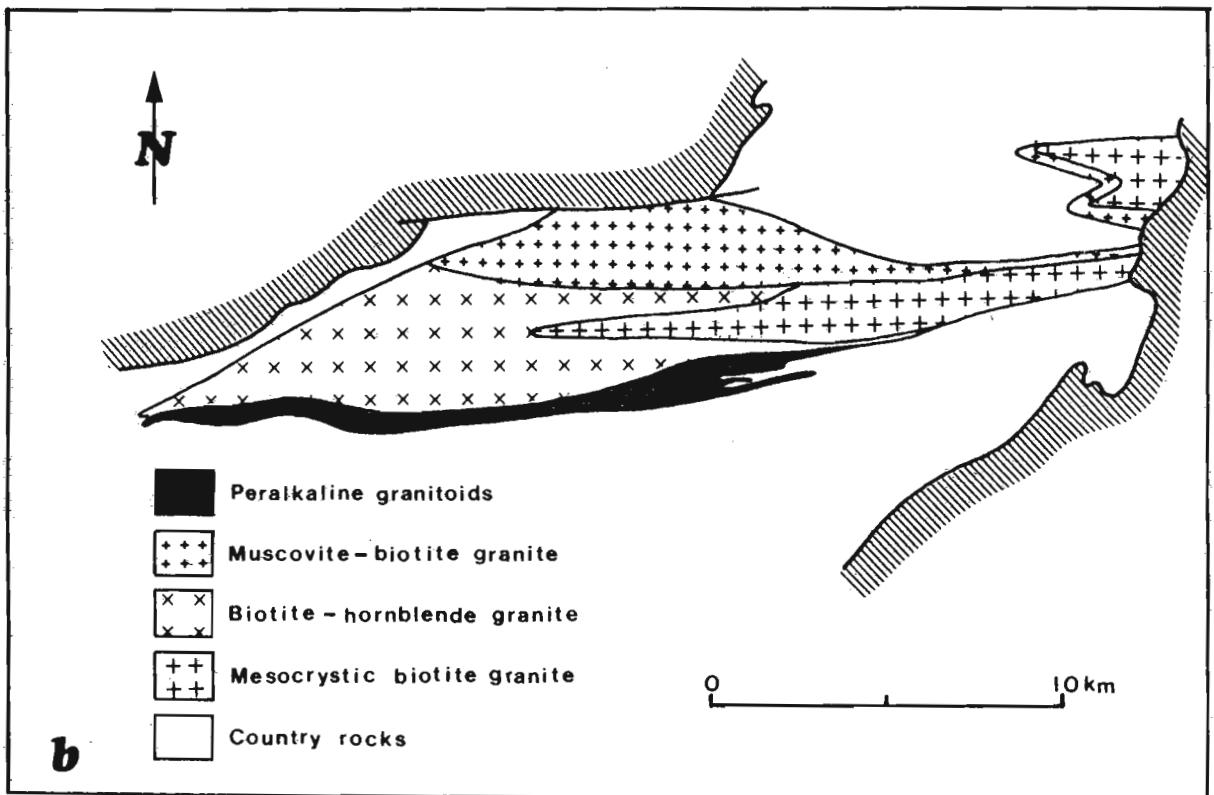
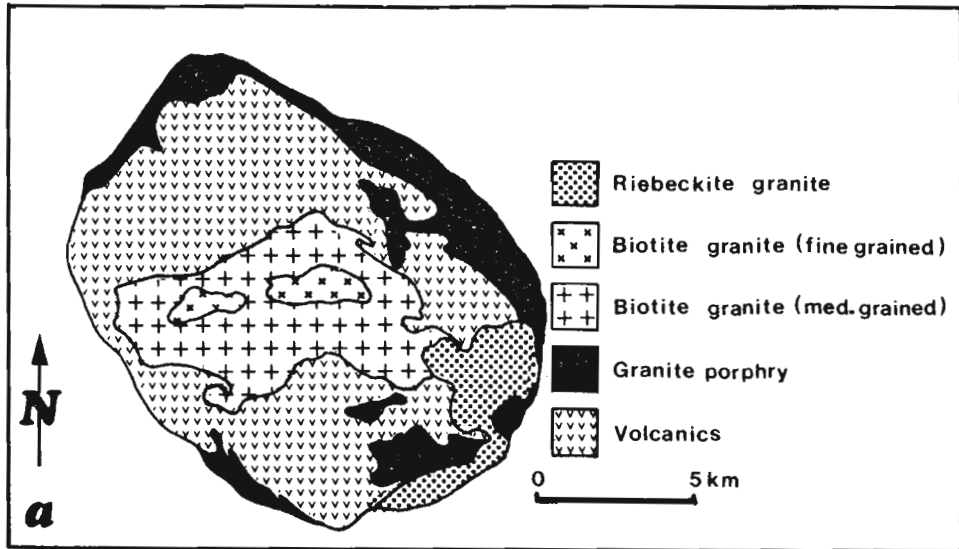


Fig. 7.3. (a), A typical "younger granite" complex, Ririwai, Nigeria (after Ekwere & Olade, 1984); (b), a simplified map of the Ngoye Formation.

Typically, ring complexes are circular to elliptical in outline (Bowden, 1974), and vary in size from 50 to 200 km² although exceptions to this do occur. Individual centres commonly show concentric structures with fine grained (microgranitic or rhyolitic) ring dykes surrounding an often composite coarser grained granitic core (Fig. 7.2). Central cauldron subsidence (Jacobsen *et al.*, 1958; Bowden & Turner, 1974) within the ring dykes may preserve earlier volcanic material (Fig. 7.3). These authors also point out that outer contacts are usually sharp and steep-dipping, and that the order of intrusion may vary from one province to another, for example in Nigeria the peraluminous granites post-date the intrusion of peralkaline types, whereas this order is reversed in Saudi Arabia and the Sudan.

Loiselle & Wones (1980) note that A-type granite complexes are characterized by highly variable ⁸⁷Sr/⁸⁶Sr ratios. They explain this by suggesting that A-type magmas are produced when a mafic mantle-derived magma enters the crust and (a) fractionates directly to yield siliceous magmas with low ⁸⁷Sr/⁸⁶Sr ratios or (b) interacts with crustal material to produce a large volume of siliceous magma with moderate to high Sr ratios. Other processes suggested include reaction melting, whereby alkali-olivine-basalt magma reacts with granulites in the lower crust and produces syenitic magmas (Barker, 1975; in Loiselle & Wones, 1980), liquid immiscibility and volatile diffusion (Hildreth, 1979) and volatile fluxing (Bailey, 1970). This latter hypothesis is related to alkali metasomatism of the lower crust by mantle derived, CO₂-rich volatiles that cause enrichment of incompatible elements and result in anhydrous magmas.

7.4 Comparison of the Ngoye Formation with A - type granites

Based on available data, the Ngoye gneissic granitoids have the geochemical characteristics of A-type, within-plate granites. They are extremely depleted in CaO, MgO and Al₂O₃, while enriched in Na₂O and K₂O relative to average granites. Incompatible element concentrations are high, particularly in the peralkaline lithologies, while Ba and Sr are depleted. Comparison of the distribution of lithologies shows that the Ngoye Formation has the form typical of granitic ring complexes ie, an outer microgranitic and fine-grained granite phase surrounding a medium to coarse-grained core. In addition, the size of the formation (about 100 Km²) is similar to that of the "type" ring

complexes in Nigeria, Sudan and Saudi Arabia. Moreover, the occurrence of a CO₂-rich phase in the monzodiorite is similar to anorogenic granite complexes in Sudan & Saudi Arabia, where carbonate veins represent the final magmatic phase (Harris, 1982). **The inference therefore is that the Ngoye Formation represents a metamorphosed peralkaline A-type granite ring complex (Scogings, in press) intrusive into continental crust, either wholly intracratonic, or in a back-arc situation on the attenuated margin of a continental plate.** The low ⁸⁷Sr/⁸⁶Sr ratios of 0.706, Charlesworth (1981) are consistent with their derivation from fractionated, mantle derived mafic magma, suggested by Loiselle & Wones (1980) as a possible method of deriving A-type granites.

The highly elongate, lensoid outline of the Ngoye Formation, as opposed to the essentially circular outline of most anorogenic granite complexes, may be ascribed to the effect of folding, lateral shearing and mylonitization during the D₂ and D₃ metamorphic events.

REFERENCES

- Almond, D.C. (1979). Younger granite complexes of Sudan. *In*, Al Shanti, A.M.S., *et al.*, Eds., *Evolution and mineralization of the Arabian - Nubian Shield*, **2**, 151-164. Pergamon Press, U.K.
- Anderson, J.L., Cullers, R.L. and van Schmus, W.R. (1980). Anorogenic meta-luminous and peraluminous granite plutonism in the Mid-Proterozoic of Wisconsin, U.S.A. *Contrib. Mineral. Petrol.*, **74**, 311-328.
- × Anderson, W. (1901). Report on the Reconnaissance Survey of Zululand. *Rep. Geol. Surv. Natal - Zululand*, **1**, 60-61.
- Bailey, D.K. (1970). Volatile flux, heat focussing, and the generation of magma. *Geol. J. Spec. Issue*, **2**, 177-186.
- Bailey, D.K. and Macdonald, R. (1970). Petrochemical variations among mildly peralkaline obsidians from the oceans and continents. *Contr. Mineral. Petrol.*, **28**, 340-351.
- Baker, P.E. (1975). Peralkaline acid volcanic rocks of oceanic islands. *Bull. Volcanol.*, **38**, 737 - 754.
- × Barth, T.F.W. (1962). *Theoretical petrology.*, 2nd ed. Wiley, New York, N.Y.
- Batchelor, R.A. and Bowden, P. (1985). Petrogenetic interpretation of granitoid rock series using multicationic parameters. *Chem. Geol.*, **48**, 43 - 55.

- Becke, F. (1903). Die eruptivgebiete des bohmischen Mittelgebirges und der amerikanischen Andes. *Tschermaks miner. petrogr. Mitt. Neue Folge*, **22**.
- Bell, T.H. and Etheridge, M.A. (1973). Microstructure of mylonites and their descriptive terminology. *Lithos*, **6**, 337-348.
- Benson, W.N. (1926), The tectonic conditions accompanying the intrusion of basic and ultrabasic igneous rocks. *Bull. nat. Sci.*, **1**, 1-90, Washington, D.C.
- Berthe', D., Choukroune, P. and Jegouzo, P. (1979). Orthogneiss, mylonite and non coaxial deformation of granites: The example of the South Armorican Shear Zone. *J. Struct. Geol.*, **1**, 31-42.
- Binns, R.A. (1965). Ferromagnesian minerals in high-grade metamorphic rocks. *Geol. Soc. Austr. Spec. Pap.* **2**, 323-332.
- Boettcher, A.L. (1970) The system $\text{CaO-Al}_2\text{O}_3\text{-SiO}_2\text{-H}_2\text{O}$ at high pressures and temperatures. *J.Petrol.*, **11**, 337-379.
- Bowden, P. (1974). Oversaturated alkaline rocks : Granites, pantellerites and comendites, 109-123. In, Sorensen, H., Ed., *The Alkaline Rocks*. Wiley Interscience, New York.
- Bowden, P. and Turner, D.C. (1974). Peralkaline and associated ring-complexes in the Nigeria-Niger province, west Africa, 330-351. In, Sorensen, H., Ed., *The Alkaline Rocks*. Wiley Interscience, New York.
- Bowden, P., Bennet, J.N., Whitley, J.E. and Moyes, A.B. (1979). Rare earths in Nigerian Mesozoic granites. *Lithos*, **7**, 15-21.
- Brown, G.C., Thorpe, R.S. and Webb, P.C. (1984) The geochemical characteristics of granitoids in contrasting arcs and comments on magma sources. *J. geol. Soc. Lond.*, **141**, 413-426.

- Bryant, B., and Reed, J.C., Jnr. (1969). Significance of lineation and minor folds near major thrust faults in the southern Appalachians and the British and Norwegian Caledonides. *Geol. Mag.*, **106**, 412-429.
- Carreras, J., Estrada, A. and White, S.H. (1977). The effects of folding on the c - axis fabrics of a quartz mylonite. *Tectonophysics*, **39**, 3-24.
- Chappell, B.W. and White, A.J.R. (1974). Two contrasting granite types. *Pacific Geology*, **8**, 173 -174.
- *Charlesworth, E.G. (1981). *Tectonics and metamorphism of the northern margin of the Namaqua-Natal Mobile Belt, near Eshowe, Natal*. Ph.D. thesis (unpubl.), Natal University, Durban.
- Collerson, K.D. (1982). Geochemistry and Rb-Sr geochronology of associated Proterozoic peralkaline and subalkaline anorogenic granites from Labrador. *Contrib. Mineral. Petrol.*, **81**, 126-147.
- Collins, W.J., Beams, S.D., White, A.J.R. and Chappell, B.W. (1982). Nature and origin of A-type granites with particular reference to South-eastern Australia. *Contrib. Mineral. Petrol.*, **80**, 189-200.
- × Cox, K.G., Bell, J.D., and Pankhurst, R.J. (1979). *The interpretation of igneous rocks*. Allen and Unwin, London.
- De la Roche, H., Leterrier, J., Grandclaude, P. and Marchal, M. (1980) A classification of volcanic and plutonic rocks using R_1 - R_2 diagram and major element analyses - its relationships with current nomenclature. *Chem. Geol.*, **29**, 183-210.
- × Deer, W.A., Howie, R.A. and Zussman, J. (1966). *An introduction to the rock-forming minerals*. Longmans, London.
- Du Preez, J.W. (1982). *The geology of the area West of Richards Bay*. Explanation to sheets 2831 DD & 2832 DC. Open file rep. geol. Surv. S. Afr., **244**, 40-41.

- Ekwere, S.J., and Olade, M.A. (1984). Geochemistry of the tin-niobium bearing granites of the Liruei (Ririwai) complex, younger granite province, Nigeria. *Chem. Geol.*, **45**, 225-243.
- Engel, A.E.J. and Engel, C.G. (1962). Hornblendes formed during progressive metamorphism of amphibolites, northwest Adirondack Mountains, New York. *Bull. geol. Soc. Am.*, **73**, 1499-1514.
- Ernst, W.G. (1960). The stability relations of magnesio-riebeckite. *Geochim. Cosmochim. Acta.*, **19**, 10-40.
- Etchecopar, A. (1974). A plane kinematic model of progressive deformation in a polycrystalline aggregate. *Tectonophysics*, **39**, 121 - 139.
- Evans, D.J. and White, S.H. (1984). Microstructural and fabric studies from the rocks of the Moine Nappe, Eriboll, NW Scotland. *J. Struct. Geol.*, **6**, 369 -389.
- Floor, P. (1974). Alkaline gneisses, 124-142. In, Sorensen, H., Ed., *The Alkaline Rocks*. Wiley Interscience, New York.
- * Ford, W.E. (1932). *Dana's textbook of mineralogy*, 4th ed. John Wiley and Sons, New York, N.Y.
- Gass, I.G. (1982). Upper proterozoic (Pan-African) calc-alkaline magmatism in north-eastern Africa and Arabia, 591-609. In, Thorpe, R.S., Ed., *Andesites*. John Wiley and Sons, London.
- Gerasimovsky, V.I. (1974). Trace elements in selected groups of alkaline rocks, 402-410. In, Sorensen, H., Ed; *The Alkaline Rocks*. Wiley Interscience, New York.
- Hanson, G.N. (1978). The application of trace elements to the petrogenesis of igneous rocks of granitic composition. *Earth Planet. Sci. Lett.*, **38**, 26-43.
- * Harker, A., (1897). *The natural history of igneous rocks*. Macmillan, New York, N.Y.

- Harpum, J.R. (1963). Petrographic classification of granitic rocks in Tanganyika by partial chemical analyses. *Records geol. Surv. Tanganyika*, **10**, 80-88.
- Harris, I.B. and Cobbold, P.R. (1984). Development of conjugate shear bands during bulk simple shearing. *J. Struct. Geol.*, **7**, 37-44.
- Harris, N.B.W. (1981). The role of fluorine and chlorine in the petrogenesis of a peralkaline complex from Saudi Arabia. *Chem. Geol.* **31**, 303-310.
- Harris, N.B.W. (1982). The petrogenesis of alkaline intrusives from Arabia and northeast Africa and their implications for within-plate magmatism. *Tectonophysics*, **83**, 243-258.
- Harris, N.B.W and Marriner, G.F. (1980). Geochemistry and petrogenesis of a peralkaline granite complex from the Midian Mountains, Saudi Arabia. *Lithos*, **13**, 325 - 337.
- Higgins, M.W. (1971). Cataclastic rocks. *Prof. Pap. U.S. geol. Surv.*, **687**, 1-97.
- Hildreth, W. (1979). The Bishop tuff: compositional zonation in a silicic magma chamber without crystal settling. *Geol. Soc. Am. Abstr. Programs*, **8**, 918.
- Hine, R., Williams, I.S., Chappell, B.W. and White, A.J.R. (1978). Contrasts between I- and S - Type granitoids of the Kosciusko Batholith. *J. geol. Soc. Aust.*, **25**, 219 -234.
- Hobbs, B.E., Means, W.D., and Williams, P.F. (1976). *An outline of structural geology*. Wiley International Edition, J.Wiley and Sons, New York, N.Y.
- Holdaway, M.J. (1972). Thermal stability of Al-Fe epidote as a function of fO₂ and Fe content. *Contrib. Mineral. Petrol.*, **37**, 307-340.

- × Hutchison, C.S. (1974) . *Laboratory handbook of petrographic techniques*, Wiley Interscience, New York.
- × Hyndman, D.W. (1972). *Petrology of igneous and metamorphic rocks*. McGraw-Hill, New York, N.Y.
- Iddings, J.P. (1892). The origin of igneous rocks. *Bull. Wash. Phil. Soc.*, **12**, 89-214.
- Irvine, T.N. and Baragar, W.R.A. (1971). A guide to the chemical classification of the common volcanic rocks. *Can. J. Earth. Sci.*, **8**, 523-548.
- × Jackson, M.P.A. (1976). *High grade metamorphism and migmatization of the Namaqua Metamorphic Complex around Uis in the southern Namib desert, S.W.A.* Chamber of Mines PreCambrian Res. Unit, Bulletin 18.
- Jacobsen, R.R.E., MacLeod, W.N. and Black, R. (1958). Ring-complexes in the younger granite province of northern Nigeria. *Mem. geol. Soc. Lond.*, **1**, 1-71.
- × Kerr, P.F. (1959). *Optical mineralogy*, 2nd ed. McGraw-hill, New York, N.Y.
- Kvale, A. (1953). Linear structures and their relationship to movement in the Caledonides of Scandinavia and Scotland. *Q. Jl. geol. Soc. Lond.*, **109**, 51-73.
- Lameyre, J. and Bowden, P. (1982). Plutonic rock type series: discrimination of various granitoid series and related rocks. In, Brousse, R. and Lameyre, J., Eds., *Magmatology. J. volcanol. geotherm. Res.*, **14**, 169-186.
- LeMaitre, R.W. (1976). The chemical variability of some common igneous rocks . *J. Petrology*, **17**, 589-637.
- Lepeltier, C. (1969). A simplified statistical treatment of geochemical data by graphical representation. *Econ. Geol.*, **64**, 538-550.

- Lister, G.S. and Snoke, A.W. (1984). S-C mylonites. *J. Struct. Geol.*, **6**, 617-638.
- Loiselle, M.C. and Wones, D.R. (1979). Characteristics of anorogenic granites. *Abstr. with Programs, A.G.M. geol. Soc. Am.*, p. 539.
- Loiselle, M.C. and Wones, D.R. (1980). *Characteristics and models for the origin of A-type granites*. Unpublished report, Virginia Polytechnic, Blackburg, Virginia.
- Macdonald, R. (1975 a). Nomenclature and petrochemistry of the peralkaline oversaturated extrusive rocks. *Bull. Volcanol.*, **38**, 498-516.
- Macdonald, R. (1975 b). Tectonic settings and magma associations. *Bull. Volcanol.*, **38**, 575-593.
- Macdonald, R., and Bailey, D.K. (1973). The chemistry of the peralkaline oversaturated obsidians. *Prof. Pap. U.S. geol. Surv.*, **440**, N1-N37.
- Martin, R.F. and Piwinskii, A.J. (1972). Magmatism and tectonic settings. *J. Geophys. Res.*, **77**, 4966-4975.
- Mason, B. (1967). *Principles of geochemistry*, 3rd ed. John Wiley and Sons, New York, N.Y.
- Mattauer, M., Faure, M. and Malavielle, J. (1981). Transverse lineation and large - scale structures related to Alpine obduction in Corsica. *J. Struct. Geol.*, **3**, 401 - 409.
- × Matthews, P.E. (1972). Possible Precambrian obduction and plate - tectonics in Southeast Africa, *Nature*, **240**, 37-39.
- × Matthews, P.E. (1981). Eastern or Natal sector of the Namaqua-Natal Mobile Belt in southern Africa. In, Hunter, D.R., Ed., *Precambrian of the southern hemisphere*, 705-725. Elsevier, Amsterdam.

- × Matthews, P.E. and Charlesworth, E.G. (1981). 1 : 140000 Map, *Northern margin of the Namaqua-Natal Mobile Belt in Natal*. Compiled at Natal University.
- × McCarthy, M.J. (1961). *The geology of the Empangeni fault area*. M.Sc. thesis (unpubl.), Natal University, Durban.
- McCarthy, T.S., and Hasty, R.A. (1976). Trace element distribution patterns and their relationships to the crystallization of granitic melts. *Geochim. Cosmochim. Acta*, **40**, 1353-1358.
- Metz, P. and Trommsdorff, V. (1968). On phase equilibria in metamorphosed siliceous dolomites. *Contrib. Mineral. Petrol.*, **18**, 305-309.
- Mukherjee, A. and Rege, S.M. (1972). Stability of wollastonite in the granulite facies: some evidence from E. Ghats, India. *Neues Jb. Miner. Abh.*, **118**, 22-43.
- Murthy, M.V.N., and Venkataraman, P.K. (1964). Petrogenetic significance of certain platform granites of the world. In, *The upper mantle symposium*, New Delhi, 127-149.
- Neary, C.R., Gass, I.G. and Cavanagh, B.J. (1976). Granitic association of northeastern Sudan. *Bull. geol. Soc. Am.*, **87**, 1501-1512.
- × Nockolds, S.R., Knox, R.W.M. and Chinner, C.A. (1978). *Petrology for students*. Cambridge University Press, Cambridge.
- Norrish, K. and Hutton, J.T. (1969). An accurate x-ray spectrographic method for the analysis of a wide range of geological samples. *Geochim. Cosmochim. Acta*, **33**, 431-453.
- O'Connor, J.T. (1965). A classification of quartz-rich igneous rocks based on feldspar ratios, *Prof. Pap. U.S. geol. Surv.*, **525 B**, B74-B84.
- Peacock, M.A. (1931). Classification of igneous rocks series. *J. Geol.*, **39**, 54-67.

- Pearce, J.A., Harris, N.B.W. and Tindle, A.G. (1984). Trace element discrimination diagrams for the tectonic interpretation of granitic rocks. *J. Petrol.*, **25**, 956-983.
- Petro, W.L. Vogel, T.A. and Wilband, J.T. (1979). Major-element chemistry of plutonic rock suites from compressional and extensional plate boundaries. *Chem. Geol.*, **26**, 217-235.
- Pitcher, W.S. (1983). Granite type and tectonic environment, 19-40. In, Hsu, K., Ed., *Mountain building process*. Academic Press, London.
- Platt, J.P. (1984). Secondary cleavages in ductile shear zones. *J. Struct. Geol.*, **6**, 439-442.
- Poldervaart, A. (1955). Zircon in rocks. 1, sedimentary rocks. *Am. J. Sci.*, **253**, 433-461.
- Poldervaart, A. (1956). Zircon in rocks. 2, igneous rocks. *Am.J.Sci.*, **254**, 521-554.
- Radain, A. and Kerrich, R. (1980). Peralkaline granite in the western part of the Arabian Shield. In, Al Shanti, A.M.S., et al. Eds., *Evolution and mineralization of the Arabian-Nubian Shield*, **2**, 117-130, Pergamon Press, U.K.
- × Ramsay, J.G. and Graham, R.H. (1970). Strain variation in shear belts. *Can. J. Earth Sci.*, **7**, 786 - 813.
- × Ramsay, J.G. (1980). Shear zone geometry; a review. *J. Struct. Geol.*, **2**, 83-99.
- Robb, L.J. (1983). Trace element trends in granites and the distinction between partial melting and crystal fractionation processes: case studies from two granites in southern Africa, 279-294. In, Augustithis, S.S., Ed., *The significance of trace elements in solving petrogenetic problems and controversies*. Theophrastus Publications S.A., Athens, Greece.

- Rosler, H.J. and Lange, H. (1972). *Geochemical tables*. Elsevier Publishing Co., Amsterdam.
- Saunders, A.D. and Tarney, J. (1979). The geochemistry of basalts from a back-arc spreading centre in the East Scotia Sea. *Geochim. Cosmochim. Acta*, **43**, 555-572.
- Saunders, A.D., Tarney, J., and Weaver, S.D. (1980). Transverse geochemical variations across the Antarctic peninsula: Implications for the genesis of calc-alkaline magmas. *Earth Planet. Sci. Lett.*, **38**, 26-43.
- Schoch, A.E., Leterrier, J. and de la Roche, H. (1977). Major element geochemical trends in the Cape granites. *Trans. geol. Soc. S. Afr.*, **80**, 197-209.
- Shand, S.J. (1947). *The eruptive rocks*, 228-230. Thomas Murby and Co., London.
- Shilling, J.G. (1973). Icelandic mantle plume: geochemical study of Reykjanes ridge. *Nature, Lond.*, **242**, 565-571.
- Schmid, S.M., Casey, M. and Starkey, J. (1981). The microfabric of calcite tectonites from the Helvetic Nappes. *In*, McClay, K.R. and Price, N.J., Eds., *Thrust and Nappe Tectonics*: Geol. Soc. Lond. Spec. Publ., **9**, 151-158.
- × Scogings, A.J. (1983). *Investigation of incompatible-element mineralization associated with the Ngoye granite gneiss, Kwa-Zulu*. Project report (unpubl.), Mining Corporation Ltd., Pretoria.
- × Scogings, A.J. (in press). Peralkaline gneissic granites in the Ngoye Formation. *Trans. geol. Soc. S. Afr.*
- Simpson, C. (1983). Strain and shape fabric variations associated with ductile shear zones. *J. Struct. Geol.*, **5**; 61-72.

- Simpson, C. and Schmid, S.M. (1983). An evaluation of criteria to deduce the sense of movement in sheared rocks. *Bull. geol. Soc. Am.*, **94**, 1281-1288.
- × South African Committee for Stratigraphy (SACS), (1980). *Stratigraphy of South Africa*, Handb. geol. Surv. S. Afr., **8**.
- × Spry, A. (1969). *Metamorphic textures*. Pergamon Press, Sydney.
- Storre, B. and Nitsch, K. H. (1973). The upper stability of margarite in the presence of quartz. *Naturwissenschaften*, **60**, 152.
- Streckeisen, A. (1976 a). Classification of the common igneous rocks by means of their chemical composition - a provisional attempt. *N. Jb. Min.*, **1**, 1-15.
- Streckeisen, A. (1976 b). To each plutonic rock its proper name. *Earth Sci. Rev.*, **12**, 1-33.
- Streckeisen, A. and LeMaitre, R.W. (1979). A chemical approximation to the modal QAPF classification of the igneous rocks. *N. Jb. Miner. Abh.*, **136**, 169-206.
- Taylor, R.P., Strong, D.F. and Kean, B.F. (1980). The Topsails igneous complex: Silurian-Devonian peralkaline magmatism in western Newfoundland. *Can. J. Earth Sci.*, **17**, 425-439.
- Thornton, C.P., and Tuttle, O.F. (1960). Chemistry of igneous rocks. 1, differentiation index. *Am. J. Sci.*, **258**, 664-684.
- Turekian, K.K. and Wedepohl, K.H. (1961). Distribution of the elements in some major units of the Earth's crust. *Bull. geol. Soc. Am.*, **72**, 175.
- × Turner, F.J. and Weiss, L.E. (1963). *Structural analysis of metamorphic tectonites*. Mc Graw - Hill Book Co., New York, N.Y.
- Twidale, C.R. (1982). *Granite landforms*. Elsevier Scientific Publishing Co., Amsterdam.

- Waters, A.C. and Campbell, C.D. (1935). Mylonites from the San Andreas fault zone. *Am. J. Sci.*, **29**, 473 - 503.
- Watson. E.B. (1971). Zircon saturation in felsic liquids: experimental results and applications to trace element geochemistry. *Contrib. Mineral. Petrol.*, **70**, 407-419
- White, S.H., Burrows, S.E., Carreras, J., Shaw, N.D. and Humphreys, F.J. (1980). On mylonites in ductile shear zones. *J. Struct. Geol.*, **2**, 175-187.
- Woodard, H.H. (1957). Diffusion of chemical elements in some naturally occurring silicate inclusions. *J. Geol.*, **65**, 61-64.
- Wright, J.B. (1969). A simple alkalinity ratio and its application to questions of non-orogenic granite genesis. *Geol. Mag.*, **106**, 370-384.

APPENDIX A

A.1 Introduction

An exploration programme over the Ngoye massif and surrounding gneissic terrain was initiated in 1982, following the discovery of radioactive, magnetite-bearing quartz-rich rocks along the southern margin of the Ngoye formation (Fig. A.1). Initial analyses of hand specimens indicated variable but essentially high concentrations of incompatible elements, eg: Ta, up to 234 ppm; Nb, up to 4700 ppm; U_3O_8 , up to 887 ppm; ThO_2 , up to 2723 ppm; REE, up to 2000 ppm; Sn, up to 29 ppm, W, up to 379 ppm; Zr, up to 11600 ppm; and Y, up to 1600 ppm.

Prospecting permission was obtained for the area covered by Bantu Reserves 7B, 9 & 17, with the major share of exploration carried out over the northern part of Reserve 9. Following an orientation survey over the discovery area and the eastern part of the Ngoye range (Scogings, 1983), an exploration programme was commenced in August 1982 using the methods outlined below:

- (i) bulk stream sediment samples (7-10 kg) collected at a density of approximately 1 sample per 2 Km². The panned concentrate (30-50 g) of each was analysed for Nb, Ta, Sn, W and U_3O_8 .
- (ii) magnetic and radiometric traverses were carried out normal to the southern granite contact, extending to 500 m south of the massif, and at 500 m intervals along strike. This spacing was later closed to 100 m apart along strike within selected areas.
- (iii) reconnaissance geological mapping of the Ngoye Formation and adjacent amphibolitic gneisses.
- (iv) it was decided that priority targets would be likely to be characterized by combined magnetic and radiometric anomalies, as well as high stream sample values.

A.2 Geochemical exploration results

A total of 172 bulk stream sediment samples were collected and panned, the values of which were plotted on log probability paper after the method described by Lepeltier (1969). The elements analysed were approximately log normally distributed, which enabled background (median value, b); standard deviation (s); and threshold level (t) to be graphically estimated. The threshold is conventionally taken as $b + 2s$, in which case only 2,5% of the population exceed this value (Lepeltier, op cit). The results are tabulated below:

Table A.1

Panned stream samples*, statistical parameters

Element	b	s	t
Nb	75	200	530
Ta	25	45	85
Sn	12	28	90
W	40	75	130
U ₃ O ₈	45	80	150

Notes:

* = all values in ppm, uranium as U₃O₈.

b = median value (background)

s = standard deviation

t = 2nd standard deviation (threshold)

Accordingly, contours of *s* & *t* values were plotted, with representative distributions of Nb and Sn given in Figs. A.2 and A.3. The following features were noted:

- (i) all elements analysed were present in low concentrations over the central part of the Ngoye massif, increasing in concentration towards the southern and north-eastern margins;
- (ii) the highest Nb, Ta and U_3O_8 concentrations were from streams draining the south-central to south-eastern margins of the Ngoye Formation; and that
- (iii) the highest Sn and W concentrations occurred in streams draining the north-east flanks of the massif.

A.3 Geophysical exploration results

During the initial phase of exploration, the geophysical traverses were widely spaced at 500 m intervals along strike in order to gain a regional appreciation of geophysical trends. This spacing was reduced to 100 m along the southern contact zone when, it became apparent that the radioactive magnetic rocks were of restricted strike extent. Geophysical data were plotted on composite graphs, as well as contoured on a 1: 25 000 base plan. Several notable points to emerge from this exercise were that:

- (i) geophysical activity is subdued south of the contact zone;
- (ii) anomalous magnetic and radiometric reading readings were most common within a 200 m wide zone along the southern granite contact zone;
- (iii) geophysical anomalies were essentially parallel to lithological boundaries, ie: they were orientated approximately east-west, parallel to the granite contact and usually located over outcrops of magnetite microgranite; and
- (iv) that geophysical traverses did not detect any anomalies along the northern flanks of the range.

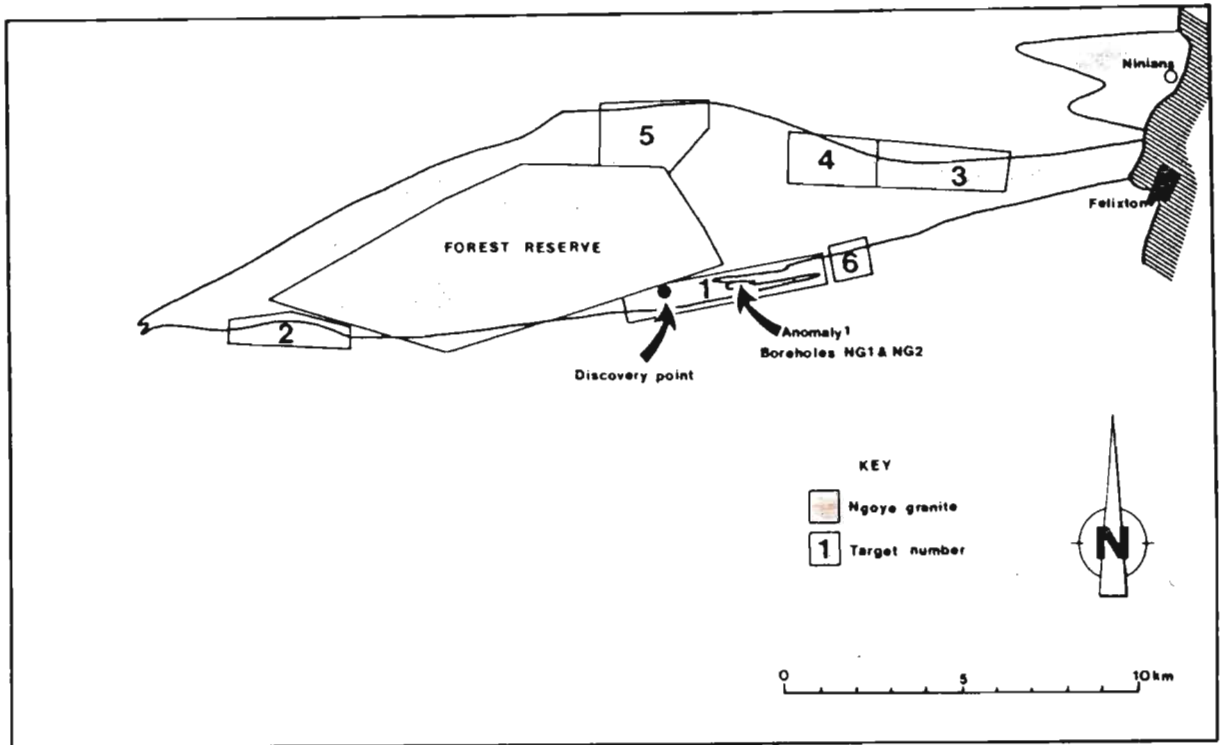


Fig. A.1. Location of the discovery point and subsequent target areas.

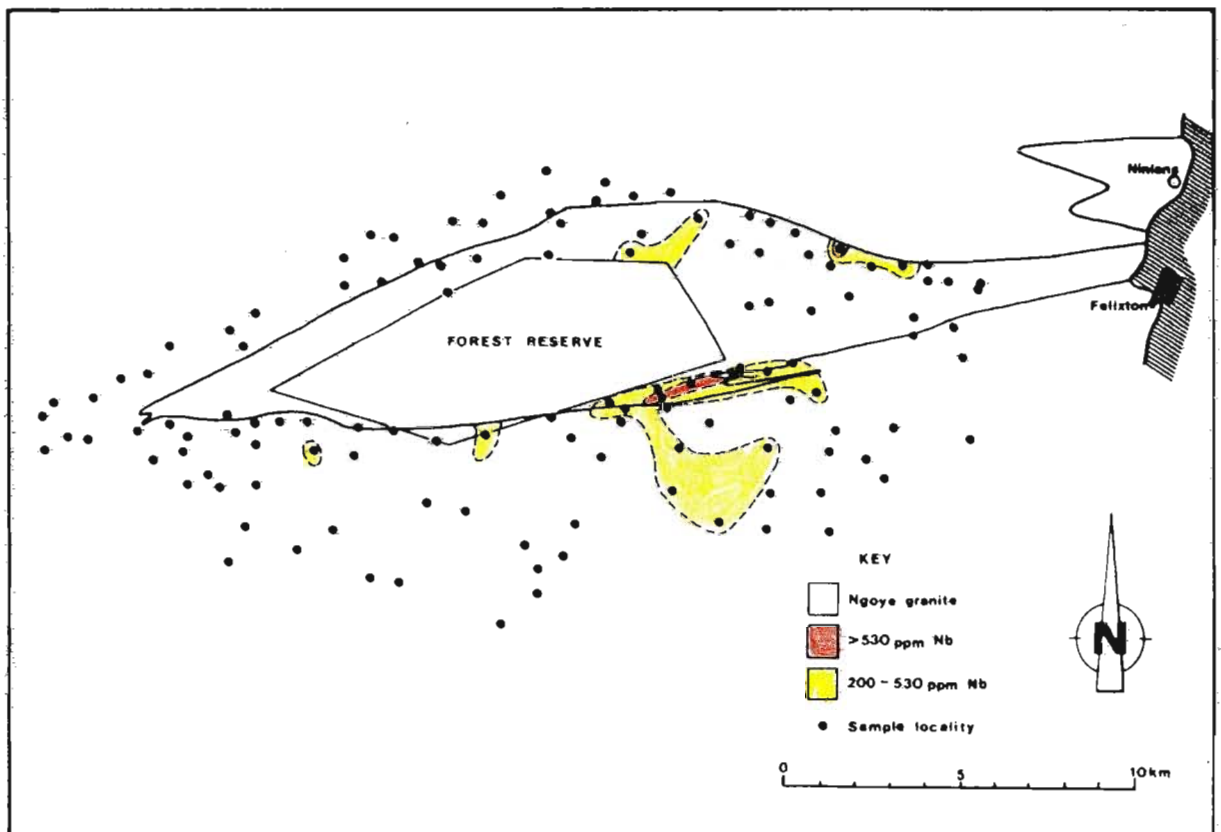


Fig.A.2. Contours of Nb (ppm) in panned stream-sediment samples.

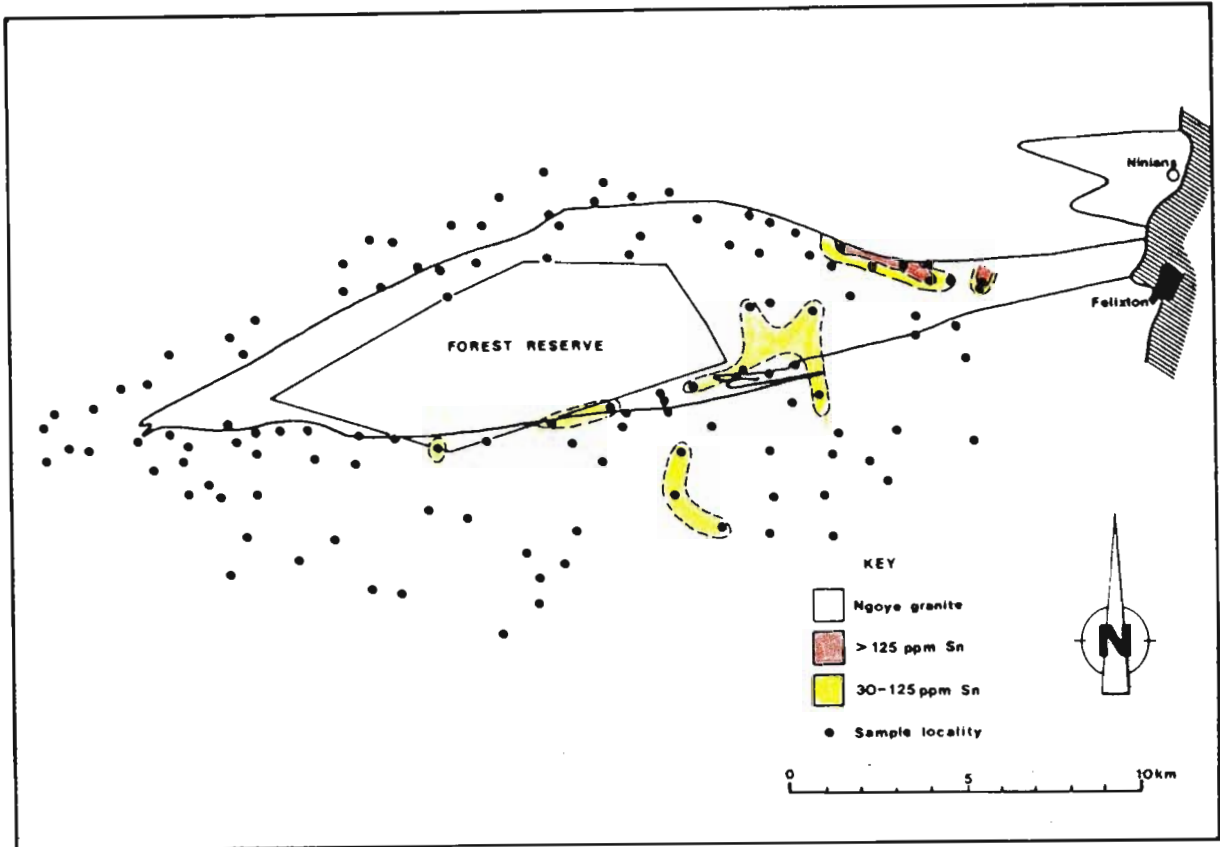


Fig. A.3. Contours of Sn (ppm) in panned stream-sediment samples.

A.4 Targets

A total of 6 targets were outlined on the basis of geochemical and geophysical evidence (Fig. A.1). Target 1 assumed priority rating as it is characterized by high combined geophysical and geochemical anomalies. The area was mapped by plane-table to a scale of 1 : 1 000 , with all of the (steeply dipping) magnetite-quartz horizons evaluated (a) by channel sampling of surface outcrops and (b) by sampling a series of 9 trenches. As shown in Table A.2, the values are extremely variable and restricted to narrow bands of radioactive quartz rock. Preliminary ore reserves calculations, from intersections over the area covered by trenches 1 to 5, indicated 1158 tonnes per metre depth over a stoping width of 1 metre, with values as follows; Nb, 1253 ppm; Ta, 46 ppm; Sn, 13 ppm; W, 60 ppm; and U308, 109 ppm. Two surface boreholes of TNW diameter were sunk (at the positions indicated in Fig. A.1) at a plunge of 55° to the north. These holes, NG 1 and NG 2, were drilled to depths of 159 and 132 m respectively and showed good correlation with surface geology, but failed to intersect any significant Nb mineralization. The project was abandoned in July 1983.

TABLE A.2

Target 1, trench channel sample analyses*

Trench	Nb	Ta	U ₃ O ₈	Sn	W	width**
1	650	34	62	32	44	1,50
2a	3135	110	309	-	122	0,45
2b	2246	87	194	-	99	0,56
3	1169	50	113	-	43	3,00
4	2558	67	199	-	94	1,13
5a	952	44	101	-	60	1,20
5b	1259	66	58	35	56	0,42
6	220	-	-	-	-	2,00
7	1640	99	186	32	85	1,00
8	932	44	120	-	46	0,55
9	2097	194	262	621	124	1,25

Notes:

* = all analyses in ppm., uranium as U₃O₈.

** = sample widths in metres.

APPENDIX B

B.1 Major and Trace Element Analyses

Twenty seven granitoid samples were analysed by M.R. Sharpe at Pretoria University, using a Siemens SRS/1 XRF machine. All major elements, with the exception of Na, were analysed using fused discs prepared after the method described by Norrish & Hutton (1969). Major elements were determined as follows: MgO, Al₂O₃, SiO₂, P₂O₅, K₂O and CaO with a Cr tube, and Fe as Fe₂O₃, MnO, Cr₂O₃, and N₂O with a W tube. Pressed, 40 mm diameter, powder briquettes were analysed for trace elements by XRF techniques. The trace elements Cu and Zn were analysed using the Au tube while the remaining elements, including Na, were analysed using a W tube. Precision in all cases is better than 40% of the absolute error.

Geochemical values for the 27 samples analysed are presented below in Tables B.1, B.2, B.3, and B.4. All major element oxides are in weight %, trace elements are in ppm., and C.I.P.W. norms are derived from 100% volatile-free recalculated analyses. Fe in all cases is given as FeO^(tot), ie 0.8998Fe₂O₃ + FeO. LOI includes H₂O- in all analyses, and D.I. = the differentiation index of Thornton & Tuttle (1960).

TABLE B.1

Major-elements, selected trace elements, and C.I.P.W. norms

	N574	C47	C48	N447	C107	N373	C106
SiO ₂	71,79	74,60	76,97	72,12	73,15	73,18	73,91
TiO ₂	0,43	0,22	0,10	0,49	0,37	0,32	0,30
Al ₂ O ₃	13,54	12,86	12,46	12,78	11,83	12,37	12,06
FeO	2,59	1,95	1,01	4,77	3,32	3,26	2,83
MnO	0,04	0,05	0,02	0,11	0,10	0,07	0,06
MgO	0,56	0,08	-	0,28	0,25	0,21	0,12
CaO	1,25	0,74	0,49	1,24	0,90	0,86	0,57
Na ₂ O	4,08	4,24	3,96	4,06	3,62	4,39	3,71
K ₂ O	4,52	5,03	5,07	4,66	4,66	4,53	5,08
P ₂ O ₅	0,14	0,06	0,02	0,08	0,06	0,05	0,04
LOI	0,36	0,29	0,25	0,34	0,53	0,21	0,51
Total	99,30	100,24	100,32	100,93	98,80	99,45	99,20
D.I.	88,40	94,00	96,70	86,70	90,30	92,00	93,20
Rb	166	210	208	90	84	126	122
Sr	202	114	127	104	52	89	46
Ba	937	753	753	1086	711	825	622
Zr	198	297	271	839	713	478	592
Zn	34	56	60	148	128	84	92
Q	26,49	28,36	33,12	25,35	31,56	27,28	30,64
Or	27,27	30,02	30,05	27,27	27,83	27,51	30,58
Ab	34,61	35,63	33,56	34,09	30,94	37,23	31,96
An	5,28	1,11	1,11	2,78	2,50	0,55	1,03
Di	0,12	1,04	1,24	2,45	1,36	3,16	1,29
Hy	4,35	1,85	0,53	5,48	3,35	3,07	2,91
Mt	0,70	0,70	0,24	1,16	0,93	0,70	0,93
Il		0,46	0,15	0,91	0,76	0,61	0,61
Ap	0,31	0,12		0,15	0,12		0,09

Notes:

N574, C47, C48 = mesocrystic biotite granite. N447, C107, N373, C106 = biotite-hornblende granite.

TABLE B.2

Major elements, selected trace elements, and C.I.P.W. norms

	N613	N682	C49	C112	N34	NG2A	NG2B
SiO ₂	75,20	77,57	73,57	77,38	77,88	63,79	65,12
TiO ₂	0,07	0,09	0,28	0,02	-	0,14	0,22
Al ₂ O ₃	12,07	12,25	13,51	12,96	13,10	17,64	18,38
FeO	1,24	1,24	2,11	0,75	0,71	5,33	3,21
MnO	0,03	0,02	0,05	0,08	0,11	0,12	0,05
MgO	0,05	0,04	0,26	0,11	0,10	0,25	0,28
CaO	0,55	0,48	1,01	0,25	0,03	0,07	0,15
Na ₂ O	4,40	3,84	4,34	4,48	5,18	3,89	2,18
K ₂ O	4,41	4,83	4,98	4,41	4,16	7,84	11,86
P ₂ O ₅	-	0,02	0,06	0,01	0,01	0,02	0,02
LOI	0,33	0,26	0,21	0,22	0,33	0,76	0,57
Total	98,35	100,64	100,34	100,67	101,67	99,94	101,39
D.I.	96,50	95,80	92,50	96,90	98,20	87,24	90,79
Rb	345	266	322	724	935	276	408
Sr	5	-	20	4	29	17	31
Ba	10	16	84	3	-	217	658
Zr	112	122	115	97	64	587	955
Zn	30	29	9	33	118	75	45
Q	31,98	34,95	26,82	33,00	30,69	7,45	6,99
Or	26,71	28,38	29,47	26,13	24,49	46,76	65,35
Ab	37,76	32,51	36,16	37,73	43,00	33,03	18,35
An	0,28	1,67	2,78	1,11	0,28	0,28	0,72
C				0,31		2,65	2,45
Di	2,16	0,50	1,92				
Hy	0,65	1,29	2,12	1,36	1,49	8,26	4,92
Mt	0,23	0,23	0,69	0,20	0,12	1,16	0,69
Il	0,15	0,17	0,45			0,30	0,46

Notes:

N613, N682 = muscovite-biotite granite. C49, C112, N34 = biotite-muscovite granite. NG2A, NG2B = lower and upper syenite intersections respectively.

TABLE B.3

Major elements, selected trace elements, and C.I.P.W. norms

	N272	C108	N211	C46	N330	N331	N145	N181
SiO ₂	76,03	76,06	76,86	78,47	76,70	76,77	77,58	77,69
TiO ₂	0,19	0,19	0,18	0,11	0,10	0,14	0,11	0,09
Al ₂ O ₃	11,53	11,21	11,63	11,40	10,93	11,26	10,87	11,02
FeO	2,55	2,24	2,30	1,16	2,35	2,77	2,36	3,06
MnO	0,05	0,05	0,05	0,02	0,01	0,04	0,03	0,06
MgO	0,06	0,13	0,06	0,08	-	0,15	0,05	0,01
CaO	0,31	0,26	0,36	0,06	0,15	0,32	-	-
Na ₂ O	4,54	3,82	4,30	4,28	4,84	5,18	4,83	4,89
K ₂ O	4,59	4,80	4,41	4,52	4,14	4,15	4,08	4,25
P ₂ O ₅	0,11	0,02	0,01	0,01	-	0,01	-	0,02
LOI	0,21	0,29	0,16	0,21	0,27	0,28	0,14	0,13
Total	100,17	99,07	100,32	100,32	99,49	101,07	100,05	101,22
A.I.	1,08	1,03	1,02	1,05	1,14	1,16	1,14	1,15
D.I.	93,10	94,20	94,90	97,00	93,20	91,50	93,60	92,00
Rb	151	144	136	156	242	152	227	267
Sr	8	8	21	2	3	7	-	-
Ba	214	212	256	49	11	49	11	11
Zr	366	527	374	344	699	848	704	690
Zn	147	142	136	35	241	173	251	328
Q	32,29	34,38	33,11	36,78	35,21	32,76	36,58	34,57
Or	27,26	28,91	26,15	26,69	24,49	24,49	23,94	25,02
Ab	33,56	30,92	35,66	33,54	33,56	34,29	33,03	32,49
Ac	1,20	1,40	0,46	0,46	1,39	1,38	0,92	1,53
Ns	0,78			0,49	1,46	1,78	1,59	1,55
Di	0,74	0,98	1,47	2,42	0,74	1,47		
Hy	3,62	2,96	2,64	1,65	3,17	3,73	3,66	4,75
Mt			0,23					
Il	0,30	0,30	0,30	0,15	0,16	0,31	0,15	0,15
Ap	0,31	0,19						

Notes:

N272, C108, N211, C46 = riebeckite-biotite granite. N330, N145, N181 = riebeckite granite. N331 = aegerine microgranite.

TABLE B.4

Major elements, selected trace elements, and C.I.P.W. norms

	C110	NG2	C111	NR189	NR80
SiO ₂	76,55	77,85	71,32	64,89	71,50
TiO ₂	0,12	0,13	0,24	1,35	0,91
Al ₂ O ₃	11,52	10,92	6,07	1,29	0,44
FeO	1,67	2,37	14,97	27,37	28,07
MnO	0,01	0,02	0,17	0,14	0,18
MgO	0,03	0,03	-	0,06	-
CaO	0,21	0,13	0,16	0,86	0,05
Na ₂ O	3,08	3,78	2,29	0,43	0,14
K ₂ O	6,14	4,82	2,58	0,45	0,04
P ₂ O ₅	0,02	0,01	0,04	0,18	0,03
LOI	0,49	0,09	0,12	0,24	0,11
Total	99,84	100,15	97,96	97,26	101,29
D.I.	95,80	94,40	72,90	50,65	54,33
Rb	155	240	95	27	2
Sr	26	14	6	15	-
Ba	189	120	56	50	21
Zr	462	458	3443	29605	3285
Zn	89	57	622	985	681
Q	34,22	36,66	40,04	44,20	53,28
Or	36,47	28,38	15,57	2,78	
Ab	25,15	29,37	17,29	3,67	1,05
An				0,26	0,28
Ac	0,88	1,39	2,31		
Ns		0,25			
Di	0,87	0,49	0,50	2,97	
Hy	1,88	3,27	19,80	36,17	36,69
Mt			3,71	6,75	6,73
Il	0,15	0,30	0,46	2,58	1,67
Ap	0,03		0,10	0,30	

Notes:

C110, NG2 = magnetite microgranite. C111, NR189, NR80 = magnetite-quartz rock.

APPENDIX C - MODAL ANALYSES OF NGOYE GRANITOIDS

TABLE C.1

Modal analyses* of Ngoye granitoids.

	N7	N219	N220	N221	N307
microcline	24,1	30,1	32,0	35,1	30,8
plagioclase	34,1	26,8	37,5	24,8	30,3
quartz	34,2	32,3	25,2	31,9	33,7
biotite	5,7	6,9	4,4	6,4	4,8
hornblende	-	-	-	-	-
muscovite	-	-	-	0,2	-
epidote	0,9	2,0	t	0,3	t
sphene	t	0,7	0,3	0,5	t
opaque	0,7	0,6	0,3	t	0,2

	N320	N323	N493	N554	N564
microcline	31,8	35,6	30,2	25,9	25,8
plagioclase	31,4	26,5	27,4	26,9	25,1
quartz	27,3	30,4	35,6	36,2	38,0
biotite	7,4	5,7	5,8	7,0	7,0
hornblende	-	-	-	-	-
muscovite	-	-	-	1,2	1,0
epidote	1,2	0,7	0,7	0,9	-
sphene	t	0,4	-	0,8	1,2
opaque	-	0,3	-	0,3	0,7

Notes:

Sample localities shown in Fig. C.1.

* : all values as volume percentages.

t : mineral species present but less than 0,2%.

- : mineral species not detected.

Sample numbers : N7, N219, N220, N221, N307, N320, N323, N493, N554 & N564 = mesocrystic biotite granite.

TABLE C.2

Modal analyses* of Ngoye granitoids.

	N576	N579	N574B	N210	N211
microcline	35,1	25,9	26,9	33,4	48,9
plagioclase	28,0	30,5	28,5	29,8	10,7
quartz	29,8	30,1	33,5	30,9	32,7
biotite	5,2	9,0	6,1	2,0	2,8
hornblende	-	-	-	3,0	3,9
muscovite	t	0,9	2,4	-	-
epidote	0,3	1,4	1,2	-	-
sphene	0,6	1,1	0,8	t	-
opaque	0,4	0,6	0,4	0,5	-

	N213	N216	N216	N329	N346A
microcline	37,2	37,2	33,3	36,2	34,9
plagioclase	21,1	22,1	29,1	12,1	16,2
quartz	34,4	30,4	28,8	41,7	42,2
biotite	3,3	4,3	3,0	2,3	1,0
hornblende	3,7	4,6	3,6	5,4	3,3
muscovite	-	-	-	-	-
epidote	-	0,5	1,0	1,2	-
sphene	t	0,3	0,5	0,7	0,3
opaque	-	t	0,3	0,4	1,6

Notes:

Sample localities shown in Fig. C.1.

* : all values as volume percentages.

t : mineral species present but less than 0,2%.

- : mineral species not detected.

Sample numbers : N576, N579, N574B = mesocrystic biotite granite.

N210, N211, N213, N215, N216, N329 & N346A = biotite-hornblende granite.

TABLE C.3

Modal analyses* of Ngoye granitoids.

	N374	N375	N447	N326	N327
microcline	50,7	32,0	44,1	35,2	30,7
plagioclase	23,4	35,1	20,2	35,0	29,8
quartz	22,9	42,2	27,4	26,6	34,8
biotite	0,4	1,6	2,9	2,7	4,4
hornblende	2,2	3,8	4,7	-	-
muscovite	-	-	-	t	0,2
epidote	-	-	-	-	-
sphene	t	t	0,5	-	-
opaque	-	t	0,1	-	t

	N434	N613	N33	N36	N556
microcline	28,2	23,8	22,4	21,9	40,3
plagioclase	33,4	28,8	38,2	35,2	22,9
quartz	35,4	44,5	34,2	37,3	32,9
biotite	2,6	2,7	-	-	0,5
muscovite	t	t	5,0	5,2	2,3
garnet	-	-	0,2	t	-
opaque	-	t	t	-	0,4
fluorite	t	t	-	-	-

Notes:

Sample localities shown in Fig. C.1.

* : all values as volume percentages.

t : mineral species present but less than 0,2%.

- : mineral species not detected.

Sample numbers : N374, N375 & N447 = biotite-hornblende granite. N326, N327, N434 & N613 = muscovite-biotite granite. N33, N36 & N556 = biotite-muscovite granite.

TABLE C.4

Modal analyses* of Ngoye granitoids.

	N566	C108	N192	N193	NR80
microcline	23,2	31,4	36,0	6,6	-
plagioclase	31,6	27,0	30,7	14,7	-
quartz	43,4	39,6	26,9	73,4	83,9
biotite	0,4	0,8	0,2	-	-
muscovite	0,9	-	-	-	-
riebeckite	-	1,0	5,9	-	-
sphene	-	-	-	-	0,5
opaque	-	-	t	3,0	12,1
zircon	-	t	t	1,8	0,7
fluorite	-	t	-	-	-
allanite	-	-	-	0,3	2,4

Notes:

Sample localities shown in Fig. C.1.

* : all values as volume percentages.

t : mineral species present but less than 0,2%.

- : mineral species not detected.

Sample numbers : N566 = biotite-muscovite granite. C108 = riebeckite-biotite granite. N192 = riebeckite granite. N193 & NR80 = magnetite-quartz rock.

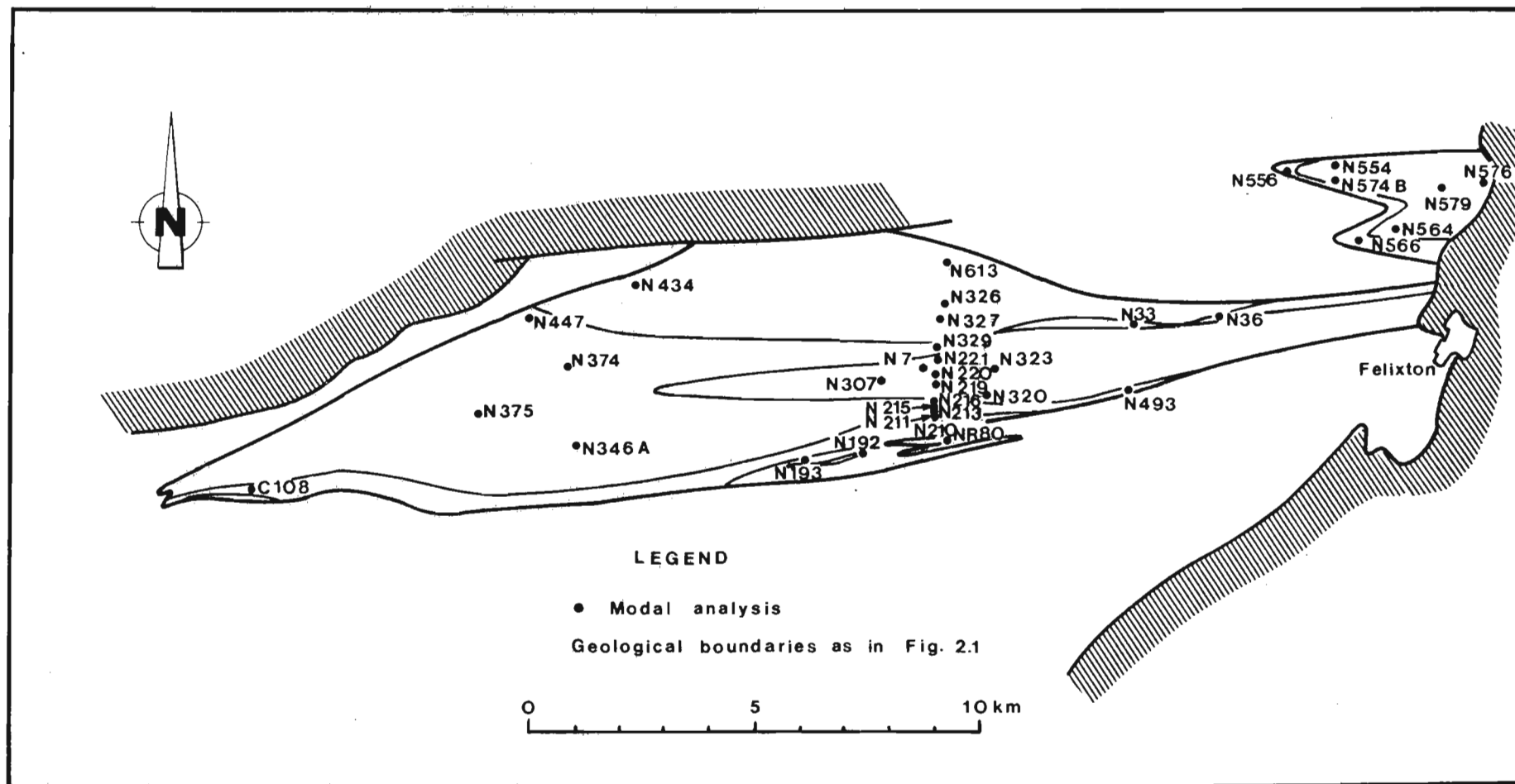


Fig. C.1 LOCATION of ADDITIONAL MODAL ANALYSES